DEVELOPMENT OF A FIBER OPTIC SENSOR FOR BIOMEDICAL ENGINEERING APPLICATION: A CASE STUDY OF CONTINUOUS BLOOD PRESSURE MEASUREMENT

By
MR. Piyawat SAMARTKIT

A Thesis Submitted in Partial Fulfillment of the Requirements
for Doctor of Philosophy ENERGY ENGINEERING
Department of MECHANICAL ENGINEERING
Silpakorn University
Academic Year 2023

การพัฒนาระบบตรวจจับชนิดใยแก้วนำแสงสำหรับการประยุกต์ใช้ในงานวิศวกรรมชีวการแพทย์: กรณีศึกษาการวัดความดันโลหิตแบบต่อเนื่อง

โดย
นายปิยวัฒน์ สามารถกิจ

วิทยานิพนธ์นี้เป็นส่วนหนึ่งของการศึกษาตามหลักสูตรปรัชญาดุษฎีบัณฑิต
สาขาวิชาวิศวกรรมพลังงาน แบบ 2.2 ปรัชญาดุษฎีบัณฑิต
ภาควิชาวิศวกรรมเครื่องกล
มหาวิทยาลัยศิลปากร
ปีการศึกษา 2566

DEVELOPMENT OF A FIBER OPTIC SENSOR FOR BIOMEDICAL ENGINEERING APPLICATION: A CASE STUDY OF CONTINUOUS BLOOD PRESSURE MEASUREMENT

By

MR. Piyawat SAMARTKIT

A Thesis Submitted in Partial Fulfillment of the Requirements
for Doctor of Philosophy ENERGY ENGINEERING
Department of MECHANICAL ENGINEERING
Academic Year 2023

Title	Development of a Fiber Optic Sensor for Biomedical Engineering Application: A Case Study of Continuous Blood Pressure Measurement
By	MR. Piyawat SAMARTKIT
Field of Study	ENERGY ENGINEERING
Advisor	Associate Professor Saroj Pullteap, (Ph.D.)

Faculty of Engineering and Industrial Technology, Silpakorn University in Partial Fulfillment of the Requirements for the Doctor of Philosophy

.....
Dean of Faculty of Engineering and Industrial Technology
(Assistant Professor Dr. Arunsri Leejeerajumnean)

Approved by

.....
Chair person
(Assistant Professor Prathan Buranasiri, (Ph.D.))

.....
Advisor
(Associate Professor Saroj Pullteap, (Ph.D.))

.....
Committee
(Assistant Professor Teerasak Hudakorn, (Ph.D.))

.....
Committee
(Assistant Professor Thosapon Katejanekarn, (Ph.D.))

.....
External Examiner
(Assistant Professor Dr. Chaowalit Hamontree)

61406802 : Major ENERGY ENGINEERING
Keyword : Fiber optic sensor, Fiber optic Fabry-Perot interferometer, Blood pressure measurement, Arterial pulse wave monitoring, Optical phase-shift demodulation

MR. Piyawat SAMARTKIT : Development of a Fiber Optic Sensor for Biomedical Engineering Application: A Case Study of Continuous Blood Pressure Measurement Thesis advisor : Associate Professor Saroj Pullteap, (Ph.D.)

In this dissertation, the development of a fiber optic sensor for non-invasive continuous blood pressure measurement has been investigated with the objective of prototyping a biomedical instrument with high accuracy, high sensitivity, and high resolution. Particularly, a fiber optic Fabry-Perot interferometer (FFPI) has been involved in the designing of pulse sensing probes and also development of a continuous blood pressure measuring system over the course of investigations. Principally, the displacement measurement capability of the FFPI is exploited to detect arterial distension on human skins, allowing pulse wave monitoring and ultimately blood pressure demodulation.

In this case, the theory of thin film deflection enabling the displacement conversion into pressure parameter has been applied to preliminarily measure the pulse pressure (PP), heart rate (HR), and arterial pulse wave detected during the examination. Furthermore, the systolic blood pressure (SBP) and diastolic blood pressure (DBP) are measured by using a modified pulse wave velocity (PWV) demodulation technique. To investigate the FFPI in non-invasive continuous blood pressure measurement, this dissertation has initiated three validation phases: 1) preliminary system implementation, 2) resolution improvement for high performance pulse monitoring, and 3) validation of FFPI in a human trial. Specifically, the system implementation phase has interrogated the technical feasibility of the FFPI in displacement and arterial pulse wave detection. In this stage, a mechanical vibrator has been employed as a surrogate pulse wave generator before applying the fiber optic sensor in human examination of three volunteers. Afterwards, the resolution of the FFPI has been improved through integration of an optical phase-shift demodulation technique with the intention of designing a robust pulse wave monitoring system for subsequent blood pressure demodulation. Here, the improved sensitivity and resolution of the FFPI has also been investigated by deploying a piezoelectric actuator as a displacement platform. Ultimately, a total of 85 human volunteers have been recruited and examined to validate the biomedical capabilities of the FFPI in the third dissertation phase. Nonetheless, the energy consumption and developed cost of the fiber optic system have been characterized and estimated, respectively, for establishing preliminary information for future instrumentation.

Following the three investigation phases, it is initially found that the FFPI system can detect arterial distension at the human wrist, thus leading to PP and HR measurement in a non-invasive way. Using the phase-shift demodulation technique, the sensitivity of the FFPI is revealed to be 1.0008 μm/μm while the resolution is 1.3199 nm which is significantly higher than the maximum approximated 700 μm of human arterial distension. Ultimately, the human trial showed high accuracy of the FFPI in all blood pressure and HR measurements of higher than 98%. Statistically, the mean absolute error (MAE) ± standard deviation (SD) in SBP, DBP, and PP measurement of 1.1500 ± 0.9544 mmHg, 0.9182 ± 0.9038 mmHg, and 0.7297 ± 0.6919 mmHg, respectively. This consequently complies with the accuracy grading of the Association for Advancement of Medical Instrumentation/European Society of Hypertension/International Organization for Standardization (AAMI/ESH/ISO) standard of "*grade A*". For the HR measurement, the mean absolute error percentage is 1.8518% with SD of 1.2868%. Meanwhile, the daily energy consumption of the FFPI system is estimated of 5,210 W·hr assuming a continuous operation in 8 working hours where the development cost to implement the fiber optic system is 319,117.91 THB. Nevertheless, the estimations concerned laboratory-grade equipment which could be optimized for small size and less expensiveness in future design. Therefore, the developed fiber optic system has been

concluded to be highly capable in non-invasive continuous blood pressure measurement and could pave ways for future development of novel biomedical instruments in cardiovascular investigations.

ACKNOWLEDGEMENTS

This dissertation has been the pursuit of my doctoral degree and would not have been possible without the help of other people for providing the opportunity and support. I would like to first and foremost express my sincere gratitude to Associate Professor Dr. Saroj Pullteap, my dissertation advisor, who has continuously provided advice and support with relentless efforts and patience. He has not only given knowledge and experience regarding research and academic aspects but also important life lessons. Furthermore, it is thanks to his broad perspective in the academic field that has expanded my point of view.

Moreover, I would like to thank Assistant Professor Dr. Prathan Buranasiri, the chairperson, Assistant Professor Dr. Teerasak Hudakorn, Assistant Professor Dr. Thosapon Katejanekarn, the internal dissertation committees, and also Assistant Professor Dr. Chaowalit Hamontree, the external committee, who had participated in my dissertation defense. With their suggestions, the dissertation has been improved with relevant information which should be of interest to those in the research and academic field.

I would like to offer my appreciation to Associate Professor Dr. Han Cheng Seat and Assistant Professor Dr. Olivier Bernal for their support during my international collaboration program at École Nationale Supérieure d'Électrotechnique, d'Électronique, d'Informatique, d'Hydraulique et des Télécommunications (ENSEEIHT), Institute Nationale Polytechnique de Toulouse (INPT), Toulouse, France. Not only has their expertise broaden my knowledge but they have also been of great help for my stay in France.

In addition, I express the utmost profound gratitude towards my family for their unyielding encouragement even in the most difficult time throughout my study. I would also like to thank all the laboratory members for their friendship, the staff of the Department of Mechanical Engineering, Silpakorn University and other personnels for the technical and administrative support.

The Royal Golden Jubilee (RGJ) PhD program of the National Research Council of Thailand (NRCT) has financially supported this dissertation under grant no. PHD/0189/2561. Due acknowledgement is also given to Silpakorn University Research, Innovation and Creativity (SURIC) administration office for approving the ethics in human research required in this dissertation. Without the opportunities, this dissertation would not have been as successful.

Piyawat SAMARTKIT

TABLE OF CONTENTS

Page

LIST OF TABLES

Page

LIST OF FIGURES

Page

LIST OF SYMBOLS AND ABBREVIATIONS

Symbol	Meaning
%Error	Error percentage
AAMI	Association for the Advancement of Medical Instrumentation
AE	Absolute error
AE%	Absolute error percentage
AI	Artificial intelligence
AWG	arbitrary waveform generator
BHS	British Hypertension Society
Bin	Bin width
c_{DBP}	Linear offset of diastolic blood pressure calibration
c_{PP}	Linear offset of pulse pressure calibration
CPU	Computer processing unit
d	Optical cavity length
DAQ	Data acquisition unit
DBP	Diastolic blood pressure
E_0	Arterial elasticity at zero pressure
ECG	Electrocardiographic
$E_{\mathrm{consumption}}$	Energy consumption
E_{film}	Elastic modulus
ESH	European Society of Hypertension
FBG	Fiber Bragg grating
FFPI	Fiber optic Fabry-Perot interferometer
FFT	Fast Fourier transform
FIR	finite impulse response
f_{mod}	Laser modulation frequency
f_{Nyquist}	Nyquist frequency
f_{original}	Frequency of signal without noise
f_{sample}	Sampling frequency
h_{artery}	Arterial wall thickness
h_{film}	Film thickness
HR	Heart rate

I	Intensity of interference signal
ICU	Intensive care unit
IEEE	Institute of Electrical and Electronics Engineers
I_r	Intensity of reference signal
I_s	Intensity of sensing signal
ISO	International Organization for Standardization
I_x	Interference signal x
I_y	Interference signal y
L	Length between arterial sites
LED	Light emitting diode
MAE	Mean absolute error
MAE%	Mean absolute error percentage
m_{DBP}	Linear slope of diastolic blood pressure calibration
mmHg	Millimeters of mercury
m_{PP}	Linear slope of pulse pressure calibration
MRI	Magnetic resonance imaging
n	Refractive index
N_{cavity}	Number of optical reflections within cavity
$N_{current}$	Current loop number
$N_{fringes}$	Number of fringes
N_{Loop}	Number of loops to perform
N_{sample}	Total number of samples
N_{sys}	Number of systolic peaks
OSA	Optical spectrum analyzer
P	Pressure
PAT	Pulse arrival time
PET	polyethylene terephthalate
PGC	phase generated carrier
P_{max}	Maximum power rating
PP	Pulse pressure
PP_{demod}	Demodulated pulse pressure
PPG	Photoplethysmographic
PSD	Power spectral density
PSD_{noise}	Power spectral density of signal noise

PTT	Pulse transit time
PWV	Pulse wave velocity
PZT	Lead zirconate titanate
R^2	Coefficient of correlation
r_{artery}	Radius of artery
r_{DBP}	Arterial radius at diastolic blood pressure
r_{film}	Deflection radius
RMS	Root mean square
RMSD	Root mean square deviation
SBP	Systolic blood pressure
SD	Standard deviation
t	Sample number
THB	Thai Baht
t_{HR}	Measurement time
t_{power}	Operating time
t_{x}	Time x
t_{y}	Time y
UI	user interface
USD	United States Dollar
V	Blood volume
WHO	World Health Organization
Δd	Displacement / Deflection
ΔP	Differential pressure
Δr_{artery}	Arterial distension
ΔV	Differential volume
$\Delta\lambda$	Difference of wavelength x and y
ε	Error
λ	Optical wavelength
Λ_{c}	Initial input wavelength
λ_{x}	Optical wavelength x
λ_{y}	Optical wavelength y
ρ	Blood density
υ	Poisson's ratio
φ	Phase-shift

χ_{in}	Input parameter
χ_m	Measurement from interrogating instrument
χ_{out}	Output parameter
χ_t	Measurement from reference device

CHAPTER 1
INTRODUCTION

1.1 MOTIVATION

Blood pressure, along with heart rate, respiratory rate, and temperature, is one of the important vital signs which indicates the health of a person. Particularly, it is applied for health monitoring, disease diagnosis, medicine prescription, and treatment management. For example, inspections of blood pressure during everyday lives allows early warning to underlying health issues such as stress and weaknesses [1]. In some instances, physicians monitor the blood pressure of patients before and after administering their medicine to ensure that the subjects have stable health conditions [2]. Moreover, life insurance companies have been one of the first organizations to consider the blood pressure information in their business [3]. Nevertheless, the most prominent application of blood pressure is, arguably, the diagnosis of hypertension.

Hypertension, or the state where high blood pressure circulates within the body, is one of the leading causes of mortality in the world. This is due to the high pressure in the circulatory system that can potentially damage internal organs and blood vessels when maintained for a long period. Over time, hypertension will lead to organ failures or major health problems, eventually leading to mortality [4, 5]. Moreover, the primary causes of hypertension are stress, unhealthy diets (e.g., high sodium intake and high cholesterol consumption), and lack of physical activities, which are more common in modern society [6]. These facts elevate the number of hypertensive patients in the present day.

From the World Health Organization (WHO) report, approximately 1.3 billion people worldwide were diagnosed with hypertension in 2023, accounting for 33% of global adults (33-79 years old) [7]. More importantly, the aforementioned percentage of hypertensive patients has insignificantly changed over the years, from 32% in 1990 to 2019. However, the global hypertensive population greatly increased from 650 million to 1.3 billion in the respective period, meaning that hypertension has become a persistent cardiovascular disease in the modern world. Importantly, 46% of the high blood pressure patients were unaware of having the disease, contributing to the untreated cardiovascular disease worldwide [7].

Globally, hypertension is similarly prevalence across all countries regardless of income level. Specifically, there are 32% of hypertensive adults in high-income nations while it is 34% for low-income countries [7]. However, more notable statistics are seen in regional variability, which can be observed in Table 1.1 [7].

Table 1.1 Prevalence of hypertension in different regions

Region	Hypertension	Diagnosis coverage
African	36%	43%
The Americas	35%	70%
Southeast Asia	32%	39%
European	37%	66%
Eastern Mediterranean	38%	49%
Western Pacific	28%	54%
Globally	33%	54%

On average, hypertension across the globe is 33% prevalent, with the Western Pacific having the least and the Eastern Mediterranean having the most percentage of hypertensive patients, respectively. However, the Americas have the highest diagnosis coverage of all the regions in contrast to Southeast Asia with the least coverage of 39%. Population wise, it is also reported that the greatest number of hypertensive patients live in the most populous areas: Western Pacific and Southeast Asia [7]. This implies that regions with the most population tend to have a significantly higher hypertension risk regardless of the diagnosis coverage in the area.

In Thailand, hypertensive cases are repeatedly reported yearly, with the statistics in 2007-2019 shown in Fig. 1.1 [8].

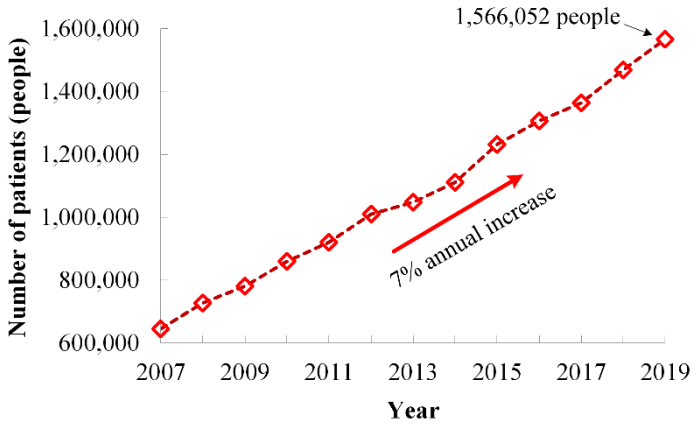

Fig. 1.1 Statistics of Thai hypertensive patients in 2007-2018

It has been investigated that Thai hypertensive patients increase at 7% rate annually, with a reported number of 1,566,052 people in 2019. In addition, hypertensive patients accounted for 2.09%, 2.25%, and 2.39% of the total population in the country from 2017-

2019, respectively [8]. This suggests that the number of hypertensive patients will gradually increase each year with a growing population. While not explicitly reported, it can however be speculated that one of the major causes of hypertension around the world is its asymptomatic nature.

Since hypertension is related to high blood pressure within the circulatory system, apparent symptoms are not clearly sensed or conveyed to the patient via their physiology unlike wounds or bodily weakness. Instead, symptoms such as headaches, dizziness, and fatigue are either observed at a severely high blood pressure level or associated with other diseases due to the common immunological responses, further leading to complications in health diagnosis. Regardless, hypertension can simply be detected by blood pressure measurement and consequently treat or control afterwards.

In modern medicine, blood pressure, along with heart rate, respiratory rate, temperature, and other vital signs, is one of the important biological parameters in health monitoring, diagnosis, and disease intervention/prevention. Primarily, blood pressure is applied to diagnose the cardiovascular health of a person as high blood pressure or hypertension can lead to potential danger to the body. Table 1.2 indicates the level of blood pressure corresponding to the hypertension category for references [9].

Table 1.2 Hypertension category

Hypertension level	**Systolic blood pressure (SBP: mmHg)**		**Diastolic blood pressure (DBP: mmHg)**
Normotensive	< 120	and	< 80
Prehypertension	120-139	or	80-89
Hypertension stage 1	140-159	or	90-99
Hypertension stage 2	≥ 160	or	≥ 100

From the table, hypertension can be categorized into 4 groups: normotensive, pre-hypertension, hypertension stage 1, and stage 2. Normotensive level describes the normal blood pressure level a healthy person is expected to have, while early hypertensive, specifically, means that blood pressure has elevated to a certain value. If untreated, early hypertension will develop into hypertension stage 1 and then stage 2, respectively, with each development increasing the risk of cardiovascular diseases such as strokes, arrhythmia, and lasting damage to the circulatory system. At this point, the systolic blood pressure of at least 140 mmHg should be treated to prevent cardiovascular risk and mortality in the immediate future. Systolic blood pressure of less than 140 mmHg will, however, benefit less from

hypertensive preventive measures, though should still be reduced for better cardiovascular health [9, 10].

Fortunately, hypertension can be prevented by initially altering the lifestyle of the patient (change of diet, sodium reduction, more frequent physical exercises, etc.) before any bodily damage occurs [11]. For instance, aerobic and isometric exercises have shown to reduce the high blood pressure level; thus, regular exercises are considered an antihypertension management strategy for patients [12]. Also, early and fast blood pressure control are preliminarily investigated as an effective, long-lasting approach in hypertension prevention [13]. This is, consequently, performed in association with regular blood pressure inspection to evaluate the hypertension level and carry out proper treatment or management strategies. Therefore, it is imperative that modern blood pressure measuring instruments accommodate this biomedical practice to the general population.

Historically, blood pressure was a concept stemming from internal body pressure only concerned when blood spurts out from wounds. This fact was later scientifically investigated and subsequently paved the way for the development of blood pressure instruments. Here, the milestones of blood pressure instrumentation can be illustrated in Fig. 1.2 [14-22].

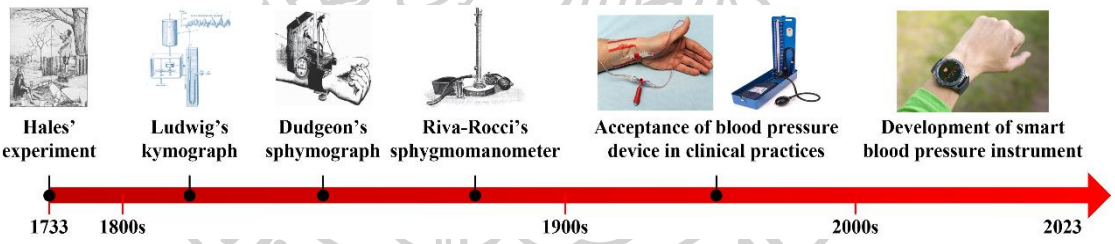

Fig. 1.2 Important milestones in blood pressure instrumentation history

Stephen Hales (1677-1761) introduced the concept of blood pressure in 1733 by cannulation of a long glass tube into a living horse. Consequently, the blood surged into the tube at approximately 2.5 m of height, proving the existence of blood pressure within a living being [14, 15]. In 1828, a mercury manometer for blood pressure measurement was then invented by Jean Léonard Marie Poiseuille (1797-1869), confirming that blood pressure resides in small arteries, leading to the advancement of clinical blood pressure in that period [16, 17]. Furthermore, a kymograph, a furthered design of Poiseuille's invention, was developed by Carl Friedrich Wilheim Ludwig (1816-1895) as an invasive blood pressure apparatus with a paper-based recording function for physiological and medical experiments [16, 17]. After the 1850s, the focus of blood pressure instrumentation had, however, shifted from invasive techniques to non-invasive approaches, such as for Karl von Vierordt (1818-

1884). Significantly, he introduced a sphygmograph which detected arterial pulse wave using the counter pressure required to neutralize the radial arterial distension [18]. Ètienne Jules Marey (1830-1904) and Robert Ellis Dudgeon (1820-1904), afterwards, improved the sphygmograph to have a pulse wave recording function on a paper sheet and more robust structure for portability, respectively [19]. Scipione Riva-Rocci (1863-1937) ultimately created a sphygmomanometer, exploiting an inflatable cuff as an external pressure inducer to measure the internal blood pressure in a non-invasive approach. This instrument revolutionized the medical field since a sphygmomanometer can be relatively simple to operate in contrast to the previous non-invasive measuring apparatus [20]. Nevertheless, it was Nikolai Korotkoff (1874-1920) who consequently elevated the potential of the sphygmomanometer when applied in association with a stethoscope. His discovery of the heart pulse sound correlation with systolic blood pressure (SBP) and diastolic blood pressure (DBP) has led to the introduction of modern auscultatory sphygmomanometers [20]. On the other hand, Marey has also investigated the cuff pressure oscillation during blood pressure measurement, contributing to the inspiration of a novel blood pressure demodulation technique, namely the oscillometric sphygmomanometry widely utilized by modern blood pressure measuring devices [21]. Afterwards, the usefulness of blood pressure measuring instruments have been realized and the concept of home health monitoring devices was introduced in 1997. Specifically, anxiety of patients undergoing a hospital visit (medically termed as a white-coat effect) can lead to incorrect blood pressure results. Thus, measurements performed in a more relaxing environment can overcome the possible error due to emotional stimulation [22]. In this perspective, novel blood pressure instruments have been developed over the years, such as smartwatches and portable digital sphygmomanometers, for convenience in daily blood pressure measurement.

Nowadays, the most widely utilized non-invasive blood pressure measuring devices are digital sphygmomanometers, owing to their simplicity in measurement setup, portability, and automatic functions that allows quick and accessible blood pressure measurement both within and outside of hospital settings [23]. Significantly, digital sphygmomanometers have been developed for commercial applications in the market and also for medical institutes to alleviate the requirements of physicians in regular health inspections. Consequently, several modern biomedical textbooks have described the digital sphygmomanometer as an essential cardiovascular tool in the field [4, 24]. However, one of their limitations is that the blood pressure measurement is at best intermittent, due to the utilization of inflatable cuffs which block the blood flow during each measurement. This, inevitably, means that a digital sphygmomanometer cannot perform continuous blood pressure measurement on a patient, and

subsequent measurement setup must be organized [25]. Moreover, the design of the inflatable cuff can adversely affect the measurement accuracy, i.e., inappropriate cuff size to the patient's upper arm might lead to erroneous blood pressure readings [26-28]. On another perspective, the patient is required to prepare themselves for each measurement, for example, seated in a relaxing environment while wearing the machine. As such, their everyday routine can be periodically disrupted by performing the blood pressure measurement, leading to inconvenience and annoyance [29]. With the fast-going lives we live today, it is reasonable to consider a continuous blood pressure measuring device that would provide more convenience in day-to-day activities.

On the other hand, continuous blood pressure measuring instruments known as arterial catheters have been in medical practice alongside the digital sphygmomanometers. Instead of using an inflatable cuff, an arterial catheter is inserted into the blood vessel, allowing the instrument to measure the blood pressure in real-time. Due to this method, this instrument is considered the most accurate blood pressure measuring device to date, as the internal blood pressure is directly measured similarly to pressure measurement in pipelines [30]. This advantage is, consequently, significant as accurate blood pressure measurement leads to accurate diagnosis and treatment of hypertension [31]. Nonetheless, this invasive blood pressure measurement technique is not appropriate for regular blood pressure checkup in the general public. The main limitations are, consequently, potential risk of infection due to catheter insertion, requirement of a trained operator, and time-consuming to perform. Thus, this blood pressure measurement method is reserved within the hospital or medical institute for intensive care unit (ICU) and high risk surgery of certain critical cases [32].

Therefore, the current topic of interest in the biomedical engineering field is to introduce novel continuous non-invasive blood pressure measuring devices for general health inspection in everyday living. Conventionally, Pressman and Peñàz had invented arterial tonometers and volume clamp finger cuffs, respectively, which exploit the emergence of electronic components and computer technology for continuous non-invasive blood pressure measurement [21]. These devices are different from the digital sphygmomanometers in that dedicated pressure sensors are employed to retrieve the arterial pulse wave information and subsequently demodulate the corresponding blood pressure onto a digital screen [33, 34]. The contributions of the aforementioned instruments have, therefore, inspired the development of novel continuous non-invasive blood pressure measuring devices. Recently, several measuring instruments have been proposed such as the application of piezoresistive [35, 36] or piezoelectric (PZT) sensors for detection of arterial distension on the human skin [35-38], photoplethysmographic (PPG) sensors which detects the blood pressure using optical

illumination techniques [39-41], electrocardiographic (ECG) electrodes that can capture the electrocardiogram signals and demodulates into blood pressure values [42-44], and also fiber optic sensors utilizing light wave to indicate the arterial pulse wave, etc. The latter sensors are, in this case, investigated in the biomedical engineering field for the advantages of small size, lightweight, high sensitivity, and electromagnetic immunity. These advantages can, consequently, lead to the development of high performance portable blood pressure measuring instruments.

In this work, the development of a continuous non-invasive blood pressure measuring instrument based on a fiber optic sensor has been investigated with the purpose of proposing a highly accurate, and sensitive measuring system of a high resolution. Particularly, this dissertation is concerned with a fiber optic Fabry-Perot interferometer (FFPI) application in arterial pulse wave detection and subsequent blood pressure demodulation. The related theories chapter, initially, introduces the concept of arterial pulse wave detection, explanation of the FFPI in arterial pulse wave detection, and ultimately the employed blood pressure demodulation techniques. This dissertation also organizes the experimental setup and experimental results into 3 main phases, reflecting the continuity of the research in this topic starting from 1) the FFPI system implementation for preliminary investigation, 2) the improvements on the performance of the developed system, and 3) the validation of the proposed system in live human trial. Finally, the dissertation concludes with a conclusion chapter summarizing all the findings, limitations, and future prospects of the investigation.

1.2 OBJECTIVE OF DISSERTATION

To develop a fiber optic sensor system for continuous non-invasive blood pressure measurement with high accuracy, high sensitivity, and high resolution.

1.3 SCOPE OF RESEARCH

- This dissertation concerns the development of a fiber optic Fabry-Perot interferometer for continuous non-invasive blood pressure measurement on humans.
- The primary blood pressure demodulation techniques are thin film deflection and pulse wave velocity theories.
- The validation process recruits human volunteers under their own volition and consent. In addition, their rights are protected under ethics in human research protocol approved by Silpakorn University Research, Innovation, and Creativity

(SURIC) administration office certified in document no. COE 65.0401-065 under the research project ID: REC 65.0131-017-0419.

- The participants are of general population, i.e. have no cardiovascular or other significant health conditions.
- The high sensitivity and resolution aspects of the developed fiber optic sensor are verified through literature review and comparison to other equivalent blood pressure sensors.
- The analysis mainly focuses on the systolic blood pressure (SBP), diastolic blood pressure (DBP), pulse pressure (PP), and heart rate (HR) measurements.

1.4 EXPECTED BENEFITS

- Knowledge regarding the development of a fiber optic sensor-based continuous non-invasive blood pressure measuring system.
- Knowledge on continuous blood pressure demodulation technique for future development of novel biomedical instruments.

1.5 LOCATION OF RESEARCH

- Main location: Mechanical Embedded System Laboratory (MESL), Department of Mechanical Engineering, Faculty of Engineering and Industrial Technology, Silpakorn University (Sanam Chandra Palace Campus), Nakhon Pathom, 73000, Thailand
- International collaboration: École Nationale Supérieure d'Électrotechnique, d'Électronique, d'Informatique, d'Hydraulique et des Télécommunications (ENSEEIHT), Institute Nationale Polytechnique de Toulouse (INPT), Toulouse, France

1.6 DISSERTATION PERIOD

This dissertation has been conducted from the academic year 2018-2023.

1.7 FUNDING SOURCES

This dissertation has been supported by the Royal Golden Jubilee (RGJ) Ph.D. Program of the National Research Council of Thailand (NRCT) grant no. PHD/0189/2561.

1.8 ETHICS IN HUMAN RESEARCH

The experiment on humans carried out in this dissertation has followed the ethics in human research protocol and approved by Silpakorn University Research, Innovation, and Creativity (SURIC) administration office certified in document no. COE 65.0401-065 under the research project ID: REC 65.0131-017-0419.

CHAPTER 2
RELATED THEORIES

In this chapter, the information associated with the principles, theories, and related concepts regarding the blood pressure measurement, sensing mechanisms of fiber optic sensors, and pressure demodulation schemes are described. This would afterwards contribute to the experiments explained in subsequent chapters.

2.1 ARTERIAL PULSE WAVE AND BLOOD PRESSURE MEASUREMENT

The human heart is one of the important organs which propagates blood to the entire body for exchanging essential biocomponents (oxygen, nutrients, waste, etc.). It functions by contracting and retracting its cardiac muscles, allowing blood to flow in a rhythmic fashion throughout the circulatory system. Thus, the blood pressure fluctuates according to the heart function, with the profile referred to as "*arterial pulse wave*" [45] and has a characteristic schemed in Fig. 2.1.

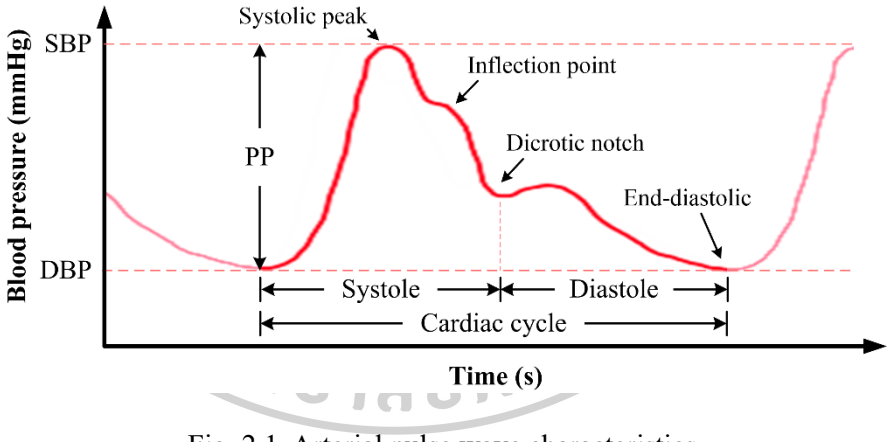

Fig. 2.1 Arterial pulse wave characteristics

At the start of any heart contraction, the blood pressure rises during the systolic upstroke phase and reaches a maximum point of systolic peak. The pressure value at this point is, thereby, called "*systolic blood pressure* (SBP)" which later reduces as the heart enters its retraction period. During this period, a superimposition between the percussion blood pressure wave of the heart contraction and a reflective wave due to the circulatory system might occur, resulting in the forming of an "*inflection point*" [46, 47]. This inflection can, interestingly, happen before or after the systolic peak according to the arterial stiffness, where it is caused before the peak in elderly people due to stiffer vessels and vice versa [48]. Regardless, a noticeable slight increase in blood pressure happens after the dicrotic notch, the

period between the heart contraction (systole) and retraction (diastole). This is due to the remaining propagation energy within the artery causing the slight increase in blood pressure before it lowers to the minimum value of "*diastolic blood pressure* (DBP)". Afterwards, a new cardiac cycle starts and continues the blood pressure fluctuation over time as the blood flows through the body. With this knowledge, the blood pressure values can be derived from the arterial pulse wave using an invasive blood pressure instrument. However, the difference between the SBP and DBP is the "*pulse pressure* (PP)", and this parameter is sensible using non-invasive pressure sensors [49]. Specifically, the major arteries, namely the radial and carotid arteries, are distended with sufficient pulse pressure that the distension can be felt on the skin above the arterial sites, i.e., on the wrist and neck, respectively. With this knowledge, it is possible to detect, and then measure, the pulse pressure of a human subject using a non-invasive blood pressure sensor.

Moreover, the arterial pulse wave is useful for extracting the "*heart rate* (HR)" of the examinee by observing the pulse wave characteristic. The systolic peaks occurred within a minute are, particularly, counted to measure the heart rate in beats per minute (bpm). Nonetheless, this can be performed in less time and subsequently interpolated to achieve an equivalent result using:

$$\mathrm{HR} = \frac{60}{t_{\mathrm{HR}}} N_{\mathrm{sys}} \tag{2.1}$$

where t_{HR} corresponds to the measurement time and N_{sys} is the number of systolic peaks counted over the t_{HR} period. While this equation can reduce the time requirement of an HR measurement, it should however be considered that the resolution of the measurement is inversely proportional to the period of interrogation. Therefore, an appropriate sampling period should be chosen to both lower the length of time while optimizing the measurement resolution. Regardless, this HR application proves the preliminary usefulness of the arterial pulse wave in blood pressure measurement.

Technically, arterial pulse wave, and by extension blood pressure, is an internal cardiovascular parameter measurable through invasive means. However, one of the by-products of blood pressure circulation is arterial distension, which is the expansion of the blood vessel in response to the pressure change during the blood propagation. This distension also exerts significant displacement on the skin surface where there are thin layers of tissues between the skin and the artery. These arterial distension areas can be referred to as arterial sites, and the common sites for detecting the distension through finger palpation are the

carotid artery at the neck and radial artery at the wrist, respectively. Owing to this knowledge, the most basic HR measurement technique is finger palpation on the arterial sites to count the heart pulse over a minute. Nevertheless, it is possible to monitor the arterial pulse wave through the arterial distension, leading to blood pressure measurement using a biomedical instrument. One common practice in the biomedical field is applanation tonometry where a pressure sensor is pressed to partially flatten the artery, causing blood pressure to enact onto the sensor [50, 51]. This method allows the PP measurement when the external applanating pressure approximately equals the DBP within the blood vessel. Note that applanation tonometry generally provides only the PP out of the three blood pressure parameters, though the concept has been effectively implemented by several continuous non-invasive blood pressure devices under research of today [52, 53].

2.2 MODERN NON-INVASIVE CONTINUOUS BLOOD PRESSURE SENSORS

In the past decade (2014-2023), several research and development have been investigating novel continuous non-invasive blood pressure measuring devices in hopes of overcoming the drawbacks of sphygmomanometers and arterial catheters. In this section, literatures regarding the development of blood pressure sensors are discussed, owing to the significance of new sensing components which enable more access into the cardiovascular information and eventually leading to new blood pressure demodulation techniques and implementations. In brief, there are 5 main sensors utilized in the current biomedical engineering field: electrocardiographic (ECG) electrodes, electronic transducers (such as piezoresistive, piezoelectric, and capacitive sensors), photoplethysmographic (PPG) sensors, ultrasound systems, and fiber optic sensors.

2.2.1 Electrocardiographic electrodes

Technically, heart contraction and retraction during blood circulation are controlled via bioelectrical signal, which conducts throughout the body. This discharge can, therefore, be detected using specialized equipment such as electrocardiographic (ECG) electrodes. Generally, the ECG electrodes are placed on the arms, legs, and chest areas of the patient to detect the electric current resulting from the cardiac function, with the setup exemplified in Fig. 2.2.

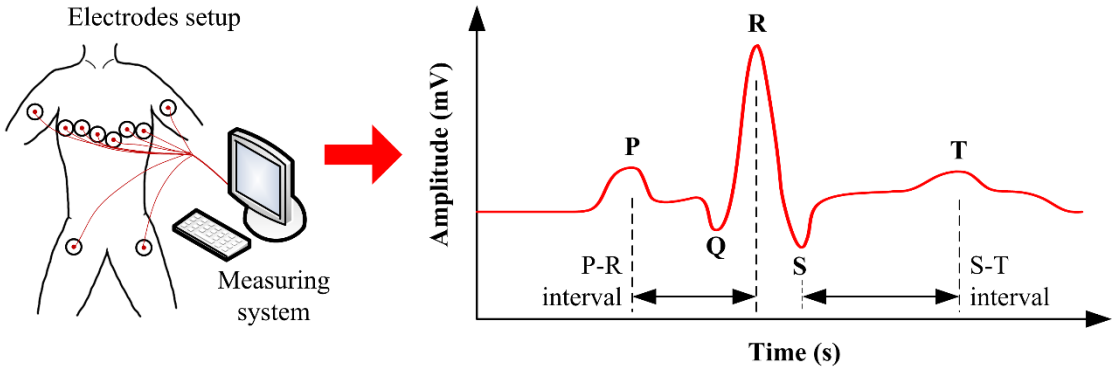

Fig. 2.2 Setup and cardiac signal of electrocardiographic electrodes

Once the electrodes are properly set up on the body, the electrical conduction can then be monitored, with the ECG signal arbitrarily labeled from the letter P to T designating the heart function. The P-wave, particularly, depicts atrial depolarization or when the right atrial chamber contracts blood to the right ventricle. The latter successively propagates blood through the aorta, performing ventricular depolarization which is characterized by the QRS-wave. The T-wave, meanwhile, corresponds to ventricular repolarization during blood filling the heart chamber at the moment of diastole. In addition, the time interval between the aforementioned parameters can also provide more cardiovascular information. For example, the P-R interval relates to the atria impulse propagation time, while S-T interval indicates the period of fully repolarized ventricular fibers[4, 45, 49].

Traditionally, ECG electrodes are exploited to investigate the heart function rather than directly utilized for blood pressure measurement. Nevertheless, recent research have been of interest to implement the ECG electrodes as novel blood pressure sensors in association with other cardiovascular transducers. In this case, the ECG signal can detect the blood propagation from the aorta, allowing the implementation of pulse arrival time (PAT) blood pressure demodulation technique when paired with another pulse sensor. This concept can, further, be described in Fig. 2.3.

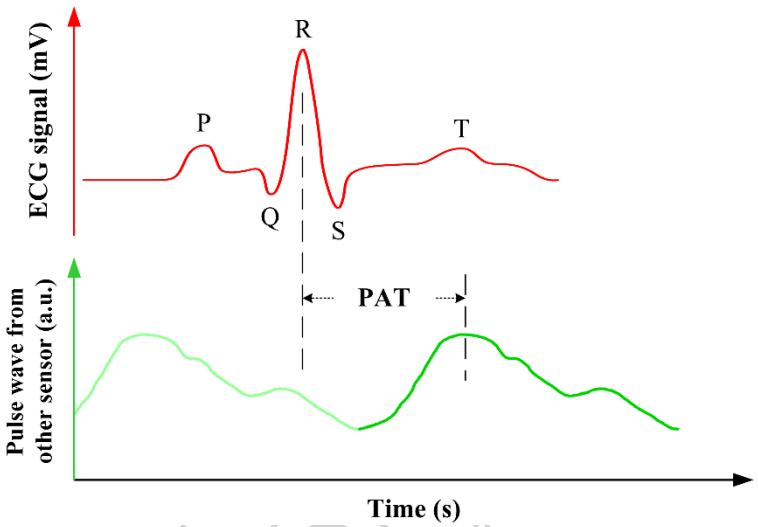

Fig. 2.3 Concept of pulse arrival time technique using ECG electrodes

From the figure, the R-peak of an ECG signal is applied as a reference point of blood propagation from the aorta. By comparing the reference point with the pulse characteristic of another pulse wave obtained from a different sensor, the time delay between the two points (the PAT) can be calculated and later applied to demodulate blood pressure. This PAT technique is, technically, similar to the pulse transit time (PTT) which will be described in other sections within this dissertation. Regardless, ECG electrodes are useful integration system for constructing compact size blood pressure measuring devices, owing to compatibility with other electronic components and small size [42-44, 54-60]. Additionally, ECG systems are unrestricted by the position of electrode attachment, as the cardio-electrical signal can be sensed from any body parts. However, it also means that a single ECG system cannot readily measure blood pressure without relying on other pulse wave detectors.

The most observed configuration of an ECG-based blood pressure measuring device requires an ECG system paired with another pulse sensor. Nevertheless, research in recent years have also investigated the implementation of ECG electrodes as standalone blood pressure instruments. Owing to the emergence of artificial intelligence (AI) and machine learning algorithms, novel ECG system adopts the latter to demodulate blood pressure from the ECG signal. With this method, large cardiovascular parameters aside from the ECG signals such as age, gender, height, weight, and other patient profile are trained into the machine learning algorithm. Afterwards, the system will be available for blood pressure measurement by monitoring the ECG signal of patients [61-63], allowing a single ECG system to perform the measurement independently from other pulse sensors. Still, the machine learning algorithm requires significant sample size and rigorous investigation to

ensure accuracy in practical settings. Regardless, this approach might lead to novel applications of ECG-based systems in future biomedical applications.

2.2.2 Electronic transducers

In this information era, electronic engineering has significantly elevated the development of advanced smart devices through the implementation of electronic sensors such as piezoresistive, piezoelectric, and capacitive sensors. Owing to the advent of modern electronics, the aforementioned sensors have become relatively cheaper, contributing to the development of commercial biomedical instruments. In the pressure sensing scheme, piezoresistive transducers modulate electrical resistance according to mechanical excitation such as arterial distension. This, subsequently, means that a piezoresistive sensor can be utilized as an arterial pulse wave detector and further as a blood pressure sensing device. Still, piezoresistive transducers require an external power source to function [35, 36]. On the contrary, piezoelectric sensors operate as active transducers without a power source, instead using the piezoelectric material (e.g., lead zirconate titanate: PZT) to discharge electricity when compressed [37, 38]. Likewise, the arterial pulse wave can be observed by using a capacitive sensor, which alternates the capacitance of an electronic system depending on the inducing pressure [64, 65]. Therefore, all electronic transducers have been of interest in the development of blood pressure measuring devices. In particular, electronic transducers are simple to operate, cheap in price, and can be integrated with embedded system design of an electronic platform such as smartwatches. Alternatively, flexible membranes comprising of these transducers can also be constructed and then placed on the skin for pulse sensing, as schemed in Fig. 2.4.

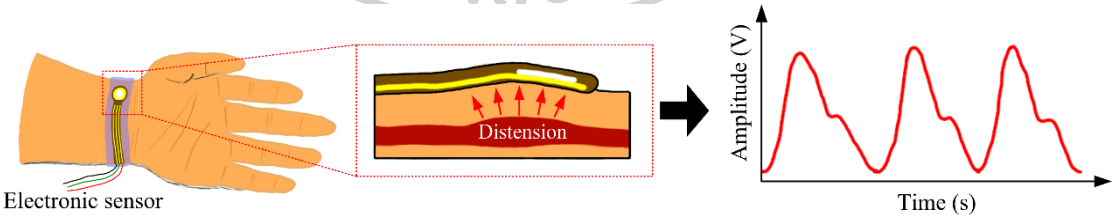

Fig. 2.4 Placement of an electronic sensor for arterial pulse wave monitoring

By ensuring the contact between the skin and the transducer, the arterial distension will induce PP onto the sensor, allowing the arterial pulse wave monitoring application. To perform this, the sensor design can either be integrated into a rigid structure or constructed inside a flexible membrane. For the former, fabrication of aa conventional sensing

probe is relatively simple, especially with mechanical tools and plastic printers [66-71]. Nonetheless, the rigidity of the probe might hinder its placement on an unstable human skin due to the curvature and bones. This, ultimately, leads to the requirement of substantial applanation force to correctly acquire the pulse wave information. Meanwhile, flexible membranes offer bendable pulse sensor structure, improving the attachability in pulse sensing setup [44, 72-76]. Moreover, flexible membranes can be implemented with a transducing array for widening the pulse detection area, reducing the difficulty of pinpointing the exact location of the arterial distension [77-80]. However, the limitations of the flexible membrane-based electronic transducers are the complexity of material selection and fabrication processes which might lead to higher development cost. Nevertheless, both the rigid and flexible design of the sensors are applicable for blood pressure measurement.

2.2.3 Photoplethysmographic sensors

In contrast to traditional pressure transducers, photoplethysmographic (PPG) sensors apply optical interaction to biological membranes. Specifically, the sensor propagates light through the skin which is successively modulated by the arterial distension before retrieved by the detector, as illustrated in Fig. 2.5.

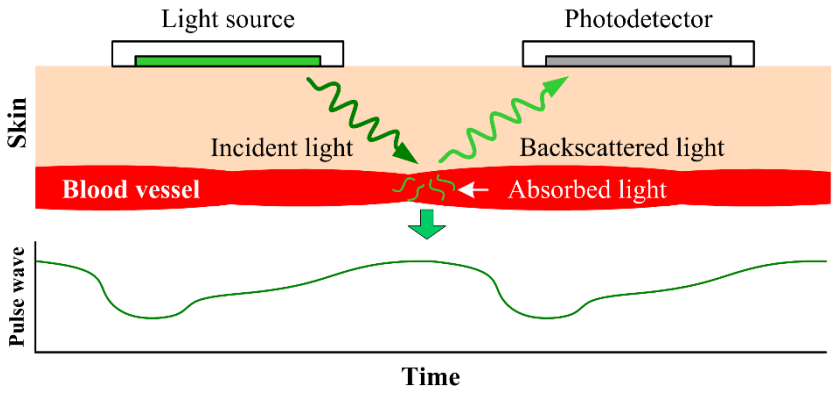

Fig. 2.5 Photoplethysmographic sensor in arterial pulse wave sensing

Typically, a PPG sensor consists of a green (approximately of 530 nm optical wavelength) light emitting diode (LED) and a photodetector for signal acquisition. In operation, the green light propagates through the tissue layer to the blood vessel, where it is absorbed proportionally to the amount of propagating hemoglobin. Afterwards, the remaining light is backscattered to the photodetector, with the intensity inversely proportional to the blood volume [39-41]. Since blood volume and blood pressure is closely related, the intensity

of the backscattered light, thus, corresponds to the arterial pulse wave and can be demodulated into blood pressure. Incidentally, a PPG sensor mainly utilized the optical principle after the device is properly placed over the skin without significant applanation force. Consequently, it is less perturbed by the anatomical aspect of the human body, contributing to convenience and higher accuracy than conventional pressure transducers.

Recently, PPG sensors have attracted several biomedical engineering research owing to the effectiveness in unobtrusive arterial pulse wave monitoring in humans. In fact, its operating principle reduces the discomfort during the monitoring process while enabling embeddable design into compact devices such as smartwatches and handheld probes. For example, wristband integrated with a PPG sensor is able to measure the HR and pulse wave, subsequently paving the way for continuous blood pressure measurement [81-84]. Furthermore, PPG sensors have generally been applied in association with ECG electrodes and electronic transducers, suggesting the high compatibility with other pulse sensing elements [85-88]. Nevertheless, the main limitation of the PPG sensor is the necessary calibration of the device to perform blood pressure measurement. This implies that an additional blood pressure instrument must be employed, thereby the PPG sensor will not be a standalone measuring system. Regardless, new demodulation techniques using artificial intelligence, machine learning algorithms, or other advanced computation schemes such as PPG intensity ratio have currently been interrogated to reduce the calibration requirement when using the PPG sensor [81].

2.2.4 Ultrasonic sound system

Arterial distension, an alteration of vessel diameter due to blood pressure, is an important parameter in continuous non-invasive blood pressure measurement. Therefore, most blood pressure sensing elements focus on acquiring arterial distension via the skin applanation. Interestingly, direct measurement of the arterial diameter has been considered to provide higher accuracy in arterial distension acquisition. Here, ultrasound systems are introduced as an alternative blood pressure measuring instrument using sound wave as the main sensing mechanisms, as shown in Fig. 2.6.

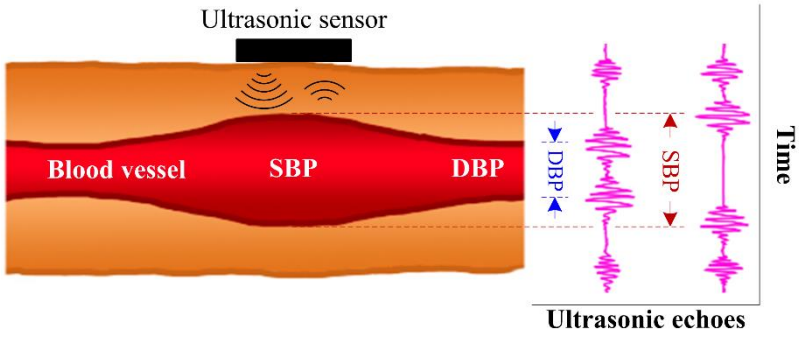

Fig. 2.6 Ultrasound mechanism in arterial distension detection

When a sound wave propagates through different mediums, an echo sound can be heard using a dedicated microphone. In biomedical engineering, the ultrasonic wave of at least 5 MHz is propagated through the human tissue where the echoes occur at the proximal and distal arterial wall of the blood vessel. This consequently generates two echoes which indicate the arterial diameter when the time delay is demodulated [89-91]. Incidentally, the arterial diameter changes depending on the blood pressure, reaching a maximum size due to SBP while reducing to the minimum diameter with DBP, respectively. In this manner, a calibration algorithm can be formed by investigating the relation between the arterial diameter and blood pressure, allowing the development of the ultrasound system into blood pressure measuring instruments [92-94]. The advantage of the ultrasound system is the direct arterial diameter acquisition which links to relative higher accuracy in blood pressure measurement since the cardiovascular parameters can directly be demodulated instead of relying on other the calibration of unavailable biological variables such as softness of skin tissue or blood density. However, biomedical ultrasound technology is currently expensive compared to other alternative blood pressure sensors, leading to high development cost and pricing. Also, recent research suggests that the ultrasound systems are still only capable of discrete blood pressure measurement. Regardless, their contribution to the biomedical engineering field will pave new concepts for future implementations.

2.2.5 Fiber optic sensors in blood pressure detection

In modern biomedical engineering, fiber optic sensors have been increasingly of interest due to the high sensitivity, compact sensor size, lightweight, and immunity to electromagnetic interference. Therefore, fiber optic sensors have been investigated and developed as arterial pulse wave monitoring instruments and consequently blood pressure measuring system [95]. In this aspect, several types of fiber optic sensors are introduced in recent blood pressure applications, with examples shown in Fig. 2.7.

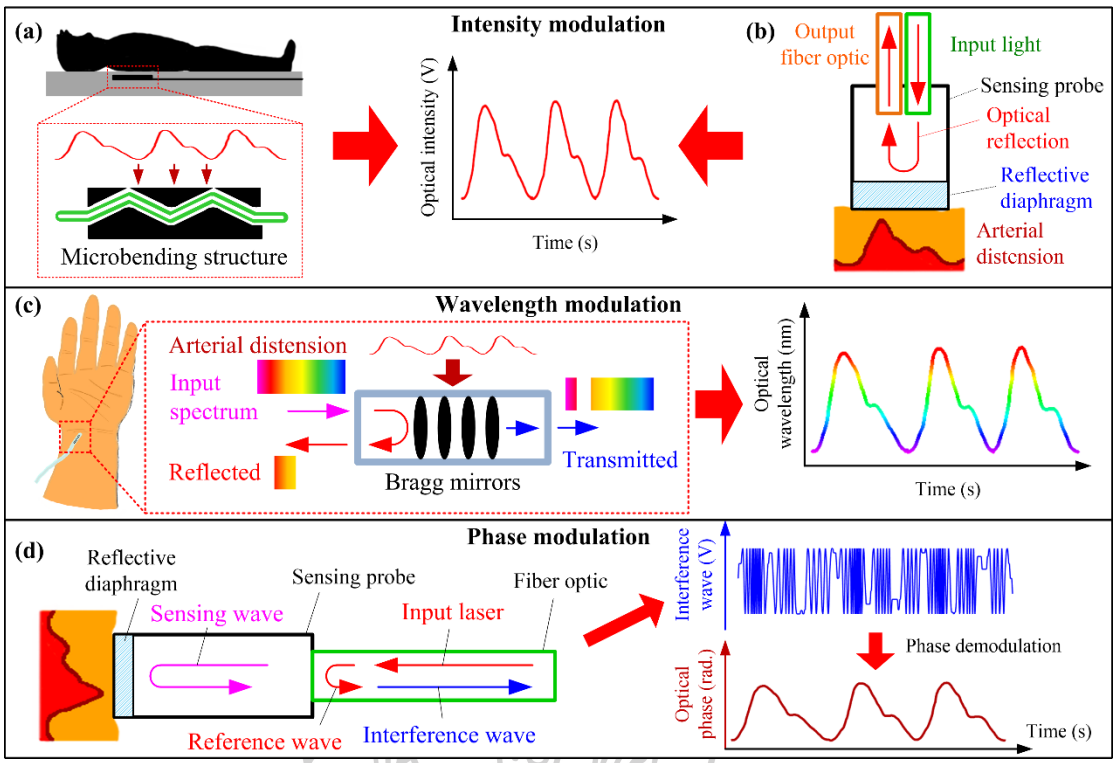

Fig. 2.7 Types of fiber optic sensors in pulse wave monitoring applications: (a) fiber microbending structure, (b) reflection-based fiber optic intensity probe, (c) fiber Bragg grating element for optical wavelength modulation, and (d) fiber optic interferometer for phase modulation

Generally, there are three main pulse sensing mechanisms for any fiber optic sensors: intensity, wavelength, and phase modulation. All of these modulations are, however, similar in pulse wave acquisition, i.e., the fiber optic sensor is modulated through physical interactions with arterial distension on the human skin. Regardless, the intensity-type fiber optic sensors primarily modulate the optical intensity according to the arterial pulse wave, either by using a fiber bending structure (in Fig. 2.7(a)) or reflective configuration scheme (Fig. 2.7(b)). The former structure is, particularly, designed for the fiber element to be bent by the arterial distension, which modulates the internal optical propagation in response to the pulse wave. In this approach, the fiber bending sensor is placed over the human skin where sufficient distension can be detected for the pulse wave monitoring [96-98]. To optimally construct a fiber bending sensor, plastic fiber optic element is generally exploited for high bending tolerance. However, plastic fiber has increased optical propagation loss compared to traditional silica fiber optics. Meanwhile, reflection-based fiber optic sensors utilize a reflective surface (generally a deflectable diaphragm) constructed on a cavity for pulse wave

detection. With this setup, the reflective surface is placed over the area of arterial distension, and the optical intensity is modulated by the displacement resulting from the pulse wave [99]. This configuration is often deployed using dual fiber-end propagation design or a single fiber optic mode for an incoherent light source system [100]. Nevertheless, the main advantage of all intensity-based fiber optic sensors is the relatively inexpensive development cost. This is due to the principal equipment required for the modulation process of a light source, photodetector, and waveform monitor. Regardless, the sensitivity and overall performance of this fiber optic sensor type depends on the optical modulation components, environmental effects, and responsiveness of the employed system.

On the other hand, wavelength modulation fiber optic sensors are generally constructed using fiber Bragg grating (FBG) elements as displayed in Fig. 2.7(c). This optical element, specifically, modulates the propagating wavelength when the Bragg mirror is induced by strain or temperature. Thus, FBG sensors have been applied for pulse wave sensing through placement on the arterial site while using a wavemeter or optical spectrum analyzer (OSA) to measure the modulated wavelength [101-105]. Since each FBG element modulates wavelength at different ranges, multiple sensing elements can be constructed on a single fiber optic to develop a distributed sensing system for simultaneous vital signs monitoring on multiple patients [106, 107]. Moreover, wavelength-type fiber optic sensors have been reported for higher sensitivity than the intensity-type; thereby, able to detect smaller pulse signal [52, 53, 108]. Still, the most prominent limitation of the wavelength fiber optic sensor is the expensiveness of the wavelength analyzer, increasing the development cost.

Phase modulation fiber optic sensors or fiber optic interferometers, otherwise, concerns the modulation of optical phase due to the arterial distension. In Fig. 2.7(d), a fiber optic Fabry-Perot interferometer (FFPI) is exemplified as one of the fiber interferometers investigated for arterial pulse wave monitoring, which shall be explained in a later section for in-depth details. Here, a fiber optic is configured similarly to the reflective intensity type yet differs in optical modulation. Particularly, a portion of an input laser is internally reflected inside the fiber as a "*reference wave*" while the rest is incident on a reflective thin film before coupling back into the fiber-end as a "*sensing wave*". Thus, the two light waves superposition within the fiber optic, forming an "*interference wave*" with its pattern determined by the phase shift caused by the displacement of the diaphragm [109]. Through the analysis of the interference wave, a corresponding displacement information associated with the arterial pulse can be acquired [110-112]. While the FFPI is described as an example, other fiber optic interferometers such as a Michelson or Mach-Zehnder interferometers can also be developed

according to the optimization, signal extraction, and sensor design [113-115]. Regardless, fiber optic interferometers require photodetector and waveform monitor as the minimal system requirement, consequently offering inexpensive development price. In addition, interferometers generally provide high sensitivity in measurement from the optical phase modulation, which also causes less amplitude-based signal noise owing to the frequency modulation technique of the phase parameters. Nevertheless, the output interference wave is a non-linear parameter that requires more complex demodulation techniques such as fringe counting, phase tracking, phase-shift demodulation, etc. Thus, a dedicated demodulation system is generally developed to enable automatic pulse wave monitoring applications.

Overall, fiber optic sensors for arterial pulse wave monitoring have higher development cost and higher sensitivity than electronic sensors. However, the exploitation of light as the interrogating medium provides several advantages in specific biomedical situation. For example, light wave is insensitive to electromagnetic interference, thus fiber optic sensors can be operated in strong magnetic zones such as during magnetic resonance imaging (MRI) examination where electronic sensors are prone to malfunction or destruction [105]. Furthermore, fiber optic sensors can be developed as distributed sensing systems for simultaneously monitoring multiple health parameters on different locations [106, 107]. In contrast, the drawbacks of fiber optic sensors are generally the high complexity in signal analysis and high equipment cost compared to electronic sensor systems. Nonetheless, novel biomedical engineering applications have continuously been investigated using fiber optic sensors, which will eventually lead to the emergence of state-of-the-art blood pressure measuring instruments.

2.3 FIBER OPTIC FABRY-PEROT INTERFEROMETER

A fiber optic Fabry-Perot interferometer (FFPI) is a type of fiber optic sensor configured by optical fiber elements to perform interferometry for measurement of a parameter of interest, such as displacement, vibration, material deflection, etc. This fiber optic sensor is, particularly, comprised of a laser source as a light source, optical fibers to construct a propagation system, and a photodetector for observing the output from sensing, with the components configured similar to Fig. 2.8.

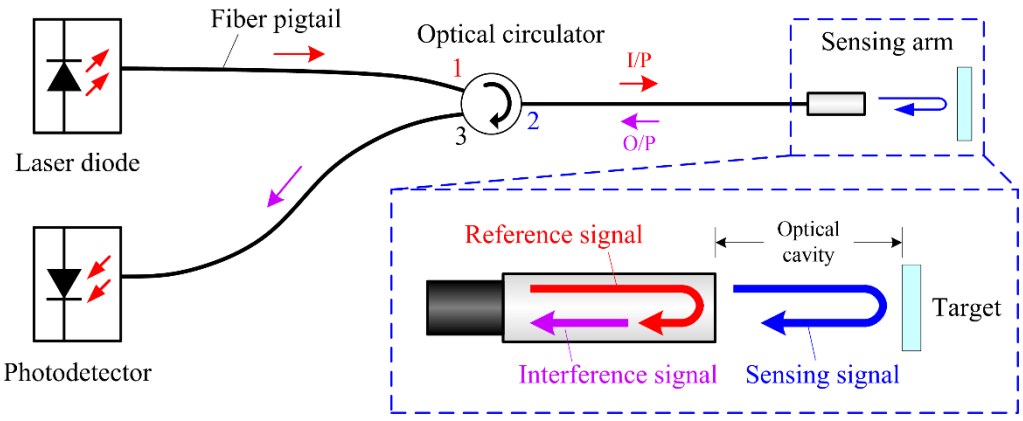

Fig. 2.8 Configuration of a fiber optic Fabry-Perot interferometer

A monochromatic light, generated by the laser diode, propagates through a fiber pigtail to an optical circulator, which guides the incoming light to a sensing arm. At the end of the sensing arm, approximately 4% of the light is internally reflected as a "*reference signal*" while the rest is ejected to be incident on a target of interrogation. The ejected light is then coupled into the sensing arm as a "*sensing signal*" and consequently superposition with the reference wave into an "*interference signal*". The latter wave subsequently propagates to the optical circulator and is ultimately sent to a photodetector, converting the optical parameter into an electrical signal for analysis.

This principle of operation allows an FFPI to detect physical parameters of interest (displacement, deflection, vibration, etc.). through observation of the output intensity of the interference signal (I) which can be mathematically explained by [109, 116]:

$$I = I_r + I_s + \sqrt{2I_r I_s}\cos(\varphi) \tag{2.2}$$

where I_r and I_s are the intensity of the reference and sensing signals, respectively, while φ is the optical phase as a function of the parameters within the optical cavity which can be calculated using [116, 117]:

$$\varphi = \frac{2\pi}{\lambda} 2nN_{\text{cavity}}d \tag{2.3}$$

where λ as the optical wavelength of the propagating light, n the refractive index of the cavity medium, N_{cavity} the number of optical reflections occurred inside the optical cavity, and d the optical cavity length. Therefore, the output interference wave corresponds to either the optical wavelength, refractive index, or optical cavity modulated during a measurement.

In particular, any modulation to these parameters will cause the interference wave to behave as a series of cosinusoidal wave pattern, as exemplified in Fig. 2.9.

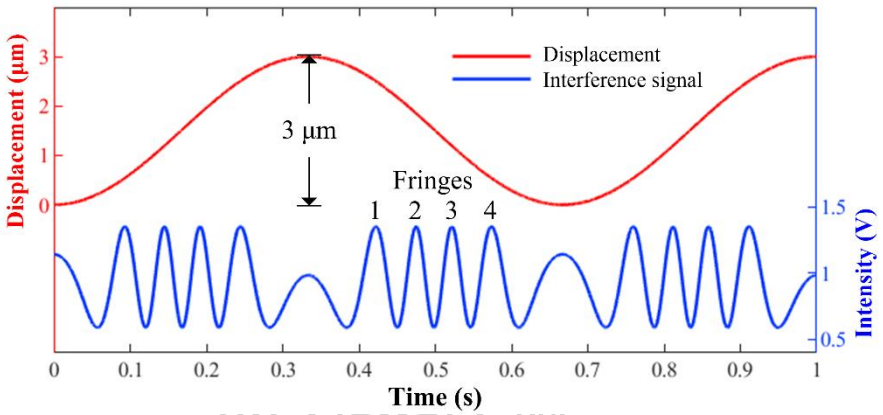

Fig. 2.9 Example of interference signal generated as a function of displacement

From the figure, an induced displacement to a target of interest leads to the generation of the interference waves with each complete cosinusoidal wave referred to as "*fringes*". To demodulate the displacement, a fringe counting technique is primarily deployed to measure the displacement (length alteration: Δd) by counting the number of fringes (N_{fringes}) before any directional changes and apply to the following [109, 117]:

$$\Delta d = N_{\text{fringes}} \frac{\lambda}{2nN_{\text{cavity}}} \tag{2.4}$$

With the fringe counting technique, the displacement of the target resulting from its movement or vibration can be measured. For example, Fig. 2.9 shows an excited 3 μm of displacement, generating 4 fringes during the displacement incline and decline. Assuming the optical wavelength is 1310 nm with a refractive index of 1, the measured displacement becomes 2.620 μm. Therefore, an FFPI can be applied to measure the displacement of a target and other associated physical parameters such as vibration, movement, and arterial distension in humans.

2.4 PHASE-SHIFT DEMODULATION FOR RESOLUTION IMPROVEMENT

As mentioned in the previous section, an FFPI can measure the target displacement using the fringe counting technique for preliminary investigation. The method, specifically, is easy to perform which leads to quick analysis of the displacement information. However, the

fringe counting technique has two major drawbacks: precision and instantaneous directional indication during real-time measurement.

The former drawback is the result of the fringe recognition during the measurement, as it is possible to underestimate or overestimate the number of fringes due to its fractured formation (sometimes referred to as fringe fractures). This means that the precision of a given FFPI using the fringe counting technique would be dependent on the input optical wavelength, refractive index, and number of reflections within the optical cavity. The precision, consequently, affects the resolution and accuracy of the fiber optic sensor by the equivalent amount of $\pm\lambda/2nN_{\text{cavity}}$. Still, the precision of the fringe counting technique can be improved by increasing the refractive index, the number of cavity reflections, or by implementing a zero-crossing fringe counting technique. One example is a modified zero-crossing fringe counting technique which counts additional fringe characteristics such as the troughs, rising, and falling slopes to increase the resolution [109]. By dividing the parameters to count from a single fringe, the resolution can be improved to $\lambda/64nN_{\text{cavity}}$ [118].

Regardless, the latter drawback of the fringe counting technique, the instantaneous directional information, can be considered a major limitation when applying the demodulation technique for continuous measurement. Preliminarily, the fringe counting technique offers relative ease in analysis based on human observations of the output interference signal. Yet, the direction of the observed displacement, vibration, or movement is not readily available to the analyzer, who opts to instead infer the direction by investigating the actual source or through another measuring instrument set up in parallel to an interrogating fiber optic sensor. Also, it is possible to reconstruct the directional information of an interrogated displacement using the fringe counting technique, albeit sufficient reference data should be provided in associated with a well-trained algorithm or human analyzer. This approach, while suitable within a laboratory setting, can nevertheless limits the application of an FFPI in real-world applications, where environmental effects and other uncertain factors can cause potential disturbance to the established analysis procedure. Thus, a continuous demodulation technique able to demodulate both the displacement and directional information from the FFPI signal should be implemented.

One of the demodulation techniques which overcome the aforementioned limitations is phase-shift demodulation, which relies on two interference signals with different optical phases between each other. In this case, the phase-shift demodulation and subsequent finding of the desired displacement can be exemplified in Fig. 2.10.

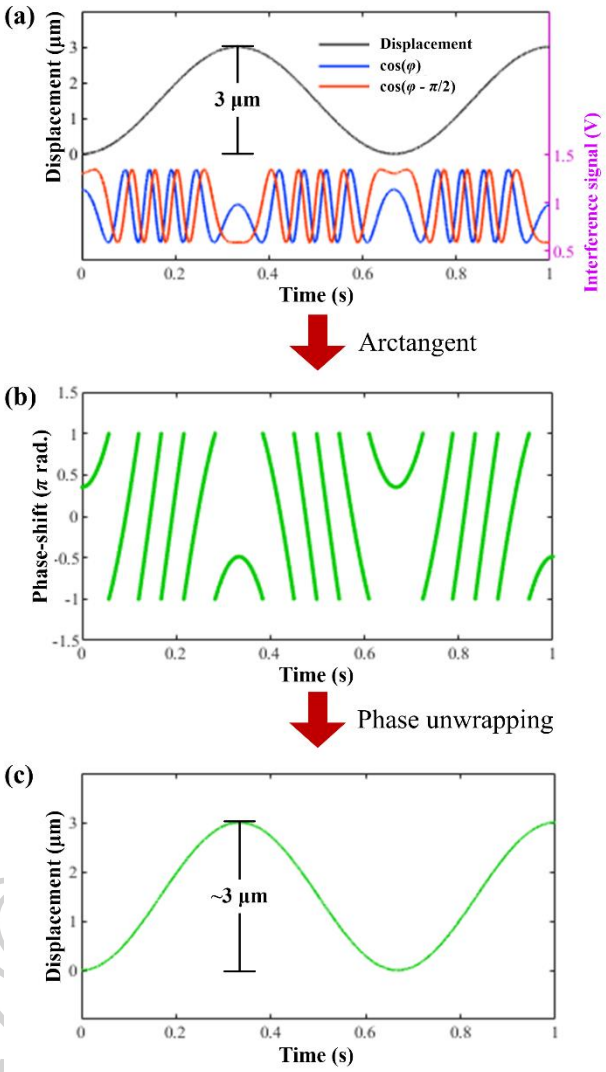

Fig. 2.10 Phase-shift demodulation process: (a) interrogating displacement and generated in-quadrature interference signals, (b) Demodulated phase-shift parameter using arctangent function, and (c) phase unwrapping and displacement demodulation

Differently from the fringe counting technique, phase-shift demodulation technique requires two interference signals with their wave phase shifted by $\pi/2$. When this phase parameter is carried out, the two signals are in quadrature to each other, with one behaving similarly to a cosinusoidal wave while another corresponds to a sinusoidal parameter (refer to Fig. 2.10(a)). This can, further, be explained in mathematical terms as follow:

$$I = I_r I_s + \sqrt{2 I_r I_s}\cos\left(\varphi + \frac{\pi}{2}\right) = I_r I_s + \sqrt{2 I_r I_s}\sin(\varphi) \tag{2.5}$$

To generate the in-quadrature interference signal pair, passive or active quadrature phase demodulation method can be configured. The former passive method is the generation of quadrature-shifted signals using physical configurations such as dual laser sources, dual cavity, birefringent crystals, and 2x2 fiber coupler-based configuration. Alternatively, the active quadrature phase demodulation method generally applies a common-path dual-wavelength fiber optic propagation system with a tunable laser source for generating a pair of in-quadrature signals. Regardless, both methods aim to create two in-quadrature interference signals for the demodulation [119].

Once the two in-quadrature interference signals are obtained, it is possible to retrieve the phase-shift information (φ) due to the target displacement using a trigonometric approach in contrast to the fringe counting technique. To ensure the output is correctly demodulated, the signals are firstly normalized to remove the amplitude and offset bias, resulting in the expressions [120, 121]:

$$I_{\cos} = \cos(\varphi) \tag{2.6}$$

$$I_{\sin} = \sin(\varphi) \tag{2.7}$$

Afterwards, the φ of the aforementioned normalized signals can be successfully acquired by applying an arctangent function using [119-121]:

$$\varphi = \tan\left(\frac{\sin(\varphi)}{\cos(\varphi)}\right)^{-1} \tag{2.8}$$

Theoretically, the above calculation should conclude the finding of the parameter. However, the resulting phase-shift information will be chipped from using the arctangent function (as shown in Fig. 2.10(b)). Therefore, a phase unwrapping process is initiated, basically connecting the chipped part of the phase-shift parameter into one coherent waveform. Ultimately, the displacement value can be calculated using the inverse of (2.4), which can be rewritten into:

$$d = \frac{\varphi\lambda}{4\pi n N_{\text{cavity}}} \tag{2.9}$$

At this point, both the displacement direction and value are readily available to the analyzer, provided that a dedicated computational system has been prepared for the

measurement (as in Fig. 2.10(c)). The apparent advantage of the phase-shift demodulation technique over the fringe counting technique is firstly the higher precision in demodulation, which is not limited by the number of fringes. Secondly, phase-shift demodulation allows for automatic displacement demodulation, a very useful advantage for continuous monitoring instruments in real-world applications. However, any fiber optic sensors implementing the phase-shift demodulation technique will require high performance and more sophisticated optoelectronics and computational components. Still, this demodulation technique contributes to fast continuous acquisition of the displacement information, especially for an FFPI-based blood pressure monitoring system in biomedical engineering applications.

2.5 THEORY OF THIN FILM DEFLECTION

As explained in the previous section, a FFPI can measure displacement by propagating light onto a target of interest before coupling the optical wave back into the optical fiber. Consequently, a reflective surface is required for the coupling of the sensing wave and the employed material should accommodate for the placement onto the interrogating target. In the case of blood pressure measurement, this scheme can be achieved by deploying a reflective thin film which deflected in response to the inducing pressure of the artery under human skin.

Particularly, the major arteries, namely the radial and carotid arteries underneath the wrist and neck, respectively, distend with sufficient pressure through the skin layers which is sensitive via finger palpation and, to an extent, pressure sensors. This also means that a FFPI can sense the arterial distension proportional to the pulse pressure of the human subject, thus can be developed for blood pressure measurement. However, the FFPI is limited in the direct acquisition of the pulse pressure, albeit the limitation can be amended by applying a thin film deflection technique, which demodulates the measured displacement from the interferometer into the desired pressure parameters.

Here, Kirchhoff-Love's plate theory is investigated for the design of a pulse sensing probe for the FFPI. In broader perspective, the inducing pressure onto a plate (or a reflective thin film) will cause the latter material to deflect in direct proportion as illustrated in Fig. 2.11.

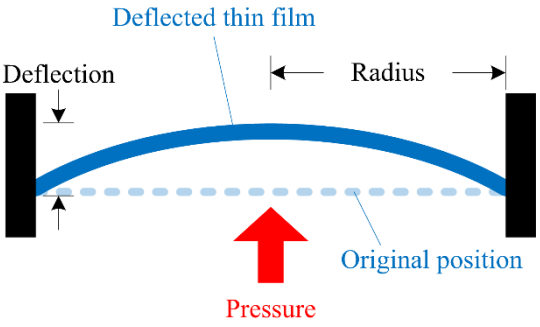

Fig. 2.11 Thin film deflection from inducing pressure

From the aforementioned figure, the thin film clamped on each end will deflect when induced by pressure. Assuming this thin film is a circular plate, the Kirchhoff-Love's plate theory shall apply the deflection-pressure relation for a clamped-edge circular diaphragm as depicted by [122-125]:

$$P = \frac{16E_{\text{film}}h_{\text{film}}^{3}\Delta d}{3r_{\text{film}}^{4}(1-\upsilon^{2})} \tag{2.10}$$

where P is the inducing pressure, Δd the deflection (synonymous with displacement), while E_{film}, h_{film}, r_{film}, and υ relates to the material properties of the thin film that is elastic modulus, thickness, deflection radius, and Poisson's ratio, respectively. Consequently, this technique can be applied to demodulate the pressure acted upon a thin film once the material properties of the film have been characterized.

2.6 PULSE TRANSIT TIME AND PULSE WAVE VELOCITY

While the aforementioned thin film deflection technique can lead to arterial distension detection, the technique is limited to only measuring the amplitude of the arterial pulse wave, namely PP. However, the blood pressure parameters of interest in modern medicine are SBP and DBP. Thus, additional blood pressure demodulation technique is encouraged to allow a measuring instrument to obtain the desired parameters. One such technique is the measurement of pulse wave velocity (PWV).

Since the heart periodically propagates blood in a rhythmic fashion, two different places of the same artery will experience arterial distension at different times. For example, the arterial distension on the forearm will firstly be sensed before the distension at the wrist. The time delay between these distensions is, consequently, termed "*pulse transit time* (PTT)" and exemplified in Fig. 2.12.

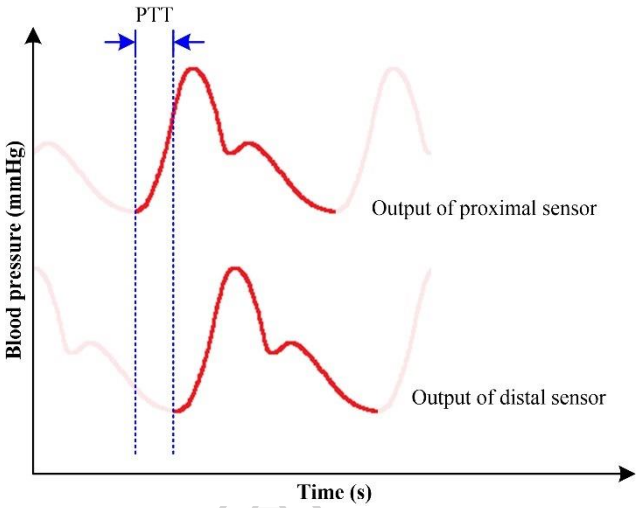

Fig. 2.12 Concept of pulse transit time

Generally, the PTT measurements will specify the point of reference for the determination using the characteristics of the arterial pulse wave, such as the end-diastolic points or the systolic peaks. Nonetheless, the point of reference is selected based on the sensor developer, since any pulse characteristics can be interchangeable without significantly altering the measurement results. Regardless, the PTT is associated with PWV as described in [126]:

$$\text{PWV} = \frac{L}{\text{PTT}} \tag{2.11}$$

where L is the length between two arterial sites. Consequently, PWV is related to blood pressure as explained using the Bramwell-Hill equation of [127, 128]:

$$\text{PWV} = \sqrt{\frac{V\Delta P}{\rho \Delta V}} \tag{2.12}$$

when V represents the blood volume, ΔP and ΔV is the differential in blood pressure and blood volume, respectively, while ρ depicts the blood density. The Bramwell-Hill equation basically links the relationship between the PWV and blood pressure through the alteration of blood volume within a given artery. Alternatively, the Moens-Korteweg and Hughes equations describe the PWV as a parameter affected by the arterial elasticity at zero pressure (E_0), arterial wall thickness (h_{artery}), radius (r_{artery}), and vessel coefficient (γ), as subsequently expressed in [126-128]:

$$\text{PWV} = \sqrt{\frac{E_0 e^{\left(\gamma h_{\text{artery}} P\right)}}{2\rho r_{\text{artery}}}} \tag{2.13}$$

While the aforementioned equations mathematically describe the relationship between PWV and blood pressure, several parameters associated with bodily components might not be measurable in a non-invasive way (such as arterial thickness and radius). Still, these equations hold significant in non-invasive continuous blood pressure demodulation in the development of novel blood pressure measuring devices. Therefore, a compromise has been introduced by characterizing the unknown variables using an available standard blood pressure device. This approach is referred to as "*calibration*" of the proposed continuous blood pressure measuring instrument, which ultimately enable the instrument to perform the measurement based on pseudo cardiovascular parameters obtained through empirical studies or the interrogating subjects for rapid operations [23, 128].

2.7 CHARACTERISTICS OF MEASURING INSTRUMENTS

The purpose of a measuring instrument is to quantify a parameter of interest such as electrical voltage, displacement, liquid volume, etc. However, the acquired value from the instrument will always have errors in measurement, owing to environmental effects, device limitations, or other undeterminable factors. Thus, it is imperative to characterize the performance of the measuring instrument to ensure desirable output during measurement. Generally, four parameters are analyzed in the characterization process: accuracy, sensitivity, precision, and resolution.

2.7.1 Accuracy

It is the degree of closeness between the measured value and the actual quantity which can commonly be evaluated by calculating the measurement error [129, 130]. In this case, the error (ε) in each measurement is the subtraction of the two aforementioned values as expressed by:

$$\varepsilon = \chi_m - \chi_t \tag{2.14}$$

with χ_m as the data obtained by the interrogating instrument, whereas χ_t is the data of the reference device. From (2.14), the calculated error depicts a true difference between the reference and measured data, leading to the estimation of bias in the interrogating instrument.

Still, the absolute error (AE) can be alternatively considered to establish the accuracy range in measurement, as calculated using[131]:

$$\mathrm{AE} = |\chi_m - \chi_t| \tag{2.15}$$

In addition, error percentage (%ε) can also be calculated to assess the uncertainty factor relative to the measured value in the following:

$$\%\varepsilon = \left|\frac{\chi_m - \chi_t}{\chi_t}\right| \tag{2.16}$$

The aforementioned equation is useful when preliminarily evaluating the relative accuracy of a measuring device. Nevertheless, the instrument under validation will generally be required to perform several repeatable measurements to statistically determine its specifications. Therefore, the mean absolute error (MAE) is considered using the following expression:

$$\mathrm{MAE} = \frac{\sum_{t=1}^{N_{\mathrm{sample}}} (\mathrm{AE}_t)}{N_{\mathrm{sample}}} \tag{2.17}$$

where the notation t denotes the sample number (t = 1, 2, 3, …, N_{sample}) and N_{sample} depicts the total number of measurement data. Note that the mean absolute error percentage (MAE%) can also be found by substituting AE_t in (2.17) with %ε of each measurement. The latter is also of significance when analyzing the accuracy of the instrument as follows:

$$\mathrm{Accuracy} = 100\% - \mathrm{MAE}\% \tag{2.18}$$

In the engineering field, a confidence of 95% in accuracy is widely adopted, which means the percentage error should not be more than 5% [132, 133]. Note that these numbers might change depending on the research discipline and area of applications (in biomedicine, construction, business evaluation, etc.), albeit the aforementioned values serve as preliminary criteria during investigations.

2.7.2 Sensitivity

On the other hand, sensitivity defines the ratio of output parameter (χ_{out}) to input quantity (χ_{in}). In most cases, the latter two values are incidentally linearly proportional, thereby the term "*linearity*" might be synonymous. As such, the sensitivity in measurement of a given machine can be characterized by considering the linear slope between the output-input relation or by using the following mathematical expression:

$$\text{Sensitivity} = \frac{\chi_{\text{out}}}{\chi_{\text{in}}} \tag{2.19}$$

In the case of non-linear relation between the output and input, an area depicting a linear trend will commonly be determined, and subsequent operational limits or thresholds are proposed. This, ultimately, compensates for the non-linear problem by introducing a working range which guarantees the linearity of the instrument. Furthermore, devices with higher sensitivity are, in general, more discriminating towards small variations, leading to measurements of smaller parameters (e.g., in the micro- or nanometric scale).

2.7.3 Precision

This parameter depicts the random errors occurring within a repeatable test environment. Differently from accuracy, precision does not intrinsically determine the closeness to truth but rather the closeness between each measured value [130]. It is consequently practical for characterizing the repeatability of the measurement and by extension the reliability of the measuring device [134]. In general, precision of an interrogating instrument can be revealed through calculation of the standard deviation (SD) of a dataset using:

$$\text{SD} = \sqrt{\frac{\sum_{t=1}^{N_{\text{sample}}} (\text{AE}_t - \text{MAE})^2}{(N_{\text{sample}} - 1)}} \tag{2.20}$$

In this approach, it is simple to characterize the precision from multiple discrete measurements. However, the method could prove difficult when characterizing a dynamic measurement system such as displacement monitoring since both the vibration and signal noise contribute to the SD. To compensate, a power spectral density approach can be applied to only extract the signal noise for precision characterization.

Power spectral density (PSD) is the distribution of signal power observed in frequency domain, useful for investigating a dynamic alteration such as vibration waves [135]. In basic terms, PSD is the square of a fast Fourier transform (FFT) of an input signal. This parameter is of interest in vibration measurement as the frequency information in each range can be retrieved and subsequently analyzed from a single source. Particularly, the output of the PSD enables the precision characterization of dynamic measured signal. For the sake of simplicity, the mathematical expression of the FFT and PSD is not entirely described in this section. Their applications are, however, elaborated to demonstrate the precision characterization.

Assuming that a mathematical simulation software (e.g., MATLAB) has a dedicated FFT function, the following shall assume the time-to-frequency conversion as a black box. Therefore, the PSD, an extension of the FFT, can be determined using:

$$\mathrm{PSD} = \frac{\mathrm{FFT}^2}{f_{\mathrm{sample}} \times N_{\mathrm{sample}}} \tag{2.21}$$

where f_{sample} is the sampling frequency of the measurement. Note that the FFT operation has multiplied the positive and negative sets of frequencies by a factor of two without accounting for the zero and Nyquist limits. This mentioned process is incidentally excluded when exploiting the FFT function, thus it must be manually programmed beforehand. Regardless, the PSD found after this operation will reveal the frequencies of various sinusoidal waves comprising the original input signal. Should a frequency corresponding to the intended vibration be removed at this point, only the signal noise will remain to be subsequently analyzed, which can be mathematically represented by:

$$\mathrm{PSD}_{\mathrm{noise}} = \int_{t=1}^{f_{\mathrm{original}}-Bin} (\mathrm{PSD}\ dt) + \int_{t=1}^{f_{\mathrm{original}}+Bin} (\mathrm{PSD}\ dt) \tag{2.22}$$

with $\mathrm{PSD}_{\mathrm{noise}}$ as the PSD of the signal noise excluding any signal in the frequency of f_{original} while Bin corresponds to the bin width calculated using:

$$Bin = \frac{f_{\mathrm{sample}}}{N_{\mathrm{sample}}} \tag{2.23}$$

In real-world experiments, utilization of a mechanical vibrator inducing a fixed frequency will be effective in the precision characterization. Afterwards, the root mean

square (RMS) of the signal noise PSD is calculated to find the precision parameter, as follows:

$$\mathrm{RMS} = \sqrt{\sum_{t=1}^{f_{\mathrm{Nyquist}}} (\mathrm{PSD}_{\mathrm{noise}}) \times Bin} \tag{2.24}$$

where t in this case depicts the frequency of interest (t = 1, 2, 3, …, f_{Nyquist}) whereas f_{Nyquist} is the Nyquist frequency or the maximum frequency to be interrogated from the PSD. To further clarify the aforementioned applications of the PSD, Fig. 2.13 illustrates the input signal, perturbing random noise, and their PSD profiles.

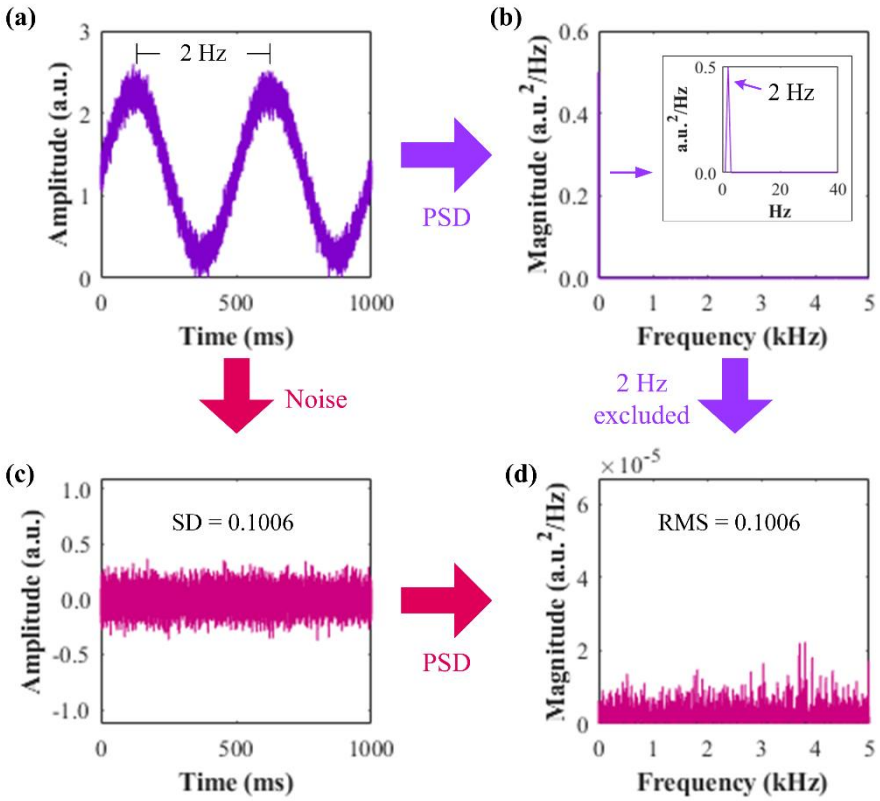

Fig. 2.13 Power spectral density in precision characterization:
(a) the original vibration signal with (b) power spectral density perturbed by signal noise in (c) time-domain and (d) frequency-domain

In Fig. 2.13(a), a vibration signal consisting of 2 Hz primary frequency and random noise is displayed while its PSD profile shown in Fig. 2.13(b) displays a distinct magnitude at 2 Hz region. Meanwhile, the signal noise that is the main cause of random error is illustrated in Fig. 2.13(c) with an SD of 0.1006. Incidentally, its power distribution profile

is almost identical to the PSD of the original signal subtracted by the 2 Hz frequency. The RMS of the latter is, moreover, equal to 0.1006, equivalent to the SD of the signal noise, as seen in Fig. 2.13(d). Therefore, the precision of dynamic vibrations can be characterized through the PSD approach.

2.7.4 Resolution

Ultimately, a measuring instrument applied for any measurement has a limit in displaying the results, such as in integer or several decimals depending on the design. This limit is, consequently, referred to as resolution which is related to the accuracy and precision of the instrument. Particularly, the higher the resolution, the smaller the discrepancy between two different measurements, thus the closer the reading will be to the true parameters. In addition, smaller discrepancies allow more repeatable results when performing several measurements of the same measurand.

To define the resolution of the instrument, the smallest discrepancy between two different measurements is the primary parameter of interest. In this case, the resolution becomes higher inversely to the smaller discrepancy found between the two measurements. For example, a ruler with 1 cm scale will have less resolution than a ruler with 1 mm line gauge. The former is, thus, less accurate and precise to measure a length of 1.2 mm. In contrast, the latter 1 mm ruler will be more suitable due to the smaller discrepancy between its line gauges. Still, electronic-based instruments are less restricted by the physical limits of the ruler, instead able to display the measurement results in several decimals. In this case, the resolution can be defined by investigating the precision of the instrument. Specifically, the random error, characterized as the precision, becomes the smallest discrepancy for indicating two different values, thereby serving as the resolution in measurement.

2.8 VALIDATION PROTOCOL OF A BLOOD PRESSURE MEASURING DEVICE

Blood pressure measuring instruments are essential biomedical tools for diagnosing not only hypertension and blood pressure-related issues but also the overall health conditions of patients. Therefore, it is imperative to ensure the performance of the instruments for prevention of erroneous measurements that might lead to mortality due to device failure or improper functionality. Here, the accuracy of the blood pressure measuring devices is the foremost parameter to consider, as inaccurate measurement results can significantly alter the diagnosis of hypertension. Thus, a validation protocol of a blood pressure measuring device is explained in this section.

After the emergence and adoption of blood pressure instruments in biomedical applications, validation protocols of such devices have been enacted to guarantee the reliability in operations. As such, the United States Association for the Advancement of Medical Instrumentation (AAMI) had introduced the first protocol for the development of accurate blood pressure measuring machines in 1987. Afterwards, the British Hypertension Society (BHS), German Hypertension League, European Society of Hypertension (ESH), and the International Organization for Standardization (ISO) had published their own protocol in 1990, 1999, 2002, and 2009, respectively [131]. In recent years, the Institute of Electrical and Electronics Engineers (IEEE) and the World Health Organization (WHO) have also created standards of blood pressure instrumentation for modern biomedical engineering [136-138]. The widely cited protocol when developing a blood pressure instrument in the current biomedical engineering field is, however, the standard of the AAMI/ESH/ISO standard which basically combines the general criteria to validate a blood pressure measuring device.

The AAMI/ESH/ISO validation protocol concerns principally the development of a cuff-based digital sphygmomanometer, though the protocol can also serve as a standard for developing a continuous non-invasive instrument owing to the rigorously proposed criteria. In this protocol, at least 85 human volunteers of any sex and from 18 years old onward must be included in the validation. A standard blood pressure measuring device must also be utilized as a reference, which might be an invasive arterial catheter or highly accurate non-invasive sphygmomanometer depending on the research objective. Mostly, the latter instrument is chosen for validating a novel device for potential commercialized applications. Regardless, a total of seven measurements must be performed using the reference and interrogating devices in sequential order in case both devices are to be applied on the same arm, as illustrated in Fig. 2.14.

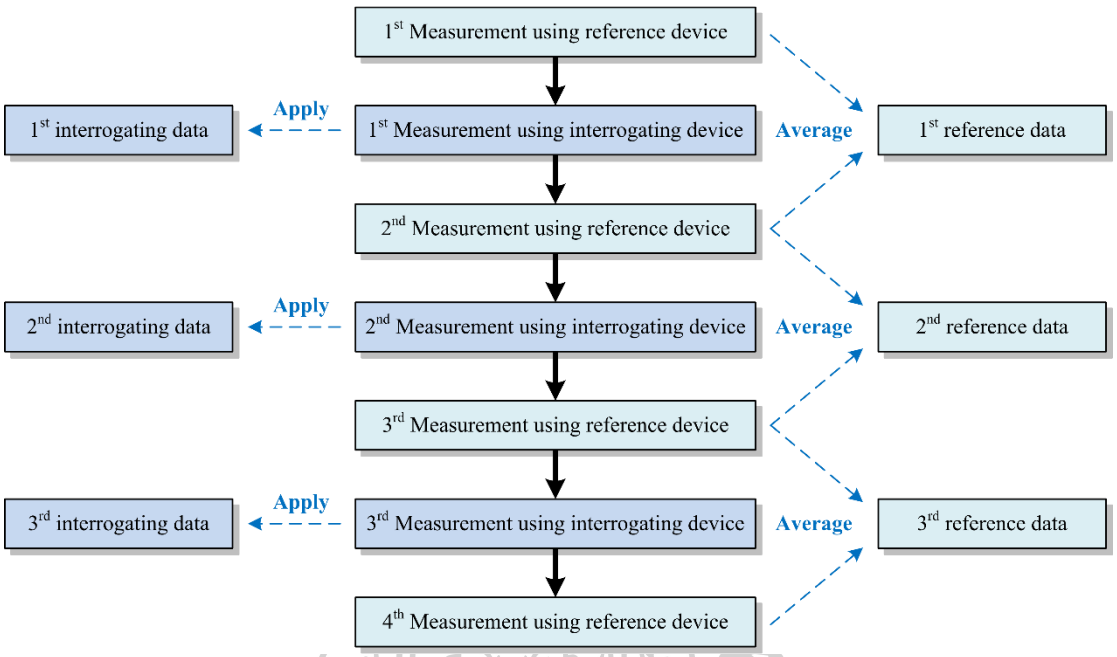

Fig. 2.14 Sequential validation procedure of blood pressure devices

Firstly, a reference blood pressure measuring device performs the measurement, followed by the instrument in interrogation within at most 1-2 minutes. This sequence is, subsequently, carried out for another two times before concluding with a fourth measurement using the reference device. To validate the results, the two reference measurement data between each operation of the interrogating instrument is averaged into three datasets. The datasets from the reference and interrogating devices are, thus, compared against each other to calculate the error or difference in blood pressure measurement. Note that the terms "*error*" and "*difference*" are interchangeable with the latter more mentioned in the biomedical field. In this dissertation, the term error will, however, be applied.

The parameters concerned by the AAMI/ESH/ISO standard is the measurement error of the interrogating blood pressure instrument and consequently its accuracy in operation. Initially, the AE is to be considered, which can be calculated using (2.15) and later be applied to find the MAE by exploiting (2.17). To further investigate the precision, and by extension its resolution, of the blood pressure instrument, its SD is also determined by using (2.20). The preliminary criterion for a passing blood pressure measuring instrument is that the MAE ± SD is less than 5 and 8 mmHg, respectively. This will imply that the interrogating instrument can be applied as a blood pressure measuring instrument in biomedical applications. Nevertheless, its accuracy grade is also suggested to further specify the dependability of the instrument in specialized settings such as in-depth cardiovascular investigation for grade A, medical

diagnosis for grade B, clinical usage for preliminary patient screening for grade C, and commercialized medical gadget for grade D, respectively. To implement this accuracy grading, Table 2.1 presents the criteria for the grading proposed by the AAMI/ESH/ISO standard.

Table 2.1 Accuracy grading criteria for a blood pressure measuring device

Grade	**Percentage of absolute error with difference ranges**		
	AE ≤ 5 mmHg	**AE ≤ 10 mmHg**	**AE ≤ 15 mmHg**
A	≥ 60%	≥ 80%	≥ 95%
B	≥ 50%	≥ 75%	≥ 90%
C	≥ 40%	≥ 65%	≥ 85%
D	Otherwise		

In order to achieve the accuracy grade A, the interrogating device must at the very least have AE of no more than 5 mmHg for 60% of the total measurement data, AE of no more than 10 mmHg for 80%, and AE of no more than 15 mmHg for 95%, respectively. All of these criteria must be true to obtain the accuracy grade A, otherwise the grading will follow from B to D. In this perspective, the expected accuracy grade of the interrogating instrument should be A or B, suggesting their high performance for cardiovascular investigation and health diagnosis applications. Devices in grade C might qualify as a sufficiently accurate blood pressure device, though it might serve as a preliminary patient screening tool. Grade D, however, implies that the interrogating device should be further developed before applying as a biomedical gadget for disease diagnosis.

2.9 LITERATURE REVIEWS OF FIBER OPTIC BLOOD PRESSURE INSTRUMENT

In recent years, fiber optic sensors have been of interest in the biomedical engineering field. For blood pressure measurement, the sensors are, particularly, investigated for the arterial pulse wave monitoring by exploiting the high sensitivity characteristics. The main idea is that arterial pulse wave relates to blood pressure, thus the fiber optic sensors have been rigorously researched in pursuit of the desired biomedical applications. Furthermore, additional cardiovascular studies have also been under consideration such as arterial stiffness identification, simultaneous patient inspection, operations in hazardous environment, etc. This section shall, consequently, review the literature involving the development of fiber optic sensors in blood pressure-related applications.

C. Leitão *et al.* [48] have investigated the technical feasibility of fiber optic sensors for arterial pulse wave monitoring in humans. Particularly, the carotid pulse wave is desirable in arterial stiffness identification since the parameter can lead to the diagnosis of cardiovascular health. Firstly, the researchers have designed a fiber Bragg grating (FBG) sensing probe which applies the wavelength modulation scheme to extract the pulse information via contact on the neck [48]. After a small human trial of 4 volunteers, it was revealed that the fiber optic sensor can detect important pulse wave characteristics during the examination. The obtained pulse waves were, then, analyzed to provide arterial augmentation index of -0.28 to 0.04. Moreover, a root mean square deviation (RMSD) of 0.53 was found from five days of repeatable testing, implying the promising results of using the FBG sensor for carotid pulse wave detection.

Afterwards, the researchers have investigated an intensity-based fiber optic sensor using plastic fiber element instead of the FBG type [100]. In this configuration, the plastic fiber optic was chosen for its relatively cheap price, which contributed to lower development cost. Also, the signal processing is less complicated than the wavelength-based FBG sensors due to the intensity modulation scheme using conventional electrical waveform analysis approach. The proposed fiber optic sensor was, consequently, investigated for carotid pulse wave monitoring, which was validated to have a sensitivity of 727 μV/μm and a resolution of 0.1 μm. This sensitivity was, then, concluded suitable for carotid pulse wave monitoring.

By further developing both the FBG and intensity-based fiber optic sensors, C. Leitão *et al.* [53] have, subsequently, performed a feasibility analysis of both instruments. Primarily, the work compared the sensitivity and resolution of the sensors, which were 21.2 pm/μm and 20 nm, respectively, for the FBG sensor. Meanwhile, the plastic intensity fiber optic sensor exhibited a sensitivity of 727.2 μV/μm and resolution of 50 nm. While the sensitivity unit between the two fiber optic sensors were different, the main consideration was the resolution for its importance in detecting small changes in arterial pulse wave amplitude. In this case, the FBG sensor had higher performance in terms of resolution. However, the plastic fiber optic sensor reportedly expended less development cost due to the materials and required equipment in operation. Consequently, the arterial distension, as described in a pathological case, can be from a few micrometers to a maximum of 700 μm, which means that both fiber optic sensors had sufficient resolution to detect the cardiovascular parameter. In conclusion, the plastic fiber optic sensor was selected for further development into a practical biomedical machine owing to the cheaper cost.

Ultimately, C. Leitão *et al.* [139] have developed a plastic fiber optic-based carotid pulse wave monitoring system for clinical validation in human participants. Specifically, a

total of 118 patients were enrolled to have their blood pressure measured by the novel fiber optic sensor and also a reference invasive pulse wave monitoring device. The investigation had, moreover, aimed to interrogate the correlation factors found by measuring the augmentation index and central SBP. From the experiment, the reference instrument had the correlation coefficients for the augmentation index of 0.79 with the central SBP correlation of 0.94. On the other hand, the proposed fiber optic sensor yielded 0.91 and 0.98 of the augmentation indices and central SBP correlation coefficients, respectively. The results have, thereby, shown that the fiber optic sensor has high correlation with the reference device, and would be appropriate for developing a novel central blood pressure measuring instrument in the future.

Still, the FBG sensor type has been applied in other aspects aside from the carotid pulse wave monitoring. Mainly, the sensing mechanism of the fiber optic sensor allows for new designs of a pulse detecting scheme. For instance, N. V. Kumar *et al.* [101] introduced a radial pulse sensing probe comprising of three FBG elements which expanded the area of pulse detection when placed over the human wrist. A cantilever structure was, further, constructed to hold the fiber optic sensor for stability during an examination. An intermittent cuff-based blood pressure device was also employed to calibrate the fiber optic system to enable its blood pressure measuring algorithm. After carrying out an experiment on 35 volunteers, radial pulse waves could successively be obtained by the proposed FBG sensor. With the tolerance limit of <10 mmHg, the developed sensor additionally yielded an average accuracy in SBP and DBP measurement of 89.85% and 94.20%, respectively. This research ultimately concluded that the wavelength-based fiber optic sensor could accurately perform the blood pressure measurement with added benefits from compatibility with engineering application software for aiding in the pulse wave monitoring.

S. Pant *et al.* [108] otherwise developed a finger plethysmographic FBG sensor utilizing the high sensitivity of the optical element to acquire the pulse wave on a human finger. In particular, an FBG sensing element was sewed on a cylindrical finger cuff which would be worn on a finger to detect arterial distension. An interrogating unit was, then, deployed to acquire and analyze the modulated wavelength caused by the arterial pulse wave bending the FBG sensor. This research, consequently, performed experiments on human participants, where their pulse waves were retrieved and compared to a reference wrist-worn pulse sensor. The results showed a high correlation between the number of heart pulses measured using the FBG sensor and the reference with coefficient of correlation (R^2) of 0.97445. The obtained pulse waves could, further, be processed into first derivative values, increasing cardiovascular parameters to be applied for constructing a blood pressure

demodulation algorithm. Thus, the researchers concluded that the finger FBG sensor has the potential of becoming an emergency heart pulse measuring gadget or a clinical pulse wave monitoring device in the future.

D. Jia *et al.* [140], meanwhile, considered the application of an FBG-based radial pulse detection in Chinese medicine. In this case, a translational cantilever system was constructed to allow the pulse wave sensed at the wrist for acting on an FBG element. By placing a protruding fingertip of the cantilever on the area of pulse sensing, the arterial distension would displace the fingertip and intentionally pull the FBG element, inducing strain corresponding to the pulse strength. In this way, the system could achieve precise placement of the fingertip on the human wrist while able to adjust the pressing force required in Chinese medicine. Consequently, the three areas around the pulse site (namely "*Chun*", "*Chi*", and "*Guan*") could be accurately obtained using the fiber optic sensor. A sensitivity of 8.236 nm/N was also found, and a comparison to a reference electrical sensor showed high similarity in measured parameters such as pulse wave period and amplitude with the largest error of 0.008. This led to the conclusion that the FBG sensor could be applied in radial pulse monitoring and, by extension, Chinese medicine owing to high sensitivity and precise sensor placement.

R. B. Gowda *et al.* [141] likewise developed an FBG-based radial pulse sensor which was constructed using 3D printing technology. The sensor was designed to accommodate pulse detection at different positions and angles around the wrist. Later, the fiber optic instrument was verified through medical trials, and found that the detected pulse wave showed high fidelity during the operation. The instrument was also utilized by medical experts under diagnostic standards, leading to the conclusion that the proposed optical technology could be applied for physiological monitoring of radial pulse waves.

Z. Tang *et al.* [142] designed a hybrid force sensitive structure for a displacement FBG sensor. Specifically, an FBG element was implemented into an orthogonal planar spring which stretches the fiber optic sensor with incoming vibration such as arterial distension on the wrist. This consequently enables an effective displacement measurement using the FBG sensor with a force sensing resolution of 0.47 mN under 0.98% of error. Its dynamic range was, further, characterized to be 0.9-2.7 N while the sensitivity was observed at 0.103 μm. In addition, the pulse waves detected using this fiber optic prototype were highly precise, thereby suggesting the effectiveness of the FBG sensor for pulse wave monitoring in humans.

From the literature reviews, it can be discussed that fiber optic sensors, as well as ECG electrodes, electronic transducers, PPG sensors, and ultrasound systems, have been of interest in modern biomedical engineering [143]. This is, consequently, owing to the

emergence of home health monitoring concept where an individual can examine their own blood pressure value and take precautions for any possible health problems. Specifically, ECG, electronic transducers, and PPG sensors have primarily been developed as alternative blood pressure sensors, especially for integration into smart devices such as smartwatches. The mentioned sensors are also attractive due to relatively inexpensive cost and unobtrusive setup, elevating the development of novel commercial blood pressure instruments. Meanwhile, fiber optic sensors and ultrasound systems have been investigated for possible innovative biomedical machines for specialized cardiovascular health monitoring. For instance, fiber optic sensors can operate under strong magnetic field, which is preferable during MRI where conventional electronic-based sensors malfunction. Likewise, ultrasound system prompted direct arterial distension measurement, bypassing the calibration process to obtain an estimate of blood pressure parameters. Thus, the latter two sensors are generally concerned in the development of innovative biomedical instruments. Overall, blood pressure measuring devices will continue to be highly regarded in the upcoming future.

2.10 SUMMARY

In this chapter, the theories and principles involving arterial pulse wave detection and blood pressure measurement have been described to serve as a fundamental for developing a fiber optic sensor for biomedical applications. In addition, the details of modern blood pressure sensors and also literature reviews of various fiber optic instruments have been discussed. The contribution of the reviewed work is, subsequently, applied as an inspiration and case study during the development of a novel cardiovascular monitoring system. From this knowledge, this dissertation initiates the concept of a continuous non-invasive blood pressure measuring system based on a fiber optic Fabry-Perot interferometer (FFPI) which would have high performance and ease of operation as generally desired by peer literatures in recent years.

CHAPTER 3
EXPERIMENTAL SETUP

In this chapter, the fiber optic sensor system configuration for continuous blood pressure measurement is explained, along with the experimental setups to implement, investigate, and validate the performance of the fiber optic sensor in the biomedical application. During the course of this dissertation, several research regarding the development of the fiber optic system has been conducted, and thus this chapter shall organize the experimentations into three main phases: 1) the implementation of fiber optic Fabry-Perot interferometer (FFPI) for preliminary arterial pulse wave detection, 2) the improvement on the measurement resolution using a phase-shift demodulation technique, and 3) the validation of the developed FFPI system for continuous blood pressure measurement through human trial. The aforementioned research phases are, consequently, described in sequential order throughout this chapter.

3.1 FIBER OPTIC FABRY-PEROT INTERFEROMETER FOR ARTERIAL PULSE DETECTION

In the initial research phase, the implementation of a fiber optic Fabry-Perot interferometer (FFPI) for arterial pulse wave acquisition is investigated. Primarily, the objective is to develop a fiber optic sensor with a capability of sensing the arterial distension on the human skin, specifically on the wrist. This research, consequently, intends to clarify the capability of applying a fiber optic interferometric sensor for firstly obtaining arterial pulse waves which shall pave the way for future development into a full-fledged blood pressure measuring system. In this phase, the research mainly concerns the design of a fiber optic pulse sensing probe, the pulse wave sensing principle, its system configuration for an experiment on a mechanical vibrator for initial validation, and also the preliminary investigation of arterial pulse wave acquisition on a small group of human volunteers.

3.1.1 Fiber optic pulse sensing probe design

To construct a pulse wave sensing probe based on an FFPI principle, the design of the probe applies the thin film deflection technique previously described in Chapter 2.4. Basically, a thin film is placed on the end of the solid cylindrical structure with a fiber optic guiding element on the opposite side to initiate the FFPI sensing principle. The design of such probe is, moreover, illustrated in Fig. 3.1.

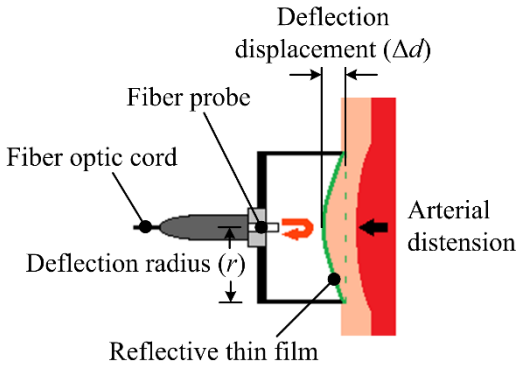

Fig. 3.1 Design of an FFPI-based pulse sensor probe

In particular, the FFPI pulse sensing probe is comprised of a solid cylindrical structure which is encased on one end with a reflective thin film (optically coated acrylic polyethylene terephthalate: PET), which will be placed above a radial arterial site or the wrist of a human. The other end of the sensing probe is, subsequently, connected to a fiber optic probe for propagating light from the FFPI system to incident on the reflective thin film. Afterwards, the arterial distension due to blood pressure will deflect the reflective thin film, causing displacement of the optical cavity, which ultimately leads to the generation of the interference signal to be later analyzed and demodulated. In this dissertation, the FFPI pulse sensing probe is intended to detect radial arterial distension on the human wrist. Thus, the probe will firstly be secured on the arterial site and subsequently detect the arterial pulse wave from the thin film deflection.

Before exploiting the FFPI sensing probe, the material properties of the PET reflective thin film are characterized using a universal tensile testing machine (*INSTRON 5969*). In this case, the reflective thin film is firstly encased within an adhesive material to prevent destruction during the investigation. Then, the ends of the film are gripped to the actuator of the machine which induce tension onto the material, as depicted in Fig. 3.2.

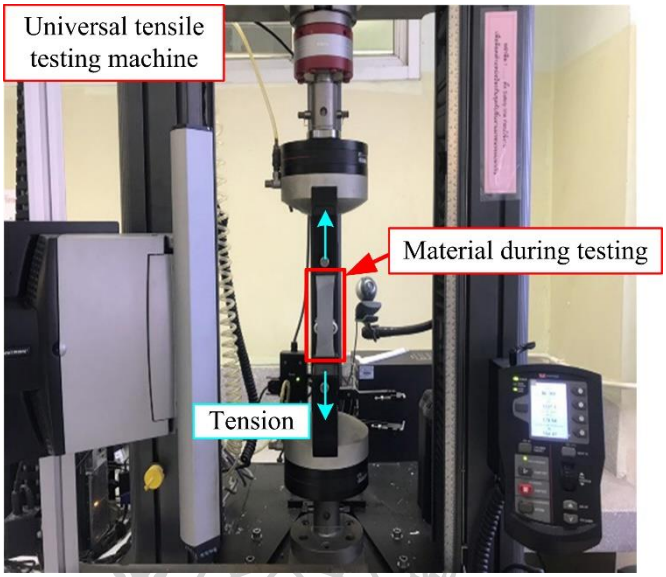

Fig. 3.2 Universal tensile testing for thin film characterization

Once the investigation is initiated, the universal tensile testing machine will stretch the reflective thin film at a certain speed until the material breaks. Afterwards, calculations of elastic modulus and Poisson's ratio can be performed along with the measurement of material thickness and deflection radius for the pressure demodulation according to (2.10). The primary material properties of the reflective thin film characterized by the aforementioned process are subsequently summarized in Table 3.1.

Table 3.1 Material properties of reflective thin film

Properties	**Value**
Elastic modulus (E_{film})	21.8668 GPa
Thickness (h_{film})	0.5500 mm
Deflection radius (r_{film})	15.0000 mm
Poisson's ratio (υ)	0.1250 -

With the summarized material properties, it is preliminarily possible to measure the pulse pressure of the detected pulse wave. However, the main focus in this research phase is to implement the FFPI probe along with its fiber optic system for arterial pulse wave detection. This would, consequently, pave ways for blood pressure demodulation in the later phases.

3.1.2 Configuration of an FFPI system for arterial pulse wave detection

To operate this sensing probe, however, an FFPI system must be implemented to effectively guide and interrogate the optical parameters resulting from the arterial pulse wave detection. Thus, an FFPI system for the light propagation and interrogation is configured as shown in Fig. 3.3.

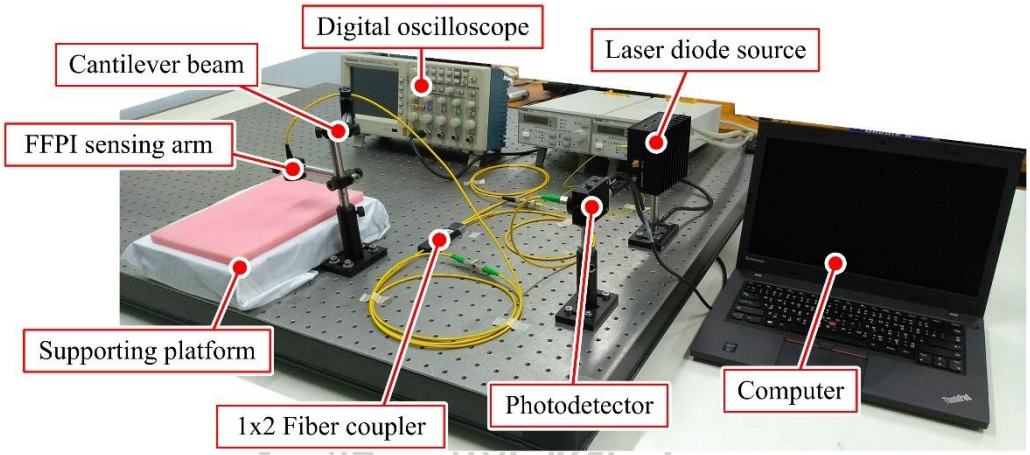

Fig. 3.3 FFPI system configuration for arterial pulse wave detection

A fiber-pigtailed monochromatic laser diode (*Thorlabs LPS-1310-FC*) emits laser wavelength of 1311.82 nm (measured by an optical spectrum analyzer: *Yokogawa AQ370D*) to a 1x2 fiber coupler. The fiber coupler, essentially a surrogate optical circulator in this configuration, then propagates the laser to the FFPI sensing arm, which is equipped with the aforementioned pulse sensing probe. The sensing site is, additionally, prepared with a supporting platform and a cantilever beam structure for accommodating the forearm of the human volunteers during an experiment. Regardless, the interference signal created by the FFPI probe is, afterwards, propagated back to the fiber coupler, and later to an InGaAs photodetector (*Thorlabs PDA10CS-EC*). At this point, the optical intensity of the interference signal is converted into electrical value to be observed using a digital oscilloscope (*Tektronix TDS 2014B*), displaying the interference signal on its screen. The data is, further, recorded through a USB drive to be analyzed using a computer, ultimately acquiring the arterial pulse wave.

3.1.3 Sensitivity characterization using a mechanical vibrator

Before the presented FFPI system and its pulse probe is exploited in real-live subjects, the fiber optic sensor is firstly investigated for its displacement measurement

capability, namely its sensitivity, through a mechanical vibrator. The experimental setup for such investigation is, thus, shown in Fig. 3.4.

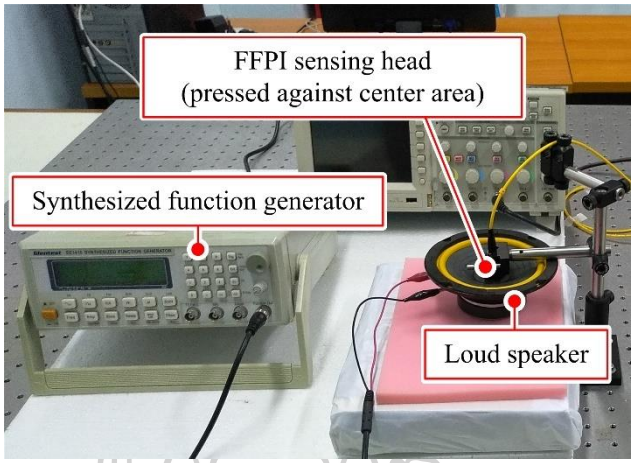

Fig. 3.4 Sensitivity characterization setup using an FFPI pulse sensing probe

In this experiment, the FFPI sensing probe is pressed on the center of a loudspeaker, which acts as a mechanical vibrating instrument generating displacement as a function of the input electrical signal from a synthesized function generator (*Glentest EE1410*). Furthermore, the excitation frequency induced on the mechanical vibrator ranges from 1-2 Hz (equivalent to a heart rate of 60-120 bpm, respectively) with an increment of 0.5 Hz (30 bpm). The amplitude of the excitation is, however, between 4-80 mV, increasing by 4 mV at a time. This setup is, consequently, intended to simulate the displacement induced via arterial distension when applying the FFPI sensing probe on a radial arterial site. The sensitivity of the fiber sensor can, therefore, be characterized through this experiment.

3.1.4 Preliminary arterial pulse wave detection in a human group

After the sensitivity characterization, the FFPI sensing probe is, lastly, exploited for radial arterial pulse wave detection in human volunteers as a preliminary validation in this dissertation. The volunteers are, firstly, recruited under their own consent and willingness. Subsequently, three individuals have participated in this experiment: one 22 years old female, one 25 years old male, and one 48 years old male. All participants are, moreover, healthy subjects, people without any medical ailments or health problems. During the pulse wave detection, the FFPI probe is set up on the right wrist of the volunteers in a sitting position, who are also asked to remain for the entire period of investigation, as can be demonstrated in Fig. 3.5.

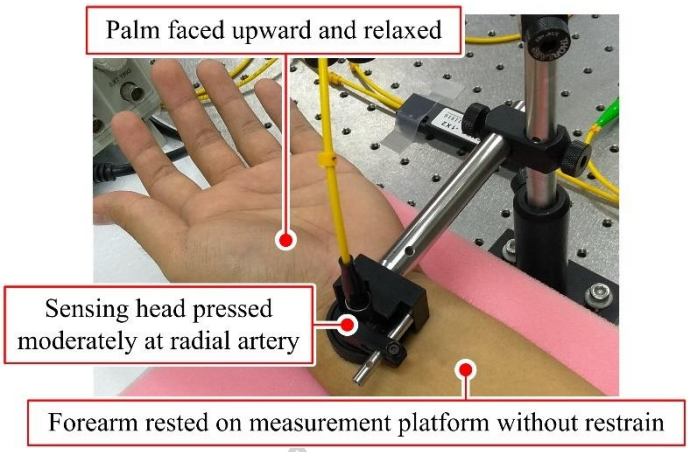

Fig. 3.5 FFPI pulse sensing probe setup on a volunteer

In addition, a digital sphygmomanometer (*OMRON HEM-7130*) as a reference blood pressure measuring device for measuring the heart rate (HR) of the volunteer as a surrogate indication of pulse wave. Generally, the sphygmomanometer measures HR by detecting the number of cuff pressure oscillations corresponding to the systolic peak of the arterial pulse wave, thereby suitable as a preliminary pulse wave reference. Regardless, the measurements on each volunteer are performed over 10 times of repeatability, using firstly the FFPI probe, followed by the reference sphygmomanometer, and interspace with a rest interval of at least one minute until all measurements are completed.

The results from this experiment are, consequently, investigated to determine the sensitivity of the FFPI system in actual pulse wave detection in humans. The HR demodulated by counting the number of heart pulses sensed by the FFPI is, additionally, compared against the HR of the reference, leading to the measurement error analysis.

3.2 RESOLUTION IMPROVEMENT FOR HIGH PERFORMANCE PULSE WAVE SENSING

Following the preliminary implementation of the FFPI system for pulse wave detection, an improvement on the measurement resolution is carried out. The main motivation is, principally, to overcome the limitations of the fringe counting technique applied in the previous research phase. Briefly, fringe counting technique limits the resolution of the FFPI system due to the demodulation principle, which might not be well-suited for continuous pulse wave acquisition on larger human trials. Therefore, this second research phase intends to implement a novel demodulation technique, namely phase-shift demodulation system, to improve the sensing capabilities of the FFPI system. In this section, the concept of phase-shift

demodulation, its application on an FFPI system, and also performance characterization through experimentation are described.

3.2.1 Principle of a laser modulation phase shift FFPI system

As previously explained in Chapter 2.4, phase-shift demodulation technique can overcome the resolution limit of the fringe counting technique and provide displacement information suitable for continuous measurement operations. Nonetheless, the applied FFPI requires two in-quadrature interference signals to propagate within the system. Here, the principle of in-quadrature interference signal generation is described based on a laser modulation technique.

Laser modulation is an interference signals generation technique which applies the relation between laser intensity and wavelength for phase-shift demodulation. Fundamentally, laser intensity affects the laser wavelength propagating within an optical system, thus the latter can be modulated by altering the input laser current of a laser diode. This can, further, be exemplified by a laser current-wavelength characterization in Fig. 3.6.

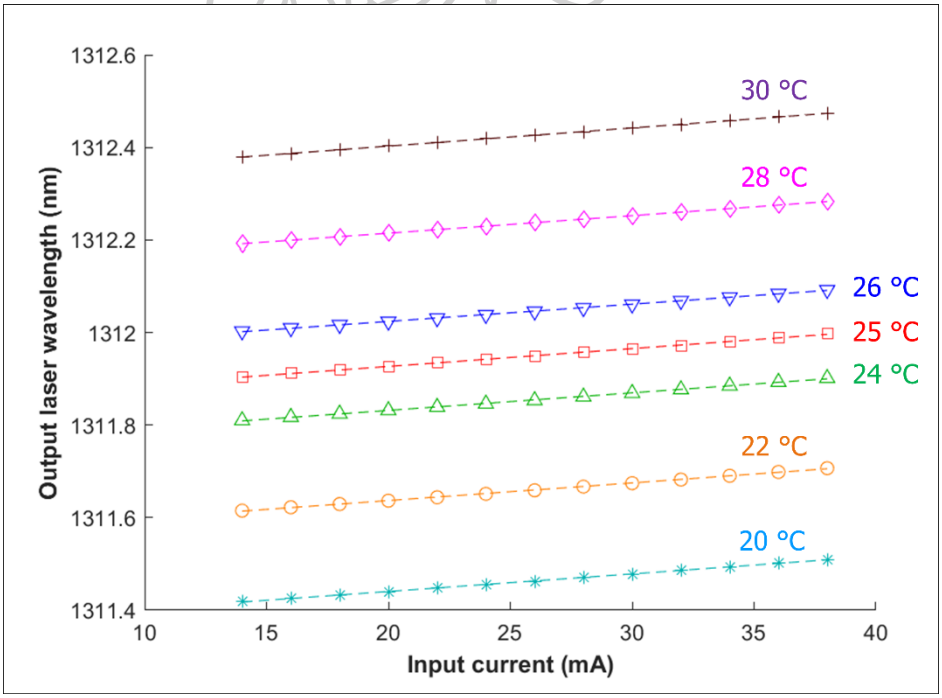

Fig. 3.6 Laser current wavelength characterization at different temperatures

According to the figure, the output optical wavelength is dependent on the input laser current and temperature. Particularly, higher input current and/or controlled temperature raise the optical wavelength of the propagating laser, as seen from the distinct

separation between each temperature range (such as between 20 °C and 22 °C). Once the controlled temperature is fixed, the output wavelength is, however, only affected by the input driving current. As such, alteration of the laser current of the light source will lead to optical wavelength modulation, meaning that a laser tuning scheme can be implemented to generate a light beam of different wavelengths within a single optical propagation system.

From the aforementioned laser characteristics, it is possible to configure a common-path dual-wavelength FFPI system which has two light beams of different wavelengths propagating within a single fiber component. In this dissertation, a phase generated carrier (PGC) configuration has been applied for the phase-shift demodulation, comprising an arbitrary waveform generator (AWG), a laser current driver, a data acquisition unit (DAQ), and two FFPIs supplied with a split laser source from a 1x2 fiber coupler, as schemed in Fig. 3.7.

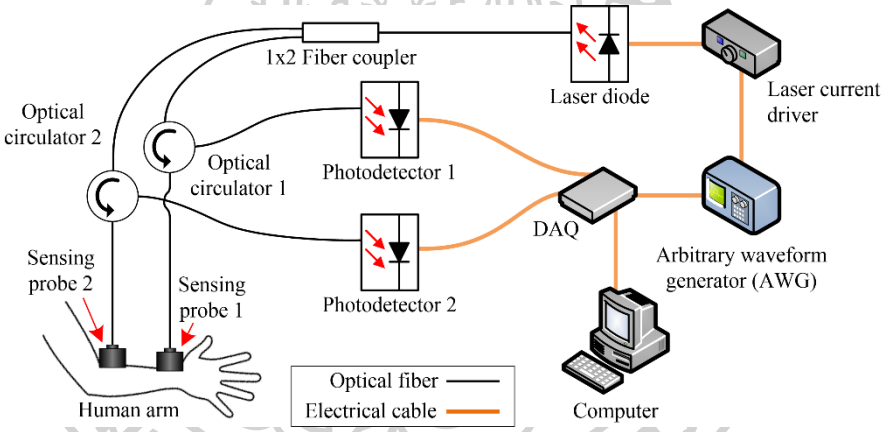

Fig. 3.7 Common-path dual-wavelength FFPI system configuration

Specifically, the AWG is utilized as a laser current modulator which generates a specific repeatable tuning signal to a laser current driver. Consequently, the initial laser current of the latter machine is further modulated at the frequency equivalent to the tuning signal. In this case, a square wave modulating signal is generated from the AWG and input to the laser driver since square waves have a period of stable signal which is desirable when extracting important parameters at high frequencies. Regardless, an example of the optical wavelength corresponding to the modulating square wave is schemed in Fig. 3.8.

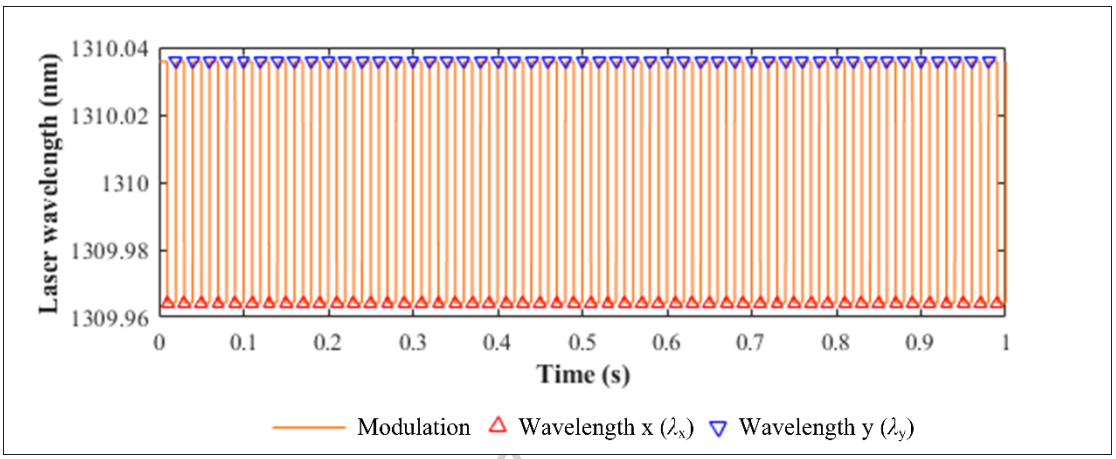

Fig. 3.8 Square wave modulating of dual wavelength laser

By inputting a square wave to modulate the laser current with a certain frequency (f_{mod}), the output optical wavelength of the laser diode can be measured at two different values. From the figure, the minimum wavelength (referred to as wavelength x: λ_x) is approximately 1,309.96 nm while the maximum modulated wavelength (termed wavelength y: λ_y) almost equals 1,310.04 nm. Importantly, these two optical wavelengths happen at a different time, i.e., λ_x occurs during time x (t_x) whereas λ_y is induced at time y (t_y) which is incidentally at half a modulation time later ($t_y = t_x + (1/2f_{mod})$). From Fig. 3.8, the simulated modulation signal is 50 Hz in frequency, meaning that the wavelength changes between λ_x and λ_y every 10 milliseconds. This information is, theoretically, applied to extract the point of wavelength alteration, leading to the separation of dual wavelength parameters for subsequent processes. In practices, finding the peaks and troughs of the modulation signal is, however, preferable as perfectly timing the wavelength shift period might be asynchronous during real-world applications. Using the modulation signal peaks and throughs, therefore, serves as a more robust point of reference, which can be automatically performed through a signal processing program. As such, square wave modulation scheme is chosen since a period of signal stability provides adequate space for error should the program experiences delays during a measurement. Note that the aforementioned laser modulation of 50 Hz has been exemplified for explanation's sake, though real-live implementation happens at a significantly faster frequency for higher resolution (i.e. more than 1 kHz). Regardless, the modulated optical wavelength causes the output interference signal to be modulated in response. Thus, the latter must be demultiplexed to form two separate interference signals of different wavelengths as demonstrated in Fig. 3.9.

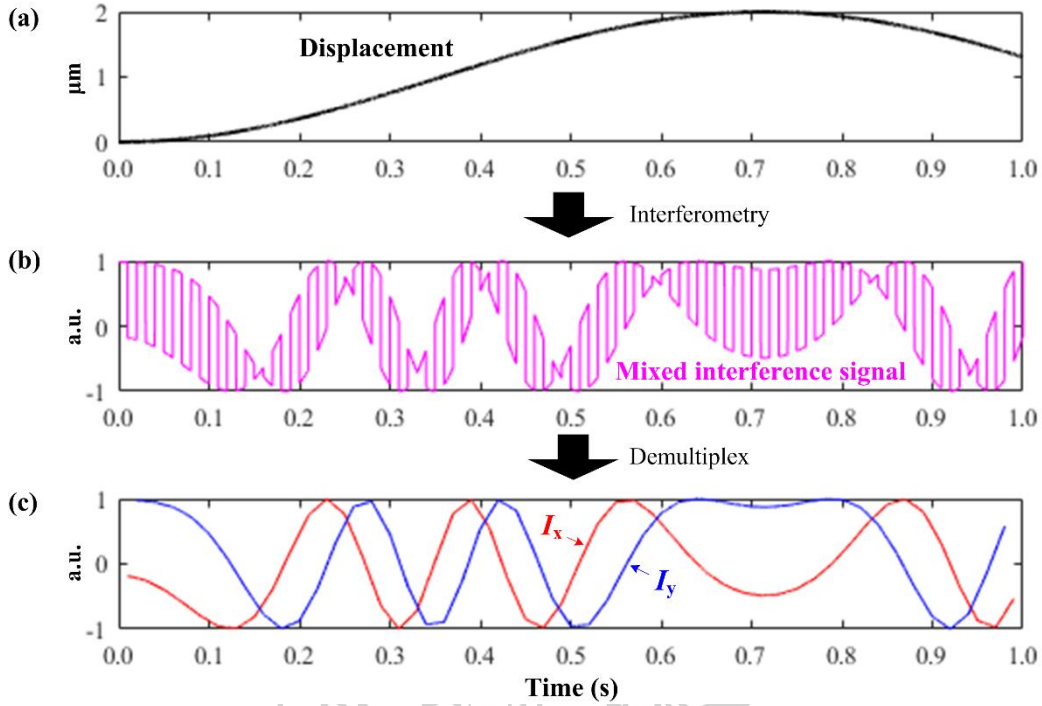

Fig. 3.9 Interference signal demultiplexing processes:
(a) input displacement, (b) interference signal multiplexing between two wavelengths, and (c) demultiplexed interference signals

In Fig. 3.9(a), a displacement of 2 μm is induced to form an interference signal with modulated wavelength during the interrogation. This is due to the laser current alteration presented in Fig. 3.8 which causes a square wave-like pattern to be observed in Fig. 3.9(b). However, the perturbed interference signal holds two separate wavelength parameters which must be demultiplexed to yield useful optical signals. Technically, a new interference signal named I_x is retrieved at t_x while another signal of I_y can be extracted at t_y, resulting in two interference signals with optical wavelength of λ_x and λ_y, respectively. At this point, the demultiplexed are obtained at two different times, though this can be remedied by waveform interpolation to match the point of occurrences between the dual interference signals. In this aspect, two interference signals are obtained by modulating a single laser source, realizing the common-path dual-wavelength FFPI system configuration as presented in Fig. 3.9(c).

Subsequently, the dual interference signals are demodulated to find the phase-shift value associated with the displacement of a measurand. Nevertheless, the phase difference between the two optical signals should be approximately in quadrature (i.e., $\pi/2$). To ensure that the demultiplexed interference signals are in quadrature, an initial wavelength-shift characterization is consequently performed. Firstly, consider the condition of the in-

quadrature interference pair which should have a phase difference of $\pi/2$. By applying the dual-wavelength modulating scheme, the condition can be described as [144]:

$$\Delta\varphi = \frac{\pi}{2} = \frac{4\pi n N_{\text{cavity}}}{(\lambda_x - \lambda_y)} d \tag{3.1}$$

where λ_x and λ_y correspond to the laser wavelength of the interference signal x and y, respectively. Assuming that the wavelength-shift ($\Delta\lambda$) is the difference between the two wavelengths ($\Delta\lambda = \lambda_x - \lambda_y$), while the initial input wavelength (λ_c) approximately substitutes both wavelength ($\lambda_c = \lambda_x \cong \lambda_y$), the wavelength-shift to be modulated is expressed to be:

$$\Delta\lambda = \frac{\lambda_c^2}{8nN_{\text{cavity}}d} \tag{3.2}$$

Ultimately, the laser wavelength which shall propagate within the FFPI system can be determined using the following:

$$\lambda_x = \lambda_c - \frac{\Delta\lambda}{2} \tag{3.3}$$

$$\lambda_y = \lambda_c + \frac{\Delta\lambda}{2} \tag{3.4}$$

With the aforementioned mathematics, the wavelength parameters for the laser modulation and subsequent phase-shift demodulation can be carried out. In this aspect, a laser current-wavelength characteristic of the utilized laser diode should be known. Alternatively, an iterative approach to indirectly characterize the modulation signal for generating the in-quadrature interference signals can be conducted in case the characterization data is unavailable (e.g., from the lack of equipment or onsite impromptu adjustments). Here, the polarization between the output interference signals can preliminarily convey the phase difference between the two signals through a Lissajous diagram. Fig. 3.10 illustrates the phase difference corresponding to the polarization of the optical signals.

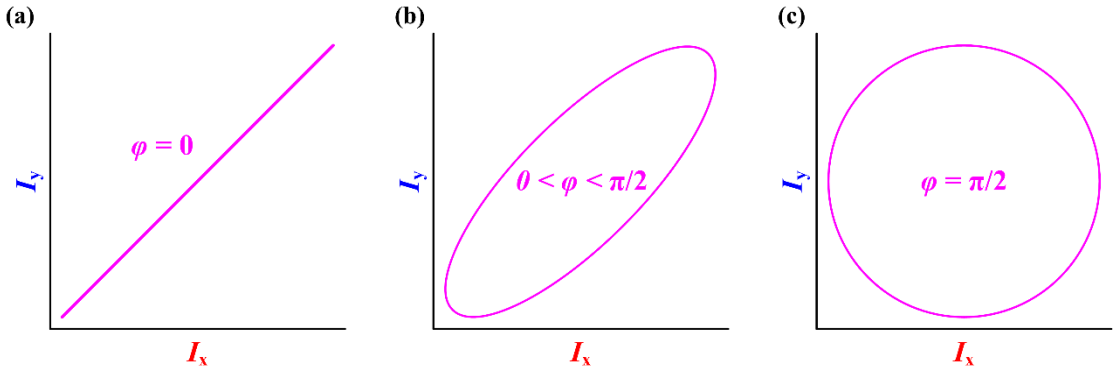

Fig. 3.10 Lissajous diagrams of different phase difference:
(a) linear, (b) elliptical, and (c) circular polarization

Considering the phase difference between the two interference signals from 0 to $\pi/2$ radians, the polarization plotted by one signal against another can incur three different polarization patterns: linear, elliptical, and circular. The former polarization (in Fig. 3.10(a)) occurs when the two interference signals are completely out-of-quadrature at a phase difference of 0, consequently disabling the phase-shift demodulation to be performed. Elliptical polarization (Fig. 3.10(b)) is, however, observed if the signal pairs are partially in-quadrature but not at $\pi/2$ (specifically, the phase difference is between 0 and $\pi/2$). While this condition is not ideal, the phase-shift demodulation can still be carried out, with some measurement error from the incomplete quadrature condition. The circular polarization shown in Fig. 3.10(c) is, in this case, the most optimal polarization to obtain as the phase difference is approximately, if not exactly, $\pi/2$. The main reason behind the polarization state is, consequently, the trigonometric function utilized to demodulate the phase-shift. Basically, the arctangent function described in (2.10) requires a sinusoidal and cosinusoidal parameter, which are obtainable when two interference signals are in quadrature. As such, circular polarization is the most desired, followed by ellipse polarization. The linear polarization is, in contrast, avoided since no phase-shift value can be demodulated. From this perspective, the configuration of a phase-shift FFPI system should allow for the adjustment of the quadrature conditions underlying the dual interference signals. One method is to iteratively adjust the laser modulation parameter until the Lissajous diagram shows an approximate circular polarization to ensure the generation of the in-quadrature interference signal pair.

3.2.2 Configuration of a phase-shift FFPI system

Continuing from the previous experiment, the utilized FFPI system for pulse wave detection has been improved to apply the phase-shift demodulation as the primary

technique of investigation. In order to achieve this, a new fiber optic system has been configured according to Fig. 3.11.

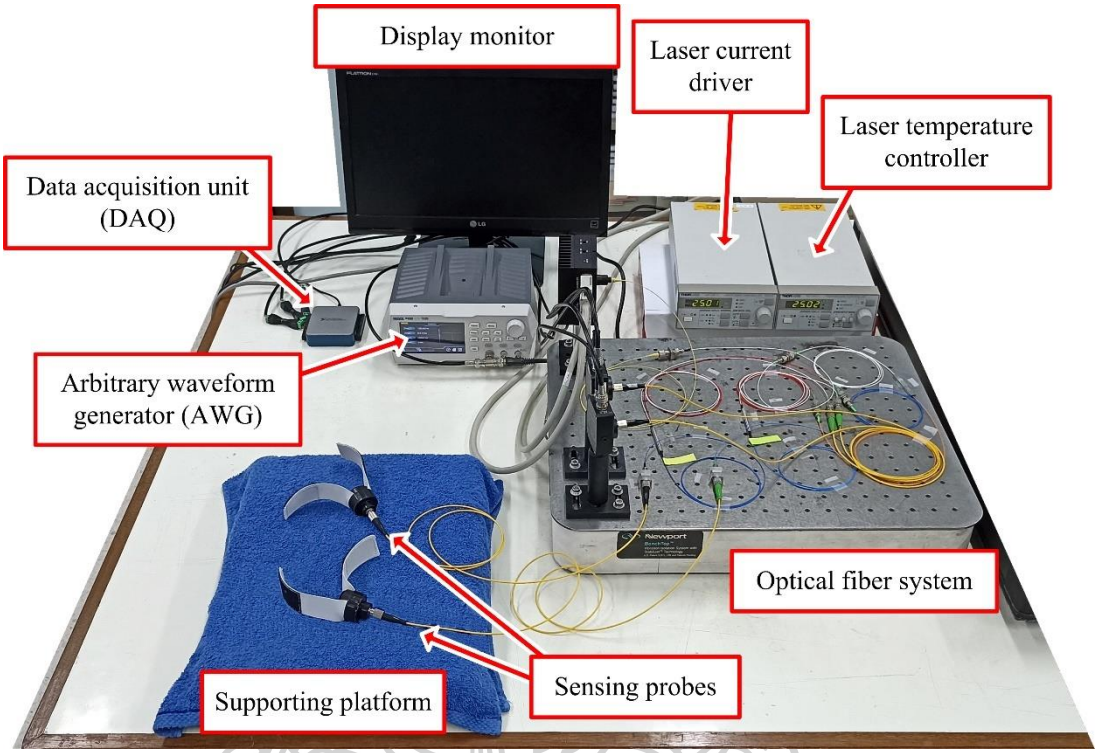

Fig. 3.11 Configuration of phase-shift FFPI pulse wave monitoring system

Similar to the schematic in Fig. 3.7, a laser diode source (*Thorlabs LPS-1310-FC*) injects a monochromatic light of 1311.9650 nm (measured by *Burleigh Wavemeter WA-1000*) to a 1x2 fiber coupler, where the light is split to two separate FFPI subsystems. Each FFPI subsystem is, however, identical to one another, comprising an optical circulator which propagates the split light to an FFPI sensing probe. At the sensing probe is a new design of interrogating fiber optic tools (explained in the next section) where the interference phenomenon occurs during the pulse wave monitoring. The interference signal from the probe is, regardless, sent back to the optical circulator before being propagated to an InGaAs photodetector (*Thorlabs PDA10CS-EC*) for optical-electrical signal conversion.

Nonetheless, additional components for phase-shift demodulation such as an AWG, laser current driver, laser temperature controller, DAQ, and computer unit have been implemented in association with the FFPI instrument. The AWG (*RIGOL DG800*) is, in this case, used to generate a square wave modulation signal at 12.5 kHz of frequency for laser parameter variation through the laser current driver (*Thorlabs LCD205C*). The modulation

amplitude is, intentionally, not fixed to allow manual adjustment of the driving laser current for forming the desirable circular polarization during real-world examination. In particular, the human skin properties can vary between individuals, causing the ideal quadrature condition in each measurement to be different, thus a dynamic compensating technique should be introduced. Nonetheless, the laser temperature controller is utilized to maintain the temperature profile of the optical system and prevent any wavelength modulation due to the temperature changes. The aforementioned laser manipulation machines, consequently, lead to the multiplexing of the interference signal which will be demultiplexed by a dedicated waveform processing unit. Here, the DAQ is applied to convert incoming analog interference signal from the photodetectors and laser modulation signal from the AWG into digital data for subsequent displacement demodulation.

In particular, a mathematical analysis software (*MATLAB 2018*) is employed to run a signal analysis scripts to sequentially analyze the input signals, demultiplex the dual-wavelength interference parameter, and demodulate the displacement measured by the FFPI. Firstly, the laser modulation signal is analyzed to determine the wave peaks and troughs which incidentally correspond to either I_x or I_y (demonstrated in Fig. 3.8). Once the points of references are found, the intensities of the multiplexing interference signal at those locations are extracted to form two separate interference signals (as shown in Fig. 3.9). Then, the obtained signals are interpolated to match their time of occurrence before applying (2.8)-(2.9) for demodulating the displacement information.

In this dissertation phase, the FFPI sensing probe has, however, been redesigned with the objective to heighten the reflectivity of the interference signal and also accommodate its setup on a human wrist. In this case, the new design of the sensing probe can be schemed in Fig. 3.12.

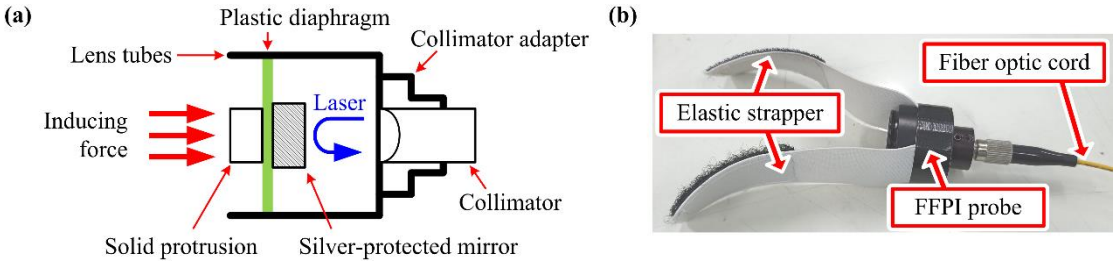

Fig. 3.12 Design of a new FFPI pulse sensing probe: (a) schematics of inner components and (b) photograph of outer appearance

The new FFPI pulse sensing probe still relies on the thin film deflection technique similar to the previous version. However, the reflective thin film has been discarded from this design since direct contact on the human skin has caused lower reflectivity due to the uneven optical alignment. The new design, thus, implements a plastic thin film secured inside a lens tube with a retaining ring, with an attached solid protrusion on its center acting as a force redirection component for displacement measurement. The protrusion can also serve as a precision arterial site locator when setting up the sensing probe on an area of interest. On its other end, a silver-protect mirror (*Thorlabs PF10-03-P01*) is secured and exploited as the new reflective surface for the FFPI, with a reflectivity of more than 0.97%. Furthermore, a collimating lens (*ThorLabs F220FC-C*) is purposedly embedded to incident laser onto the mirror, lessening the loss due to light dispersion when ejected from a typical fiber optic cord. The slightly extended part of the probe also allows for suitable skin accommodation that leads to stable sensor placement on a human. Moreover, the FFPI sensing probe is constructed with elastic strappers for wrapping around the human wrist, therefore additional cantilever systems are negligible. Overall, this new probe design not only increases the reflectivity of the FFPI but also accommodates for the force redirection to the thin film, enabling more stable and faster sensor setup during examination.

3.2.3 Investigation of phase-shift FFPI system on a mechanical vibrator

While the entire FFPI system presented in previous sections is developed for continuous pulse wave monitoring, the fiber optic system is initially investigated for its performance before validation through human trials. In this aspect, an investigation on a mechanical vibrator, namely a piezoelectric actuator *PI-753.1CD*, is exploited to generate displacement onto an FFPI probe. The experimental setup for such investigation can, consequently, be shown in Fig. 3.13.

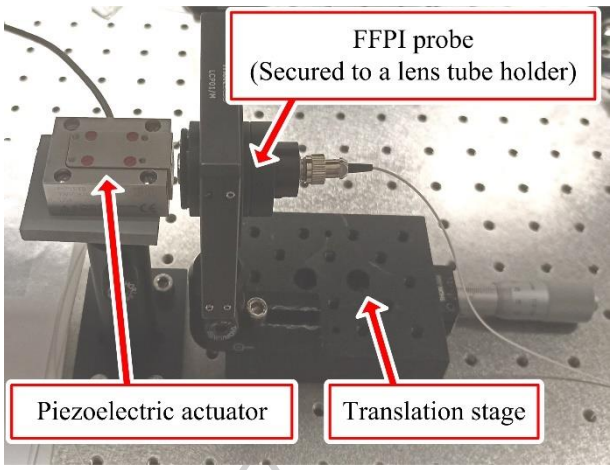

Fig. 3.13 Experimental setup to investigate FFPI performance: (a) configuration and (b) mechanical vibrator setup

From the figure, an FFPI pulse sensing probe is secured on a lens tube holder (*Thorlabs LCP01/M* cage plate with an additional lens tube adapter) which is connected to a translation stage (*Thorlabs PT1*). The translation stage is exploited to press the pulse probe onto the mechanical vibrator, where its actuation will displace the thin film during the investigation. Note that an FFPI probe is validated though the characteristics are shared between the two pulse probes due to the identical components. Nonetheless, the piezoelectric actuator is excited with a function generator, which displaces its translational platform by 0.03-7.50 μm in a sinusoidal wave pattern. Additionally, a displacement frequency of 0.10-3.00 Hz is induced to investigate the FFPI capability to detect an equivalent heart rate of 6-180 bpm, respectively. This experiment is, intentionally, conducted to analyze the improved sensitivity, resolution, and accuracy of the phase-shift FFPI system.

3.3 VALIDATION OF FIBER OPTIC SYSTEM FOR BLOOD PRESSURE MEASUREMENT

The developed FFPI system, after the preliminary implementation and improvement stage, is ultimately validated for its continuous blood pressure measurement capability. To achieve this goal, the previously described phase-shift FFPI system has been applied in this research phase. However, additional components of the system, namely an engineering application software and blood pressure demodulation algorithm, are developed to assist in this endeavor. This section, therefore, explains the developed engineering application software, the demodulation algorithm, and also the human trial carried out to validate the FFPI system in this dissertation.

3.3.1 Engineering application software for arterial pulse wave monitoring

To measure the blood pressure in human volunteers, the arterial pulse wave of the person must initially be monitored to acquire all important parameters for subsequent demodulation. In section 3.2, the phase-shift FFPI system can successfully obtain the displacement information which is related to the arterial pulse wave acquisition. Nonetheless, the parameters were analyzed intermittently, by recording the data to be processed using an offsite computer. While this method can also be implemented to obtain the arterial pulse, it is preferable to have an available pulse wave display on the examination site. Thus, an engineering application software for arterial pulse wave monitoring has been developed using LabVIEW programming, specifically LabVIEW 2020 version, with a user interface (UI) for inputting important parameters and displaying the pulse wave in quasi real-time. Fig. 3.14 indicates the UI of the developed software exploited during an actual human trial.

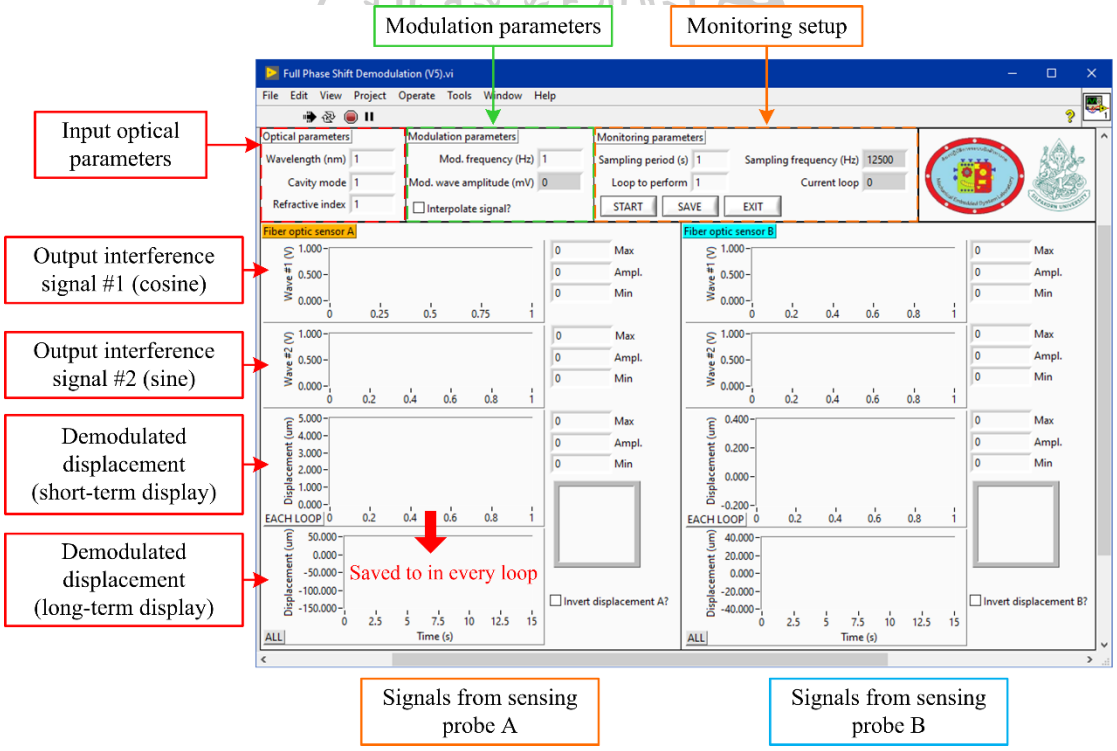

Fig. 3.14 User interface of developed pulse wave monitoring software

The application software is comprised of four main interfaces: input optical parameters, modulation parameters, monitoring setup, and FFPI signal display. The first interface allows the user to input related optical parameters such as laser wavelength, cavity mode (equivalent to the number of cavity reflections: N_{cavity}), and refractive index. These parameters are crucial for the displacement demodulation by the software in a later process.

Meanwhile, the modulating parameter interface includes the modulating frequency induced by the AWG when multiplexing the laser current. The interface also tracks the modulation amplitude in case of hardware failure. The third interface, the monitoring parameters, is responsible for the sampling period of a signal acquisition along with the number of acquisition loops to perform. This interface also houses the "*Start*", "*Save*", and "*Exit*" buttons which initiate the pulse wave monitoring, record the data, and terminate the software, respectively. Finally, the FFPI signal display is the acquired parameters from the two FFPI pulse sensing probes, showing the demultiplexed interference signal pairs, their polarization, and successive displacement demodulation. Here, the demodulated displacement will firstly be projected on the short-term display, with a sampling period defined in the monitoring interface. In case the "*Loop to perform*" input is not "1", a new demodulated displacement information will appear on the short-term screen, while the previous one is recorded and then displayed on the long-term panel. Generally, the sampling period is set to be 1 second with 15 loops to perform, meaning that the total monitoring time is 15 seconds. This function is, consequently, designed in this manner to accommodate the higher-resolution pulse wave monitoring in a shorter period, while enabling the pulse wave tracking over longer examination time. Nevertheless, the displacement information in the long-term display is recorded using the "*Save*" button, as well as all long-term monitored interference signals not shown in any of the interfaces in case of any signal analysis outside of this application software.

3.3.2 Blood pressure demodulation algorithm

Although the engineering application software can monitor the arterial pulse wave on the examination site, an excluded blood pressure demodulation algorithm is to be applied in a separate platform. Here, a blood pressure demodulation algorithm is developed using MATLAB programming, which obtains the FFPI information from the application software to process the pulse wave, characterize the essential components, and demodulate the blood pressure. The overall process of this algorithm is, further, schemed in Fig. 3.15.

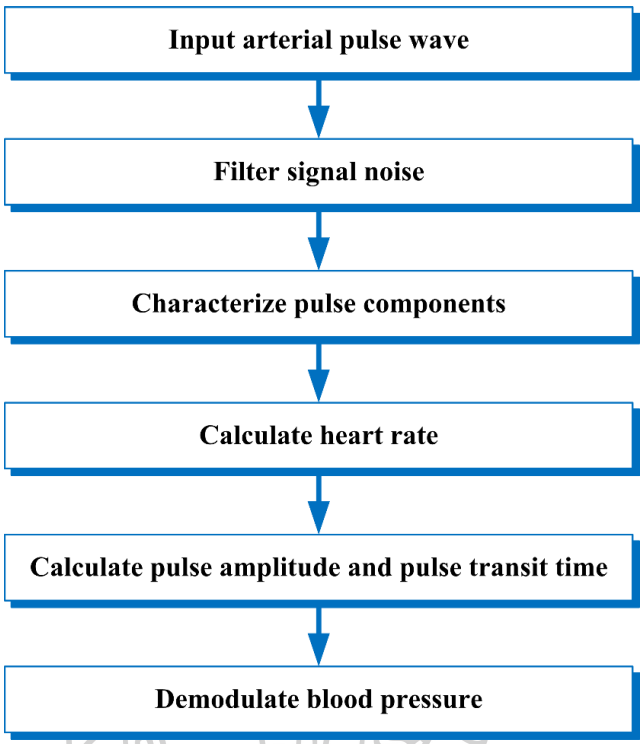

Fig. 3.15 Workflow of blood pressure demodulation algorithm

Firstly, the arterial pulse wave acquired by the engineering application software is input into the algorithm, followed by a signal noise filtering function. Particularly, a finite impulse response (FIR) filter designed using the "*Filter Designer*" function in MATLAB programming is carried out, using 5000-order Hamming window method to filter any signal noise outside the bandpass of 0.5-10.0 Hz. This bandpass is, intentionally, equivalent to 30-300 bpm of heart rate, which is deemed suitable for filtering any The FIR filter, additionally, has another benefit of sufficiently removing the motion artifact (unwanted bodily movements) from the pulse wave, as most movements have less than 30 bpm of frequency.

Afterwards, the arterial pulse characteristics such as its peak and trough are characterized to indicate the systolic peaks and end-diastolic points, respectively. This step is critical for all subsequent blood pressure demodulation processes. Next, the heart rate (HR) is calculated based on the number of systolic peaks detected over a period (15 seconds) using (2.1). The pulse wave amplitude is, however, utilized to find the pulse pressure (PP) according to (2.10). To reiterate, the demodulated PP (PP_{demod}) can be found based on the thin film deflection technique using:

$$\mathrm{PP}_{\mathrm{demod}} = \frac{16E_{\mathrm{film}}h_{\mathrm{film}}^{3}\Delta d}{3r_{\mathrm{film}}^{4}(1-\upsilon^{2})} \tag{3.5}$$

Since the FFPI pulse sensing probe has been redesigned, the exploited plastic thin film is also verified for its material properties using a universal tensile testing machine. The characterization of the thin film is then summarized in Table 3.2.

Table 3.2 Material properties of plastic thin film

Properties	**Value**
Elastic modulus (E_{film})	448.4255 MPa
Thickness (h_{film})	0.2000 mm
Deflection radius (r_{film})	12.5000 mm
Poisson's ratio (υ)	0.1400 -

Through the thin film characterization, the PP of an examined human volunteer can be demodulated. However, the skin property of the volunteer can significantly affect the placement and, by extension, the acquisition accuracy of the pulse amplitude. Therefore, a calibration value is defined by performing a linear regression analysis on three consecutive arterial pulse wave monitoring and blood pressure measurement using a reference digital sphygmomanometer. For the case of PP demodulation, the following calibration value is applied:

$$\mathrm{PP} = (m_{\mathrm{PP}} \times \mathrm{PP}_{\mathrm{demod}}) + c_{\mathrm{PP}} \tag{3.6}$$

where m_{PP} and c_{PP} as the linear slope and offset obtained from the linear regression, respectively. This calibration process lessens the skin perturbation effects on the arterial pulse amplitude.

On the other hand, the systolic peaks are applied for the pulse transit time (PTT) calculation, leading to the pulse wave velocity (PWV). Specifically, this dissertation introduces a modified PWV calculation which derives from (2.11)-(2.12) and exploits the displacement acquisition of the developed FFPI system. From the Bramwell-Hill equation:

$$\mathrm{PWV} = \sqrt{\frac{V\Delta P}{\rho\Delta V}} \tag{3.7}$$

The pressure difference (ΔP) can be substituted with the calibrated PP value, while the blood density (ρ) is defined as 1,060 kg/m^3. Also, assuming that the human radial artery is a cylindrical tube with a circular surface, the equation can be rewritten as:

$$\mathrm{PWV} = \sqrt{\frac{PP \times r_{\mathrm{DBP}}^2}{\rho\left(\Delta r_{\mathrm{artery}}\right)^2}} \tag{3.8}$$

when r_{DBP} is the arterial radius at diastolic blood pressure (DBP) and $\Delta r_{\mathrm{artery}}$ is the arterial distension. Interestingly, the size of the artery at a certain pressure is proportional to the internal pressure at the time, implying that r_{DBP} correlates to DBP. Consequently, a linear regression analysis can be conducted to find the calibration parameters to demodulate PWV into DBP, as expressed by:

$$\mathrm{DBP} = m_{\mathrm{DBP}} \frac{\mathrm{PWV}^2 \rho \Delta r_{\mathrm{artery}}}{\mathrm{PP}} + c_{\mathrm{DBP}} \tag{3.9}$$

Here, m_{DBP} and c_{DBP} are the linear slope and offset acquired through the linear regression of PWV to three reference DBP measured by a digital sphygmomanometer, respectively. In addition, $\Delta r_{\mathrm{artery}}$ is measured as the displacement due to the arterial distension monitored using the developed FFPI system. At this point, the systolic blood pressure (SBP) can be calculated with:

$$\mathrm{SBP} = \mathrm{PP} + \mathrm{DBP} \tag{3.10}$$

With all of the mentioned processes, the SBP, DBP, PP, and HR can be measured by the developed FFPI in addition to the arterial pulse wave profile.

3.3.3 Validation of FFPI system through human trial

Once the configuration of the FFPI system and associated demodulation algorithm have been developed, a human trial including 85 volunteers is carried out. In particular, the volunteers participate under their own consent and willingness, coupled with an ethics in human research approval by Silpakorn University Research, Innovation, and Creativity (SURIC) administration office to ensure protocol compliance. The statistics of the volunteer participating in this trial is, further, indicated in Table 3.3.

Table 3.3 Statistics of human volunteers

Characteristics	Participants	Percentage
Total	85	100.00%
Gender:		
Male	44	51.76%
Female	41	48.24%
Age:		
18-25 years	73	85.88%
26-35 years	5	5.88%
36-45 years	7	8.24%

In this human trial, participants may be of either gender and any age from 18 years and above. However, this trial only includes healthy volunteers, i.e., people who do not have any significant health problems to cardiovascular diseases. The participants are, after giving consents and instructions regarding the experiment, seated and have their left forearm installed with the developed FFPI probes and a reference digital sphygmomanometer *OMRON HEM-7130*, as depicted in Fig. 3.16.

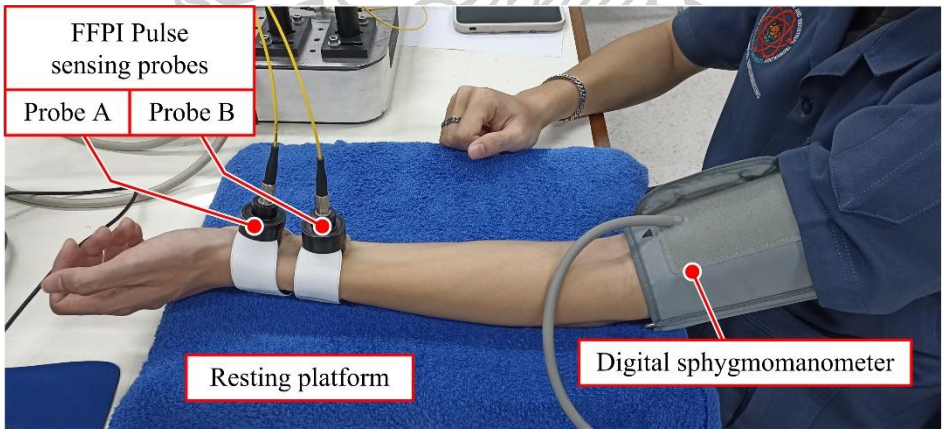

Fig. 3.16 Instrument setup on a human participant

The two FFPI pulse sensing probes are placed on the wrist of the participants, monitoring the arterial distension at the area. The probe proximal to the hand is, further, labeled as "*Probe A*" while the other is named "*Probe B*". The "*A*" and "*B*" shall subsequently be the suffix for denoting the signals from the respective sensing probes in the analysis. Meanwhile, an inflatable cuff of the digital sphygmomanometer is inserted around the upper arm. The participant is, subsequently, asked to not cause any movements during the

examination, which lasts approximately 15-20 minutes. The blood pressure measurement is, then, performed for 7 consecutive times of repeatability, utilizing the sphygmomanometer interlaying with the FFPI probes in a sequential manner. The four reference blood pressure readings are, afterwards, averaged into three referable datasets to be compared against the FFPI results.

3.4 ENERGY CONSUMPTION CONSIDERATIONS

Once the FFPI system has been configured, operated, and investigated for its capabilities in continuous blood pressure measurement, this dissertation also interrogates the energy expenditure of the system. The intent is to preliminarily characterize the energy consumption of the fiber optic system which could prove useful for optimizing the sensor to be sustainable in terms of power usage. The findings would, further, contribute to the designing of an emergency backup system, net-zero energy building, or integration into state-of-the-art technology such as smart driver seats [145], all of which generally prefers low energy consuming instrument. As such, the energy consumption profile of the developed FFPI sensor has been characterized.

Primarily, the system to be considered is the phase-shift FFPI system for continuous blood pressure measurement configured according to Fig. 3.11. Thus, all utilized equipment expending energy during operations can be listed in Table 3.4.

Table 3.4 Lists of power consuming optoelectrical equipment

Device	Amount
Laser diode driver	1
Laser temperature controller	1
InGaAs Photodetector	2
Multifunction data acquisition unit (DAQ)	1
Arbitrary waveform generator (AWG)	1
Desktop computer	1
Display monitor	1

In operation, the laser diode driver is modulated by the AWG while the temperature controller stabilizes the laser temperature at a constant level. Two InGaAs photodetectors are

consequently employed to convert the optical parameter sensed during the system operation into electrical analog signal, further retrieved using a multifunction DAQ for conversion into digital signal. The desktop computer, afterwards, processes the digital signal into arterial pulse wave and subsequently blood pressure readings to be shown on a display monitor. All the aforementioned devices are, ultimately, required to be active when measuring blood pressure of a participant. Therefore, these devices will consume energy during any measurement. To evaluate the energy consumption, the power specifications of the devices are applied in the calculation.

Here, the maximum energy consumption of the optoelectrical components has been studied by assuming that the device operates at maximum capacity. This is intentionally conducted to estimate the maximum possible energy usage of the fiber optic system which could prove useful in future research and development. Moreover, the minimum operation period of the fiber optic system is determined based on the examination time spent to achieve the blood pressure results from the volunteers. As such, the energy consumption of the optoelectrical equipment can be calculated using:

$$E_{\text{consumption}} = P_{\text{max}} \times t_{\text{power}} \tag{3.11}$$

where $E_{\text{consumption}}$ denotes the energy consumption of a device with P_{max} and t_{power} as the maximum power rating and operating time, respectively. The maximum power rating can be defined via specification sheet of a device of interest. The operating time is, however, dependent on the period of system operation. Consequently, the energy consumption is characterized according to the required time in practical blood pressure measurement, which can be divided into three consecutive periods: equipment preparation period (warm-up period), examination period, and post-operation period.

The first period is, technically, carried out to prepare the fiber optic system, basically initiating the computer unit, engineering application software, and display monitor. Additionally, the warm-up period allows the laser components to be stabilized, reducing potential signal drift as the current driver and temperature controller are adjusting the laser parameters. In this FFPI configuration, 10 minutes time is determined as the minimum warm-up period to ensure signal stability and also for turning on all relevant computer software.

Meanwhile, the examination period concerns the application of the fiber optic system for continuous blood pressure measurement, which is approximately 15-20 minutes per volunteer. For consistency's sake, the examination period is set to be 20 minutes per person.

Note that the fiber optic system is not turned off or restarted for each examination but instead continuously powered until the last measurement is done.

Afterwards, the FFPI system can be partially terminated with the computer unit still operating. In particular, the laser components, AWG, and photodetectors can be powered down since the blood pressure measurement will not be further carried out. The computer unit is, therefore, utilized to analyze any remaining arterial pulse wave records yet to be demodulated into blood pressure parameters. This procedure also allows the user to inspect, analyze, and transfer the measurement records after patient examinations. In this aspect, the post-operation period can infinitely be conducted, though the energy consumption analysis posts a set time amount of 30 minutes before a complete system shutdown.

Since the developed fiber optic system could be further researched for real-world applications, the energy consumption characterization shall assume its operation in a working environment. Assuming that the place of operation regularly opens from 8.00-17.00 working hours, the daily operation period of the system is 8 hours long. Thus, the preparation period, examination period, and post-operation period must fit within this timeframe. The fiber optic system is, furthermore, determined to be powered on for the entire day until the place of operation closes. In this manner, the daily energy consumption of the developed FFPI system can be characterized as preliminary information regarding the energy usage in practical implementation.

3.5 DEVELOPMENT COST ESTIMATION

The objective of this dissertation is to develop a fiber optic sensor for continuous blood pressure measurement in hopes that the research will elevate the competitiveness of biomedical engineering in Thailand. One of the considerations is, therefore, the commercial viability of the developed fiber optic system for future biomedical applications. Thus, it is important to estimate the development cost of the measuring system to preliminarily provide adequate financial information for possible investment.

In this dissertation, the development cost is primarily calculated based on the procurement price of the required equipment. The latter is, specifically, determined by the configuration of the FFPI system shown in Fig. 3.11, mainly concerning the optical and electrical components needed to operate the fiber optic sensor. The cost estimation has, however, not considered the cost regarding labor, software engineering, utility fees (e.g., electricity, water, gas, etc.), and administrative expenses. Consequently, the estimation focuses on analyzing the procurement cost of the fiber optic system due to predictable pricing which could become useful information when developing a commercial instrument in the

future. The disregarded costs could, nevertheless, be considered once the fiber system has been investigated for financial feasibility or cost analysis when operated in practical settings such as in hospitals.

In this perspective, the price of the utilized equipment for developing the FFPI system is surveyed either via product catalog of the providers/manufacturers or the issued cost recorded in invoices. To summarize the equipment to be considered, Table 3.5 lists the items and sources of price survey.

Table 3.5 Lists of equipment applied in developed fiber optic system

Item	Survey method	Ref.	Amount	Purpose
Near infrared fiber-pigtailed laser diode (LPS-1310-FC)	Catalog	[146]	1	Signal processing
Temperature-controlled laser diode mount	Catalog	[146]	1	Signal processing
Laser diode driver	Catalog	[146]	1	Signal processing
Laser diode temperature controller	Catalog	[146]	1	Signal processing
1x2 Fiber coupler	Invoice	[146]	1	Signal processing
Fiber Optical circulator	Catalog	[146]	2	Signal processing
Fiber patch cord	Invoice	[146]	2	Signal processing
InGaAs Photodetector	Catalog	[146]	2	Signal processing
Multifunction data acquisition unit	Catalog	[147]	1	Signal processing
Arbitrary waveform generator	Invoice	[148]	1	Signal processing
Desktop computer	Catalog	[149]	1	Signal processing
Collimating lens	Catalog	[146]	2	Probe design
Collimator adapter	Catalog	[146]	2	Probe design
Lens tube	Catalog	[146]	4	Probe design
Retaining ring	Catalog	[146]	2	Probe design
Silver-protected mirror	Catalog	[146]	2	Probe design
Plastic thin film	Invoice	-	1	Probe design
Protruding structure	Invoice	-	1	Probe design

From the table, the price survey of the equipment is classified into two groups: catalog and invoice type. The former type is the procurement price displayed by the provider of the component either through internet website or paper-based catalog. Consequently, the price survey is conducted in this manner since the equipment has been procured prior to the

configuration of the fiber optic system. Thus, the price is surveyed from recent sources to account for the procurement cost in present value. On the other hand, the invoice-based price survey depicts the equipment purchased during the system configuration, thereby allowing the actual price to be recorded.

Furthermore, the procured items shown in Table 3.5 are required for either the signal processing or fiber optic probe design. Specifically, equipment of the former group is exploited to propagate signals, either optical or electrical, through the fiber optic system and also allow the demodulation process to be initiated. This, thus, implies that most laser manipulation components are listed in this group and generally consists of a fixed unit regardless of the system size. Meanwhile, the probe design group is comprised of any component necessary to construct a fiber optic pulse sensing probe. Here, the components are commonly small in size compared to the equipment in the signal processing group. However, the number of items is proportional to the number of fiber pulse sensing probes to be implemented. Nevertheless, Table 3.5 lists all components applied in this dissertation, considering the construction of two fiber optic probes for blood pressure measurement. Note that the plastic thin film and protruding structure amount for one item since the components are larger than required size in the probe design, thus several portions can be divided from a single item. With this approach, the development cost of the fiber optic system can be preliminarily investigated.

3.6 SUMMARY

The experimental setups explained in this chapter primarily aim to investigate a fiber optic Fabry-Perot interferometer (FFPI) for continuous blood pressure measurement. By following the dissertation phase, the FFPI has been developed to preliminarily detect arterial pulse wave in human volunteers, with the results consider for resolution improvement. Consequently, a phase-shift demodulation technique has been integrated to enable higher measurement capabilities of the FFPI. The sensitivity and resolution of the improved FFPI have, then, been characterized using a displacement actuator. After confirming the potential of the proposed FFPI, human volunteers have, subsequently, been recruited to ultimately validate its biomedical function of the blood pressure measurement. Lastly, the energy consumption and also development cost have been considered and evaluated as supplemental data for future research. In the next chapter, the results following the investigation of the aforementioned experiments are, therefore, described which shall reveal the important information of the FFPI development from a preliminary arterial pulse detector into a continuous blood pressure measuring system.

CHAPTER 4
EXPERIMENTAL RESULTS

In this chapter, the experimental results concerning the experimental setups in the previous chapter are described in detail. This chapter, thus, organizes the experimental results to be presented in sequential order following the structure of the previous chapter. Moreover, the energy consumption and cost analysis in the development of the fiber optic system for continuous blood pressure measurement has been discussed to pave the way for future consideration of the novel biomedical instrument.

4.1 FIBER OPTIC FABRY-PEROT INTERFEROMETER FOR ARTERIAL PULSE DETECTION

After the configuration of the FFPI system using a reflective thin film as the interrogating arterial pulse wave detecting agent, the fringe counting technique is employed to demodulate the pulse wave information. Consequently, the displacement of a target of interest can be acquired, which is firstly investigated using a mechanical vibrator and secondly via small human trial.

4.1.1 Sensitivity characterization using a mechanical vibrator

By applying the FFPI pulse sensing probe to measure the displacement on a mechanical vibrator, it is found that the fiber optic system can successfully detect the inducing force on its probe. This can be exemplified in Fig. 4.1.

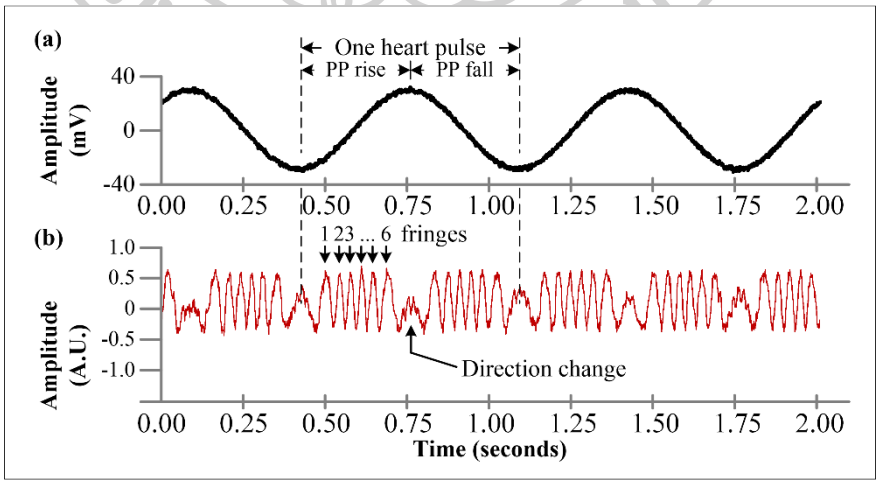

Fig. 4.1 Displacement measurement using fringe counting technique:
(a) excitation signal corresponding to displacement and (b) interference signals

In this experiment, an excitation signal of approximately 70 mV is induced to cause displacement of the mechanical actuator (in Fig. 4.1(a)). This results in the diaphragm actuation of the loud speaker, which subsequently deflects of the reflective thin film of the FFPI probe, generating an interference signal with 6 fringes (see Fig. 4.1(b)). By applying (2.10) in associated with the characterized thin film properties in Table 3.1, the pressure of 11.496 mmHg can, thus, be demodulated from the fiber optic system. To further investigate the sensor capability, an excitation of 4-80 mV at the frequency of 60, 90, and 120 bpm is also induced, with the investigation results illustrated in Fig. 4.2.

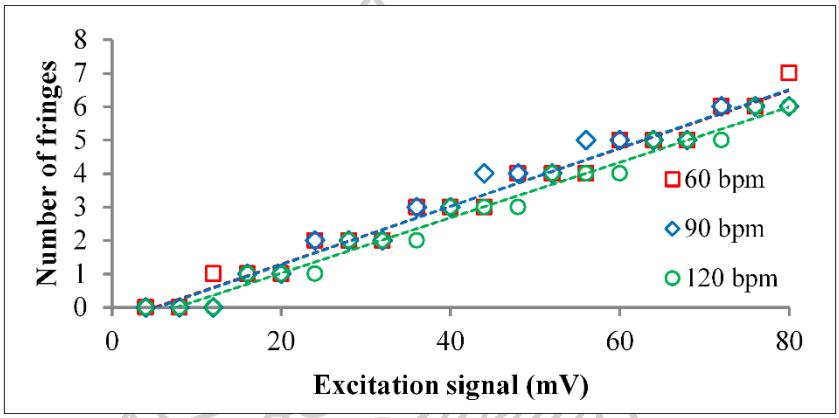

Fig. 4.2 FFPI outputs relation to excitation signal of a mechanical vibrator

It is found that the number of fringes directly corresponds to the input excitation signal. Additionally, the frequency of the fringe packet generations matches the frequency of the vibrator, implying that the FFPI probe can correctly detect the rate of actuation. However, some small signal alterations might not sufficiently cause significant change in the number of fringes. This is, consequently, due to the intrinsic resolution of the FFPI applying the fringe counting technique, that is 1.916 mmHg. In this aspect, the accuracy in displacement measurement becomes ±1.916 mmHg.

Nevertheless, the sensitivity of the FFPI pulse sensing probe for arterial pulse wave detection is also investigated, with the results summarized in Fig. 4.3.

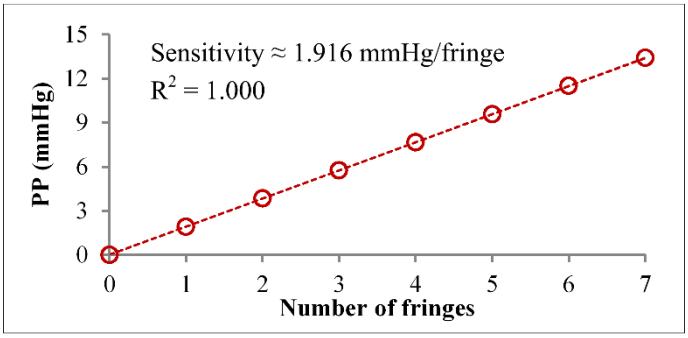

Fig. 4.3 Sensitivity characterization of FFPI sensing probe

From the analysis, it is found that the number of fringes and demodulated PP using the thin film deflection technique relationship has high linearity, with a coefficient of correlation (R^2) of 1.000 and a sensitivity of 1.916 mmHg/fringe, respectively. The results, ultimately, suggest a high correlation between the FFPI output to demodulated PP which will pave the way for future human trial.

4.1.2 Preliminary pulse wave detection using fiber optic sensing probe

Afterwards, the FFPI pulse sensing probe is preliminarily applied for human arterial pulse wave detection, and an example of the detection can be shown in Fig. 4.4.

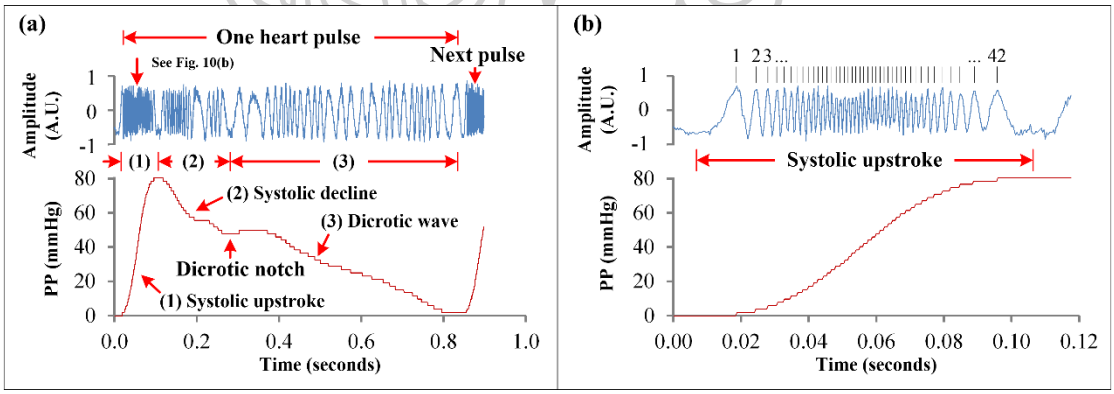

Fig. 4.4 FFPI fringe outputs in arterial pulse wave:
(top) interference signal, (bottom) reconstructed arterial pulse wave,
(a) data from a heart pulse and (b) fringes during a systolic upstroke

When the FFPI pulse sensing probe is placed on a volunteer's wrist, an interference signal is generated in response to the arterial distension, as seen in Fig. 4.4(a). The reconstructed displacement, consequently, exhibits a strong similarity to an arterial pulse

wave. This implies the capability of the FFPI probe for arterial pulse wave detection. Meanwhile, the number of fringes during a systolic upstroke (see Fig. 4.4(b)) is 42 fringes, which demodulates to 80.472 mmHg of PP. Additionally, two heart pulses can be identified by observing the dense fringe packets that indicates rapid rise in pressure.

To preliminarily verify the FFPI pulse sensing probe in arterial pulse wave detection, a reference sphygmomanometer (*OMRON HEM-7130*) is employed. Since a typical sphygmomanometer cannot display any arterial pulse waves, the heart rate (HR) measured by both the reference device and FFPI sensor are compared. This is due to the HR measurement principle which counts the number of heart pulses within a specified period, thus both instruments can compare their HR readings as a surrogate technique. In this experiment, the HR measurement results on three volunteers, each with 10 times of repeatability, are indicated in Fig. 4.5.

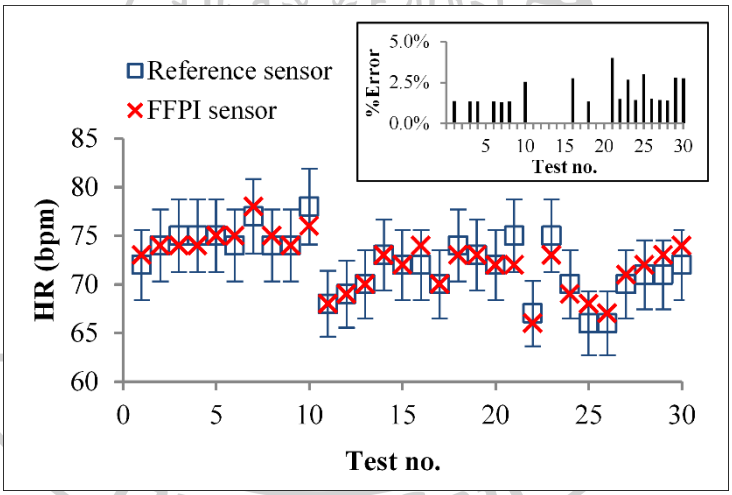

Fig. 4.5 Heart rate measurement results and error analysis

From the HR measurement, a good correspondence between the readings of the FFPI and reference device is observed, with a mean error ± standard deviation (SD) of 1.24% ± 1.16%, respectively. The difference is, incidentally, found to be from the discrepancy in the period of measurement utilized for the calculation. Namely, the sphygmomanometer has an internal timer that decides the period of HR measurement without relaying any information to the user. Meanwhile, a stopwatch is exploited to time the period of measurement for the FFPI. Therefore, an asynchronization issue between the two sensors could contribute to the difference in HR measurement. Regardless, the mean difference lower than 5% suggests the high accuracy of the FFPI system in HR measurement, and by extent in arterial pulse wave detection.

4.2 RESOLUTION IMPROVEMENT FOR HIGH PERFORMANCE PULSE WAVE SENSING

While the fringe counting technique can be applied to develop an FFPI-based arterial pulse wave monitoring system, the limited resolution in measurement is not desirable, especially in case the pulse wave has low amplitude. Therefore, a phase-shift demodulation technique is instead implemented to increase the resolution of the fiber optic system. Subsequently, the phase-shift demodulation technique is investigated in displacement monitoring of a piezoelectric actuator. An example of this investigation is portrayed in Fig. 4.6.

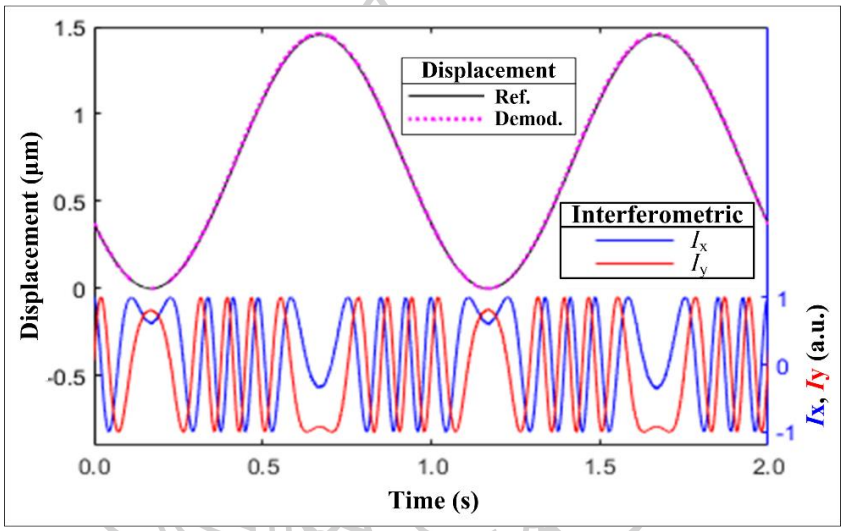

Fig. 4.6 Demodulated displacement via a phase-shift demodulation technique

As seen from the figure, the phase-shift FFPI system can successfully demultiplex two in-quadrature interference signals and then demodulate a corresponding displacement overlapping the reference movement. The demodulated displacement, moreover, has a high resolution in contrast to the fringe counting technique. To further investigate the phase-shift demodulation technique, the FFPI is subsequently tested with various displacement amplitude and frequencies, with the results from the latter illustrated in Fig. 4.7.

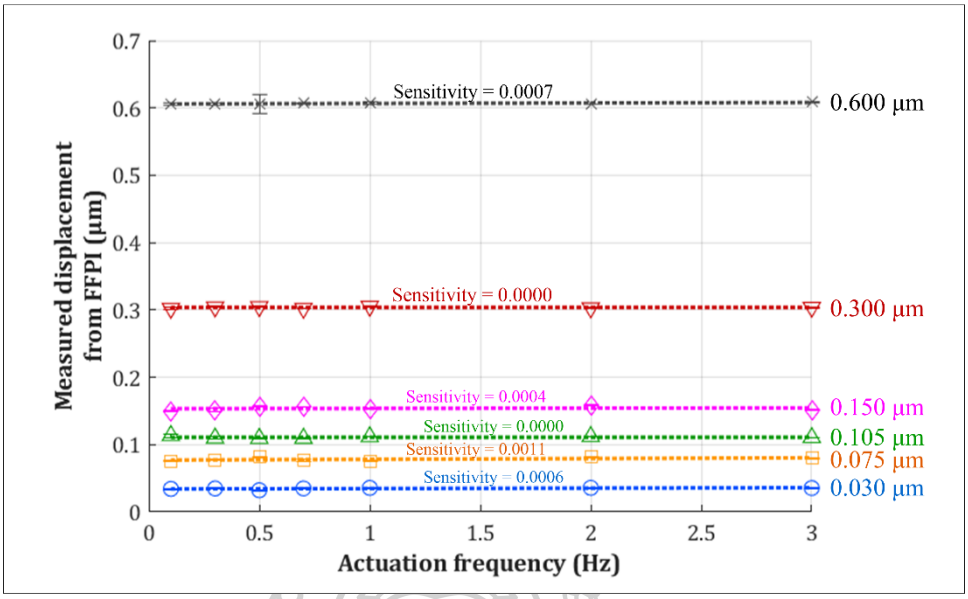

Fig. 4.7 Measured displacement at different actuation frequencies

After the experiment, it is revealed that the displacement in all ranges is linearly correlated to any actuation frequencies. Statistically, the average sensitivity of the displacement is approximately 0.0005 μm/Hz. This means that the actuation frequency does not significantly affect the measured displacement. In conclusion, there is no significant changes in the measured displacement when the input frequency is altered. The main reason is consequently that the FFPI can perform the phase-shift demodulation independently from the frequency of the moving target. This implies that different heart rates of an individual will not affect the displacement measurement during the arterial pulse wave monitoring.

Still, relatively more important information to be investigated is the arterial distension measurement capability of the FFPI system. In this case, the different displacement amplitude experiment has been performed, and Fig. 4.8 shows the results from the investigation, respectively.

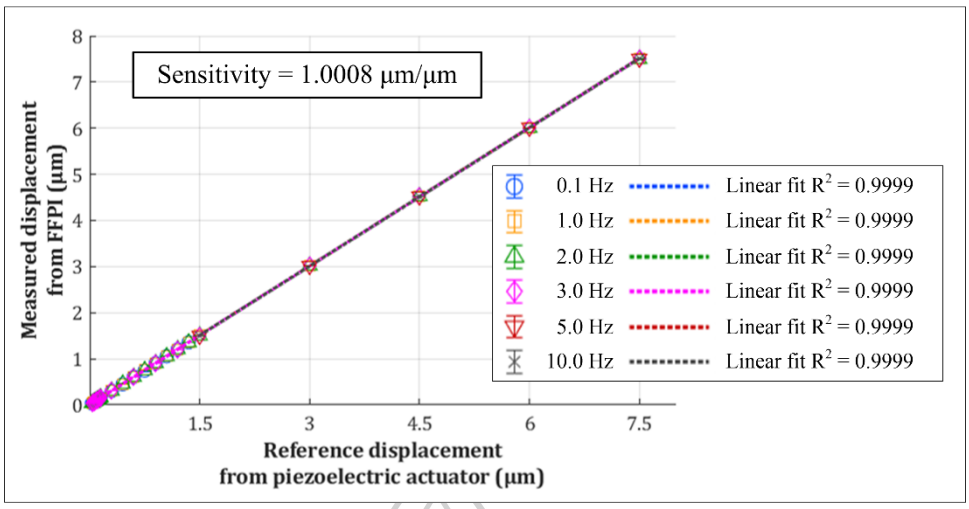

Fig. 4.8 Correlation analysis from actuator experiment

The comparison between the reference and measured displacement reveals high linearity between the parameters, with an average linear fit R^2 in all tested frequencies of 0.9999. This implies the high linearity of the reference and measured displacement. Furthermore, the sensitivity of the phase-shift FFPI found in the displacement measurement is characterized to be 1.0008 µm/µm, which consequently suggests a very high correlation between the measured values and the reference input, contributing to high accuracy of the FFPI system. Still, the resolution of the system is interrogated, and the results can be summarized in Fig. 4.9.

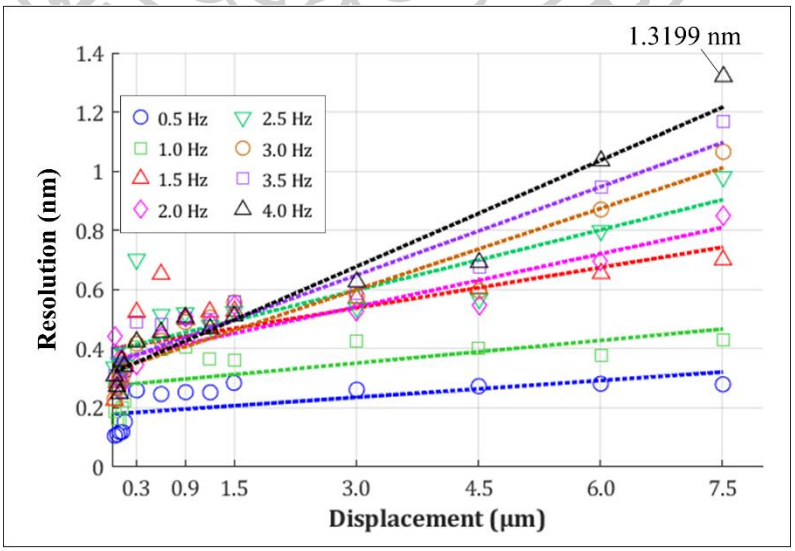

Fig. 4.9 Resolution investigation of phase-shift FFPI system

From the investigation, it is found that the linear slope in each frequency is different, causing the resolution to alternate between different values. Nevertheless, a more consistent relationship can be analyzed by considering the velocity of the actuation (displacement × frequency). In this perspective, it is revealed that the resolution of the phase-shift FFPI is inversely proportional to the velocity profile. At minimum, the resolution is 1.3199 nm at 30 mm/s of movement velocity. This resolution value is considered acceptable for pulse wave monitoring since arterial distension generally has low velocity.

4.3 VALIDATION OF FIBER OPTIC SYSTEM FOR BLOOD PRESSURE MEASUREMENT

Following the displacement measurement verification of the phase-shift FFPI system, it is validated for the blood pressure demodulation capability. Firstly, the FFPI system is applied to monitor the arterial pulse wave of volunteers using the developed engineering application software before the interferometric and demodulated displacement information are analyzed with a dedicated algorithm. By implementing both computation processes, the arterial pulse wave of the participants can be successfully acquired as exemplified in Fig. 4.10.

Once the FFPI probes are set up on a volunteer and the fiber optic system is initiated, the interference signals caused by arterial distension (Fig. 4.10(a)) are monitored by the DAQ. Furthermore, the engineering application software automatically perform the phase-shift demodulation, resulting in the displacement information displayed in Fig. 4.10(b). However, the demodulated displacement, while exhibits the characteristics of a human pulse wave, is slightly unstable. This is due to the motion artifact unintentionally induced during the monitoring, causing a noticeable perturbation to the arterial pulse wave profile. Therefore, the FIR signal filter scheme is employed, which results in the arterial pulse wave to be reconstructed on an arbitrary guideline (as in Fig. 4.10(c)). At this point, the pulse wave characteristics are identified for further usage in the blood pressure demodulation algorithm. Fig. 4.11 shows the identification of the pulse wave characteristics during the period of 3-6 seconds from Fig. 4.10(c).

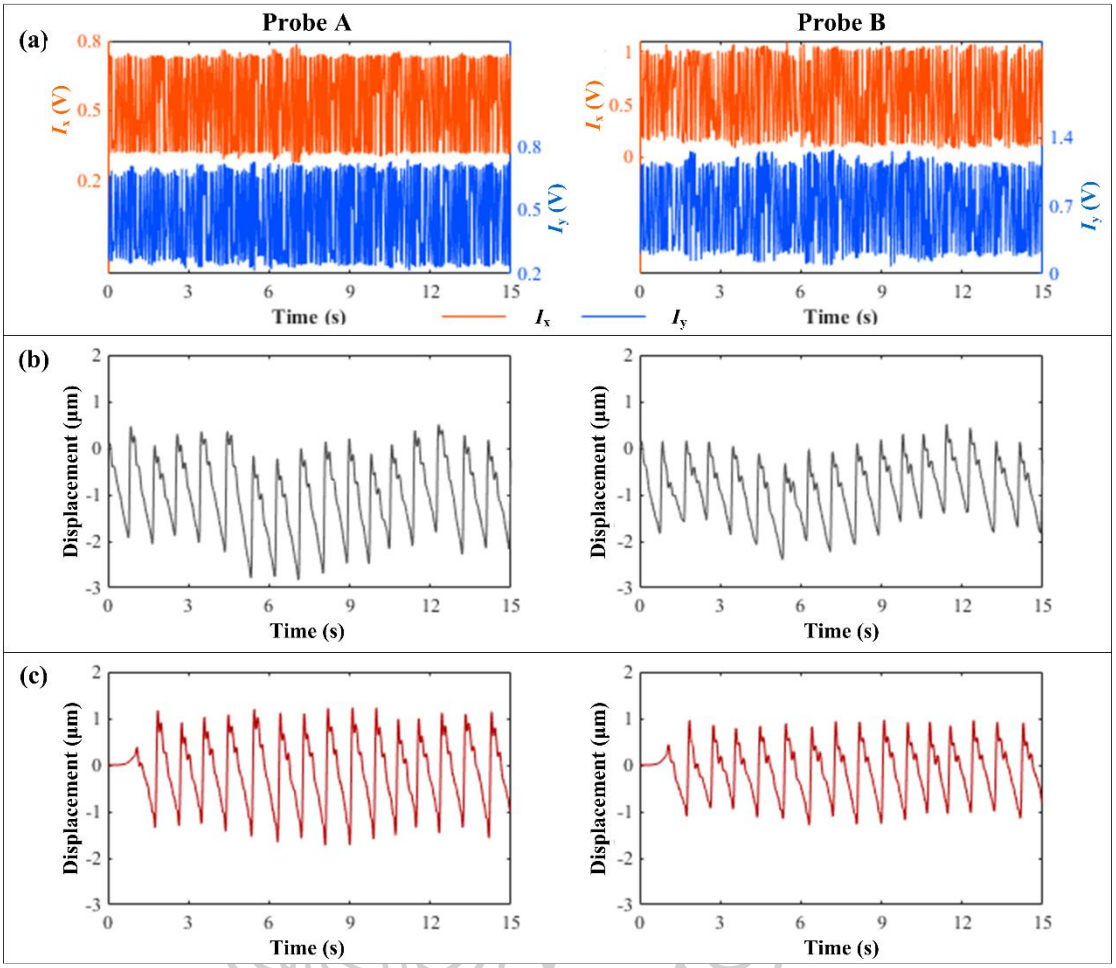

Fig. 4.10 Signals acquired by fiber optic system:
(a) interference signal, (b) demodulated displacement, and (c) filtered displacement of probe A (left) and probe B (right)

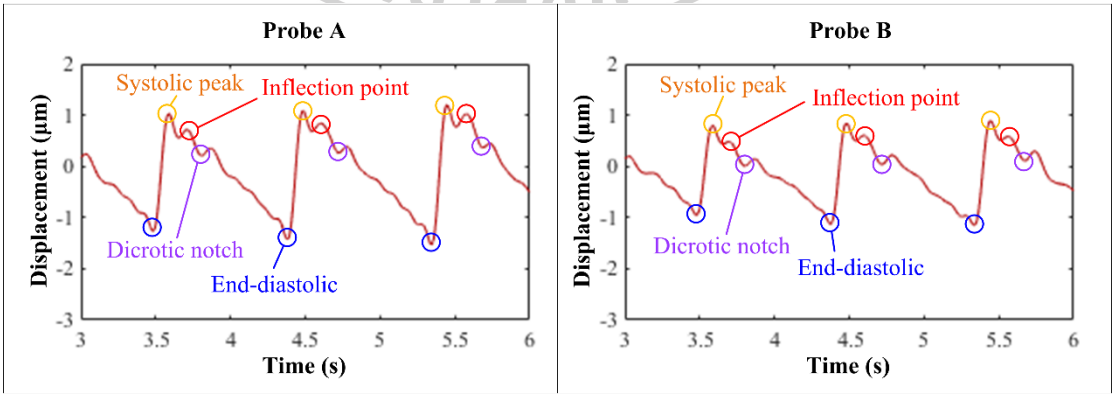

Fig. 4.11 Pulse wave characteristics identification from fiber optic pulse probes

Here, the acquired arterial pulse waves from the FFPI probes A and B have sufficiently high resolution, which allows the identification of the systolic peaks, inflection points, dicrotic notches, and end-diastolics for subsequent analysis. Specifically, the most important parameter to identify in this process is the systolic peaks, which would be counted to demodulate the heart rate of the volunteer. For example, a total of 15 systolic peaks are detected from probe A in Fig. 4.10(c) over 15 seconds, thus the calculated HR using (2.1) equals 60 bpm. Moreover, the pulse transit time (PTT) is determined from the time delay between systolic peaks of probe A and B, which can be demonstrated in Fig. 4.12.

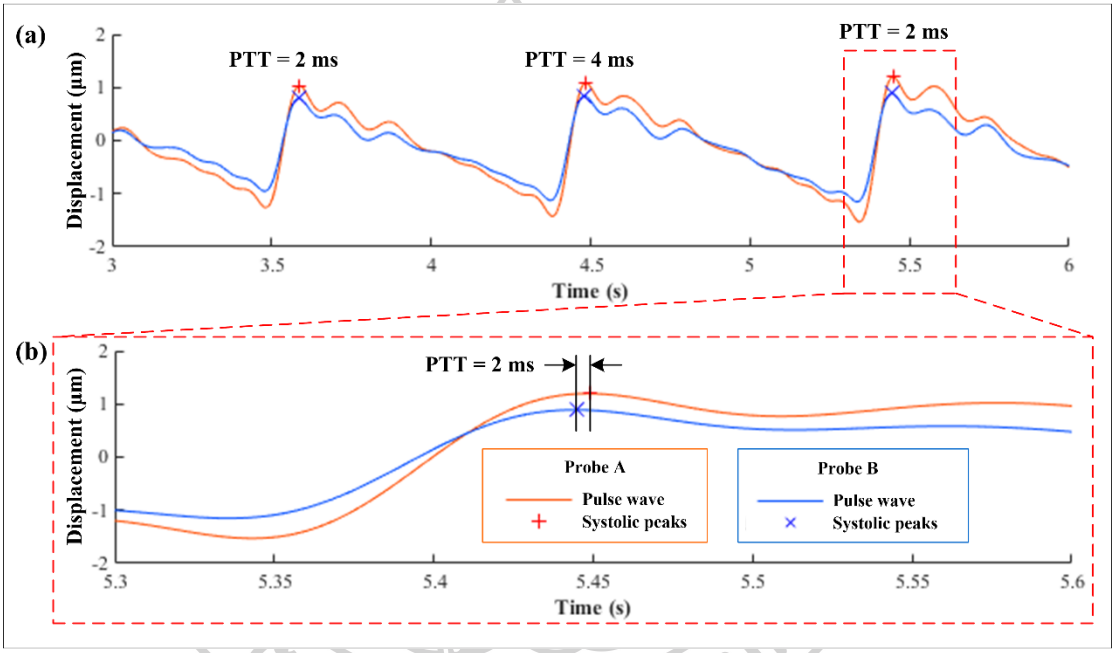

Fig. 4.12 Pulse transit time determination: (a) comparison between pulse waves and (b) time delay between systolic peaks

Since the two FFPI pulse sensing probes are set up on the same radial artery, the probe proximal to the heart (i.e., probe B) will detect the propagating pulse wave before the other (probe A). This results in a slight time delay between the captured systolic peaks as seen in Fig. 4.12(a). Upon closer inspection, the PTT between the peaks can be found, with the value of 2 ms in the case of Fig. 4.12(b). This parameter is, consequently, applied to compute the pulse wave velocity (PWV) in associated with an extrinsically obtained length between the sensors (L), which is 38 mm in this case. Thus, a PWV of 19 m/s is calculated using (2.11). To ensure consistency, the PTT and PWV acquisition is determined to be performed on three consecutive pulse waves selected from the 15-second period and then averaged into a

single value for each measurement. This single PWV value would then be obtained three times from each volunteer to initiate the linear regression analysis for finding a correlation value between PWV and diastolic blood pressure (DBP). Lastly, the measured PWV is calibrated using the correlation parameters into the demodulated DBP to be compared with the reference blood pressure value.

Meanwhile, the pulse pressure (PP) is mainly determined by measuring the pulse amplitude. However, several pulse waves are observed during the 15 seconds period of interrogation. As such, three consecutive pulse waves are selected for the PP measurement, which basically measures the mean difference between the systolic peak and its surrounding two end-diastolic values. Ultimately, the three PP values are averaged into one parameter representing the demodulated PP. Still, a linear regression analysis comparing the measured and reference PP is performed to compensate for the discrepancy due to skin properties. Once the analysis is done, the measured PP is recalculated into the calibrated PP which is later compared against the reference PP to analyze the accuracy of the FFPI system.

After examining all 85 volunteers in the human trial, a comparison between the demodulated and reference blood pressure can be carried out. In broader perspective, the three blood pressure parameters: systolic blood pressure (SBP), diastolic blood pressure (DBP), and pulse pressure (PP), are analyzed and presented in similar statistics. Particularly, the comparison between reference and measured values, absolute error percentage (AE%), and absolute error (AE) categorized in a group of less than 5, 10, and 15 mmHg are analyzed, respectively. In addition, the mean absolute error (MAE) and standard deviation (SD) in percentage and also mmHg are calculated to determine the accuracy of the FFPI system in continuous blood pressure measurement. This format of statistics is, thereby, proposed for the following experimental results, initially by the SBP analysis in Fig. 4.13.

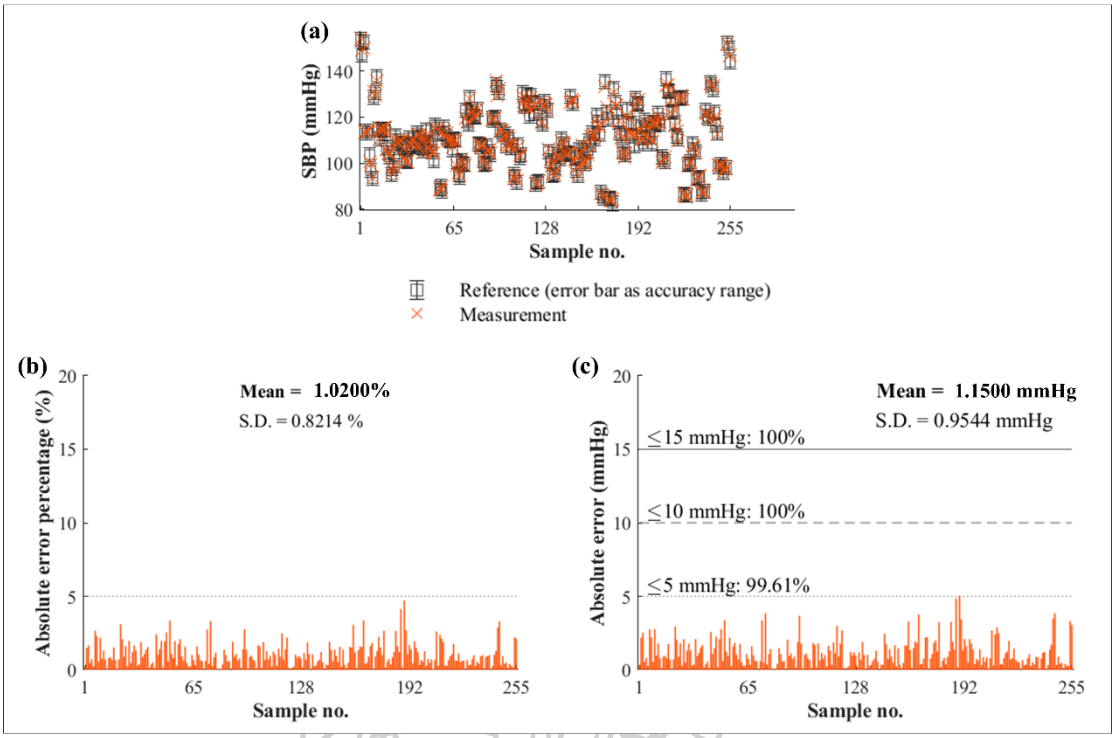

Fig. 4.13 Statistics of demodulated systolic blood pressure analysis: (a) comparison between reference and measured values, (b) absolute error percentage, and (c) absolute error below different criteria

The demodulated SBP from the FFPI system shows high correspondence to the reference readings of the employed reference digital sphygmomanometer with all absolute error percentage below 5%. Moreover, the mean absolute error percentage ± SD is 1.0200% ± 0.8214%, respectively. This indicates a high accuracy in SBP measurement. Nonetheless, the AE in mmHg of unit is also analyzed to categorize the accuracy grade of the FFPI system according to the AAMI/ESH/ISO standard for a blood pressure measuring instrument. In this case, the mean absolute error ± SD in mmHg is 1.1500 ± 0.9544 mmHg, with the percentage of AE within no more than 5, 10, and 15 mmHg at 99.61%, 100.00%, and 100.00%, respectively. Accordingly, the accuracy grade in SBP measurement is determined to be of "*grade A*".

Likewise, the DBP measurement analysis performed in a similar fashion to the aforementioned SBP results can be illustrated in Fig. 4.14.

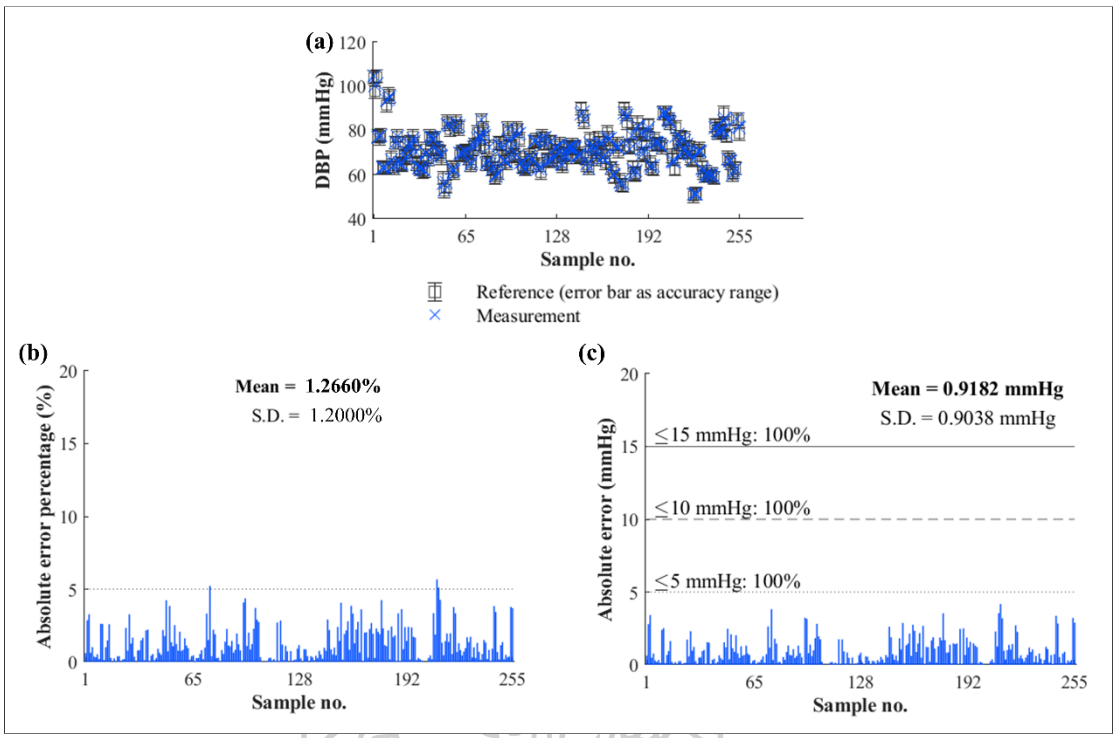

Fig. 4.14 Statistics of demodulated diastolic blood pressure analysis: (a) comparison between reference and measured values, (b) absolute error percentage, and (c) absolute error below different criteria

Similarly, the demodulated DBP presents a high correspondence when compared to the reference sphygmomanometer with the mean absolute error percentage ± SD of 1.2660% ± 1.2000%, respectively. Furthermore, the mean absolute error ± SD in mmHg is found to be respectively 0.9182 ± 0.9038 mmHg, with 100% of the AE below 5, 10, and 15 mmHg of defined error range. Thus, the accuracy grade in DBP measurement is of "*grade A*".

Ultimately, the PP measurement analysis obtained from the examination in 85 volunteers is shown accordingly in Fig. 4.15.

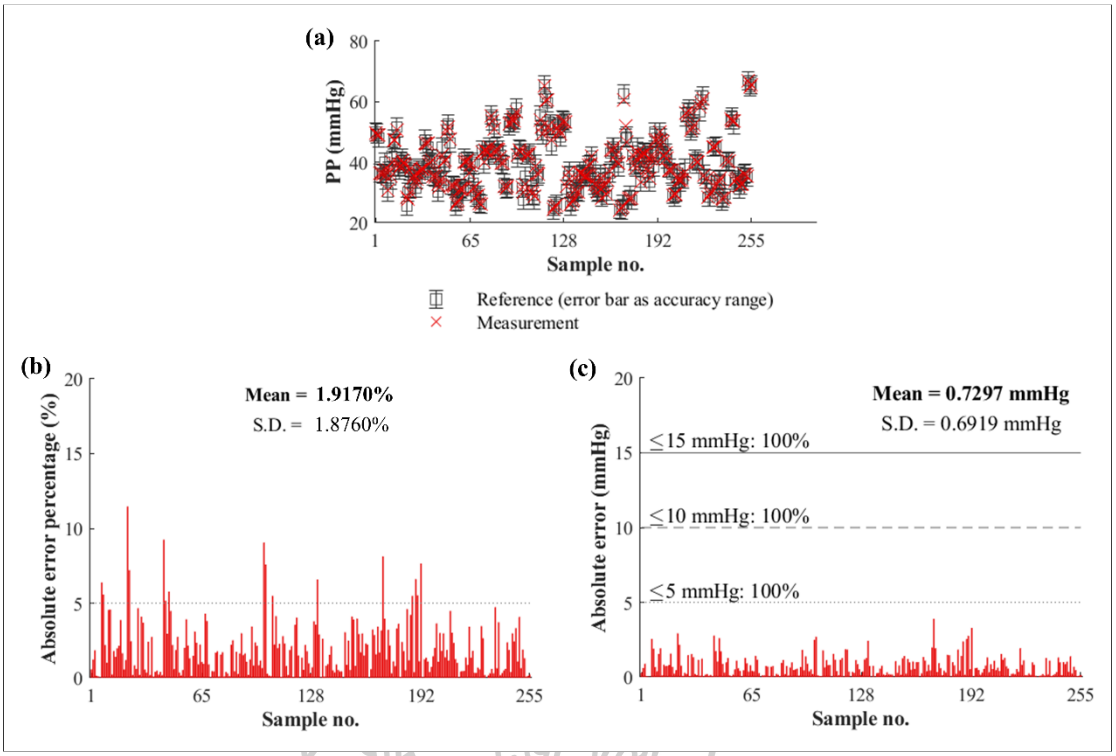

Fig. 4.15 Statistics of demodulated pulse pressure analysis:
(a) comparison between reference and measured values, (b) absolute error percentage, and (c) absolute error below different criteria

The demodulated PP, indifferent from the SBP and DBP measurement, also reveals good correspondence to the reference PP of the sphygmomanometer. In this case, the mean absolute error percentage ± SD of 1.2660% ± 1.2000% corresponding to the error in mmHg of 0.7297 ± 0.6919 mmHg are found from the analysis, respectively. In addition, all AE values are determined to be less than 5 mmHg of error range, meaning that the accuracy grade in PP measurement of the developed FFPI system is of "*grade A*".

Nevertheless, it is important to note the spikes in the absolute error and also its percentage during the SBP, DBP, and PP measurements. Firstly, the absolute error percentage in PP measurement is significantly higher than the other blood pressure parameters due to the lower reference value. To clarify, consider a reference PP of 40 mmHg compared to an arbitrary measured pressure of 41 mmHg. The absolute error between the two values is 1 mmHg with the error percentage of 2.50%. On the other hand, a reference SBP of 120 mmHg compared against an arbitrary reading of 121 mmHg will have an equivalent 1 mmHg of absolute error though the error percentage is instead 0.83%. Therefore, the level of absolute error percentage is inversely proportional to the reference blood pressure, with PP having the

most tendency for higher error percentage, followed by DBP, and then SBP. Regardless, the main reason for the spiking error is due to the calibration process in each individual. In particular, the three measurements taken to establish a calibration curve directly influence the output of blood pressure demodulation. If the three consecutively measured blood pressure (either SBP, DBP, or PP) have not significantly distributed between one another, the calibration curve would exhibit good correlation, resulting in more accurate and less erroneous blood pressure readings. In contrast, highly distributed blood pressure values will cause less correlation in the calibration curve fitting, consequently leading to higher error as observed from the experiments. In this aspect, it is suggested that the calibration process in each individual should be carefully conducted to prevent significant errors from occurring. Nonetheless, the error spikes are still analyzed to provide the overall accuracy rating of the developed FFPI.

From the aforementioned analyses of SBP, DBP, and PP measurement, the overall capability of the FFPI system as a blood pressure instrument can be considered of high accuracy with a "*grade A*" level when categorized using the AAMI/ESH/ISO standard. The human trial, furthermore, indicates the dynamic blood pressure measurement range of the FFPI system, which is 17.6425-154.7240 mmHg as experimentally validated.

However, the FFPI system is also intended to be validated for its HR measurement capability, thus additional statistics in HR measurement are conducted. The results of this analysis are, consequently, presented in Fig. 4.16.

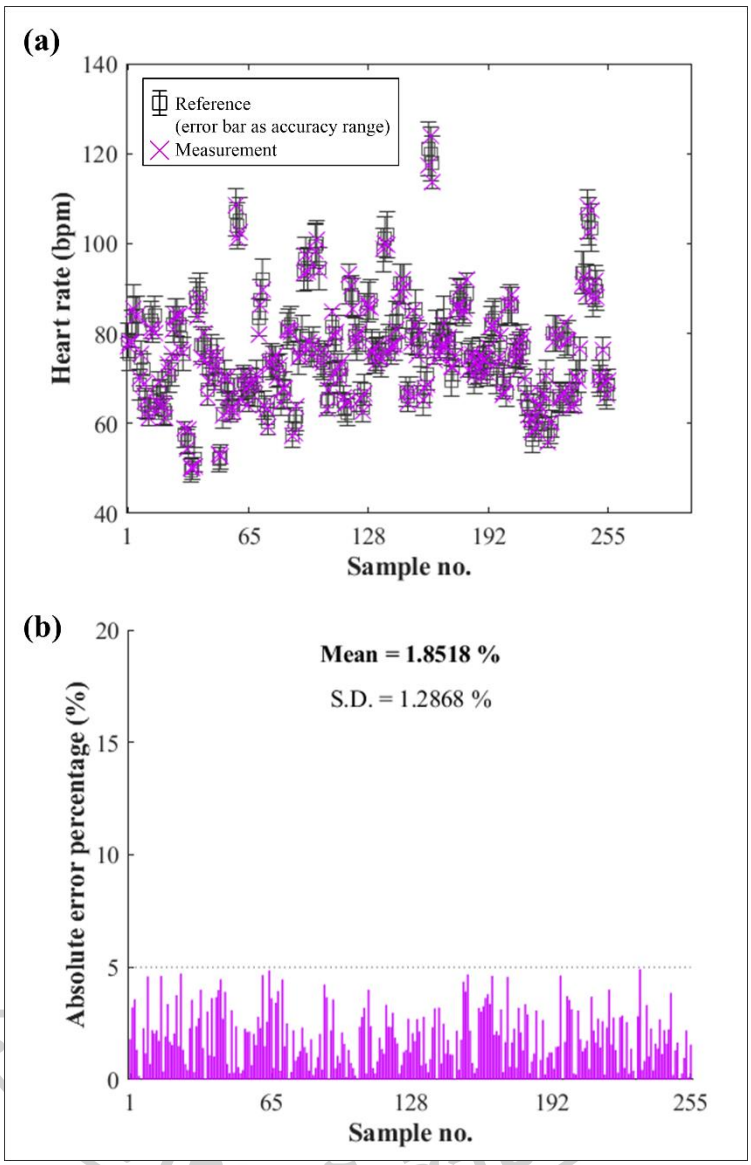

Fig. 4.16 Statistics of demodulated heart rate analysis:
(a) comparison between reference and measured values and (b) absolute error percentage

In contrast to the blood pressure analysis, the HR statistics mainly concern the absolute error percentage of the instrument in interrogation, which is averaged to be 1.8518% ± 1.2868% of SD, respectively. Moreover, all demodulated HR lies below 5% of absolute error, showing high correspondence between the measured and reference readings. In this aspect, the proposed FFPI system is considered highly accurate in HR Measurement. From the human trial, it is also found that the dynamic HR measurement range of the fiber optic system is 49.9735-123.9185 bpm. Therefore, the overall capabilities of the FFPI system in continuous blood pressure measurement can be summarized in Table 4.1.

Table 4.1 FFPI system capabilities in continuous blood pressure measurement

Parameters	Mean absolute error	Standard deviation	Accuracy	Accuracy grade
Systolic blood pressure (SBP)	1.1500 mmHg	0.9544 mmHg	98.9800%	A
Diastolic blood pressure (DBP)	0.9182 mmHg	0.9038 mmHg	98.7340%	A
Pulse pressure (PP)	0.7297 mmHg	0.6919 mmHg	98.0830%	A
Heart rate (HR)	1.8518%	1.2868%	98.1482%	-

In the table, the accuracy values of all parameters are an inverse of the mean absolute error percentage described in the aforementioned statistics. Regardless, the overall accuracy in blood pressure and HR measurement is above 98%, which is considered high. The accuracy grade in blood pressure measurement is, further, of the "*grade A*", the highest grade in the AAMI/ESH/ISO standard. This, consequently, suggests the high accuracy of the FFPI system as a blood pressure measuring instrument, paving ways for future development of the fiber optic sensor into novel biomedical devices.

Ultimately, the performance of the developed FFPI system for blood pressure measurement can be summarized in Table 4.2

Table 4.2 Summarized specifications of developed FFPI system

Parameters	Value
Sensitivity	1.0008 μm/μm
Resolution	1.3199 nm
Accuracy:	Grade A
Systolic blood pressure (SBP)	98.9800%
Diastolic blood pressure (DBP)	98.7340%
Pulse pressure (PP)	98.0830%
Heart rate (HR)	98.1482%
Dynamic range:	
Blood pressure measurement	17.6425-154.7240 mmHg
Heart rate measurement	49.9735-123.9185 bpm

In general, the FFPI system exhibits a sensitivity in displacement measurement of 1.0008 μm/μm while its resolution is 1.3199 nm. This, consequently, allows the fiber optic sensor to detect a very small arterial distension from an arterial site of interest (in this work, the radial artery on the wrist). Thus, the pulse wave can be monitored at a very low pressure owing to the high sensitivity. The high resolution, meanwhile, enables the pulse wave characterization of the systolic peaks, inflection points, dicrotic notches, and also end-diastolics, which are essential in subsequent blood pressure demodulation. To further investigate the performance of the FFPI sensor developed in this dissertation, a comparison of the work to other literature is performed according to Table 4.3.

Table 4.3 Sensitivity and resolution comparison between literatures

Research	Ref.	Sensor type	Sensitivity	Resolution (nm)
Developed FFPI	-	FFPI	1.0008 μm/μm	1.3199
Leitão *et al.*	[48]	FBG	21.2000 pm/μm	20.0000
Leitão *et al.*	[100]	Intensity-based fiber optic	727.2000 μV/μm	50.0000
Jia *et al.*	[140]	FBG	8.2360 nm/N	-
Tang *et al.*	[142]	FBG	0.103 pm/mm	0.4700

From the comparison, it is found that the sensitivity values characterized in each literature have different units of measurement. This is due to the characterization process, specifically the output parameters from the developed fiber optic sensors compared to the input displacement of a reference device. For example, the FFPI sensor developed in this dissertation has characterized the sensitivity by using a piezoelectric actuator. Incidentally, both instruments yield the displacement information, leading to the unit of μm/μm or unitless. Leitão *et al.*'s work [48] however characterized an FBG sensor against a reference arterial distension simulating device, the former providing an output optical wavelength in pm while the latter generating a displacement in μm. Moreover, another of the researcher's work [100] utilized the same reference device though applied an intensity-based fiber optic sensor instead. Since the intensity-based optical sensor output the voltage in response to the reflected light, the sensitivity was consequently determined in μV/μm. For Jia *et al.* [140], the proposed pulse wave detecting fiber optic sensor was tested with a force generating actuator, thus the sensitivity was provided in nm/N. Therefore, the sensitivity values presented in each literature are different in the unit of measurement. Nevertheless, the input displacement using the reference instruments is generally given in μm, meaning that an arterial pulse sensing fiber optic system should be highly sensitive to at least detect the displacement as low as in

micrometer scale. Therefore, it can be concluded that the developed FFPI in this dissertation has high sensitivity.

On the other hand, the resolution in pulse wave monitoring has also been investigated in several literatures. Unlike the sensitivity value, the measurement resolution is, however, determined using the similar unit of nanometers. In metrology, lower discrimination value is inversely proportional to higher resolution when an instrument is modulated by external perturbations such as arterial distension. In this case, the instrument with the highest resolution rating is Tang *et al.*'s FBG sensor [142] with a resolution of 0.47 nm. This is, however, followed secondly by the developed FFPI in this work with the rating of 1.1399 nm and thirdly by Leitão *et al.*'s FBG pulse sensing probe [48]. Regardless, it is reported in a pathological case that arterial distension can have an amplitude of a few micrometers to approximately 700 μm [53]. This implies that an arterial pulse monitoring machine should have a resolution rating in the micrometric scale. Therefore, this dissertation concludes that the FFPI system has high resolution in arterial pulse wave monitoring and blood pressure measurement.

Furthermore, the dynamic range of the FFPI system can be theoretically determined by calculating the lowest possible pressure to be demodulated. Using (2.10), the lowest possible blood pressure to be measured would be 1.9665 picometers of mercury (pmHg) whereas the upper limit is infinite. However, this dynamic range has not been experimentally verified and has only been proven in paper. From the human trial, the dynamic range in blood pressure measurement of the fiber optic sensor is, consequently, defined by the lowest to highest blood pressure demodulated from the experiment, which is 17.6425-154.7240 mmHg, respectively. Meanwhile, the HR measurement is also validated in this dissertation, which exhibits a different dynamic range due to different demodulation techniques. Here, the HR dynamic range is experimentally found to be 49.9735-123.9185 bpm.

From the human trial, the accuracy of the FFPI system in SBP, DBP, PP, and HR measurement exceeds 98%, implying high accuracy in blood pressure measurement. Also, the accuracy grade of "*A*" has been categorized according to the AAMI/ESH/ISO standard, further validating the high accuracy aspect of the fiber optic sensor. The experiment, moreover, characterized the dynamic range in blood pressure measurement to be 17.6425-154.7240 mmHg, whereas the heart rate measurement range is 49.9735-123.9185 bpm, respectively. In conclusion, the developed FFPI system is proven to have high accuracy, high sensitivity, and high resolution in blood pressure measurement. This system could, therefore, be developed further into a novel continuous blood pressure measuring instrument in the biomedical engineering field.

4.4 ENERGY CONSUMPTION CONSIDERATIONS

After the validation of the developed FFPI system in blood pressure measurement, this dissertation also analyzes the energy consumption required to operate the system in practice. In Table 4.4, the list of power consuming equipment of the FFPI system is summarized.

Table 4.4 Lists of power consuming optoelectrical equipment

Device	Amount	Power consumption per unit (W)	Total power consumption (W)
Laser diode driver	1	30	30
Laser diode temperature controller	1	60	60
InGaAs Photodetector	2	6	12
Multifunction data acquisition unit (DAQ)	1	0	0
Arbitrary waveform generator	1	30	30
Desktop computer	1	280	280
Display monitor	1	176	176
Total power consumption			**588**

From the analysis, it is found that the most power consuming component is the desktop computer with the power rating of 280 W. Furthermore, the display monitor connected to the computer has the second-most power consumption at 176 W. In this perspective, the computer unit, including the computer processing unit (CPU) and also the monitor, consumes high power relative to the optical components such as the laser diode driver and controller. Note that the multifunction DAQ reported 0 W of power consumption due to very low electricity requirements, which is supplied indirectly by the computer. Regardless, the total power consumption of the developed FFPI system equals 588 W.

However, the energy consumption of an electrical system is generally characterized by considering the operation period. For the FFPI system, equipment is recommended to be activated at least 10 minutes before operation for stability and accuracy. Therefore, the initial energy consumption due to device preparation totals 98 W·hr. From the validation through human trials, the operation period of the FFPI system to complete a blood pressure measurement of a single volunteer is 15-20 minutes. This means the energy consumption is

147-196 W·hr per measurement of one volunteer. Afterwards, the system can be shut down, leaving only the computer unit for post-measurement analysis, which takes approximately 30 minutes to complete. Consequently, the post-operation energy consumption of the fiber optic sensor is reduced to 228 W·hr.

Nevertheless, the FFPI system would be continuously activated throughout the entire working day to perform blood pressure measurement in practical applications. Therefore, the energy consumption of the fiber optic sensor considering the working period from 8.00 to 17.00 hours can be demonstrated in Fig. 4.17.

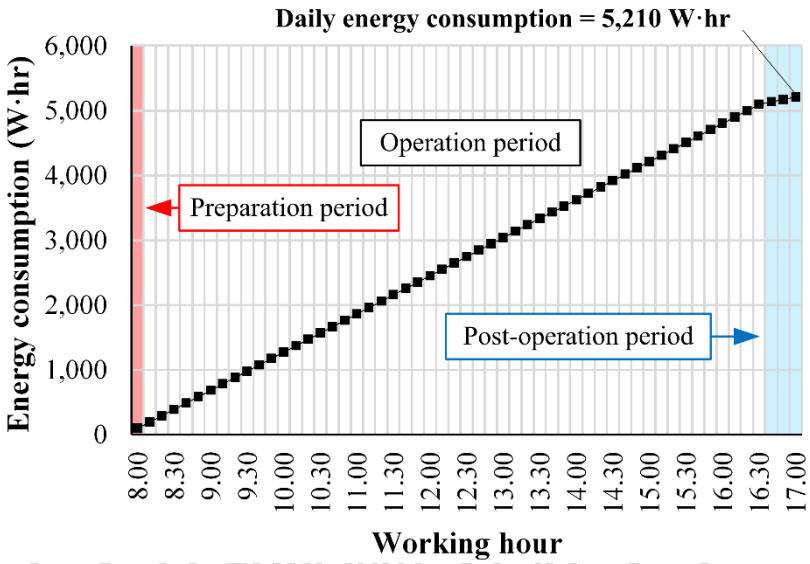

Fig. 4.17 Daily energy consumption of developed fiber optic system

Assuming that the developed fiber optic system is exploited in the working hours, the first 10 minutes will be spent to prepare the equipment before operation. The system is, subsequently, activated and continuously performed the blood pressure measurement throughout the day until 16.30 when the last examination ensued. After 16.30, the collected arterial pulse wave data is, consequently, demodulated and analyzed before the entire system is shut down after work. Overall, the daily energy consumption of the FFPI system would be 5,210 W·hr, which would also not be spiked due to sudden device activation. In economic terms, only the energy consumption during the preparation period can be considered as an initial cost, while the rest contributes to operation cost.

4.5 COST ANALYSIS OF A FIBER OPTIC BLOOD PRESSURE MEASURING SYSTEM

From the experiments, it is concluded that the phase-shift FFPI system is able to perform continuous blood pressure measurement on humans with high accuracy, sensitivity, and resolution. Still, it is imperative to analyze the development cost of the fiber optic sensor for future development of a commercial biomedical instrument in the future. In this case, the procurement cost of equipment utilized to configure the fiber optic system is preliminarily described in this section.

In this dissertation, the optical instruments applied to construct the fiber optic sensor mainly involve the assembly of laboratory-grade equipment purchased from specialized manufacturers in the optical engineering field. Here, the procurement cost of the equipment is based on the price listed by the distribution in the product catalogue. From the price survey, it is however found that any components imported from overseas are quoted in foreign currency, generally in United States Dollars (USD). Thus, the price is converted from USD into Thai Baht (THB) using the conversion rate of 36.4102 THB/USD [150]. Nevertheless, some items are, consequently, implied to be procured within Thailand, commonly from local stores and manufacturers, contributing to lower price. Still, all equipment prices shall be summarized in THB as the basis for this analysis.

The following are the procurement costs for the configuration of a fiber optic system for continuous blood pressure measurement categorized into two main groups: fiber optic probe design and signal processing system. Table 4.6, subsequently, lists the cost for the former group.

Table 4.5 Development cost of a fiber optic pulse sensing probe

Item	Amount	Price per unit (THB)	Total price (THB)
Collimating lens	1	6,590.25	6,590.25
Collimator adapter	1	1,232.49	1,232.49
Lens tube	2	495.91	991.82
Retaining ring	1	177.32	177.32
Silver-protected mirror	1	1,255.42	1,255.42
Plastic diaphragm	1	120.00	120.00
Protruding structure	1	50.00	50.00
Total cost			**10,417.30**

When constructing a fiber optic sensing probe, optical components such as lens and mirrors are revealed to have high cost due to guaranteed performance by the manufacturers

which also increases the product value. Likewise, the optomechanical parts of retaining rings, lens tubes, and collimating adapters are purposedly designed to integrate with the mentioned optics, thereby having their values added. The relatively lower price components, in this case, are the plastic thin film and protruding structures purchased from local stores. While the performance has not been guaranteed, the items have effectively been exploited in the blood pressure measurement. In this regard, components can be procured from local shops to reduce the development cost of the fiber optic probe, provided that the functionality is not impeded. Note that the presented price in Table 4.5 is for a single fiber optic probe, meaning that the total development cost of the two probes used in this dissertation is 20,834.60 THB.

Furthermore, the development cost of the signal processing system enabling the application of the fiber optic sensing probes is explained in Table 4.6.

Table 4.6 Development cost of a signal processing system

Item	Amount	Price per unit (THB)	Total price (THB)
Near infrared fiber-pigtailed laser diode (LPS-1310-FC)	1	19,679.71	19,679.71
Temperature-controlled laser diode mount	1	27,562.89	27,562.89
Laser diode driver	1	44,067.63	44,067.63
Laser diode temperature controller	1	42,733.20	42,733.20
1x2 Fiber coupler	1	11,505.62	11,505.62
Fiber Optical circulator	2	19,853.39	39,706.78
Fiber patch cord	2	2,215.56	4,431.12
InGaAs Photodetector	2	17,344.36	34,688.72
Multifunction data acquisition unit	1	22,428.68	22,428.68
Arbitrary waveform generator	1	11,978.96	11,978.96
Desktop computer	1	39,500.00	39,500.00
Total cost			**298,283.31**

The signal processing system includes the optical propagation and signal demodulation components for the operations of the FFPI system in continuous blood pressure measurement. Thus, the procurement cost is due to the installation of the laser source, fiber optic transmission paths, and signal acquisition using electronic machines. Incidentally, all optical components have been procured from a specialized laboratory-grade manufacturer and lead to high development cost. The electronic components for the signal acquisition and analysis are relatively cheaper in comparison. Nevertheless, the utilized optical equipment

ensures high reliability in the experimentation which primarily aims to investigate the potential of the fiber optic sensor in blood pressure measurement.

Overall, the total cost of system development is 319,117.91 THB, mostly due to the initial optical machines required to activate the fiber optic sensor. In particular, the laser diode driver is the most expensive component to procure, followed secondly by the laser diode temperature, and thirdly the computer for signal processing, respectively. This, consequently, implies that the optical components are the main contributor of high development cost when constructing a fiber optic system. In fact, the expensive equipment for both the optical propagation system and fiber optic pulse sensing probe stems from the optical components such as collimating lens, silver-protected mirror, fiber-pigtailed laser diode, fiber optical circulator, etc. However, the objective of this dissertation is to develop a fiber optic blood pressure sensor prototype for investigating its potential in future implementation. Therefore, laboratory-grade equipment has been implemented in the designing while the development cost has not been mainly concerned. Nevertheless, it is important to note that the applied system components can be optimized for cost reduction in the production stage. For example, the laser diode mount, laser driver, and temperature controller can be replaced with alternative laser manipulation devices of cheaper price. Similarly, the arbitrary waveform generator is required to modulate the laser current at an unchanged frequency, thus a dedicated laser modulating module might be employed instead. This would, ultimately, lower the implementation cost of the fiber optic blood pressure measuring system for market competitions.

To analyze the commercial viability of the developed fiber optic sensor, a comparison between commercially available blood pressure instruments is shown in Table 4.7.

Table 4.7 Price comparison of modern blood pressure instruments

Instrument	**Measurement**	**Availability**	**Target group**	**Pricing (THB)**	**Price survey**
Phase-shift FFPI	Continuous	Under research	N/A	319,117.91	Procurement
OMRON HEM-7130	Discrete	Commercial	Home user	1,800.00	Quotation
SphygmoCor	Continuous	Commercial	Hospital	1,300,000.00	Quotation
Finapres NOVA	Continuous	Commercial	Hospital	27,797.00	Online

The presented commercial blood pressure devices discussed in this section are surveyed either from online commercial sources or quotation from the distributors. The *OMRON HEM-7130*, in this case, has been applied as the reference instrument in the investigation, and the price is from the procurement. The price of *SphygmoCor* has, however, been quoted directly from the manufacturer, while the *Finapres NOVA* has been surveyed online. The latter two blood pressure measuring devices are, nevertheless, considered comparable to the fiber optic sensor in terms of continuous non-invasive blood pressure measurement. From the comparison, it is found that the *SphygmoCor* has the highest price in contrast to *OMRON HEM-7130* which is the cheapest. This is speculatively due to the purpose of the instruments; *SphygmoCor* is exploited for arterial pulse wave interrogation, thus has higher cost in exchange for higher reliability. Meanwhile, *OMRON HEM-7130* is designed for portable home health monitoring and optimized for availability to the general public. *Finapres NOVA*, on the other hand, is more prevalent in hospital settings where continuous non-invasive blood pressure measurement is preferred over intermittent sphygmomanometer usage. Competitively, this suggests that the developed fiber optic sensor lies between the *Finapres NOVA* and *SphygmoCor*, meaning that it might be viable as a novel hospital-based biomedical instruments. While the development cost could be less preferrable compared to the *OMRON HEM-7130* in home health monitoring, the fiber optic system might play a more crucial role in specific cardiovascular health investigation within medical institutions rather than in the commercial market.

4.6 SUMMARY

From the experimentations in all dissertation phases, the results have been investigated and subsequently shown the capabilities of the developed FFPI system in continuous blood pressure measurement. Firstly, a preliminary arterial pulse wave detection using a fringe counting technique has been conducted and found that the fiber optic system can retrieve human pulse waves in continuous operation. The sensitivity and resolution analyzed in this phase were, moreover, found to be 1.916 mmHg/fringe, and had then been improved via a phase-shift demodulation technique. Subsequently, sensing probe characterization through a displacement actuation has concluded the improved measurement sensitivity of 1.0008 μm/μm with resolution of 1.3199 nm. Following these findings is, ultimately, the validation of the FFPI in human examination, and the improved sensitivity and resolution of the system proved useful in arterial pulse wave characterization for further analysis. At this point, the blood pressure demodulation was carried out and revealed highly accurate blood pressure readings compared to a reference sphygmomanometer. The accuracy

of the FFPI in blood pressure measurement is, therefore, validated to have a "*grade A*" performance, equivalent to high accuracy in the biomedical application. Afterwards, the energy consumption profile of the developed FFPI system has been evaluated at 5,210 W·hr assuming a daily operation in a working environment. Moreover, the development cost of the fiber optic system has been considered, which yielded a total of 319,117.91 THB. While this number is relatively high for a commercial blood pressure instrument, the main cause is the price of laboratory-grade equipment that could potentially be replaced by optimizing the essential components of the FFPI system to reduce both the price and the size of the entire system. This shall, also, lead to a more compact and practical fiber optic instrument for operations in the field. With the aforementioned findings, the dissertation is concluded with remarks on the limitations during the investigation and future prospects of the developed fiber optic sensor additionally summarized in the next chapter.

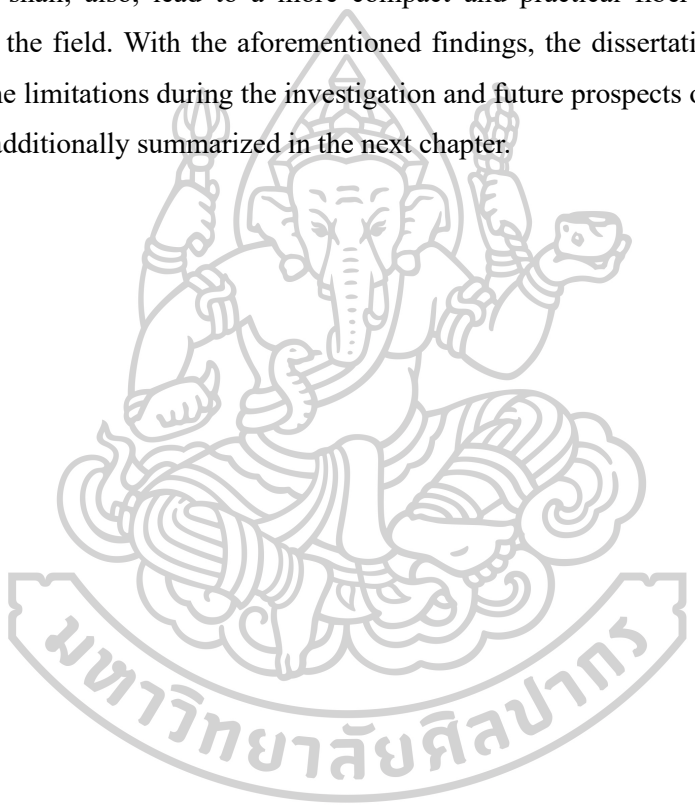

CHAPTER 5
CONCLUSION

In this chapter, the conclusion of this dissertation as well as the limitations and future prospects of the research are discussed. The former section, particularly, summarizes the findings from the experimental results, while the limitations part discusses the primary problems during the research. The future prospect, then, provides suggestions to overcome the limitations in this dissertation.

5.1 CONCLUSION

In this dissertation, the development of a fiber optic sensor for continuous blood pressure measurement has been investigated with high accuracy, high sensitivity, and high resolution in operation. Particularly, a fiber optic Fabry-Perot interferometer (FFPI) has been considered owing to the advantage in small size, lightweight, high sensitivity, and electromagnetic immunity. Moreover, thin film deflection and pulse wave velocity theories have been applied as the main blood pressure demodulation techniques. After the implementation of a preliminary FFPI system for arterial pulse wave detection, subsequent improvement of its resolution for continuous pulse wave monitoring, and finally validation through human trial, the developed FFPI system has demonstrated its capability for continuous blood pressure measurement. In summary, the performance of the FFPI system is presented in Table 5.1.

Table 5.1 Summary of FFPI system capabilities in blood pressure measurement

Parameters	Value
Sensitivity	1.0008 μm/μm
Resolution	1.3199 nm
Accuracy:	Grade A
Systolic blood pressure (SBP)	98.9800%
Diastolic blood pressure (DBP)	98.7340%
Pulse pressure (PP)	98.0830%
Heart rate (HR)	98.1482%
Blood pressure measurement	17.6425-154.7240 mmHg
Heart rate measurement	49.9735-123.9185 bpm
Energy consumption	588 W
Estimated development cost	319,117.91 THB

In general, the FFPI system exhibits a sensitivity in displacement measurement of 1.0008 while its resolution is 1.3199 nm. This, consequently, allows the fiber optic sensor to detect a very small arterial distension from an arterial site of interest (in this work, the radial artery on the wrist). Thus, the pulse wave can be monitored at a very low pressure owing to the high sensitivity. The high resolution, meanwhile, enables the pulse wave characterization of the systolic peaks, inflection points, dicrotic notches, and also end-diastolics, which are essential in subsequent blood pressure demodulation. From the human trial, the accuracy of the FFPI system in SBP, DBP, PP, and HR measurement exceeds 98%, implying high accuracy in blood pressure measurement. Also, the accuracy grade of "*A*" has been categorized according to the AAMI/ESH/ISO standard, further validating the high accuracy aspect of the fiber optic sensor. The experiment, moreover, characterized the dynamic range in blood pressure measurement to be 17.6425-154.7240 mmHg, whereas heart rate measurement range is 49.9735-123.9185 bpm, respectively. In conclusion, the developed FFPI system is proven to have high accuracy, high sensitivity, and high resolution in blood pressure measurement. Additionally, the energy consumption of the developed FFPI system is determined to be 588 W, which contributes to an approximated daily energy usage of 5,210 W·hr assuming the system is operated for an entire working day. For the development cost, the system is estimated to have 319,117.91 THB, with the expensiveness mostly due to the high prices of the optoelectrical devices such as laser controlling and computer units. This could, however, be reduced by optimizing the fiber optic system to utilize specially designed smaller cost-effective optoelectrical components which not only decrease the procurement cost but might also increase the compactness of the FFPI system. In conclusion, the developed fiber optic sensor demonstrates high capabilities in continuous blood pressure measurement and could be further considered in future research of novel biomedical instruments.

5.2 LIMITATIONS

While the proposed FFPI system has high accuracy, high sensitivity, and also high resolution in blood pressure measurement, several limitations and obstacles should be discussed. Firstly, the high sensitivity of the fiber optic sensor allows the detection of very small displacement on the human skin. However, this high sensitivity can be perturbed by motion artifacts, which results from the movement of the volunteer during the pulse wave monitoring. Since remaining still can prove to be challenging, it is almost always observed that the motion artifact affects the pulse wave, generally by offsetting the waveform with slight inclination or declination. Secondly, the employed thin film (either reflective or non-

reflective) directly affects the quality of the acquiring pulse wave. In specific, more elastic thin film would lead to greater deflection and by extension the system sensitivity. However, the reflection of the laser might misalign and disable the FFPI principle if the sensing signal cannot be coupled back into the fiber probe. In contrast, more rigid thin film reduces the misalignment possibility, though the deflection would be lower and decrease the sensitivity of the FFPI system. Lastly is the physiological aspect of the human volunteer under examination, which can significantly alter the principles behind the FFPI system. For example, soft forearm tissue could be difficult to set up the sensing probe, as it causes uneven alignment of the deflecting thin film. On the other hand, dense muscular wrist could prevent any palpation of the FFPI probe, leading to unobtainable or difficult acquisition of the arterial distension. These obstacles, while solved within this dissertation, could potentially limit the application of the proposed FFPI system in blood pressure measurement. Nevertheless, it can be possible to compensate for the effects of such obstacles, as described in the next section.

5.3 FUTURE PROSPECTS

In summary, the limitations of the FFPI system are generally due to the physiological aspects of the human to be examined, combined with the misalignment and choices of FFPI probe design. Therefore, one solution is to consider a fiber optic pulse sensing probe which can accommodate all physiques. For example, the probe might require a cuff inflated with a certain air pressure to secure the FFPI sensing probe to the wrist. Alternatively, several replaceable sensing probe designs might be introduced according to the different human characteristics (e.g., longer protruding part for soft tissue person or smaller probe size for small wrists). For the motion artifact problems, a novel movement-compensating algorithm or signal filtering may, however, be developed to reduce the unwanted movement during the examination. These recommendations could be useful for the future development of the FFPI system for continuous blood pressure measurement.

REFERENCES

[1] B. Zhou, P. Perel, G. A. Mensah, and M. Ezzati, "Global epidemiology, health burden a effective interventions for elevated blood pressure and hypertension," *Nature Revie Cardiology,* vol. 18, no. 11, pp. 785-802, 2021.

[2] "Types of Blood Pressure Medications", American Heart Association. Accessed on: 14 M 2024 [Online]. Available: https://www.heart.org/en/health-topics/high-bloc pressure/changes-you-can-make-to-manage-high-blood-pressure/types-of-blood-pressure- medications

[3] C. M. McEniery, J. R. Cockcroft, M. J. Roman, S. S. Franklin, and I. B. Wilkinson, "Cent blood pressure: current evidence and clinical importance," *European Heart Journal,* vol. 3 no. 26, pp. 1719-1725, 2014.

[4] J. E. Hall and M. E. Hall, *Guyton and Hall Textbook of Medical Physiology*, 14 Philadephia: Elsevier, 2021.

[5] F. D. Fuchs and P. K. Whelton, "High Blood Pressure and Cardiovascular Diseas *Hypertension,* vol. 75, no. 2, pp. 285-292, 2020.

[6] Tahani Saleem Alsinani, Ahmed Anis Abdullah, S. A. S. A. Talal Abdullah Algham Malik Dham Alanazi, , Mohammed Ayedh Alkahtani, Thikra Abdullah Alzahrani, and E. Alabdrabalrasol, "Lifestyle Modifications for Hypertension Management," *The Egypti Journal of Hospital Medicine,* vol. 70, no. 12, pp. 2152-2156, 2018.

[7] "Global report on hypertension: the race against a silent killer," World Health Organizati Geneva, 2023.

[8] "Thai Nationwide Population Statistics of December 2020," Bereau of Registrati Administration, Department of Provincial Administration Registration, Thailand, 2020.

[9] E. Martinez-Ríos, L. Montesinos, M. Alfaro-Ponce, and L. Pecchia, "A review of machi learning in hypertension detection and blood pressure estimation based on clinical a physiological data," *Biomedical Signal Processing and Control,* vol. 68, p. 102813, 2021.

[10] M. Brunström and B. Carlberg, "Association of Blood Pressure Lowering With Mortal and Cardiovascular Disease Across Blood Pressure Levels: A Systematic Review and Me analysis," *JAMA Internal Medicine,* vol. 178, no. 1, pp. 28-36, 2018.

[11] B. Williams, G. Mancia, W. Spiering, E. Agabiti Rosei, M. Azizi, M. Burnier, D. Clement, A. Coca, G. de Simone, A. Dominiczak, T. Kahan, F. Mahfoud, J. Redon, Ruilope, A. Zanchetti, M. Kerins, S. E. Kjeldsen, R. Kreutz, S. Laurent, G. Y. H. Lip, McManus, K. Narkiewicz, F. Ruschitzka, R. E. Schmieder, E. Shlyakhto, C. Tsioufis, Aboyans, I. Desormais, and E. S. D. Group, "2018 ESC/ESH Guidelines for the manageme of arterial hypertension: The Task Force for the management of arterial hypertension of t European Society of Cardiology (ESC) and the European Society of Hypertension (ESH *European Heart Journal,* vol. 39, no. 33, pp. 3021-3104, 2018.

[12] S. Lopes, J. Mesquita-Bastos, A. J. Alves, and F. Ribeiro, "Exercise as a tool hypertension and resistant hypertension management: current insights," *Integrated Blo Pressure Control,* vol. 11, no. null, pp. 65-71, 2018.

[13] M. Volpe, G. Gallo, and G. Tocci, "Is early and fast blood pressure control important hypertension management?," *International Journal of Cardiology,* vol. 254, pp. 328-3 2018.

[14] F. Rader and R. G. Victor, "The Slow Evolution of Blood Pressure Monitoring: But Wa Not So Fast!∗," *JACC: Basic to Translational Science,* vol. 2, no. 6, pp. 643-645, 2017.

[15] J. Booth, "A Short History of Blood Pressure Measurement," *Proceedings of the Roy Society of Medicine,* vol. 70, no. 11, pp. 793-799, 1977.

[16] X. R. Ding, N. Zhao, G. Z. Yang, R. I. Pettigrew, B. Lo, F. Miao, Y. Li, J. Liu, and Y. Zhang, "Continuous Blood Pressure Measurement From Invasive to Unobtrusiv Celebration of 200th Birth Anniversary of Carl Ludwig," *IEEE Journal of Biomedical a Health Informatics,* vol. 20, no. 6, pp. 1455-1465, 2016.

[17] R. Kumar, P. K. Dubey, A. Zafer, A. Kumar, and S. Yadav, "Past, present and future blood pressure measuring instruments and their calibration," *Measurement,* vol. 172, 108845, 2021.

[18] A. Roguin, "Scipione Riva-Rocci and the men behind the mercury sphygmomanomete *International Journal of Clinical Practice,* vol. 60, no. 1, pp. 73-79, 2006.

[19] C. P. Lau, "The sphygmograph," *Hong Kong Medical Journal,* vol. 22, no. 4, pp. 402-4(2016.

[20] E. Verrij, G. Van Montfrans, and J. Bos, "Reintroduction of Riva-Rocci measurements determine systolic blood pressure," *The Netherlands Journal of Medicine,* vol. 66, no. pp. 480-482, 2008.

[21] A. Benmira, A. Perez-Martin, I. Schuster, I. Aichoun, S. Coudray, F. Bereksi-Reguig, a M. Dauzat, "From Korotkoff and Marey to automatic non-invasive oscillometric blo pressure measurement: does easiness come with reliability?," *Expert Review of Medi Devices,* vol. 13, no. 2, pp. 179-189, 2016.

[22] M. G. Myers, "A Short History of Automated Office Blood Pressure – 15 Years SPRINT," *The Journal of Clinical Hypertension,* vol. 18, no. 8, pp. 721-724, 2016.

[23] M. Sharma, K. Barbosa, V. Ho, D. Griggs, T. Ghirmai, S. K. Krishnan, T. K. Hsiai, J. Chiao, and H. Cao, "Cuff-Less and Continuous Blood Pressure Monitoring: Methodological Review," *Technologies,* vol. 5, no. 2, p. 21, 2017.

[24] S. I. Fox and K. Rompolski, *Human Physiology*, 15 ed. New York: McGraw-Hill, 2019.

[25] G. S. Stergiou, R. Mukkamala, A. Avolio, K. G. Kyriakoulis, S. Mieke, A. Murray, Parati, A. E. Schutte, J. E. Sharman, R. Asmar, R. J. McManus, K. Asayama, A. De Sierra, G. Head, K. Kario, A. Kollias, M. Myers, T. Niiranen, T. Ohkubo, J. Wang, Wuerzner, E. O'Brien, R. Kreutz, and P. Palatini, "Cuffless blood pressure measuri devices: review and statement by the European Society of Hypertension Working Group Blood Pressure Monitoring and Cardiovascular Variability," *Journal of Hypertension,* v 40, no. 8, 2022.

[26] J. S. Ringrose, D. McLean, P. Ao, F. Yousefi, S. Sankaralingam, J. Millay, and R. Padw "Effect of Cuff Design on Auscultatory and Oscillometric Blood Pressure Measurement *American Journal of Hypertension,* vol. 29, no. 9, pp. 1063-1069, 2016.

[27] J. Ishigami, J. Charleston, E. R. Miller, III, K. Matsushita, L. J. Appel, and T. M. Brad "Effects of Cuff Size on the Accuracy of Blood Pressure Readings: The Cuff(S Randomized Crossover Trial," *JAMA Internal Medicine,* vol. 183, no. 10, pp. 1061-10 2023.

[28] G. Bilo, O. Sala, C. Perego, A. Faini, L. Gao, A. Głuszewska, J. E. Ochoa, D. Pellegrini, M. Lonati, and G. Parati, "Impact of cuff positioning on blood pressure measureme accuracy: may a specially designed cuff make a difference?," *Hypertension Research,* v 40, no. 6, pp. 573-580, 2017.

[29] R. Mukkamala, G. S. Stergiou, and A. P. Avolio, "Cuffless Blood Pressure Measuremen *Annual Review of Biomedical Engineering,* vol. 24, no. Volume 24, 2022, pp. 203-2 2022.

[30] B. Saugel, K. Kouz, A. S. Meidert, L. Schulte-Uentrop, and S. Romagnoli, "How to measu blood pressure using an arterial catheter: a systematic 5-step approach," *Critical Care,* v 24, no. 1, p. 172, 2020.

[31] P. Muntner, D. Shimbo, R. M. Carey, J. B. Charleston, T. Gaillard, S. Misra, M. G. Mye G. Ogedegbe, J. E. Schwartz, R. R. Townsend, E. M. Urbina, A. J. Viera, W. B. White, a J. T. Wright, "Measurement of Blood Pressure in Humans: A Scientific Statement From t American Heart Association," *Hypertension,* vol. 73, no. 5, pp. e35-e66, 2019.

[32] A. S. Meidert and B. Saugel, "Techniques for Non-Invasive Monitoring of Arterial Blo Pressure," *Frontiers in Medicine,* Mini Review vol. 4, 2018.

[33] B. Saugel, R. Dueck, and J. Y. Wagner, "Measurement of blood pressure," *Best Practice Research Clinical Anaesthesiology,* vol. 28, no. 4, pp. 309-322, 2014.

[34] J. Y. Wagner, I. Negulescu, M. Schöfthaler, A. Hapfelmeier, A. S. Meidert, W. Huber, R. Schmid, and B. Saugel, "Continuous noninvasive arterial pressure measurement using t volume clamp method: an evaluation of the CNAP device in intensive care unit patient *Journal of Clinical Monitoring and Computing,* vol. 29, no. 6, pp. 807-813, 2015.

[35] M. Farhath and M. F. Samad, "Design and simulation of a high sensitive stripped-shap piezoresistive pressure sensor," *Journal of Computational Electronics,* vol. 19, no. 1, p 310-320, 2020.

[36] S. Stassi, V. Cauda, G. Canavese, and C. F. Pirri, "Flexible Tactile Sensing Based Piezoresistive Composites: A Review," *Sensors,* vol. 14, no. 3, pp. 5296-5332, 2014.

[37] A. Panahi, A. Hassanzadeh, and A. Moulavi, "Design of a low cost, double triang piezoelectric sensor for respiratory monitoring applications," *Sensing and Bio-Sensi Research,* vol. 30, p. 100378, 2020.

[38] D. S. Aulakh and S. Bhalla, "3D torsional experimental strain modal analysis for structu health monitoring using piezoelectric sensors," *Measurement,* vol. 180, p. 109476, 2021.

[39] N. Sviridova, T. Zhao, K. Aihara, K. Nakamura, and A. Nakano, "Photoplethysmogram green light: Where does chaos arise from?," *Chaos, Solitons & Fractals,* vol. 116, pp. 15 165, 2018.

[40] M. P. D. Pont and J. L. B. Marques, "Reflective Photoplethysmography Acquisiti Platform With Monitoring Modules and Noninvasive Blood Pressure Calculation," *IE Transactions on Instrumentation and Measurement,* vol. 69, no. 8, pp. 5649-5657, 2020.

[41] Z. Cohen and S. Haxha, "Optical-Based Sensor Prototype for Continuous Monitoring of t Blood Pressure," *IEEE Sensors Journal,* vol. 17, no. 13, pp. 4258-4268, 2017.

[42] M. Kachuee, M. M. Kiani, H. Mohammadzade, and M. Shabany, "Cuffless Blood Pressu Estimation Algorithms for Continuous Health-Care Monitoring," *IEEE Transactions Biomedical Engineering,* vol. 64, no. 4, pp. 859-869, 2017.

[43] Q. Zhang, X. Zeng, W. Hu, and D. Zhou, "A Machine Learning-Empowered System
Long-Term Motion-Tolerant Wearable Monitoring of Blood Pressure and Heart Rate W
Ear-ECG/PPG," *IEEE Access,* vol. 5, pp. 10547-10561, 2017.

[44] N. Luo, W. Dai, C. Li, Z. Zhou, L. Lu, C. C. Y. Poon, S.-C. Chen, Y. Zhang, and N. Zh
"Flexible Piezoresistive Sensor Patch Enabling Ultralow Power Cuffless Blood Pressu
Measurement," *Advanced Functional Materials,* vol. 26, no. 8, pp. 1178-1187, 2016.

[45] R. E. Klabunde, *Cardiovascular physiology concepts*, 2 ed. Baltimore: Lippincott Willia
& Wilkins, 2012.

[46] N. A. Shirwany and M.-h. Zou, "Arterial stiffness: a brief review," *Acta Pharmacolog
Sinica,* vol. 31, no. 10, pp. 1267-1276, 2010.

[47] E. Patvardhan, K. S. Heffernan, J. Ruan, M. Hession, P. Warner, R. H. Karas, and J.
Kuvin, "Augmentation Index Derived from Peripheral Arterial Tonometry Correlates w
Cardiovascular Risk Factors," *Cardiology Research and Practice,* vol. 2011, p. 2537
2011.

[48] C. Leitao, L. Bilro, N. Alberto, P. Antunes, H. Lima, P. André, R. Nogueira, and J. Pin
"Feasibility studies of Bragg probe for noninvasive carotid pulse waveform assessmen
Journal of Biomedical Optics, vol. 18, no. 1, p. 017006, 2013.

[49] K. E. Barrett, S. M. Barman, S. Boitano, and H. L. Brooks, *Ganong's Review of Medi
Physiology*. New York: McGraw-Hill Education, 2010.

[50] M. F. O'Rourke, "Carotid Artery Tonometry: Pros and Cons," *American Journal
Hypertension,* vol. 29, no. 3, pp. 296-298, 2015.

[51] R. P. Schnall, J. Sheffy, and T. Penzel, "Peripheral arterial tonometry–PAT technolog
Sleep Medicine Reviews, vol. 61, p. 101566, 2022.

[52] C. Leitão, P. Antunes, P. André, J. L. Pinto, and J. M. Bastos, "Central arterial pu
waveform acquisition with a portable pen-like optical fiber sensor," *Blood Pressu
Monitoring,* vol. 20, no. 1, pp. 43-46, 2015.

[53] C. Leitão, P. Antunes, J. Pinto, J. Mesquita Bastos, and P. André, "Optical fiber sensors
central arterial pressure monitoring," *Optical and Quantum Electronics,* vol. 48, no. 3,
218, 2016.

[54] M. Nordine, M. Pille, J. Kraemer, C. Berger, P. Brandhorst, P. Kaeferstein, R. Kopetsch,
Wessel, R. F. Trauzeddel, and S. Treskatsch, "Intraoperative Beat-to-Beat Pulse Tran
Time (PTT) Monitoring via Non-Invasive Piezoelectric/Piezocapacitive Peripheral Sens
Can Predict Changes in Invasively Acquired Blood Pressure in High-Risk Surgical Patient
Sensors, vol. 23, no. 6, doi: 10.3390/s23063304.

[55] Z. Sagirova, N. Kuznetsova, N. Gogiberidze, D. Gognieva, A. Suvorov, P. Chomakhidze, Omboni, H. Saner, and P. Kopylov, "Cuffless Blood Pressure Measurement Using Smartphone-Case Based ECG Monitor with Photoplethysmography in Hypertensi Patients," *Sensors,* vol. 21, no. 10, p. 3525, 2021.

[56] V. G. Ganti, A. M. Carek, B. N. Nevius, J. A. Heller, M. Etemadi, and O. T. Inan, "Wearal Cuff-Less Blood Pressure Estimation at Home via Pulse Transit Time," *IEEE Journal Biomedical and Health Informatics,* vol. 25, no. 6, pp. 1926-1937, 2021.

[57] J. Choi, Y. Kang, J. Park, Y. Joung, and C. Koo, "Development of Real-Time Cuffl Blood Pressure Measurement Systems with ECG Electrodes and a Microphone Using Pu Transit Time (PTT)," *Sensors,* vol. 23, no. 3, p. 1684, 2023.

[58] F. Miao, Z. D. Liu, J. K. Liu, B. Wen, Q. Y. He, and Y. Li, "Multi-Sensor Fusion Approa for Cuff-Less Blood Pressure Measurement," *IEEE Journal of Biomedical and Hea Informatics,* vol. 24, no. 1, pp. 79-91, 2020.

[59] W. Liu, J. Cheng, Z. Wu, J. Li, W. Shi, W. Yang, N. Jin, Y. Mu, B. Weng, J. Wu, D. Hao, Liu, Z. Wang, G. Li, and L. Dong, "A Wearable and Flexible Photoplethysmogram Sens Patch for Cuffless Blood Pressure Estimation With High Accuracy," *IEEE Sensors Journ* vol. 22, no. 20, pp. 19818-19825, 2022.

[60] J. Q. Li, R. Li, Z. Z. Chen, G. Q. Deng, H. Wang, C. X. Mavromoustakis, H. Song, and Ming, "Design of a Continuous Blood Pressure Measurement System Based on Pulse Wa and ECG Signals," *IEEE J Transl Eng Health Med,* vol. 6, p. 1900114, 2018.

[61] F. Miao, B. Wen, Z. Hu, G. Fortino, X.-P. Wang, Z.-D. Liu, M. Tang, and Y. "Continuous blood pressure measurement from one-channel electrocardiogram signal usi deep-learning techniques," *Artificial Intelligence in Medicine,* vol. 108, p. 101919, 2020.

[62] C.-M. Wu, C. Y. Chuang, Y.-J. Chen, and S.-C. Chen, "A new estimate technology of no invasive continuous blood pressure measurement based on electrocardiograph," *Advances Mechanical Engineering,* vol. 8, no. 6, p. 1687814016653689, 2016.

[63] M. Simjanoska, M. Gjoreski, M. Gams, and A. Madevska Bogdanova, "Non-Invasive Blo Pressure Estimation from ECG Using Machine Learning Techniques," *Sensors,* vol. 18, 4, 2018.

[64] Bijender and A. Kumar, "Flexible and wearable capacitive pressure sensor for blo pressure monitoring," *Sensing and Bio-Sensing Research,* vol. 33, p. 100434, 2021.

[65] P. Rwei, C. Qian, A. Abiri, Y. Zhou, E.-F. Chou, W. C. Tang, and M. Khine, "Soft Iontro Capacitive Sensor for Beat-to-Beat Blood Pressure Measurements," *Advanced Materi Interfaces,* vol. 9, no. 18, p. 2200294, 2022.

[66] T.-V. Nguyen, Y. Mizuki, T. Tsukagoshi, T. Takahata, M. Ichiki, and I. Shimoyan "MEMS-Based Pulse Wave Sensor Utilizing a Piezoresistive Cantilever," *Sensors,* vol. 2 no. 4, p. 1052, 2020.

[67] P. Tan, Y. Xi, S. Chao, D. Jiang, Z. Liu, Y. Fan, and Z. Li, "An Artificial Intelligen Enhanced Blood Pressure Monitor Wristband Based on Piezoelectric Nanogenerato *Biosensors,* vol. 12, no. 4, p. 234, 2022.

[68] C.-Y. Guo, K.-J. Wang, and T.-L. Hsieh, "Piezoelectric Sensor for the Monitoring of Arter Pulse Wave: Detection of Arrhythmia Occurring in PAC/PVC Patients," *Sensors,* vol. 2 no. 20, p. 6915, 2021.

[69] T.-W. Wang and S.-F. Lin, "Wearable Piezoelectric-Based System for Continuous Beat-Beat Blood Pressure Measurement," *Sensors,* vol. 20, no. 3, p. 851, 2020.

[70] Y. Osawa and T. Dohi, "Extraction and Evaluation of Discriminative Indexes of the Weari Condition for High-Precision Blood Pressure Pulse Wave Measurement," *Micromachin* vol. 13, no. 5, p. 679, 2022.

[71] T. Panula, T. Koivisto, M. Pänkäälä, T. Niiranen, I. Kantola, and M. Kaisti, "An instrum for measuring blood pressure and assessing cardiovascular health from the fingerti *Biosensors and Bioelectronics,* vol. 167, p. 112483, 2020.

[72] X. Guan, Z. Wang, W. Zhao, H. Huang, S. Wang, Q. Zhang, D. Zhong, W. Lin, N. Di and Z. Peng, "Flexible Piezoresistive Sensors with Wide-Range Pressure Measureme Based on a Graded Nest-like Architecture," *ACS Applied Materials & Interfaces,* vol. 12, 23, pp. 26137-26144, 2020.

[73] Z. Wang, S. Wang, J. Zeng, X. Ren, A. J. Y. Chee, B. Y. S. Yiu, W. C. Chung, Y. Yang, C. H. Yu, R. C. Roberts, A. C. O. Tsang, K. W. Chow, and P. K. L. Chan, "High Sensitivi Wearable, Piezoresistive Pressure Sensors Based on Irregular Microhump Structures and Applications in Body Motion Sensing," *Small,* vol. 12, no. 28, pp. 3827-3836, 2016.

[74] X. Chen, D. Zhang, M. Tang, C. Yang, and H. Luan, "Microstructured Flexible Pressu Sensor Based on Nanofibrous Films for Human Motions and Physiological Detection," *IE Sensors Journal,* vol. 22, no. 20, pp. 19191-19197, 2022.

[75] J. Li, H. Jia, J. Zhou, X. Huang, L. Xu, S. Jia, Z. Gao, K. Yao, D. Li, B. Zhang, Y. Liu, Huang, Y. Hu, G. Zhao, Z. Xu, J. Li, C. K. Yiu, Y. Gao, M. Wu, ..., and X. Yu, "Thin, so wearable system for continuous wireless monitoring of artery blood pressure," *Natu Communications,* vol. 14, no. 1, p. 5009, 2023.

[76] P. Fang, Y. Peng, W. H. Lin, Y. Wang, S. Wang, X. Zhang, K. Wu, and G. Li, "Wrist Pu Recording With a Wearable Piezoresistor-Piezoelectret Compound Sensing System and Applications in Health Monitoring," *IEEE Sensors Journal,* vol. 21, no. 18, pp. 209 20930, 2021.

[77] C. Dagdeviren, Y. Su, P. Joe, R. Yona, Y. Liu, Y.-S. Kim, Y. Huang, A. R. Damadoran Xia, L. W. Martin, Y. Huang, and J. A. Rogers, "Conformable amplified lead zircon titanate sensors with enhanced piezoelectric response for cutaneous pressure monitorin *Nature Communications,* vol. 5, no. 1, p. 4496, 2014.

[78] L. Gao, C. Zhu, L. Li, C. Zhang, J. Liu, H.-D. Yu, and W. Huang, "All Paper-Based Flexi and Wearable Piezoresistive Pressure Sensor," *ACS Applied Materials & Interfaces,* vol. no. 28, pp. 25034-25042, 2019.

[79] M. Chattopadhyay and D. Chowdhury, "Design and performance analysis of ME capacitive pressure sensor array for measurement of heart rate," *Microsystem Technologi* vol. 23, no. 9, pp. 4203-4209, 2017.

[80] K.-H. Huang, F. Tan, T.-D. Wang, and Y.-J. Yang, "A Highly Sensitive Pressure-Sensi Array for Blood Pressure Estimation Assisted by Machine-Learning Techniques," *Senso* vol. 19, no. 4, doi: 10.3390/s19040848.

[81] X. R. Ding, Y. T. Zhang, J. Liu, W. X. Dai, and H. K. Tsang, "Continuous Cuffless Blo Pressure Estimation Using Pulse Transit Time and Photoplethysmogram Intensity Rati *IEEE Transactions on Biomedical Engineering,* vol. 63, no. 5, pp. 964-972, 2016.

[82] J. Joung, C.-W. Jung, H.-C. Lee, M.-J. Chae, H.-S. Kim, J. Park, W.-Y. Shin, C. Kim, Lee, and C. Choi, "Continuous cuffless blood pressure monitoring usi photoplethysmography-based PPG2BP-net for high intrasubject blood pressure variation *Scientific Reports,* vol. 13, no. 1, p. 8605, 2023.

[83] J.-W. Chen, H.-K. Huang, Y.-T. Fang, Y.-T. Lin, S.-Z. Li, B.-W. Chen, Y.-C. Lo, P.- Chen, C.-F. Wang, and Y.-Y. Chen, "A Data-Driven Model with Feedback Calibrati Embedded Blood Pressure Estimator Using Reflective Photoplethysmography," *Senso* vol. 22, no. 5, doi: 10.3390/s22051873.

[84] Q. Zhang, D. Zhou, and X. Zeng, "Highly wearable cuff-less blood pressure and heart r monitoring with single-arm electrocardiogram and photoplethysmogram signal *BioMedical Engineering OnLine,* vol. 16, no. 1, p. 23, 2017.

[85] C.-Y. Guo, H.-C. Chang, K.-J. Wang, and T.-L. Hsieh, "An Arterial Compliance Sensor Cuffless Blood Pressure Estimation Based on Piezoelectric and Optical Signal *Micromachines,* vol. 13, no. 8, 2022.

[86] Y.-J. Wang, C.-H. Chen, C.-Y. Sue, W.-H. Lu, and Y.-H. Chiou, "Estimation of Blo Pressure in the Radial Artery Using Strain-Based Pulse Wave and Photoplethysmograp Sensors," *Micromachines,* vol. 9, no. 11, 2018.

[87] P. Samartkit, S. Pullteap, and O. Bernal, "A non-invasive heart rate and blood pressu monitoring system using piezoelectric and photoplethysmographic sensors," *Measureme* vol. 196, p. 111211, 2022.

[88] R. Byfield, M. Miller, J. Miles, G. Guidoboni, and J. Lin, "Towards Robust Blood Pressu Estimation From Pulse Wave Velocity Measured by Photoplethysmography Sensors," *IE Sensors Journal,* vol. 22, no. 3, pp. 2475-2483, 2022.

[89] P. M. Nabeel, J. Jayaraj, K. Srinivasa, S. Mohanasankar, and M. Chenniappan, "Bi-Mo Arterial Compliance Probe for Calibration-Free Cuffless Blood Pressure Estimation," *IE Transactions on Biomedical Engineering,* vol. 65, no. 11, pp. 2392-2404, 2018.

[90] J. Seo, S. J. Pietrangelo, H. S. Lee, and C. G. Sodini, "Noninvasive arterial blood pressu waveform monitoring using two- element ultrasound system," *IEEE Transactions Ultrasonics, Ferroelectrics, and Frequency Control,* vol. 62, no. 4, pp. 776-784, 2015.

[91] A. M. Zakrzewski and B. W. Anthony, "Noninvasive Blood Pressure Estimation Usi Ultrasound and Simple Finite Element Models," *IEEE Transactions on Biomedi Engineering,* vol. 65, no. 9, pp. 2011-2022, 2018.

[92] S. Shin, M. Kim, and S. B. Choi, "Ultrasonic Distance Measurement Method With Crosst Rejection at High Measurement Rate," *IEEE Transactions on Instrumentation a Measurement,* vol. 68, no. 4, pp. 972-979, 2019.

[93] C. Wang, X. Li, H. Hu, L. Zhang, Z. Huang, M. Lin, Z. Zhang, Z. Yin, B. Huang, H. Go S. Bhaskaran, Y. Gu, M. Makihata, Y. Guo, Y. Lei, Y. Chen, C. Wang, Y. Li, T. Zhang, Chen, A. P. Pisano, L. Zhang, Q. Zhou, and S. Xu, "Monitoring of the central blood pressu waveform via a conformal ultrasonic device," *Nature Biomedical Engineering,* vol. 2, no. pp. 687-695, 2018.

[94] C. Peng, M. Chen, H. K. Sim, Y. Zhu, and X. Jiang, "Noninvasive and Nonocclusive Blo Pressure Monitoring via a Flexible Piezo-Composite Ultrasonic Sensor," *IEEE Sens Journal,* vol. 21, no. 3, pp. 2642-2650, 2021.

[95] E. Vorathin, Z. M. Hafizi, N. Ismail, and M. Loman, "Review of high sensitivity fibre-op pressure sensors for low pressure sensing," *Optics & Laser Technology,* vol. 121, p. 1058 2020.

[96] A. G. Leal-Junior, C. R. Díaz, C. Leitão, M. J. Pontes, C. Marques, and A. Frizera, "Polyn optical fiber-based sensor for simultaneous measurement of breath and heart rate unc dynamic movements," *Optics & Laser Technology,* vol. 109, pp. 429-436, 2019.

[97] Y. Koyama, M. Nishiyama, and K. Watanabe, "Smart Textile Using Hetero-Core Opti Fiber for Heartbeat and Respiration Monitoring," *IEEE Sensors Journal,* vol. 18, no. 15, 6175-6180, 2018.

[98] X. Yang, Z. Chen, C. S. M. Elvin, L. H. Y. Janice, S. H. Ng, J. T. Teo, and R. Wu, "Text Fiber Optic Microbend Sensor Used for Heartbeat and Respiration Monitoring," *IE Sensors Journal,* vol. 15, no. 2, pp. 757-761, 2015.

[99] Y. G. Y. Yhuwana, R. Apsari, and M. Yasin, "Fiber optic sensor for heart rate detectio *Optik,* vol. 134, pp. 28-32, 2017.

[100] C. S. J. Leitão, P. F. d. C. Antunes, J. A. Bastos, J. Pinto, and P. S. d. B. André, "Plas Optical Fiber Sensor for Noninvasive Arterial Pulse Waveform Monitoring," *IEEE Sens Journal,* vol. 15, no. 1, pp. 14-18, 2015.

[101] N. V. Kumar, S. Pant, S. Sridhar, V. Marulasiddappa, S. Srivatzen, and S. Asokan, "Fil Bragg Grating-Based Pulse Monitoring Device for Real-Time Non-Invasive Blood Pressu Measurement—A Feasibility Study," *IEEE Sensors Journal,* vol. 21, no. 7, pp. 9179-91 2021.

[102] Y. Haseda, J. Bonefacino, H.-Y. Tam, S. Chino, S. Koyama, and H. Ishizawa, "Measurem of Pulse Wave Signals and Blood Pressure by a Plastic Optical Fiber FBG Sensor," *Senso* vol. 19, no. 23, p. 5088.

[103] J. Bonefacino, H.-Y. Tam, T. S. Glen, X. Cheng, C.-F. J. Pun, J. Wang, P.-H. Lee, M.-L. Tse, and S. T. Boles, "Ultra-fast polymer optical fibre Bragg grating inscription for medi devices," *Light: Science & Applications,* vol. 7, no. 3, pp. 17161-17161, 2018.

[104] D. Lo Presti, D. Bianchi, C. Massaroni, A. Gizzi, and E. Schena, "A Soft and Sk Interfaced Smart Patch Based on Fiber Optics for Cardiorespiratory Monitorin *Biosensors*, vol. 12, no. 6, p. 363.

[105] Jan Nedoma, Marcel Fajkus, Martin Novak, Nela Strbikova, Vladimir Vasinek, Hon Nazeran, Jan Vanus, Frantisek Perecar, and R. Martinek, "Validation of a Novel Fiber-Op Sensor System for Monitoring Cardiorespiratory Activities During MRI Examination *Advances in Electrical and Electronic Engineering,* vol. 15, no. 3, pp. 536-543, 2017.

[106] D. Lo Presti, F. Santucci, C. Massaroni, D. Formica, R. Setola, and E. Schena, "A mu point heart rate monitoring using a soft wearable system based on fiber optic technolog *Scientific Reports,* vol. 11, no. 1, p. 21162, 2021.

[107] M. Fajkus, J. Nedoma, R. Martinek, V. Vasinek, H. Nazeran, and P. Siska, "A Non-Invasi Multichannel Hybrid Fiber-Optic Sensor System for Vital Sign Monitoring," *Sensors,* v 17, no. 1, p. 111, 2017.

[108] S. Pant, S. Umesh, and S. Asokan, "A Novel Approach to Acquire the Arterial Pulse Finger Plethysmography Using Fiber Bragg Grating Sensor," *IEEE Sensors Journal,* vol. 1 no. 11, pp. 5921-5928, 2020.

[109] S. Pullteap and H. C. Seat, "An extrinsic fiber Fabry-Perot interferometer for dynan displacement measurement," *Photonic Sensors,* vol. 5, no. 1, pp. 50-59, 2015.

[110] L. Li, Y. Li, L. Yang, F. Fang, Z. Yan, and Q. Sun, "Continuous and accurate blood pressu monitoring based on wearable optical fiber wristband," *IEEE Sensors Journal,* vol. 21, no. pp. 3049-3057, 2020.

[111] J. Wang, K. Liu, Q. Sun, X. Ni, F. Ai, S. Wang, Z. Yan, and D. Liu, "Diaphragm-bas optical fiber sensor for pulse wave monitoring and cardiovascular diseases diagnosi *Journal of Biophotonics,* vol. 12, no. 10, p. e201900084, 2019.

[112] N. A. Ushakov, A. A. Markvart, and L. B. Liokumovich, "Pulse Wave Veloc Measurement With Multiplexed Fiber Optic Fabry–Perot Interferometric Sensors," *IE Sensors Journal,* vol. 20, no. 19, pp. 11302-11312, 2020.

[113] T. Sirkis, Y. Beiderman, S. Agdarov, Y. Beiderman, and Z. Zalevsky, "Fiber sensor for nc contact estimation of vital bio-signs," *Optics Communications,* vol. 391, pp. 63-67, 2017.

[114] W. Lyu, W. Xu, F. Yang, S. Chen, F. Tan, and C. Yu, "Non-Invasive Measurement Cardiac Variations Using a Fiber Optic Sensor," *IEEE Photonics Technology Letters,* v 33, no. 18, pp. 990-993, 2021.

[115] W. Lyu, S. Chen, F. Tan, and C. Yu, "Vital Signs Monitoring Based on Interferometric Fil Optic Sensors," *Photonics*, vol. 9, no. 2, p. 50.

[116] A. Ghatak, *Optics*, 4 ed. New Delhi: Tata McGraw-Hill, 2009.

[117] S. Pullteap, "Development of an optical fiber-based interferometer for strain measureme in non-destructive application," *Electrical Engineering,* vol. 99, no. 1, pp. 379-386, 2017.

[118] S. Pullteap, H.-C. Seat, and T. Bosch, "Modified fringe-counting technique applied to a du cavity fiber Fabry-Pérot vibrometer," *Optical Engineering,* vol. 46, no. 11, p. 115603, 200

[119] Q. Liu and W. Peng, "Fast interrogation of dynamic low-finesse Fabry-Perot interferomete A review," *Microwave and Optical Technology Letters,* vol. 63, no. 9, pp. 2279-2291, 202

[120] C. Hou, J. Zhu, B. Liu, P. Shi, M. Zhang, H. Wang, J. Luo, and B. Yu, "Phase-shift demodulation scheme for fiber-optic interferometric sensors with combined waveform pha modulation," *Optical Fiber Technology,* vol. 75, p. 103211, 2023.

[121] A. Acharya and N. Kawade, "A Fabry–Perot Interferometer-Based Fiber Optic Dynan Displacement Sensor With an Analog in-Phase/Quadrature Generator," *IEEE Sens Journal,* vol. 20, no. 24, pp. 14764-14771, 2020.

[122] F. Maurin, F. Greco, L. Coox, D. Vandepitte, and W. Desmet, "Isogeometric collocation Kirchhoff–Love plates and shells," *Computer Methods in Applied Mechanics a Engineering,* vol. 329, pp. 396-420, 2018.

[123] S. K. Jindal, A. Mahajan, and S. K. Raghuwanshi, "A complete analytical model for clamp edge circular diaphragm non-touch and touch mode capacitive pressure senso *Microsystem Technologies,* vol. 22, no. 5, pp. 1143-1150, 2016.

[124] J. Zhu, M. Wang, L. Chen, X. Ni, and H. Ni, "An optical fiber Fabry–Perot pressure sen using corrugated diaphragm and angle polished fiber," *Optical Fiber Technology,* vol. pp. 42-46, 2017.

[125] F. Yu, Q. Liu, X. Gan, M. Hu, T. Zhang, C. Li, F. Kang, M. Terrones, and R. I "Ultrasensitive Pressure Detection of Few-Layer MoS2," *Advanced Materials,* vol. 29, no. 2017.

[126] D. Zambrana-Vinaroz, J. M. Vicente-Samper, C. G. Juan, V. Esteve-Sala, and J. M. Sabat Navarro, "Non-Invasive Device for Blood Pressure Wave Acquisition by Means Mechanical Transducer," *Sensors,* vol. 19, no. 19, p. 4311, 2019.

[127] X. Ding and Y.-T. Zhang, "Pulse transit time technique for cuffless unobtrusive blo pressure measurement: from theory to algorithm," *Biomedical Engineering Letters,* vol. no. 1, pp. 37-52, 2019.

[128] D. Barvik, M. Cerny, M. Penhaker, and N. Noury, "Noninvasive Continuous Blood Pressu Estimation From Pulse Transit Time: A Review of the Calibration Models," *IEEE Revie in Biomedical Engineering,* vol. 15, pp. 138-151, 2022.

[129] E. Prenesti and F. Gosmaro, "Trueness, precision and accuracy: a critical overview of t concepts as well as proposals for revision," *Accreditation and Quality Assurance,* vol. no. 1, pp. 33-40, 2015.

[130] A. Menditto, M. Patriarca, and B. Magnusson, "Understanding the meaning of accura trueness and precision," *Accreditation and Quality Assurance,* vol. 12, no. 1, pp. 45-2007.

[131] G. S. Stergiou, B. Alpert, S. Mieke, R. Asmar, N. Atkins, S. Eckert, G. Frick, B. Friedma T. Graßl, T. Ichikawa, J. P. Ioannidis, P. Lacy, R. McManus, A. Murray, M. Myers, Palatini, G. Parati, D. Quinn, J. Sarkis, A. Shennan, T. Usuda, J. Wang, C. O. Wu, and O'Brien, "A universal standard for the validation of blood pressure measuring devic Association for the Advancement of Medical Instrumentation/European Society Hypertension/International Organization for Standardization (AAMI/ESH/IS Collaboration Statement," *Journal of Hypertension,* vol. 36, no. 3, pp. 472-478, 2018.

[132] J. Leppink, K. Winston, and P. O'Sullivan, "Statistical significance does not imply a r effect," *Perspectives on Medical Education,* vol. 5, no. 2, pp. 122-124, 2016.

[133] M. A. Durivage, *Practical Engineering, Process, and Reliability Statistics*, 2 ed. Unit States of America: American Society for Quality, 2022.

[134] P. Teller, "The concept of measurement-precision," *Synthese,* vol. 190, no. 2, pp. 189-2(2013.

[135] R. Matar, N. Abcha, I. Abroug, N. Lecoq, and E.-I. Turki, "A Multi-Approach Analysis Monitoring Wave Energy Driven by Coastal Extremes," *Water,* vol. 16, no. 8, p. 1145, 202

[136] L. Wang, H. Xian, J. Guo, W. Li, J. Wang, Q. Chen, X. Fu, H. Li, Q. Chen, W. Zhang, a Y. Chen, "A novel blood pressure monitoring technique by smart HUAWEI WATCH: validation study according to the ANSI/AAMI/ISO 81060-2:2018 guidelines," *Frontiers Cardiovascular Medicine,* vol. 9, 2022.

[137] I. S. Association, "IEEE standard for wearable cuffless blood pressure measuring device *IEEE Std,* pp. 1708-2014, 2014.

[138] I. S. Association, "IEEE Standard for Wearable, Cuffless Blood Pressure Measuring Devic - Amendment 1," *1708a-2019 (Amendment to IEEE Std 1708-2014),* pp. 1-35, 2019.

[139] C. Leitão, V. Ribau, V. Afreixo, P. Antunes, P. André, J. L. Pinto, P. Boutouyrie, S. Laure and J. M. Bastos, "Clinical evaluation of an optical fiber-based probe for the assessment central arterial pulse waves," *Hypertension Research,* vol. 41, no. 11, pp. 904-912, 2018.

[140] D. Jia, J. Chao, S. Li, H. Zhang, Y. Yan, T. Liu, and Y. Sun, "A Fiber Bragg Grating Sens for Radial Artery Pulse Waveform Measurement," *IEEE Transactions on Biomedi Engineering,* vol. 65, no. 4, pp. 839-846, 2018.

[141] R. B. Gowda, P. Sharan, S. K, M. Braim, and A. N. Alodhayb, "An FBG-based opti pressure sensor for the measurement of radial artery pulse pressure," *Journal Biophotonics,* p. e202400083,

[142] Z. Tang, S. Wang, and C. Shi, "Development of a Hybrid Force-Displacement Sensor Bas on Fiber Bragg Grating for Radial Artery Pulse Waveform Measurement," *IEEE Sens Journal,* vol. 21, no. 18, pp. 20045-20054, 2021.

[143] P. Samartkit and S. Pullteap, "Non-invasive continuous blood pressure sensors in biomedi engineering research: A review," *Sensors and Actuators A: Physical,* vol. 367, p. 1150 2024.

[144] H. C. Seat, P. Chawah, M. Cattoen, A. Sourice, G. Plantier, F. Boudin, J. Chéry, C. Brun P. Bernard, and M. Suleiman, "Dual-modulation fiber Fabry-Perot interferometer w double reflection for slowly-varying displacements," *Optics Letters,* vol. 37, no. 14, 2886-2888, 2012.

[145] S. J. Park, S. Hong, D. Kim, I. Hussain, and Y. Seo, "Intelligent In-Car Health Monitori System for Elderly Drivers in Connected Car," in *Proceedings of the 20th Congress of International Ergonomics Association (IEA 2018)*, Cham, 2019// 2019: Spring International Publishing, pp. 40-44.

[146] "Thorlabs Product Catalogue", Accessed on: 20 May 2024 [Online]. Availab https://www.thorlabs.com/

[147] "NI USE-6002 Specifications", National Instruments Corporation. Accessed on: 20 M 2024 [Online]. Available: https://www.ni.com/en-th/shop/model/usb-6002.html

[148] "RIGOL product catalogue", RIGOL Technologies Co., Ltd. Accessed on: 20 May 20 [Online]. Available: https://int.rigol.com/

[149] "J.I.B. Desktop Computer Catalogue", J.I.B. Computer Group Co., Ltd. Accessed on: May 2024 [Online]. Available: https://www.jib.co.th/

[150] "Daily Foreign Exchange Rates (20 May 2024)", Bank of Thailand. Accessed on: 20 M 2024 [Online]. Available: https://www.bot.or.th/th/statistics/exchange-rate.html

APPENDICES

APPENDIX A
ALGORITHM OF DEVELOPED APPLICATION SOFTWARE

In this dissertation, two primary engineering application software have been developed for continuous signal demodulation and blood pressure measurement: an arterial pulse wave monitoring program based on LabVIEW 2020 and blood pressure demodulation program developed on MATLAB 2018 platform. This appendix consequently expands upon the developed algorithm for their functions. Owing to the complexity of the programming platform, either flowcharts or pseudo codes are however described to elaborate the intentions of the algorithm which should prove more relevant when implementing or further developing novel signal processing software in the future.

A.1 ARTERIAL PULSE WAVE MONITORING PROGRAM

The principal purpose of the arterial pulse wave monitoring program is to continuously record the interference signal corresponding to arterial distension of volunteers and display the demodulated pulse wave in a quasi-real-time manner. This is to assist in fast pulse wave acquisition before initiating the blood pressure demodulation. In particular, the examiner must secure the FFPI pulse sensing probe on the arterial site with adequate pulse amplitude to guarantee correct blood pressure demodulation in subsequent processes. As such, a pulse wave monitor becomes very practical, if not essential, for the sensor placement on participants. Moreover, the application software is also included with a pulse wave recording function which is needed to transfer the examination data to other computers for in-depth analysis. Also important to note is that the employed laser modulation components are not an integrated one-unit machine, instead consisting of an arbitrary waveform generator (AWG), photodetectors, a data acquisition unit (DAQ), and a dedicated computer. All aforementioned equipment must, then, be connected and effectively controlled for synchronous operation. The application software is, thus, developed to unify the functions of the equipment into a coherent working instrument based on LabVIEW 2020 programming which accommodates the control of the machines.

In broader perspective, the user interface (UI) of the LabVIEW-based application software has been shown in Fig. 3.14 and its overall design has been described in the section. Here, the flowchart concerning the operation of the software is illustrated in Fig. A1.

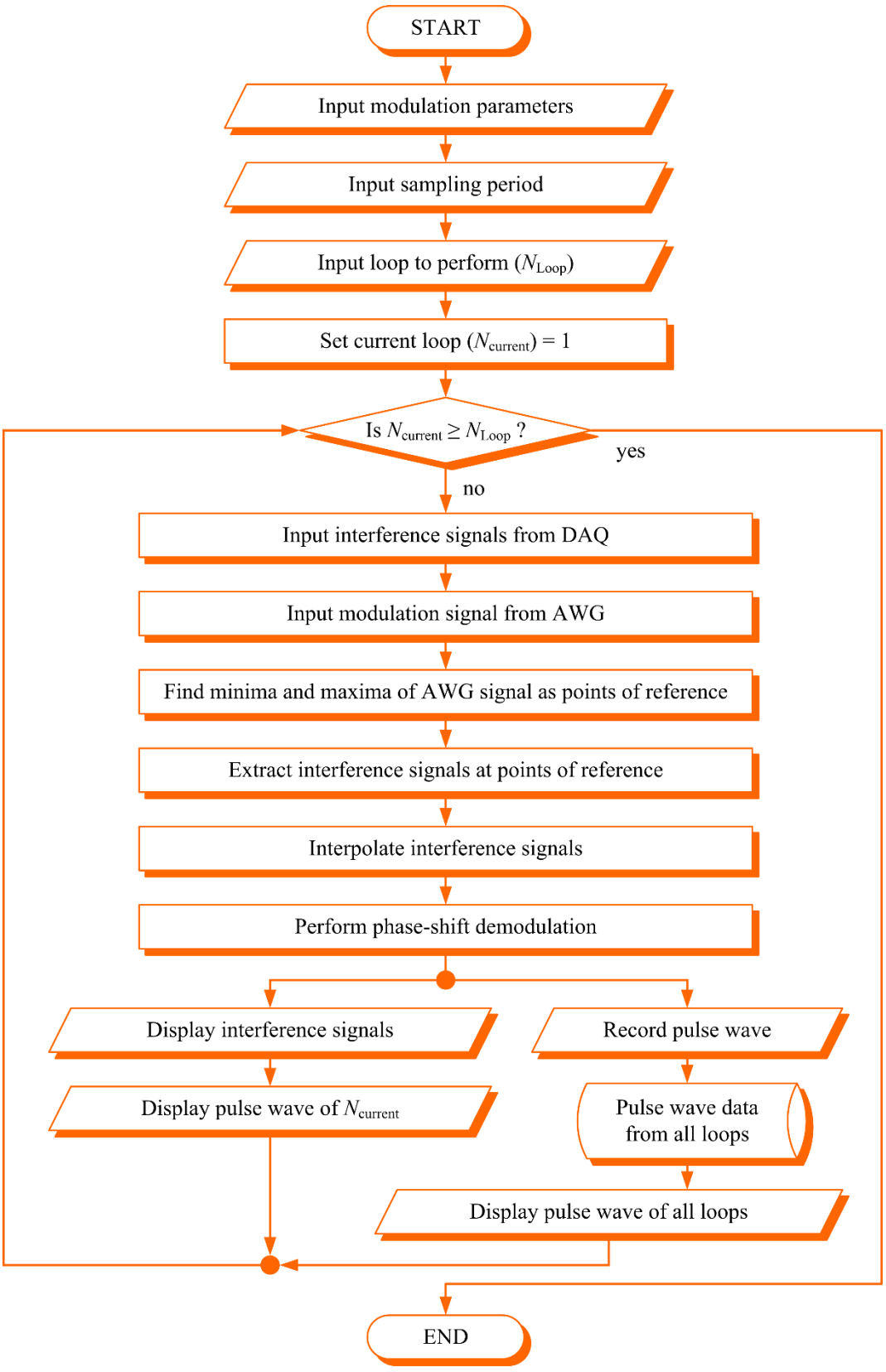

Fig. A1 Flowchart of arterial pulse wave monitoring algorithm

At the start of the software, the user is requested to input modulation parameters such as optical wavelength, refractive index, modulation frequency, etc. These parameters are not automatically found by the software and must instead be extrinsically obtained from the laser source and AWG. However, the sampling period to be input is determined by the user depending on the period of interest during the pulse wave monitoring. Next, the number of loops to perform (N_{Loop}) is included to repeat the pulse wave acquisition over a predetermined number of times. The main difference between the sampling period and the loop to perform lies in the pulse wave display algorithm and shall be explained during a more critical step in the flowchart. Regardless, the software sets an arbitrary variable of "*current loop number* ($N_{current}$)" for reference and will carry out subsequent operations until the current loop is more than the loop to perform ($N_{current} > N_{Loop}$).

In each loop of operation, the interference signals from the photodetectors are input into the algorithm. Secondly, the modulation signal generated by the AWG is obtained, followed by the finding of its minima and maxima to establish points of reference for signal demultiplex process. Incidentally, the minima and maxima of the modulation signal corresponds to either I_x or I_y, allowing the extraction of important interference parameters. Afterwards, the discrete demultiplexed interference signals are interpolated to construct a continuous wave and then applied the phase-shift demodulation to form the pulse waves. At this point, two display processes can be indicated in parallel where the difference between the sampling period and loop to perform is distinctively revealed.

Overall, the total time of monitor is the multiplication of the sampling period and loop to perform. The sampling period is intentionally designed to execute the pulse wave monitoring in a shorter time frame, where the demodulated pulse wave is periodically displayed until the software terminates. Due to the underlying algorithm of LabVIEW, the acquired pulse wave data over the sampling period will always be erased when the system is initiated for subsequent pulse acquisition. To preserve the former data over a longer time, the loop to perform function is exploited which firstly records the pulse wave of the current loop into a database and later displays the entirety of saved data into a single coherent arterial pulse wave. Thus, there are two windows of pulse wave display in the UI of the arterial pulse wave monitoring software. In practice, the pulse wave displayed over the set sampling period has greater resolution while the collective pulse waves shown in every consecutive loop provide a quasi-real-time pulse wave monitoring ability to the software.

A.2 BLOOD PRESSURE DEMODULATION PROGRAM

After the pulse wave acquisition in volunteers, the data is analyzed and demodulated into blood pressure. Therefore, a corresponding blood pressure demodulation software is developed using MATLAB 2018 platform. In this case, the arterial pulse wave monitoring and blood pressure demodulation software are separately developed and applied due to two main reasons: limitation in computation power and lack of fully automatic procedure. The former limitation is, in this scenario, the concern over the performance of the computer when activating both the arterial pulse wave monitoring and blood pressure demodulation simultaneously. Specifically, the arterial pulse wave monitoring must be synchronous with all hardware, needing fast response. Meanwhile, the blood pressure demodulation software employs complex mathematics to obtain the results which could slow the response rate during computation. Also, most relevant mathematical functions are built in MATLAB programming, significantly reducing the algorithm development time. As such, the software are separately operated. Still, it is possible to overcome this limitation by improving the computational power of the computer. However, the main obstacle comes from the lack of fully automatic procedure in demodulating blood pressure.

In this dissertation, the blood pressure demodulation procedure requires sufficiently correct arterial pulse wave which includes systolic peaks and end-diastolics. In theory, human pulse wave exhibits the necessary pulse wave characteristics as a function of the heart. In practice however, motion artifact during the examination can potentially deform the pulse wave and the pulse wave characteristics cannot be identified. Moreover, the signal noise detected in association with the pulse wave might hinder the identification process performed by machines, albeit remediable with human recognition. Therefore, the blood pressure demodulation procedure is conducted by a human operator who ensures accurate pulse wave identification for subsequent analysis.

Nevertheless, several automatic functions are still employed to improve convenience and ease of operation for the human operator as much as possible. Consequently, the algorithm based on MATLAB programming is developed with four respective phases: noise filtering, period of interest selection, pulse pressure finding, and blood pressure demodulation. The first function is the filtering of arterial pulse waves obtained from the aforementioned LabVIEW software. The overall operation of this function is accordingly illustrated in Fig. A2.

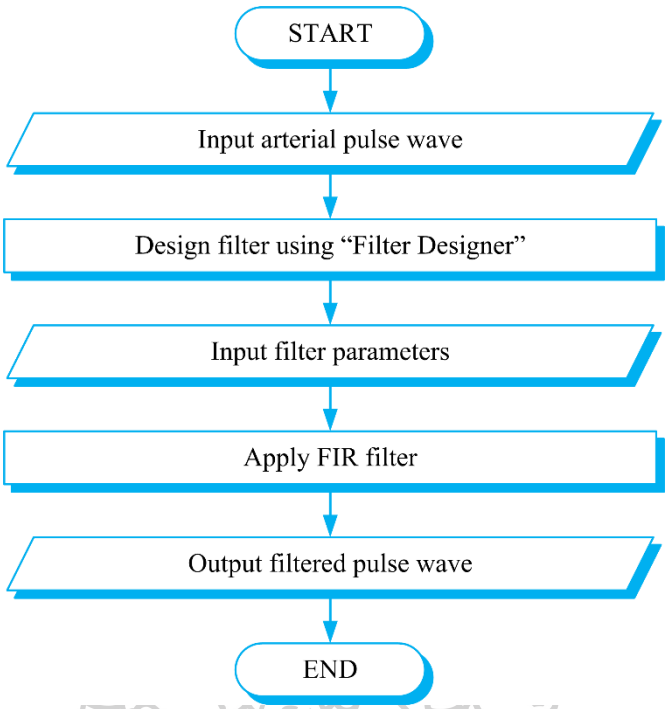

Fig. A2 Flowchart of pulse wave filter function

The objective of the filter function is to eliminate signal noise from the arterial pulse wave, ensuring accuracy blood pressure demodulation in subsequent processes. Furthermore, it is intended to remedy any motion artifact caused by the movement of the examinee during measurement. In this MATLAB function, the arterial pulse wave is initially input into the platform while a built-in “Filter Designer” MATLAB program is activated to generate filter parameters such as filter type (infinite impulse response: IIR or finite impulse response: FIR), filter order (in the latter case), bandpass frequency, etc. In this dissertation, the selected filter found via experimentation is an FIR filter with 5000 filter orders at the bandpass frequency of 0.5-10.0 Hz, corresponding to the heart rate of 30-600 bpm, respectively. These filter parameters are, incidentally, revealed to be practical when processing the arterial pulse waves in the human trial. As such, all input parameters are included into the developed MATLAB function and subsequently applied to filter the signal noise and motion artifact. The resulting pulse wave is, at this point, considered clean of undesirable perturbations.

However, the mentioned MATLAB function can remove the influence of small noise amplitude caused by unintentional movements of fingers, wrists, or other farther body parts. It could not effectively negate significant movement such as shaking of the hands, torso, or head of the examinee. This was, nonetheless, due to unawareness or discomfort of the examinees that led them to move their bodies during the blood pressure measurement. While another

measurement can be performed, it is inappropriate to prolong the examination time on each individual as the examinee could become anxious from loss time, contributing to more erroneous actions and abnormal blood pressure due to stress. Still, these incidents are not frequent across the 15 seconds examination period, thus a portion of the monitored pulse wave can be extracted for demodulation. To amend this situation, the second MATLAB function focuses on selecting the pulse wave period deemed usable and appropriate by the user. The flowchart of such function can be schemed in Fig. A3.

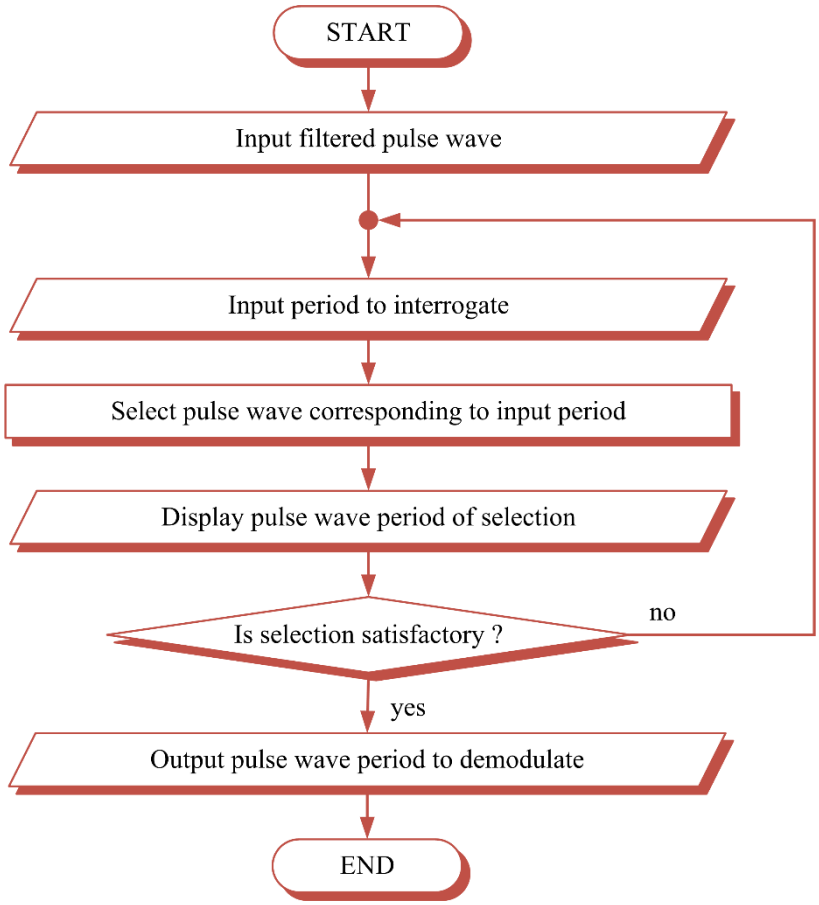

Fig. A3 Flowchart of pulse wave period selection function

Here, the filtered pulse wave is input into the programming while the period of interest is determined. Specifically, the period of interest must be within 15 seconds of examination time and is manually defined by the user. Once the period is selected, the MATLAB function automatically extracts the pulse wave within the particular period to investigate. The latter is also displayed to the user for considering the correctness and potential usefulness. If the selected pulse wave is judged to be unsuitable, a new period of

interest will be queried until the user achieves a satisfactory pulse wave. Ultimately, pulse wave period to be demodulated is output from the function.

Afterwards, the third function of pulse wave characterization is deployed to indicate the systolic peaks and end-diastolics which are essential in blood pressure demodulation. The corresponding flowchart for this function is, thus, presented in Fig. A4.

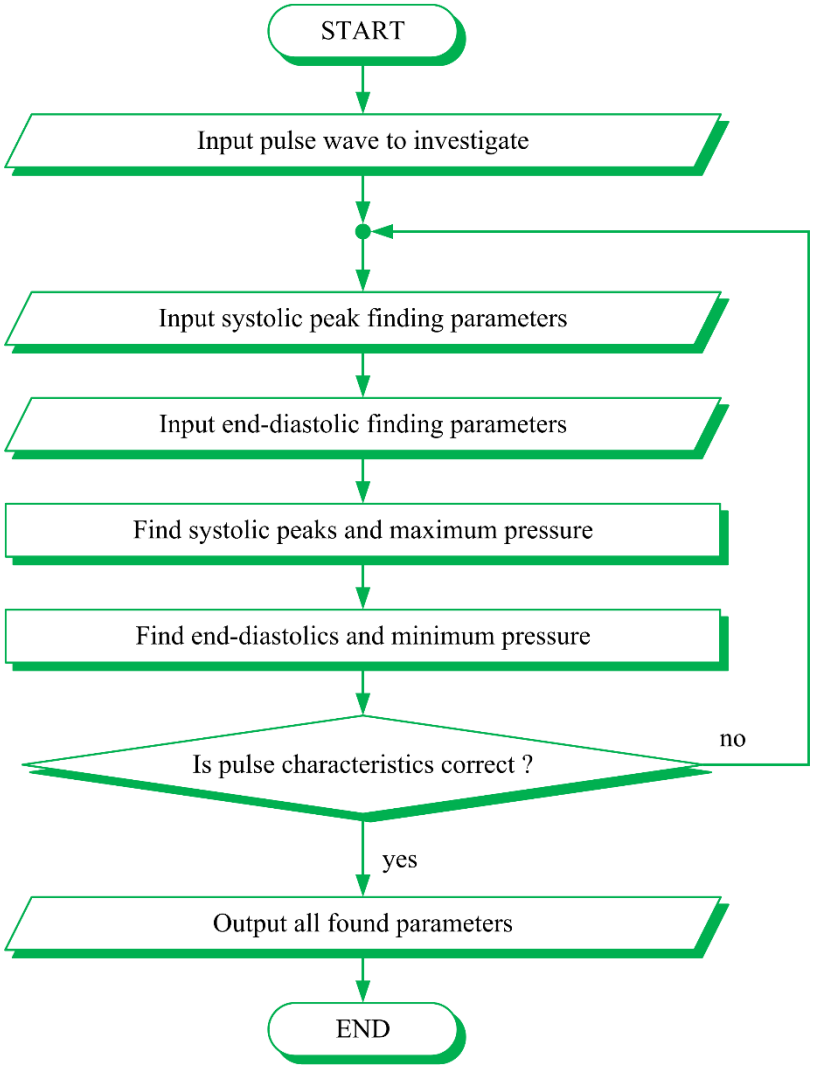

Fig. A4 Flowchart of pulse wave characterization function

As mentioned in Section 2.1, arterial pulse wave and blood pressure is closely related with the systolic peaks and end-diastolics revealing the systolic blood pressure (SBP) and diastolic blood pressure (DBP), respectively. Therefore, this MATLAB function allows quasi-automatic pulse wave characterization of an input pulse wave. Nevertheless, the peaks and end-points finding parameters such as minimum peak height and peak prominence are

manually determined. This is due to the "*findpeaks*" coding in MATLAB language that enables further accurate minimal and maximal points finding. Furthermore, the pulse wave amplitude measured from each volunteer is generally different, thereby a dynamic parameter adjustment is necessary. In this perspective, a human operator is required in this MATLAB function to properly operate rather than an automatic process. On the other hand, the human operator is more efficient in recognizing the important pulse characteristics. To accommodate, an automatic pulse characteristic display is implemented which will prompt the user to input new finding parameters until they consider the extracted systolic peaks and end-diastolics are correct. Then, the function outputs all pulse wave characteristics for the next operation.

Lastly is the blood pressure demodulation function that basically calculates the pressure values according to the determined pulse wave characteristics. Nonetheless, this function can be divided into two parts depending on the human operator requirements. The first part is consequently the three consecutive pulse period selection to calculate the pulse amplitude and pulse transit time (PTT) with the flowchart shown in Fig. A5.

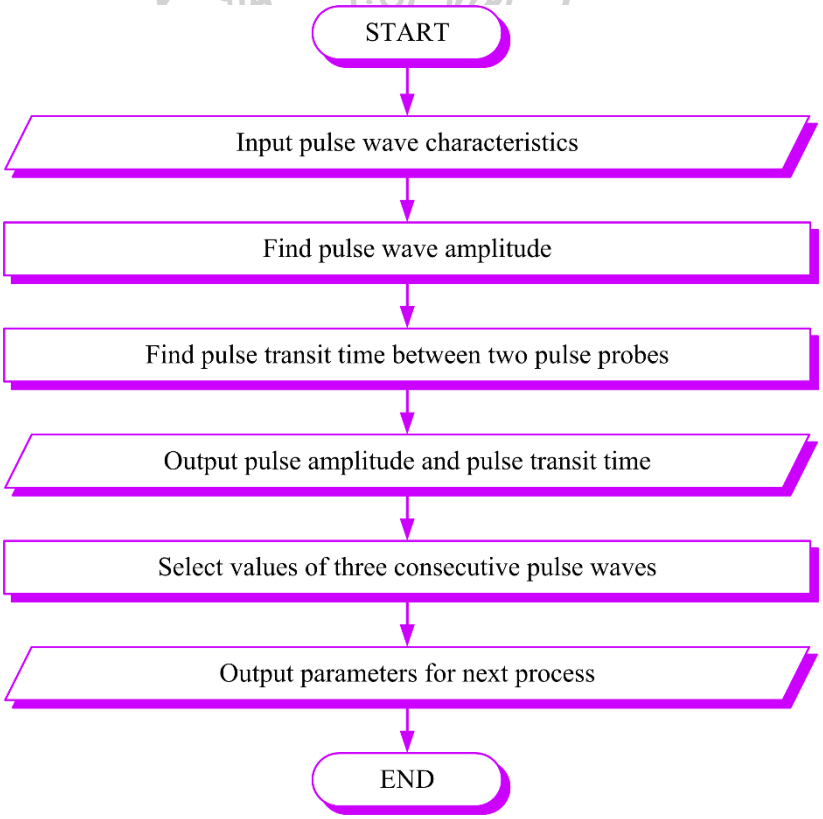

Fig. A5 Flowchart of pulse wave selection for blood pressure demodulation

After using the previously described MATLAB functions, the determined pulse wave characteristics are, consequently, applied to find the pulse amplitude for pulse pressure demodulation. Likewise, the PTT between pulse waves obtained from two different probes is calculated for subsequent diastolic blood pressure. Afterwards, the parameters are displayed to the operator who select a portion of interrogating period to perform blood pressure demodulation. Here, three consecutive arterial pulses are considered to be calibrated using the second part of the blood pressure demodulation function, which can be summarized in Fig. A6.

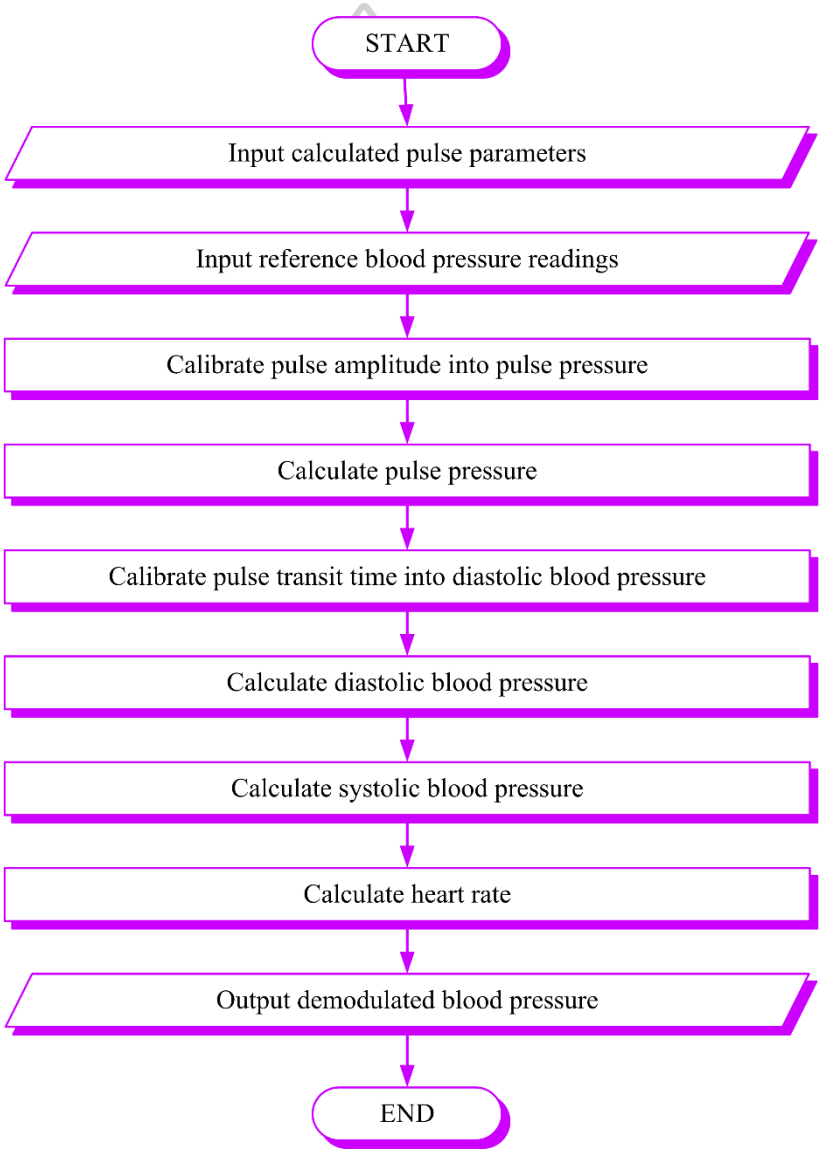

Fig. A6 Flowchart of blood pressure demodulation process

At this point, the reference blood pressure readings from the employed reference blood pressure instrument are input to initiate the calibration process. Here, the correlation between reference and measured blood pressure is established, allowing the demodulation function to calculate the corresponding pulse pressure from the pulse amplitude and diastolic blood pressure from pulse transit time, respectively. Thus, systolic blood pressure can be found as the summation between pulse pressure and diastolic blood pressure. Moreover, the heart rate is demodulated by counting the number of systolic peaks. In conclusion, all blood pressure parameters can be demodulated using this MATLAB function.

As explained in this chapter, application software for arterial pulse wave monitoring and blood pressure demodulation are developed to assist in the human examination. Mostly, the software developed either via LabVIEW or MATLAB programming proves helpful during the experiments as significant portions of the operation can be automated. However, the main limitation found in the utilization is the requirement of a human operator to define essential processing parameters and pulse wave recognition. At the moment, these manual inputs are adjusted to obtain accurate and correct blood pressure parameters and have not been automated to prevent erroneous outcomes. Regardless, the majority of the presented functions are practical in the operations and contribute to lessening the burden of human labor. The advantages and also limitations of these algorithms can, therefore, inspire new development of robust biomedical engineering application software in the future.

APPENDIX B
BLOOD PRESSURE DEMODULATION DATA

In Section 4.3, an example of blood pressure demodulation using the developed FFPI system has been demonstrated to provide an understanding of the process. Here, additional information shall be shown for deepening the knowledge in the demodulation. This appendix contains mostly graphical illustrations and mathematical expressions related to blood pressure demodulation without significant discussion on each item, which has already been explained in Chapter 3 and Chapter 4. The aim is, consequently, to showcase a more detailed process to those interested in learning and developing novel blood pressure demodulation algorithm.

In the FFPI system validation in blood pressure measurement, a total of 85 volunteers have participated in the experiment. This appendix, however, presents arterial pulse waves of several participants for the purpose of demonstration. For the following figures, three main data are illustrated: arterial pulse wave obtained through FFPI probe A (proximal to the wrist), pulse wave monitored using probe B (proximal to the heart), and their comparison which leads to pulse transit time (PTT) finding. The associated subfigures are plotted from (a) to (c), respectively. The former two of (a) and (b) show the original pulse wave directly obtained from the arterial pulse wave monitoring software with also the filtered pulse wave using FIR filter. The subplot (c), further, includes the pulse wave of probes A and B on an equivalent time-domain. Afterwards, the determined variables such as pulse pressure (PP), heart rate (HR), PTT, calibrated parameters, and demodulated blood pressure are described.

Nevertheless, the blood pressure demodulation data of all participants are included in this appendix.

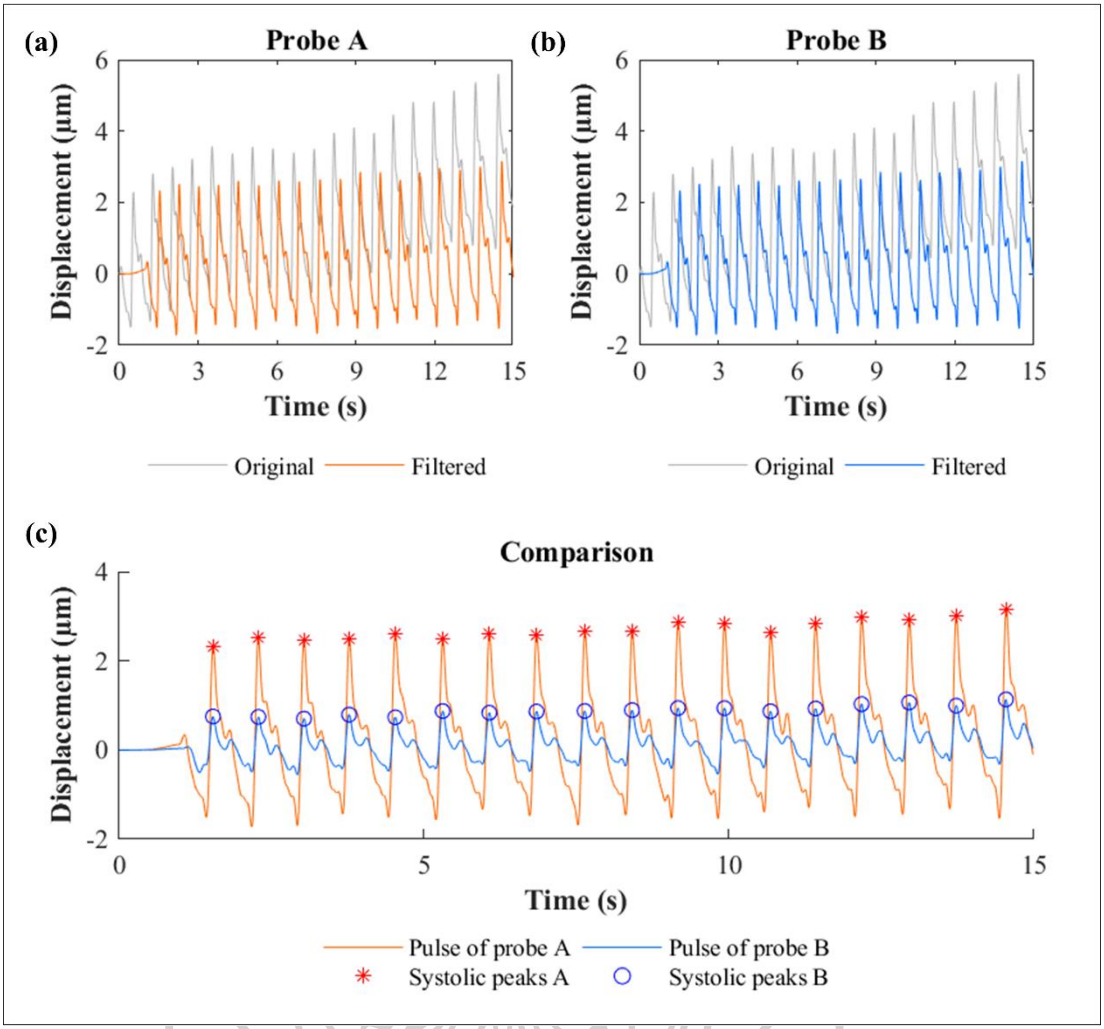

Fig. B1 Pulse waves of volunteer A measurement no. 1 :
(a) Pulse wave of probe A, (b) pulse wave of probe B, and (c) pulse wave comparison

Table B1 Measured parameters of volunteer A measurement no. 1

Probe A				Probe B			
Displacement	=	4.1791	µm	Displacement	=	1.2750	µm
Measured PP	=	0.0295	mmHg	Measured PP	=	0.0090	mmHg
Calibrated PP	=	43.2797	mmHg	Calibrated PP	=	41.4942	mmHg
Combine							
HR of probe A	=	72.8571	bpm	Mean PP	=	42.3869	mmHg
HR of probe B	=	72.8571	bpm	PTT	=	2.8267	ms
Mean HR	=	72.8571	bpm	PWV	=	16.9809	m/s

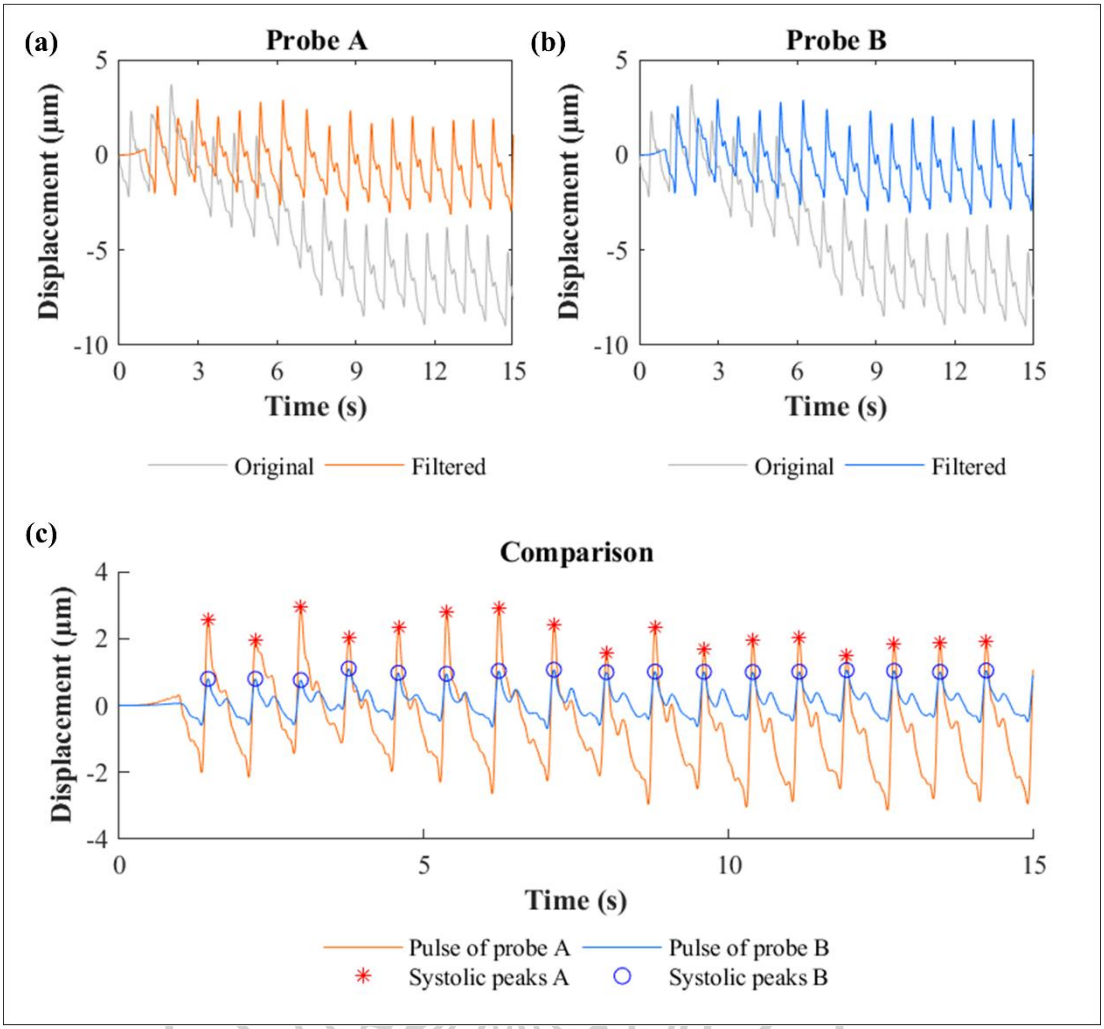

Fig. B2 Pulse wave showcase of volunteer A no. 2 :
(a) Pulse wave of probe A, (b) pulse wave of probe B, and (c) pulse wave comparison

Table B2 Measured parameters of volunteer A measurement no. 2

Probe A				Probe B			
Displacement	=	4.5757	μm	Displacement	=	1.4733	μm
Measured PP	=	0.0323	mmHg	Measured PP	=	0.0104	mmHg
Calibrated PP	=	43.7806	mmHg	Calibrated PP	=	44.4651	mmHg
Combine							
HR of probe A	=	72.8571	bpm	Mean PP	=	44.1228	mmHg
HR of probe B	=	72.8571	bpm	PTT	=	3.2500	ms
Mean HR	=	72.8571	bpm	PWV	=	14.7692	m/s

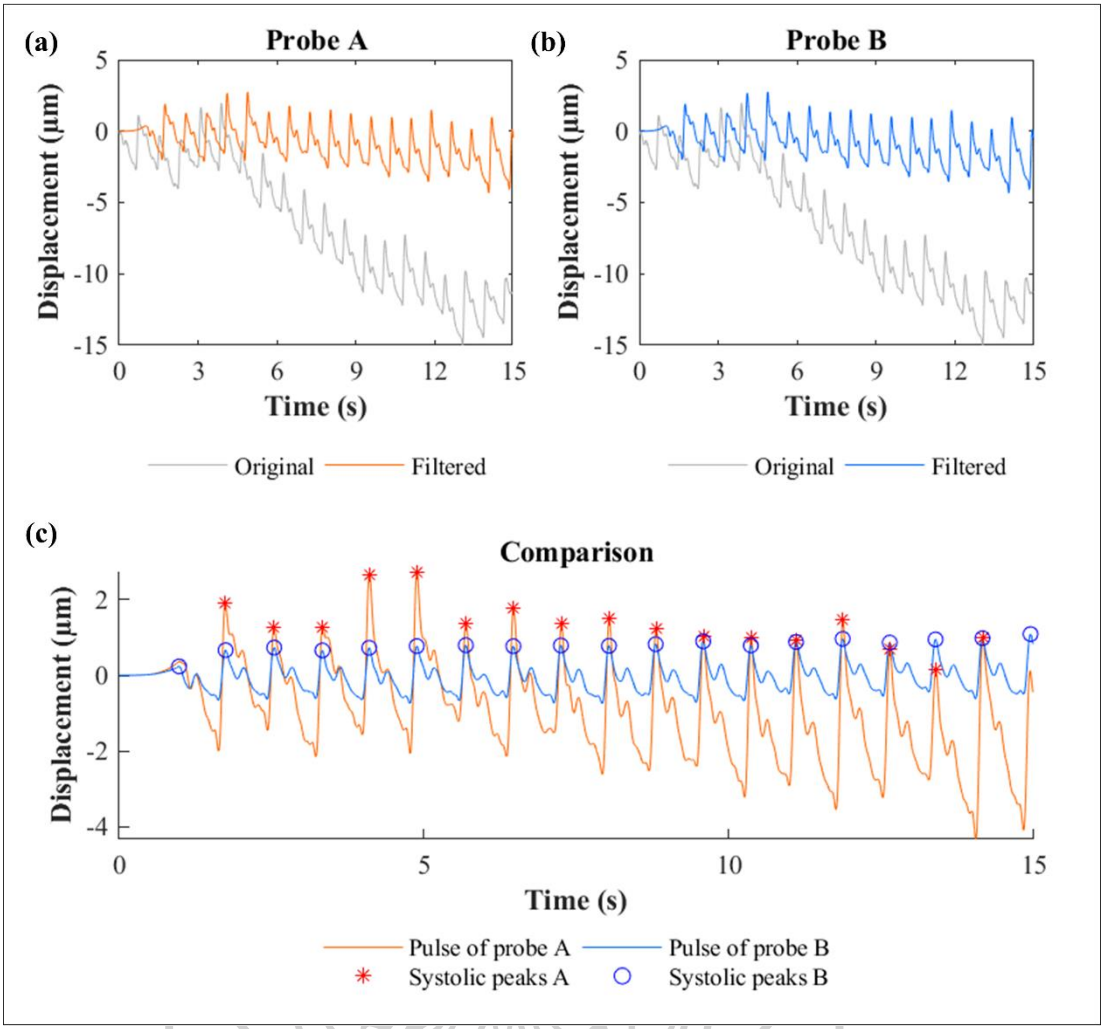

Fig. B3 Pulse wave showcase of volunteer A no. 3 :
(a) Pulse wave of probe A, (b) pulse wave of probe B, and (c) pulse wave comparison

Table B3 Measured parameters of volunteer A measurement no. 3

Probe A				Probe B			
Displacement	=	3.9099	μm	Displacement	=	1.4450	μm
Measured PP	=	0.0276	mmHg	Measured PP	=	0.0102	mmHg
Calibrated PP	=	42.9398	mmHg	Calibrated PP	=	44.0407	mmHg
Combine							
HR of probe A	=	71.1111	bpm	Mean PP	=	43.4902	mmHg
HR of probe B	=	71.1111	bpm	PTT	=	4.3250	ms
Mean HR	=	71.1111	bpm	PWV	=	11.0983	m/s

Table B4 Blood pressure demodulation of volunteer A

Parameters	No. 1	No. 2	No. 3
PP measurement (mmHg)	42.3869	44.1228	43.4902
PWV measurement (m/s)	16.9809	14.7692	11.0983
DBP coefficient $\frac{\mathrm{PWV}^2 \rho \Delta r_{\mathrm{artery}}}{\mathrm{PP}}$	43.2998	32.7551	18.4958
m_{DBP}	0.1731	0.1731	0.1731
c_{DBP}	64.7116	64.7116	64.7116
DBP measurement (mmHg) $\mathrm{DBP} = m_{\mathrm{DBP}} \frac{\mathrm{PWV}^2 \rho \Delta r_{\mathrm{artery}}}{\mathrm{PP}} + c_{\mathrm{DBP}}$	72.2061	70.3810	67.9129
SBP measurement (mmHg) $\mathrm{SBP} = \mathrm{DBP} + \mathrm{PP}$	114.5930	114.5038	111.4032

Table B5 Error analysis of volunteer A

Parameters		SBP	DBP	PP	HR
No. 1	Measurement (mmHg)	114.59	72.21	42.39	78.10
	Reference (mmHg)	114.50	73.00	41.50	76.50
	Absolute error (AE: mmHg)	0.09	0.79	0.89	1.60
	AE percentage (%)	0.08	1.09	2.14	2.09
No. 2	Measurement (mmHg)	114.50	70.38	44.12	75.28
	Reference (mmHg)	113.50	69.00	44.50	76.50
	Absolute error (AE: mmHg)	1.00	1.38	0.38	1.22
	AE percentage (%)	0.88	2.00	0.85	1.59
No. 3	Measurement (mmHg)	111.40	67.91	43.49	77.41
	Reference (mmHg)	112.50	68.50	44.00	77.50
	Absolute error (AE: mmHg)	1.10	0.59	0.51	0.09
	AE percentage (%)	0.97	0.86	1.16	0.12

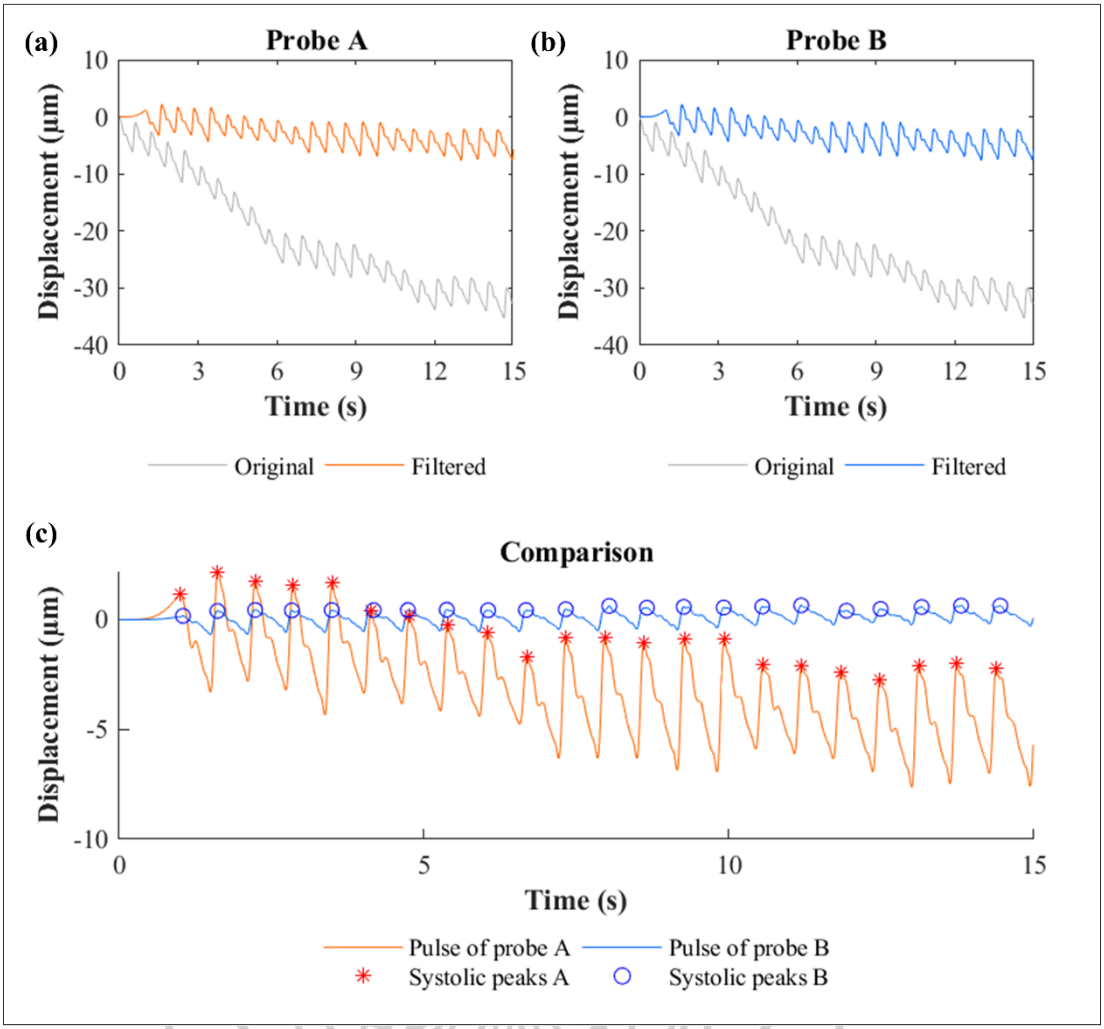

Fig. B4 Pulse wave showcase of volunteer B no. 1 :
(a) Pulse wave of probe A, (b) pulse wave of probe B, and (c) pulse wave comparison

Table B6 Measured parameters of volunteer B measurement no. 1

Probe A				Probe B			
Displacement	=	4.8449	μm	Displacement	=	0.9208	μm
Measured PP	=	0.0342	mmHg	Measured PP	=	0.0065	mmHg
Calibrated PP	=	33.8089	mmHg	Calibrated PP	=	29.6019	mmHg
Combine							
HR of probe A	=	90.0000	bpm	Mean PP	=	31.7054	mmHg
HR of probe B	=	90.0000	bpm	PTT	=	25.1400	ms
Mean HR	=	90.0000	bpm	PWV	=	1.4718	m/s

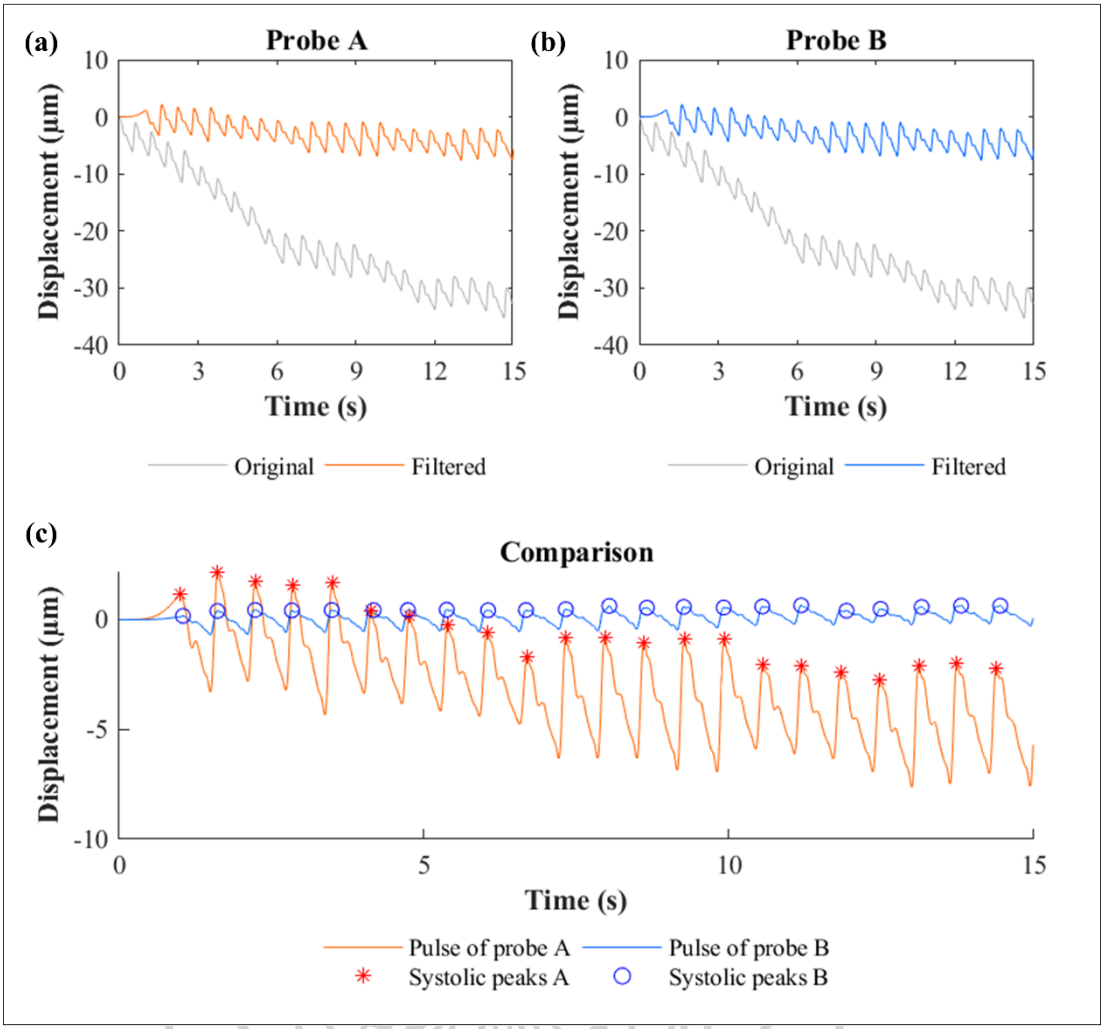

Fig. B5 Pulse wave showcase of volunteer B no. 2 :
(a) Pulse wave of probe A, (b) pulse wave of probe B, and (c) pulse wave comparison

Table B7 Measured parameters of volunteer B measurement no. 2

Probe A				Probe B			
Displacement	=	4.3349	μm	Displacement	=	1.1333	μm
Measured PP	=	0.0306	mmHg	Measured PP	=	0.0080	mmHg
Calibrated PP	=	28.3880	mmHg	Calibrated PP	=	31.5883	mmHg
Combine							
HR of probe A	=	95.6522	bpm	Mean PP	=	29.9882	mmHg
HR of probe B	=	95.6522	bpm	PTT	=	17.2545	ms
Mean HR	=	95.6522	bpm	PWV	=	2.1444	m/s

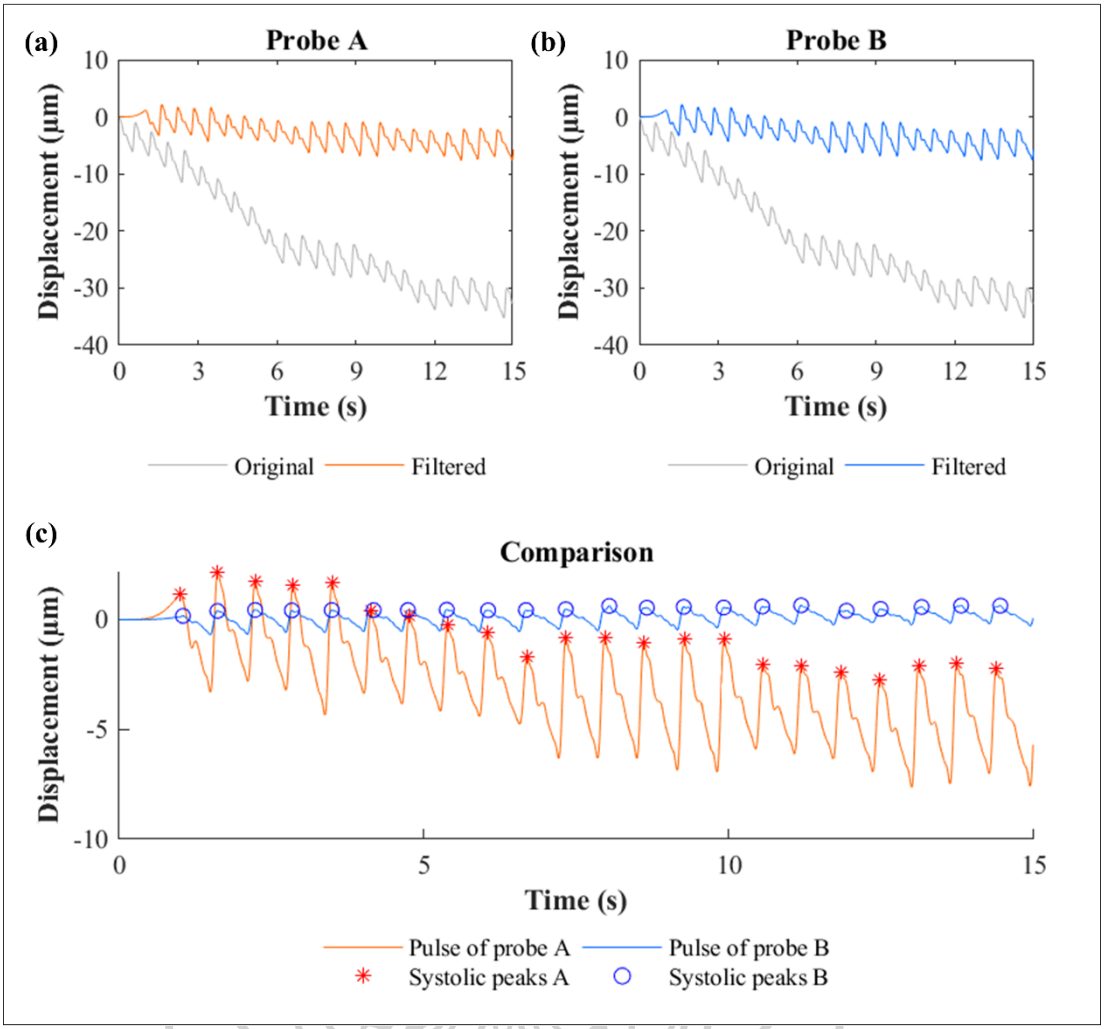

Fig. B6 Pulse wave showcase of volunteer B no. 3 :
(a) Pulse wave of probe A, (b) pulse wave of probe B, and (c) pulse wave comparison

Table B8 Measured parameters of volunteer B measurement no. 3

Probe A				Probe B			
Displacement	=	4.7032	μm	Displacement	=	1.3175	μm
Measured PP	=	0.0332	mmHg	Measured PP	=	0.0093	mmHg
Calibrated PP	=	32.3031	mmHg	Calibrated PP	=	33.3098	mmHg
Combine							
HR of probe A	=	90.0000	bpm	Mean PP	=	32.8065	mmHg
HR of probe B	=	90.0000	bpm	PTT	=	19.1238	ms
Mean HR	=	90.0000	bpm	PWV	=	1.9348	m/s

Table B9 Blood pressure demodulation of volunteer B

Parameters	No. 1	No. 2	No. 3
PP measurement (mmHg)	31.7054	29.9882	32.8065
PWV measurement (m/s)	1.4718	2.1444	1.9348
DBP coefficient $\frac{\mathrm{PWV}^2 \rho \Delta r_{\mathrm{artery}}}{\mathrm{PP}}$	0.3253	0.6905	0.5621
m_{DBP}	-5.0292	-5.0292	-5.0292
c_{DBP}	81.6451	81.6451	81.6451
DBP measurement (mmHg) $\mathrm{DBP} = m_{\mathrm{DBP}} \frac{\mathrm{PWV}^2 \rho \Delta r_{\mathrm{artery}}}{\mathrm{PP}} + c_{\mathrm{DBP}}$	80.0093	78.1725	78.8182
SBP measurement (mmHg) $\mathrm{SBP} = \mathrm{DBP} + \mathrm{PP}$	111.7147	108.1606	111.6247

Table B10 Error analysis of volunteer B

Parameters		SBP	DBP	PP	HR
No. 1	Measurement (mmHg)	111.71	80.01	31.71	93.72
	Reference (mmHg)	112.50	81.00	31.50	99.50
	Absolute error (AE: mmHg)	0.79	0.99	0.21	5.78
	AE percentage (%)	0.70	1.22	0.65	5.81
No. 2	Measurement (mmHg)	108.16	78.17	29.99	100.74
	Reference (mmHg)	107.50	80.00	27.50	100.00
	Absolute error (AE: mmHg)	0.66	1.83	2.49	0.74
	AE percentage (%)	0.61	2.28	9.05	0.74
No. 3	Measurement (mmHg)	111.62	78.82	32.81	94.02
	Reference (mmHg)	111.50	76.00	35.50	94.50
	Absolute error (AE: mmHg)	0.12	2.82	2.69	0.48
	AE percentage (%)	0.11	3.71	7.59	0.51

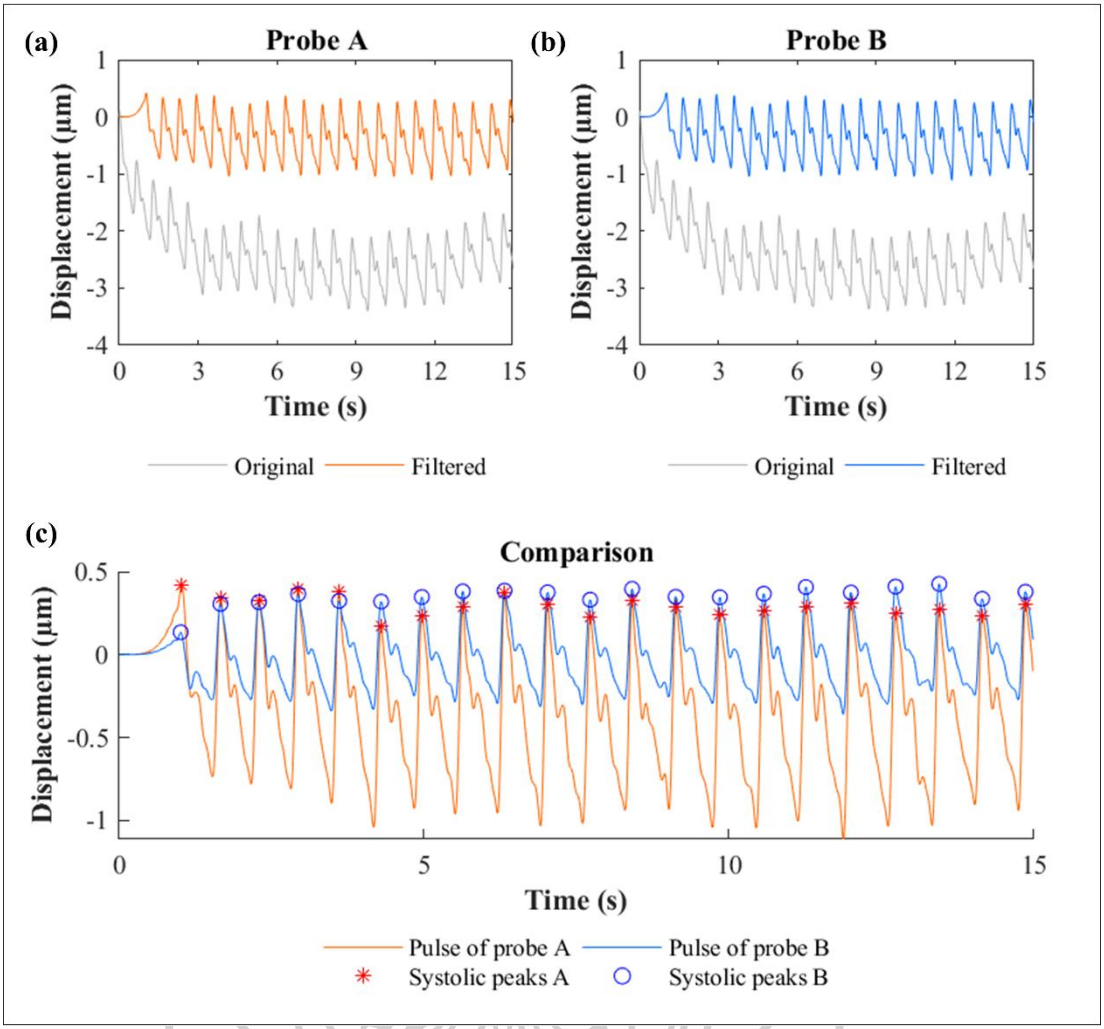

Fig. B7 Pulse wave showcase of volunteer C no. 1 :
(a) Pulse wave of probe A, (b) pulse wave of probe B, and (c) pulse wave comparison

Table B11 Measured parameters of volunteer C measurement no. 1

Probe A				Probe B			
Displacement	=	1.2466	μm	Displacement	=	0.6517	μm
Measured PP	=	0.0088	mmHg	Measured PP	=	0.0046	mmHg
Calibrated PP	=	29.1496	mmHg	Calibrated PP	=	29.2143	mmHg
Combine							
HR of probe A	=	86.2512	bpm	Mean PP	=	29.1819	mmHg
HR of probe B	=	86.2225	bpm	PTT	=	2.3059	ms
Mean HR	=	86.2369	bpm	PWV	=	20.8162	m/s

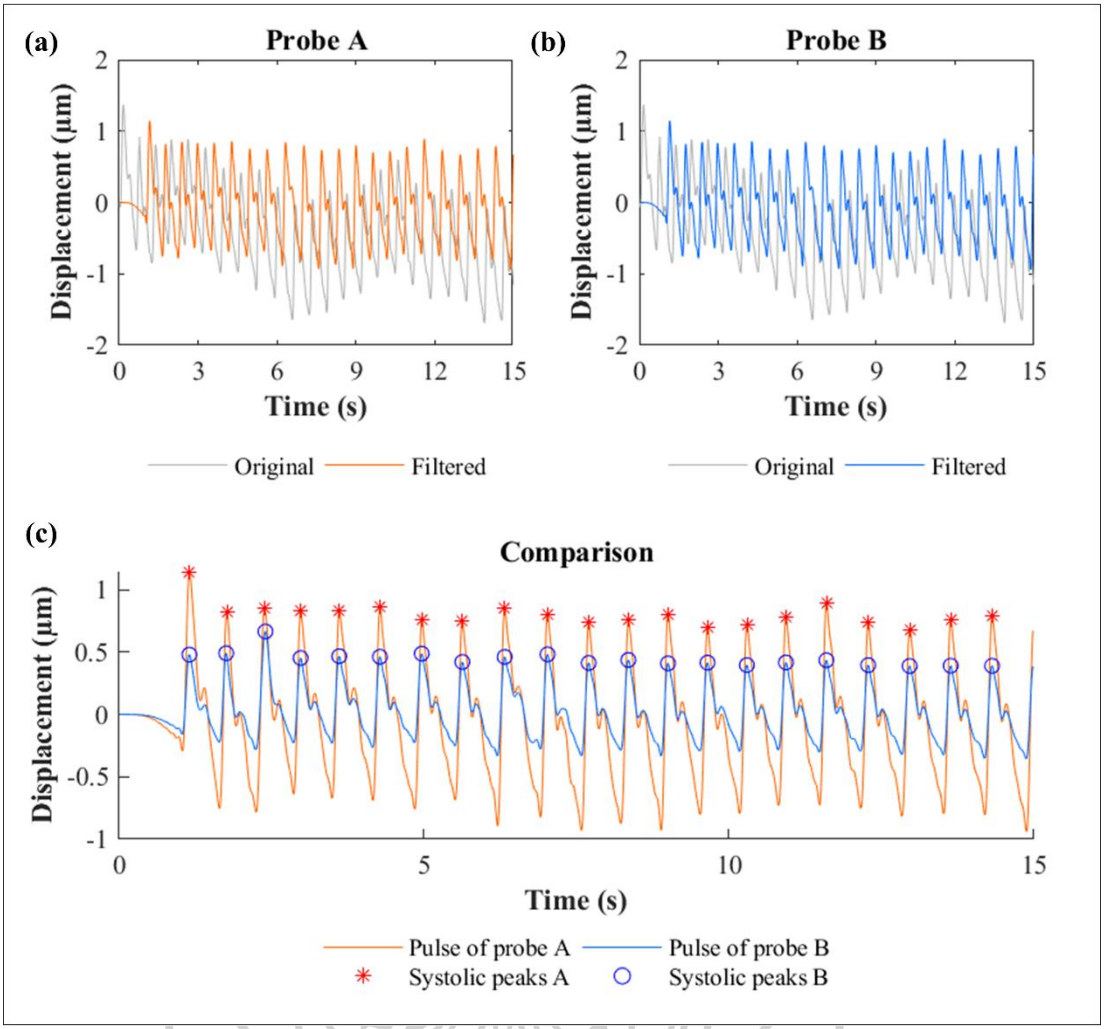

Fig. B8 Pulse wave showcase of volunteer C no. 2 :
(a) Pulse wave of probe A, (b) pulse wave of probe B, and (c) pulse wave comparison

Table B12 Measured parameters of volunteer C measurement no. 2

Probe A				Probe B			
Displacement	=	1.5725	µm	Displacement	=	0.7366	µm
Measured PP	=	0.0111	mmHg	Measured PP	=	0.0052	mmHg
Calibrated PP	=	29.3541	mmHg	Calibrated PP	=	29.3571	mmHg
Combine							
HR of probe A	=	91.0273	bpm	Mean PP	=	29.3556	mmHg
HR of probe B	=	91.0405	bpm	PTT	=	2.9200	ms
Mean HR	=	91.0339	bpm	PWV	=	16.4384	m/s

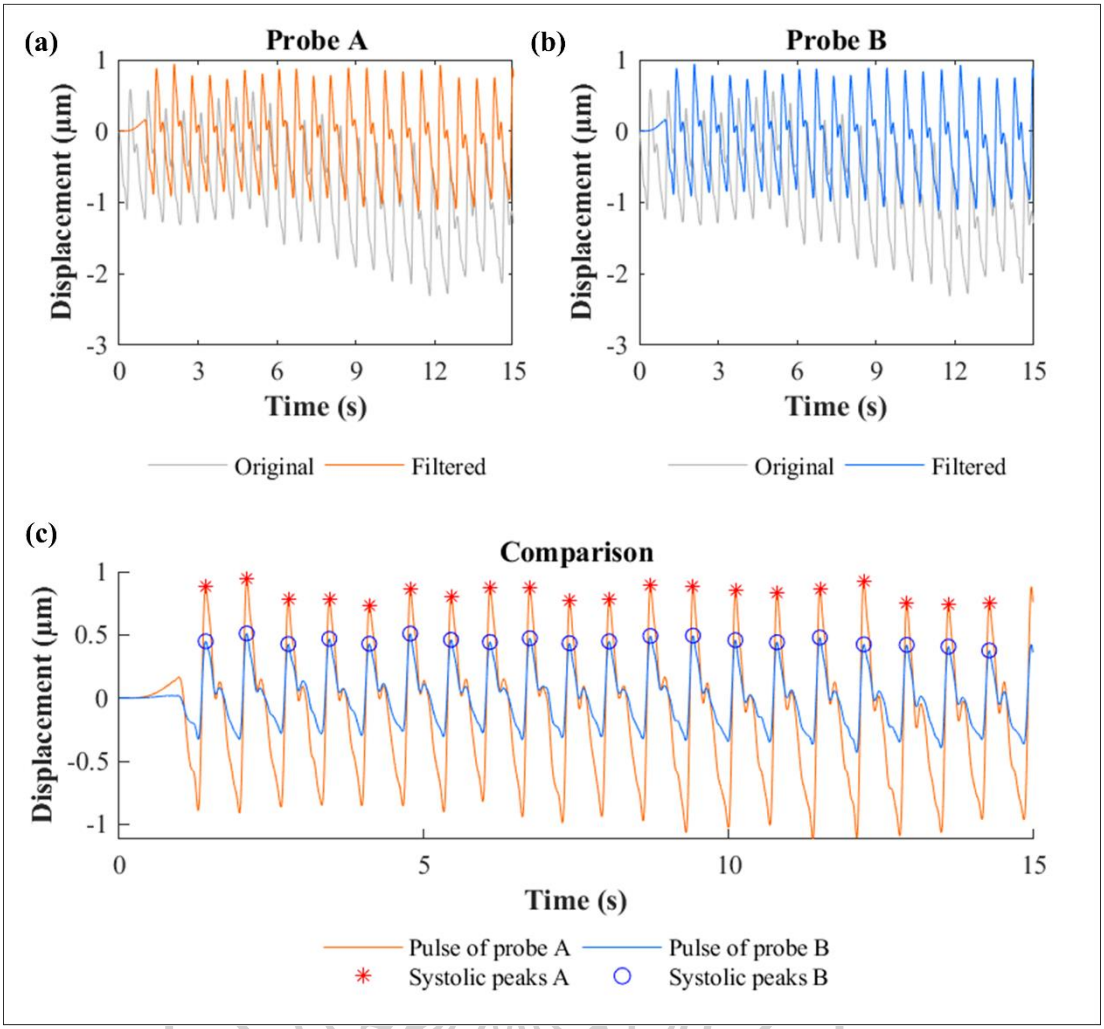

Fig. B9 Pulse wave showcase of volunteer C no. 3 :
(a) Pulse wave of probe A, (b) pulse wave of probe B, and (c) pulse wave comparison

Table B13 Measured parameters of volunteer C measurement no. 3

Probe A				Probe B			
Displacement	=	1.7991	μm	Displacement	=	0.7791	μm
Measured PP	=	0.0127	mmHg	Measured PP	=	0.0055	mmHg
Calibrated PP	=	29.4963	mmHg	Calibrated PP	=	29.4286	mmHg
Combine							
HR of probe A	=	88.6184	bpm	Mean PP	=	29.4624	mmHg
HR of probe B	=	88.6708	bpm	PTT	=	1.9600	ms
Mean HR	=	88.6446	bpm	PWV	=	24.4898	m/s

Table B14 Blood pressure demodulation of volunteer C

Parameters	No. 1	No. 2	No. 3
PP measurement (mmHg)	29.1819	29.3556	29.4624
PWV measurement (m/s)	20.8162	16.4384	24.4898
DBP coefficient $\frac{\mathrm{PWV}^2 \rho \Delta r_{\mathrm{artery}}}{\mathrm{PP}}$	65.0676	40.5770	90.0603
m_{DBP}	0.0000	0.0000	0.0000
c_{DBP}	88.0000	88.0000	88.0000
DBP measurement (mmHg) $\mathrm{DBP} = m_{\mathrm{DBP}} \frac{\mathrm{PWV}^2 \rho \Delta r_{\mathrm{artery}}}{\mathrm{PP}} + c_{\mathrm{DBP}}$	88.0000	88.0000	88.0000
SBP measurement (mmHg) $\mathrm{SBP} = \mathrm{DBP} + \mathrm{PP}$	117.1819	117.3556	117.4624

Table B15 Error analysis of volunteer C

Parameters		SBP	DBP	PP	HR
No. 1	Measurement (mmHg)	117.18	88.00	29.18	86.24
	Reference (mmHg)	117.50	88.00	29.50	86.00
	Absolute error (AE: mmHg)	0.32	0.00	0.32	0.24
	AE percentage (%)	0.27	0.00	1.08	0.28
No. 2	Measurement (mmHg)	117.36	88.00	29.36	91.03
	Reference (mmHg)	116.50	88.00	28.50	86.50
	Absolute error (AE: mmHg)	0.86	0.00	0.86	4.53
	AE percentage (%)	0.73	0.00	3.00	5.24
No. 3	Measurement (mmHg)	117.46	88.00	29.46	88.64
	Reference (mmHg)	118.00	88.00	30.00	86.00
	Absolute error (AE: mmHg)	0.54	0.00	0.54	2.64
	AE percentage (%)	0.46	0.00	1.79	3.08

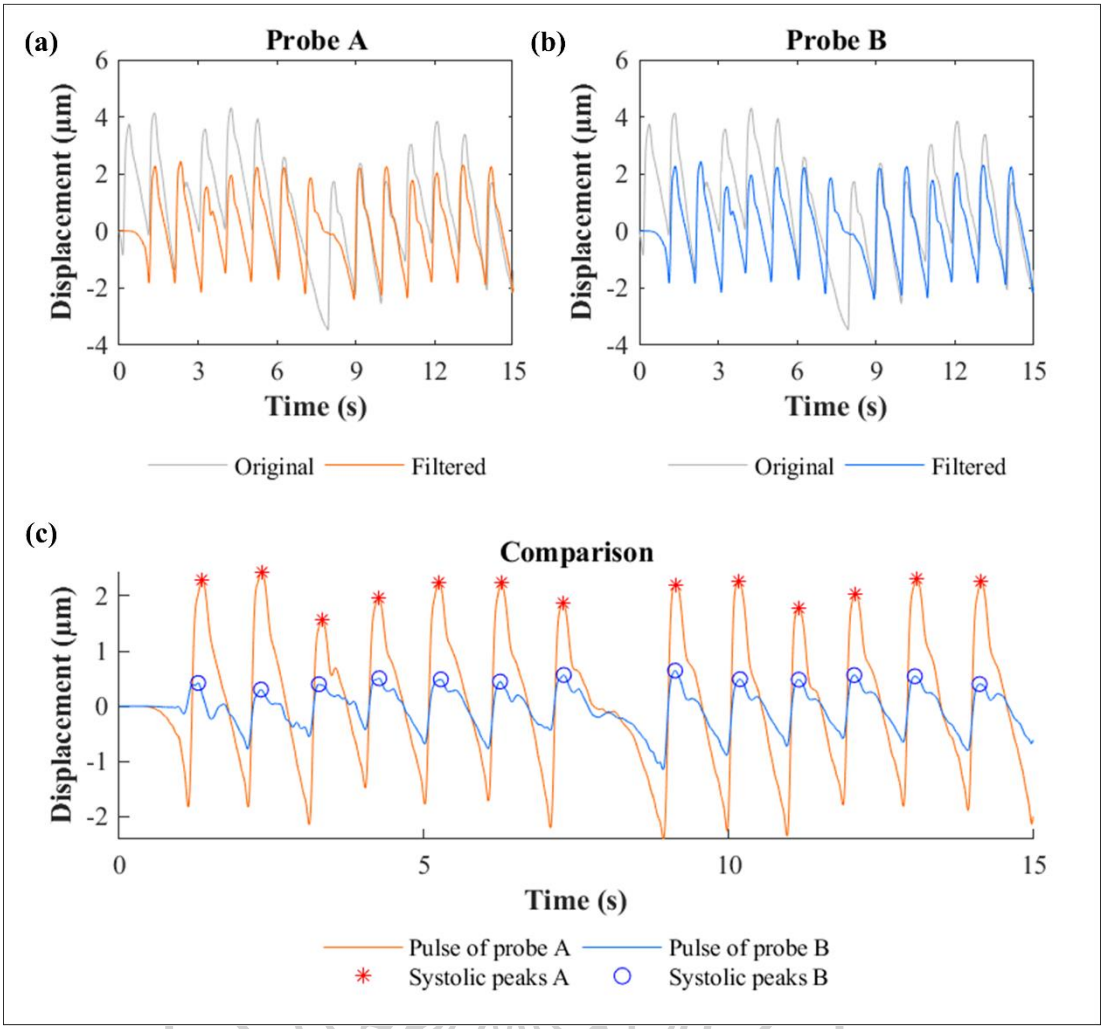

Fig. B10Pulse wave showcase of volunteer D no. 1 :
(a) Pulse wave of probe A, (b) pulse wave of probe B, and (c) pulse wave comparison

Table B16 Measured parameters of volunteer D measurement no. 1

Probe A				Probe B			
Displacement	=	4.0657	µm	Displacement	=	1.1900	µm
Measured PP	=	0.0287	mmHg	Measured PP	=	0.0084	mmHg
Calibrated PP	=	35.9991	mmHg	Calibrated PP	=	35.7500	mmHg
Combine							
HR of probe A	=	55.9038	bpm	Mean PP	=	35.8745	mmHg
HR of probe B	=	55.8981	bpm	PTT	=	21.4909	ms
Mean HR	=	55.9009	bpm	PWV	=	2.0008	m/s

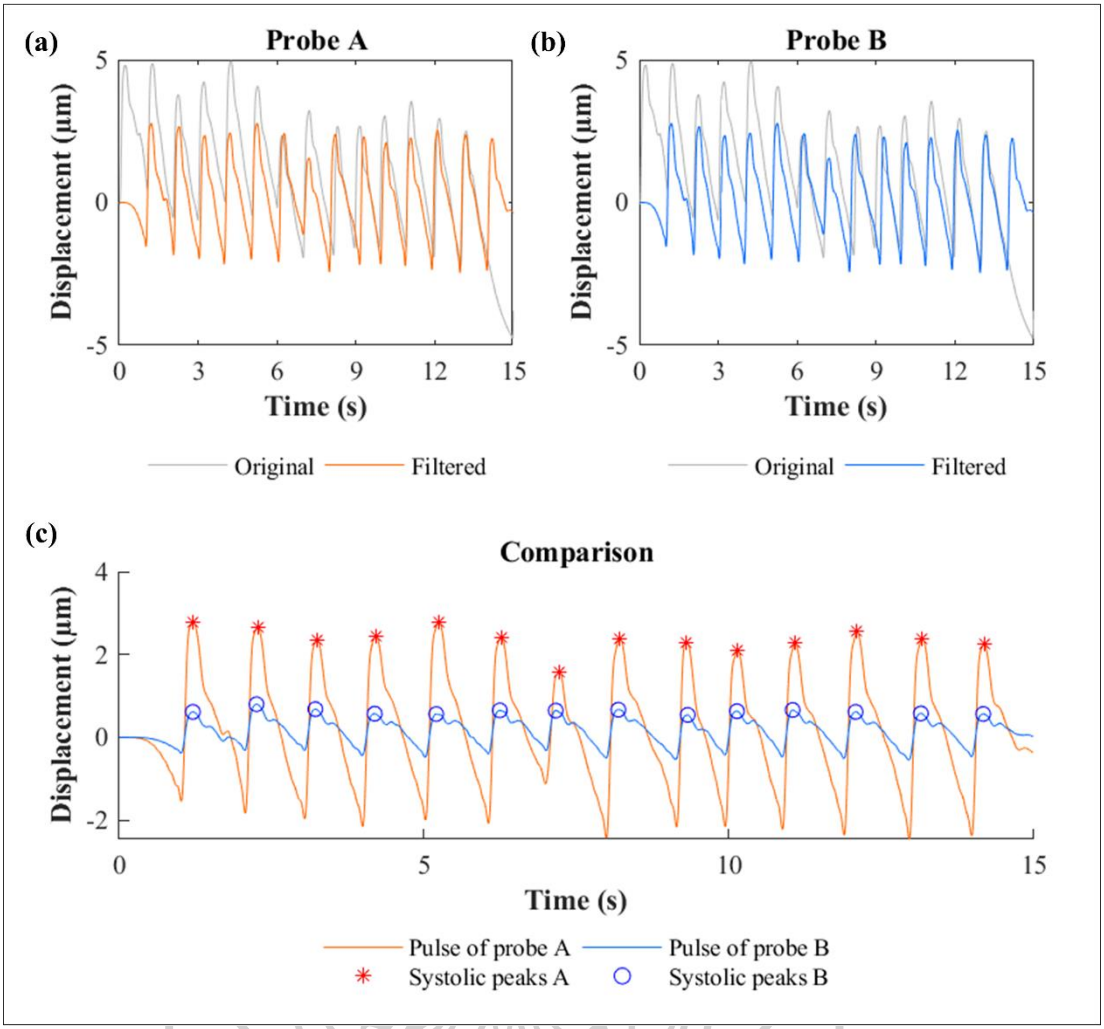

Fig. B11Pulse wave showcase of volunteer D no. 2 :
(a) Pulse wave of probe A, (b) pulse wave of probe B, and (c) pulse wave comparison

Table B17 Measured parameters of volunteer D measurement no. 2

Probe A				Probe B			
Displacement	=	4.4624	µm	Displacement	=	1.0766	µm
Measured PP	=	0.0315	mmHg	Measured PP	=	0.0076	mmHg
Calibrated PP	=	34.5268	mmHg	Calibrated PP	=	34.2500	mmHg
Combine							
HR of probe A	=	60.1740	bpm	Mean PP	=	34.3884	mmHg
HR of probe B	=	60.1703	bpm	PTT	=	28.6154	ms
Mean HR	=	60.1722	bpm	PWV	=	1.5027	m/s

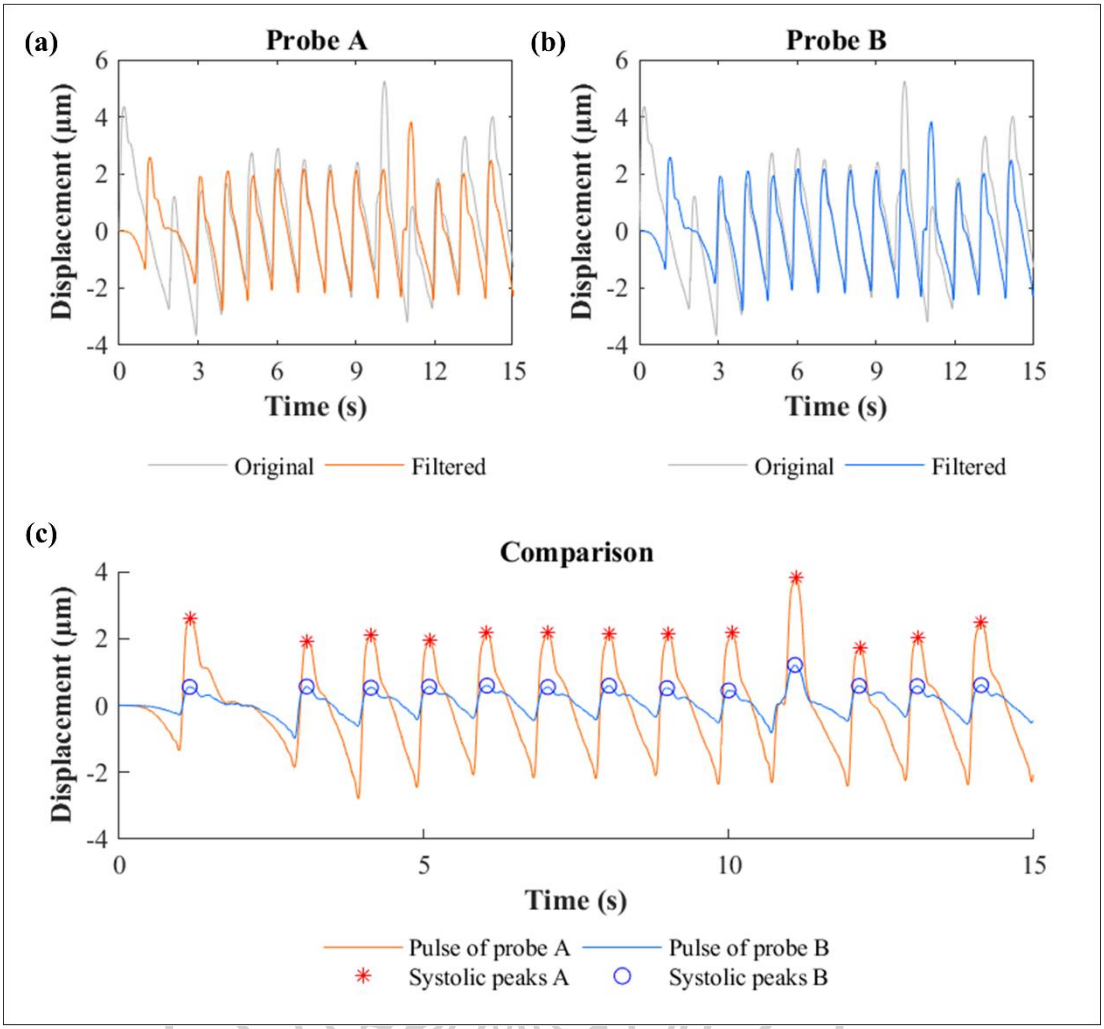

Fig. B.12 Pulse wave showcase of volunteer D no. 3 :
(a) Pulse wave of probe A, (b) pulse wave of probe B, and (c) pulse wave comparison

Table B18 Measured parameters of volunteer D measurement no. 3

Probe A				Probe B			
Displacement	=	4.4766	µm	Displacement	=	1.1333	µm
Measured PP	=	0.0316	mmHg	Measured PP	=	0.0080	mmHg
Calibrated PP	=	34.4742	mmHg	Calibrated PP	=	35.0000	mmHg
Combine							
HR of probe A	=	55.6586	bpm	Mean PP	=	34.7371	mmHg
HR of probe B	=	55.6965	bpm	PTT	=	16.0000	ms
Mean HR	=	55.6776	bpm	PWV	=	2.6875	m/s

Table B19 Blood pressure demodulation of volunteer D

Parameters	No. 1	No. 2	No. 3
PP measurement (mmHg)	35.8745	34.3884	34.7371
PWV measurement (m/s)	2.0008	1.5027	2.6875
DBP coefficient $\frac{\mathrm{PWV}^2 \rho \Delta r_{\mathrm{artery}}}{\mathrm{PP}}$	0.6012	0.3391	1.0846
m_{DBP}	0.2579	0.2579	0.2579
c_{DBP}	50.9926	50.9926	50.9926
DBP measurement (mmHg) $\mathrm{DBP} = m_{\mathrm{DBP}} \frac{\mathrm{PWV}^2 \rho \Delta r_{\mathrm{artery}}}{\mathrm{PP}} + c_{\mathrm{DBP}}$	51.1476	51.0800	51.2723
SBP measurement (mmHg) $\mathrm{SBP} = \mathrm{DBP} + \mathrm{PP}$	87.0222	85.4684	86.0094

Table B20 Error analysis of volunteer D

Parameters		SBP	DBP	PP	HR
No. 1	Measurement (mmHg)	87.02	51.15	35.87	55.90
	Reference (mmHg)	86.50	50.50	36.00	57.50
	Absolute error (AE: mmHg)	0.52	0.65	0.13	1.60
	AE percentage (%)	0.60	1.28	0.35	2.78
No. 2	Measurement (mmHg)	85.47	51.08	34.39	60.17
	Reference (mmHg)	86.00	51.50	34.50	58.50
	Absolute error (AE: mmHg)	0.53	0.42	0.11	1.67
	AE percentage (%)	0.62	0.82	0.32	2.86
No. 3	Measurement (mmHg)	86.01	51.27	34.74	55.68
	Reference (mmHg)	86.00	51.50	34.50	60.00
	Absolute error (AE: mmHg)	0.01	0.23	0.24	4.32
	AE percentage (%)	0.01	0.44	0.69	7.20

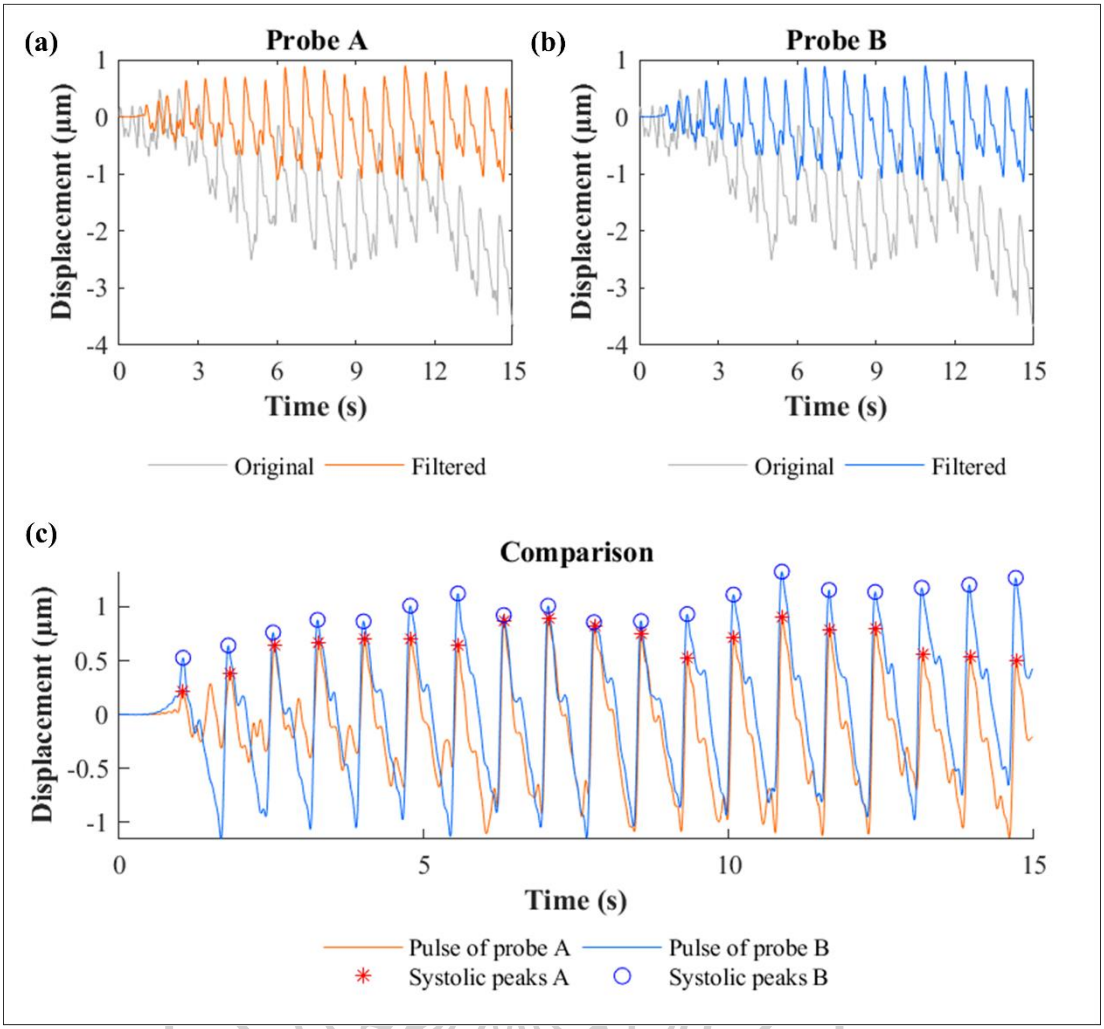

Fig. B13Pulse wave showcase of volunteer E no. 1 :
(a) Pulse wave of probe A, (b) pulse wave of probe B, and (c) pulse wave comparison

Table B21 Measured parameters of volunteer E measurement no. 1

Probe A				Probe B			
Displacement	=	1.5441	μm	Displacement	=	1.9550	μm
Measured PP	=	0.0109	mmHg	Measured PP	=	0.0138	mmHg
Calibrated PP	=	28.5830	mmHg	Calibrated PP	=	28.0920	mmHg
Combine							
HR of probe A	=	76.9184	bpm	Mean PP	=	28.3375	mmHg
HR of probe B	=	78.9889	bpm	PTT	=	13.8353	ms
Mean HR	=	77.9537	bpm	PWV	=	3.3248	m/s

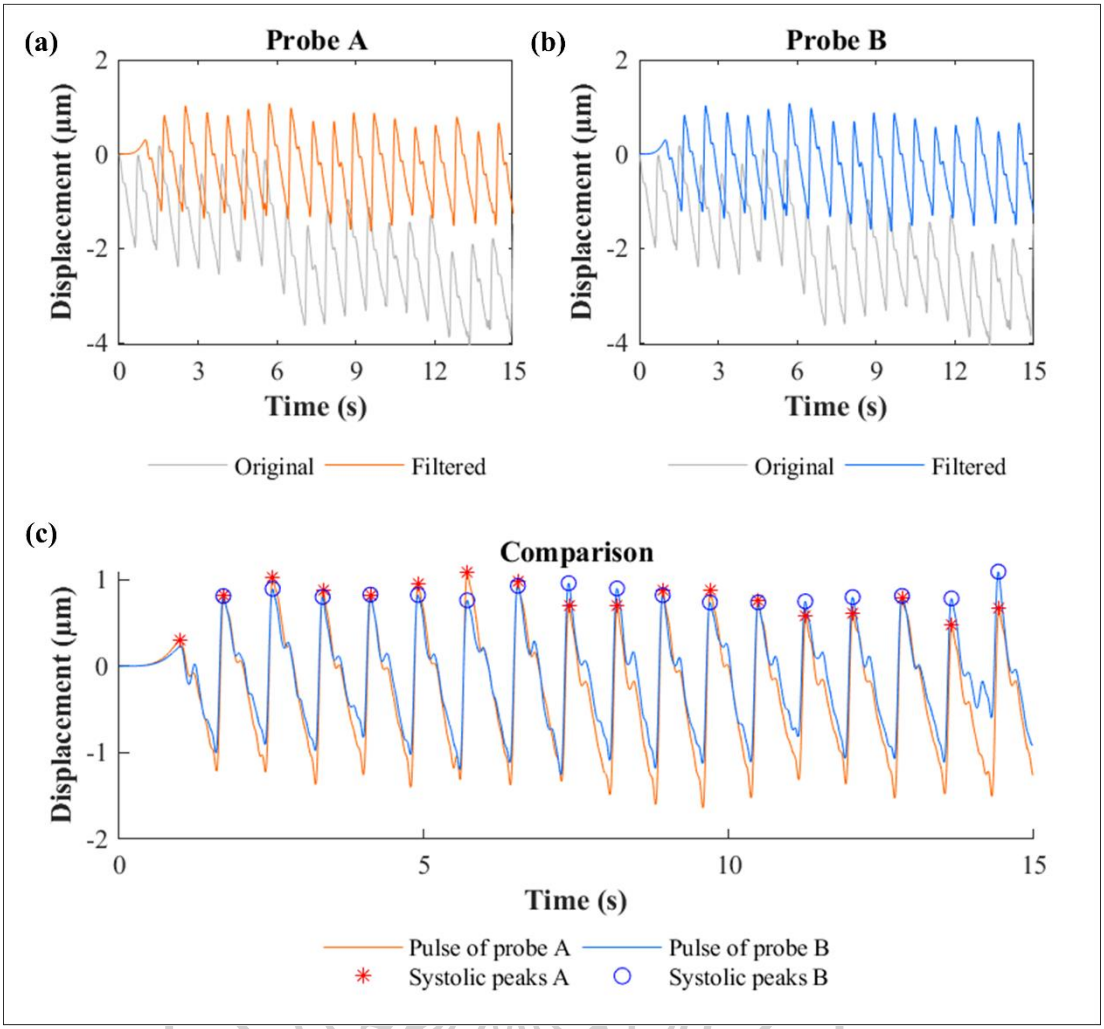

Fig. B14Pulse wave showcase of volunteer E no. 2 :
(a) Pulse wave of probe A, (b) pulse wave of probe B, and (c) pulse wave comparison

Table B22 Measured parameters of volunteer E measurement no. 2

Probe A				Probe B			
Displacement	=	2.2241	μm	Displacement	=	1.8558	μm
Measured PP	=	0.0157	mmHg	Measured PP	=	0.0131	mmHg
Calibrated PP	=	29.7448	mmHg	Calibrated PP	=	29.2254	mmHg
Combine							
HR of probe A	=	75.5026	bpm	Mean PP	=	29.4851	mmHg
HR of probe B	=	75.4836	bpm	PTT	=	4.7750	ms
Mean HR	=	75.4931	bpm	PWV	=	9.6335	m/s

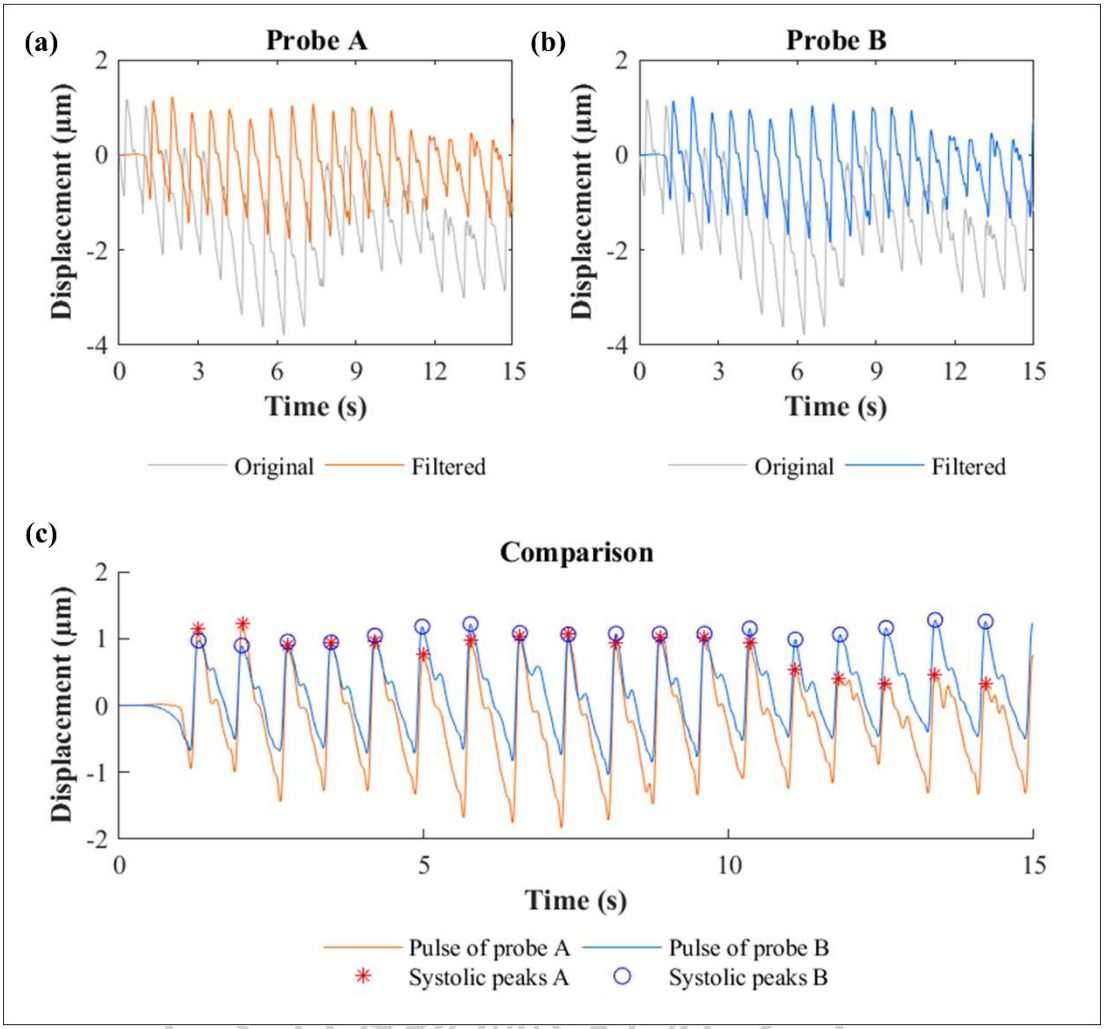

Fig. B15Pulse wave showcase of volunteer E no. 3 :
(a) Pulse wave of probe A, (b) pulse wave of probe B, and (c) pulse wave comparison

Table B23 Measured parameters of volunteer E measurement no. 3

Probe A				Probe B			
Displacement	=	2.1816	µm	Displacement	=	1.7283	µm
Measured PP	=	0.0154	mmHg	Measured PP	=	0.0122	mmHg
Calibrated PP	=	29.6722	mmHg	Calibrated PP	=	30.6826	mmHg
Combine							
HR of probe A	=	78.9174	bpm	Mean PP	=	30.1774	mmHg
HR of probe B	=	78.8713	bpm	PTT	=	6.0444	ms
Mean HR	=	78.8944	bpm	PWV	=	7.6104	m/s

Table B24 Blood pressure demodulation of volunteer E

Parameters	No. 1	No. 2	No. 3
PP measurement (mmHg)	28.3375	29.4851	30.1774
PWV measurement (m/s)	13.8353	4.7750	6.0444
DBP coefficient $\frac{\mathrm{PWV}^2 \rho \Delta r_{\mathrm{artery}}}{\mathrm{PP}}$	3.3248	9.6335	7.6104
m_{DBP}	1.6600	13.9358	8.6971
c_{DBP}	0.0266	0.0266	0.0266
DBP measurement (mmHg) $\mathrm{DBP} = m_{\mathrm{DBP}} \frac{\mathrm{PWV}^2 \rho \Delta r_{\mathrm{artery}}}{\mathrm{PP}} + c_{\mathrm{DBP}}$	70.4511	70.4511	70.4511
SBP measurement (mmHg) $\mathrm{SBP} = \mathrm{DBP} + \mathrm{PP}$	70.4953	70.8221	70.6826

Table B25 Error analysis of volunteer E

Parameters		SBP	DBP	PP	HR
No. 1	Measurement (mmHg)	98.83	70.50	28.34	77.95
	Reference (mmHg)	99.50	71.00	28.50	80.00
	Absolute error (AE: mmHg)	0.67	0.50	0.16	2.05
	AE percentage (%)	0.67	0.71	0.57	2.56
No. 2	Measurement (mmHg)	100.31	70.82	29.49	75.49
	Reference (mmHg)	100.00	71.50	28.50	80.00
	Absolute error (AE: mmHg)	0.31	0.68	0.99	4.51
	AE percentage (%)	0.31	0.95	3.46	5.63
No. 3	Measurement (mmHg)	100.86	70.68	30.18	78.89
	Reference (mmHg)	100.50	69.50	31.00	80.00
	Absolute error (AE: mmHg)	0.36	1.18	0.82	1.11
	AE percentage (%)	0.36	1.70	2.65	1.38

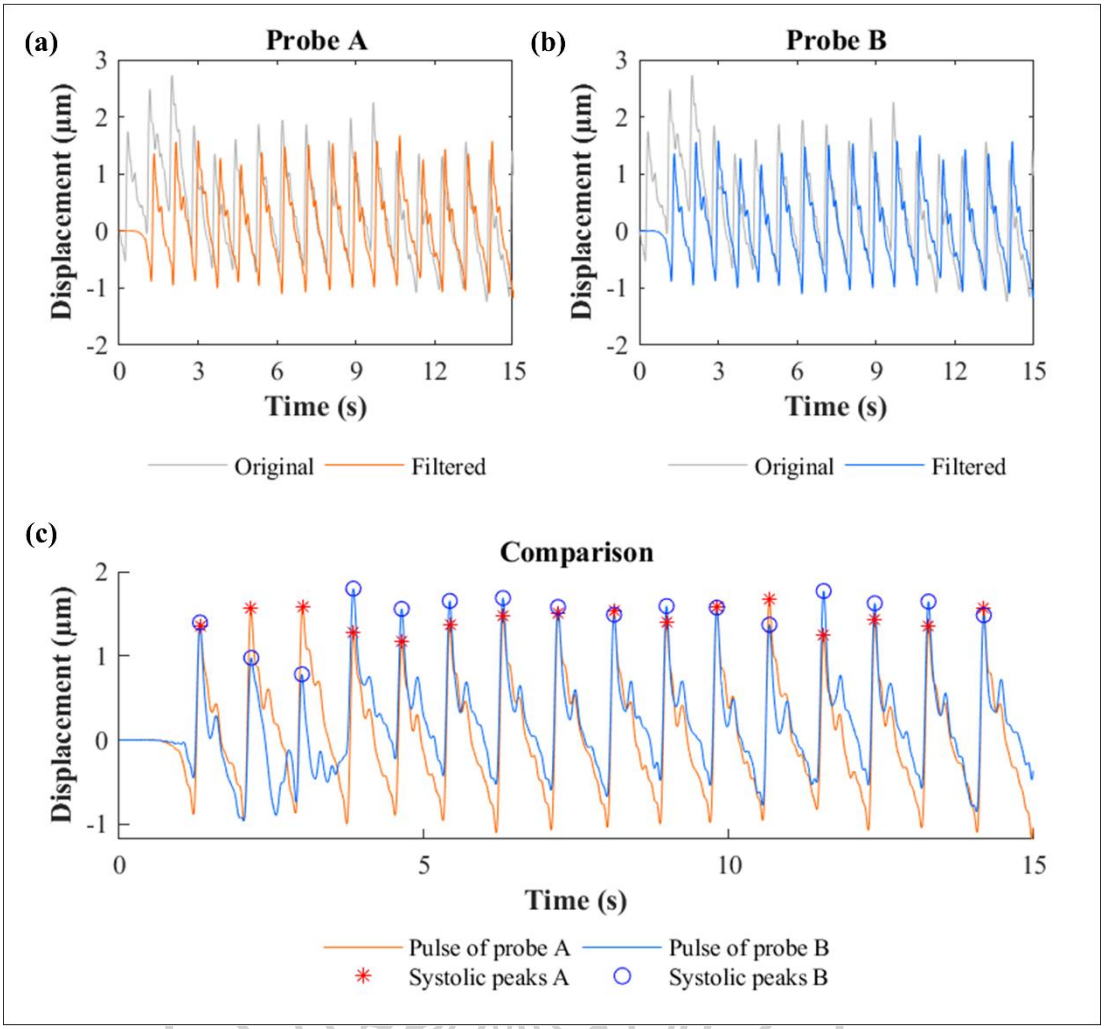

Fig. B16Pulse wave showcase of volunteer F no. 1 :
(a) Pulse wave of probe A, (b) pulse wave of probe B, and (c) pulse wave comparison

Table B26 Measured parameters of volunteer F measurement no. 1

Probe A				Probe B			
Displacement	=	2.4224	µm	Displacement	=	2.1674	µm
Measured PP	=	0.0171	mmHg	Measured PP	=	0.0153	mmHg
Calibrated PP	=	44.9502	mmHg	Calibrated PP	=	45.2143	mmHg
Combine							
HR of probe A	=	69.6567	bpm	Mean PP	=	45.0822	mmHg
HR of probe B	=	67.6336	bpm	PTT	=	2.2800	ms
Mean HR	=	68.6452	bpm	PWV	=	20.1754	m/s

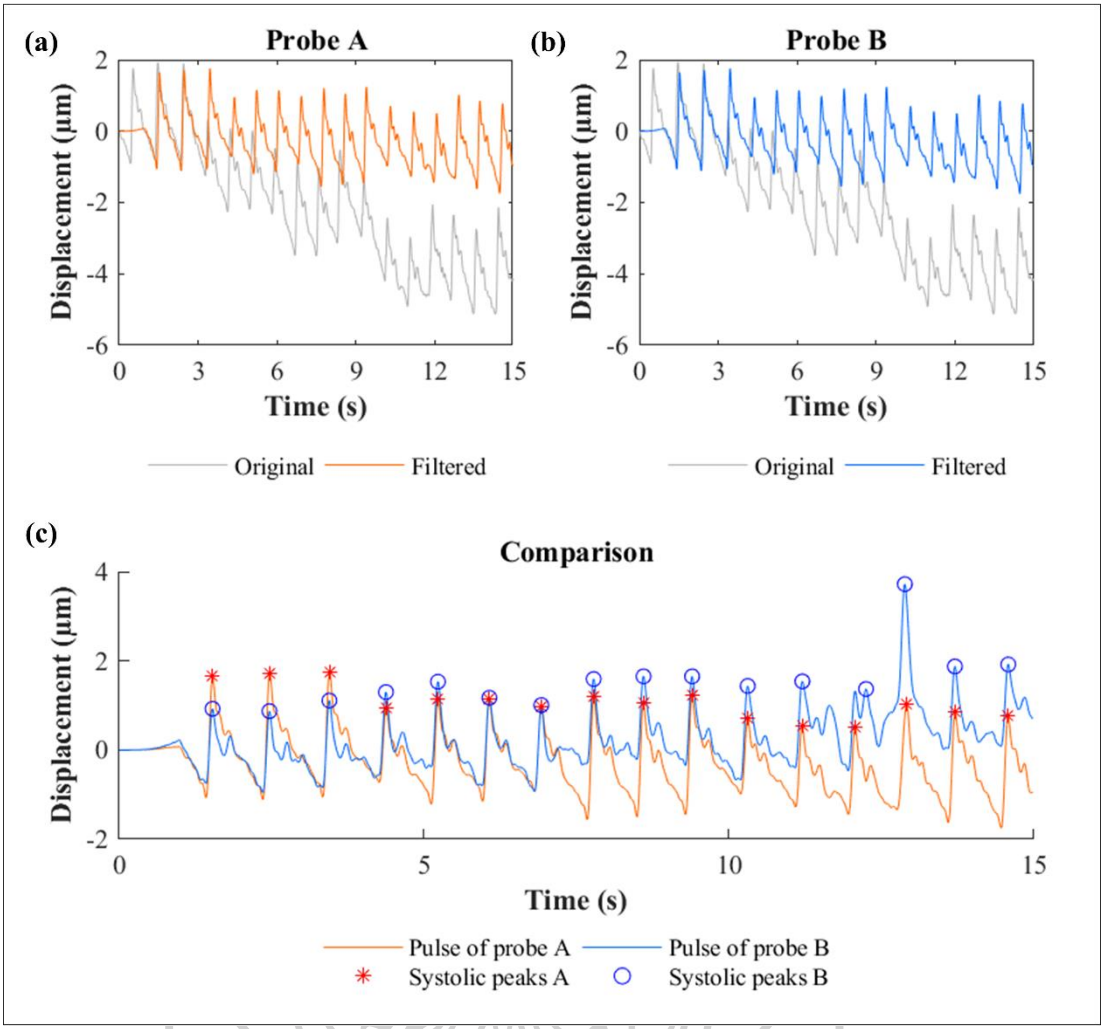

Fig. B17Pulse wave showcase of volunteer F no. 2 :
(a) Pulse wave of probe A, (b) pulse wave of probe B, and (c) pulse wave comparison

Table B27 Measured parameters of volunteer F measurement no. 2

Probe A				Probe B			
Displacement	=	2.3658	µm	Displacement	=	1.9125	µm
Measured PP	=	0.0167	mmHg	Measured PP	=	0.0135	mmHg
Calibrated PP	=	45.0631	mmHg	Calibrated PP	=	44.9286	mmHg
Combine							
HR of probe A	=	68.3527	bpm	Mean PP	=	44.9958	mmHg
HR of probe B	=	68.3553	bpm	PTT	=	2.4667	ms
Mean HR	=	68.3540	bpm	PWV	=	18.6484	m/s

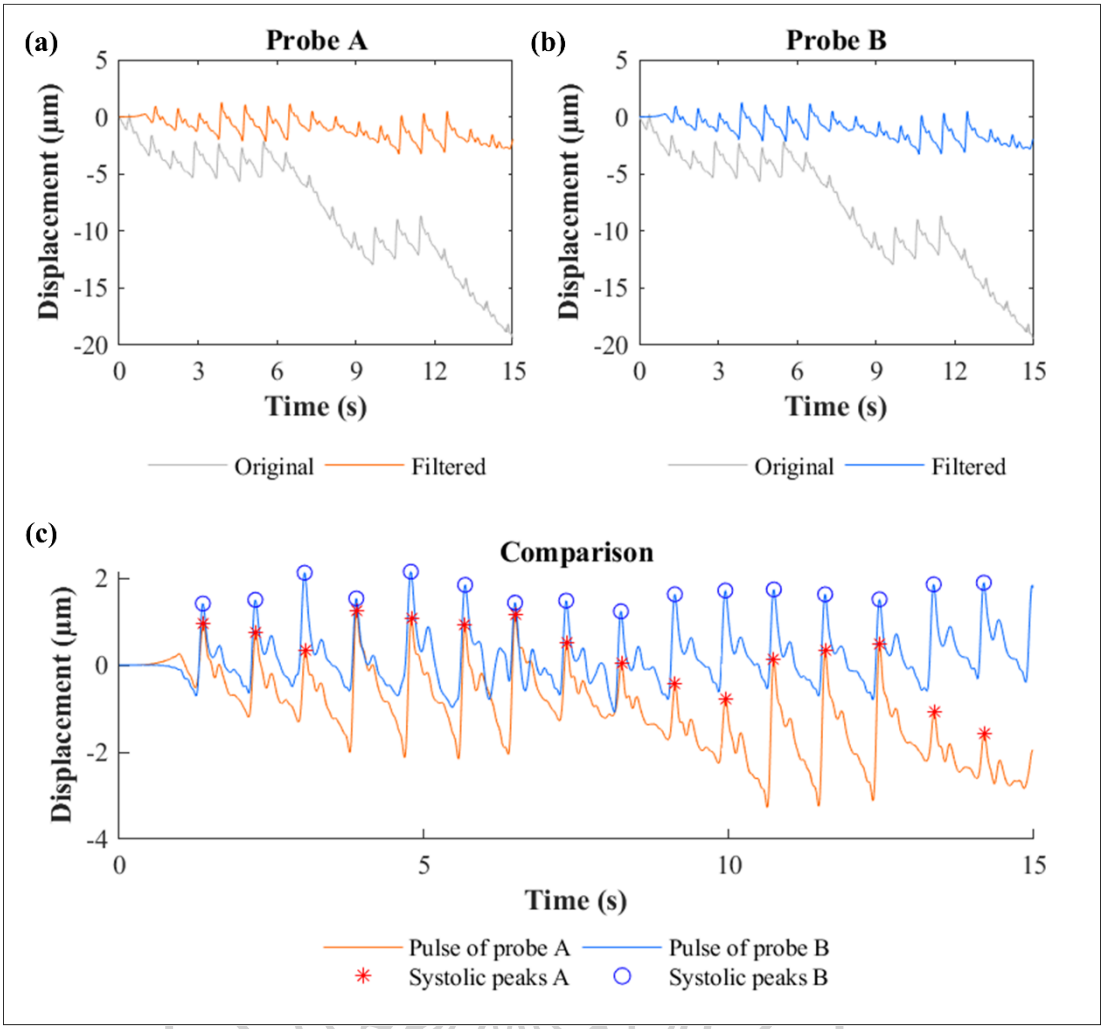

Fig. B18Pulse wave showcase of volunteer F no. 3 :
(a) Pulse wave of probe A, (b) pulse wave of probe B, and (c) pulse wave comparison

Table B28 Measured parameters of volunteer F measurement no. 3

Probe A				Probe B			
Displacement	=	2.1533	µm	Displacement	=	2.2949	µm
Measured PP	=	0.0152	mmHg	Measured PP	=	0.0162	mmHg
Calibrated PP	=	45.4867	mmHg	Calibrated PP	=	45.3571	mmHg
Combine							
HR of probe A	=	70.8624	bpm	Mean PP	=	45.4219	mmHg
HR of probe B	=	70.6732	bpm	PTT	=	5.6500	ms
Mean HR	=	70.7678	bpm	PWV	=	8.1416	m/s

Table B29 Blood pressure demodulation of volunteer F

Parameters	No. 1	No. 2	No. 3
PP measurement (mmHg)	45.0822	44.9958	45.4219
PWV measurement (m/s)	20.1754	18.6484	8.1416
DBP coefficient $\frac{\mathrm{PWV}^2 \rho \Delta r_{\mathrm{artery}}}{\mathrm{PP}}$	61.1236	52.2211	9.9536
m_{DBP}	0.0647	0.0647	0.0647
c_{DBP}	58.6723	58.6723	58.6723
DBP measurement (mmHg) $\mathrm{DBP} = m_{\mathrm{DBP}} \frac{\mathrm{PWV}^2 \rho \Delta r_{\mathrm{artery}}}{\mathrm{PP}} + c_{\mathrm{DBP}}$	62.6298	62.0534	59.3167
SBP measurement (mmHg) $\mathrm{SBP} = \mathrm{DBP} + \mathrm{PP}$	107.7121	107.0493	104.7387

Table B30 Error analysis of volunteer F

Parameters		SBP	DBP	PP	HR
No. 1	Measurement (mmHg)	107.71	62.63	45.08	68.65
	Reference (mmHg)	108.50	63.50	45.00	66.00
	Absolute error (AE: mmHg)	0.79	0.87	0.08	2.65
	AE percentage (%)	0.73	1.37	0.18	4.01
No. 2	Measurement (mmHg)	107.05	62.05	45.00	68.35
	Reference (mmHg)	106.00	61.00	45.00	65.50
	Absolute error (AE: mmHg)	1.05	1.05	0.00	2.85
	AE percentage (%)	0.99	1.73	0.01	4.36
No. 3	Measurement (mmHg)	104.74	59.32	45.42	70.77
	Reference (mmHg)	105.00	59.50	45.50	65.00
	Absolute error (AE: mmHg)	0.26	0.18	0.08	5.77
	AE percentage (%)	0.25	0.31	0.17	8.87

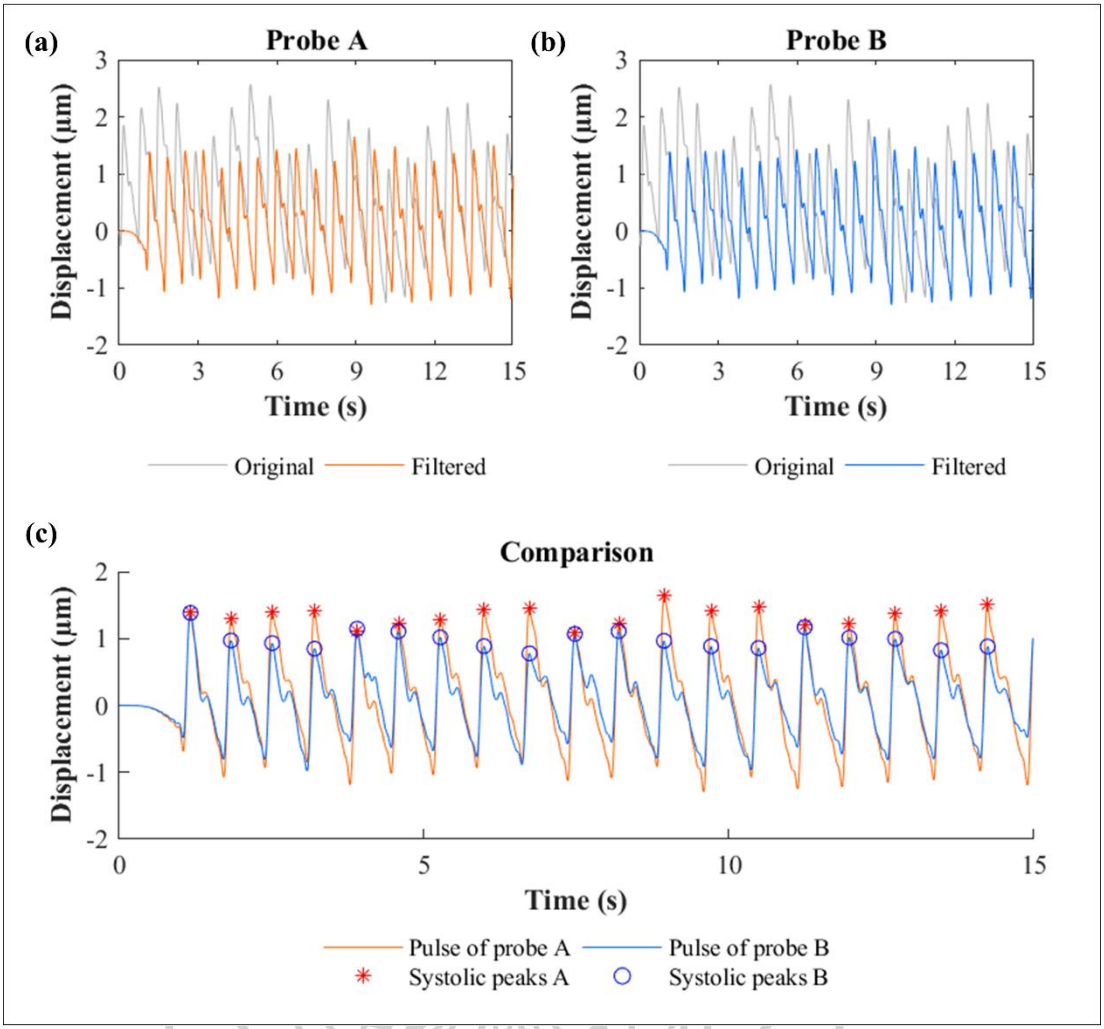

Fig. B19Pulse wave showcase of volunteer G no. 1 :
(a) Pulse wave of probe A, (b) pulse wave of probe B, and (c) pulse wave comparison

Table B31 Measured parameters of volunteer G measurement no. 1

Probe A				Probe B			
Displacement	=	2.4083	µm	Displacement	=	1.7425	µm
Measured PP	=	0.0170	mmHg	Measured PP	=	0.0123	mmHg
Calibrated PP	=	32.5153	mmHg	Calibrated PP	=	32.6812	mmHg
Combine							
HR of probe A	=	82.3580	bpm	Mean PP	=	32.5982	mmHg
HR of probe B	=	82.3628	bpm	PTT	=	2.4667	ms
Mean HR	=	82.3604	bpm	PWV	=	15.8106	m/s

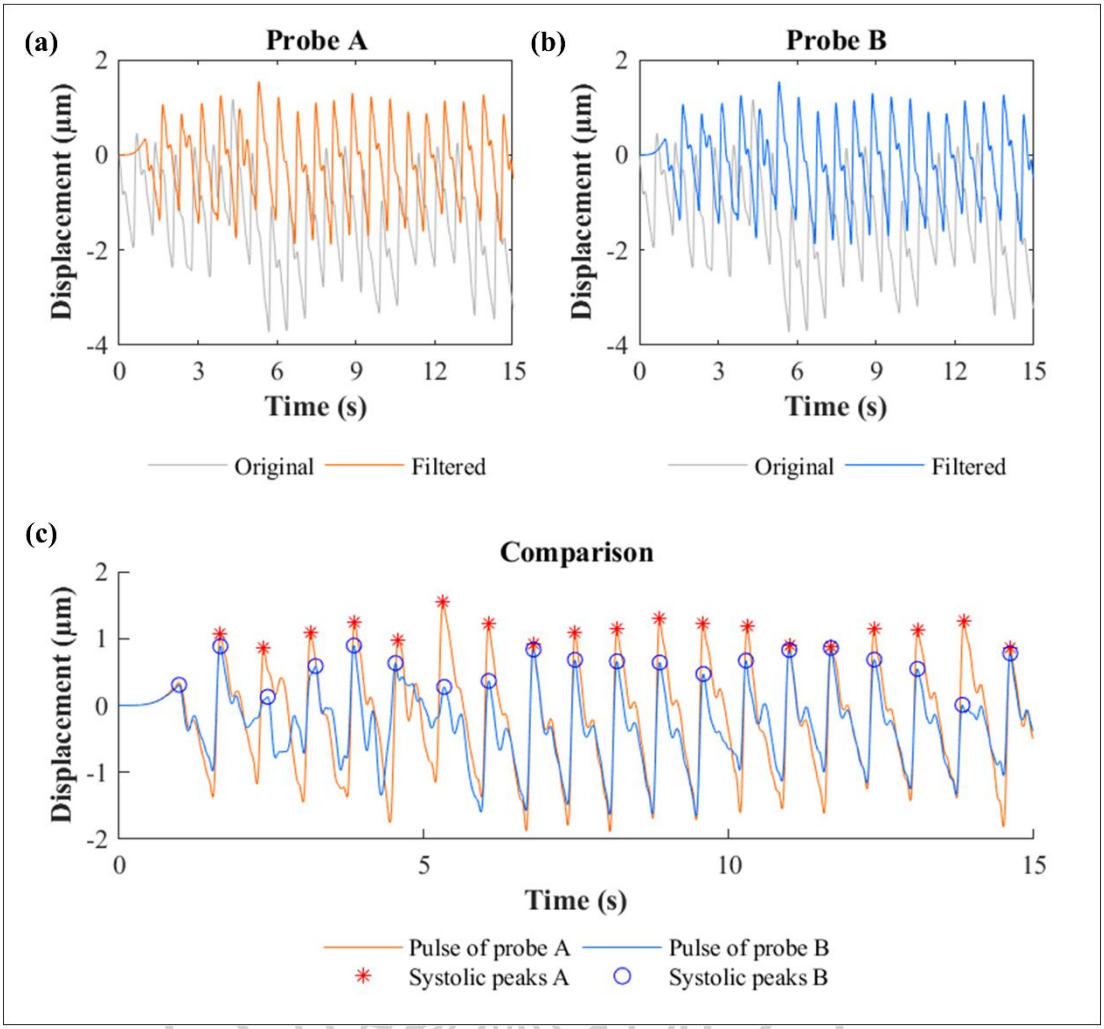

Fig. B20Pulse wave showcase of volunteer G no. 2 :
(a) Pulse wave of probe A, (b) pulse wave of probe B, and (c) pulse wave comparison

Table B32 Measured parameters of volunteer G measurement no. 2

Probe A				Probe B			
Displacement	=	2.6491	μm	Displacement	=	1.9833	μm
Measured PP	=	0.0187	mmHg	Measured PP	=	0.0140	mmHg
Calibrated PP	=	33.9475	mmHg	Calibrated PP	=	33.6477	mmHg
Combine							
HR of probe A	=	83.2896	bpm	Mean PP	=	33.7976	mmHg
HR of probe B	=	83.2742	bpm	PTT	=	7.7647	ms
Mean HR	=	83.2819	bpm	PWV	=	5.0227	m/s

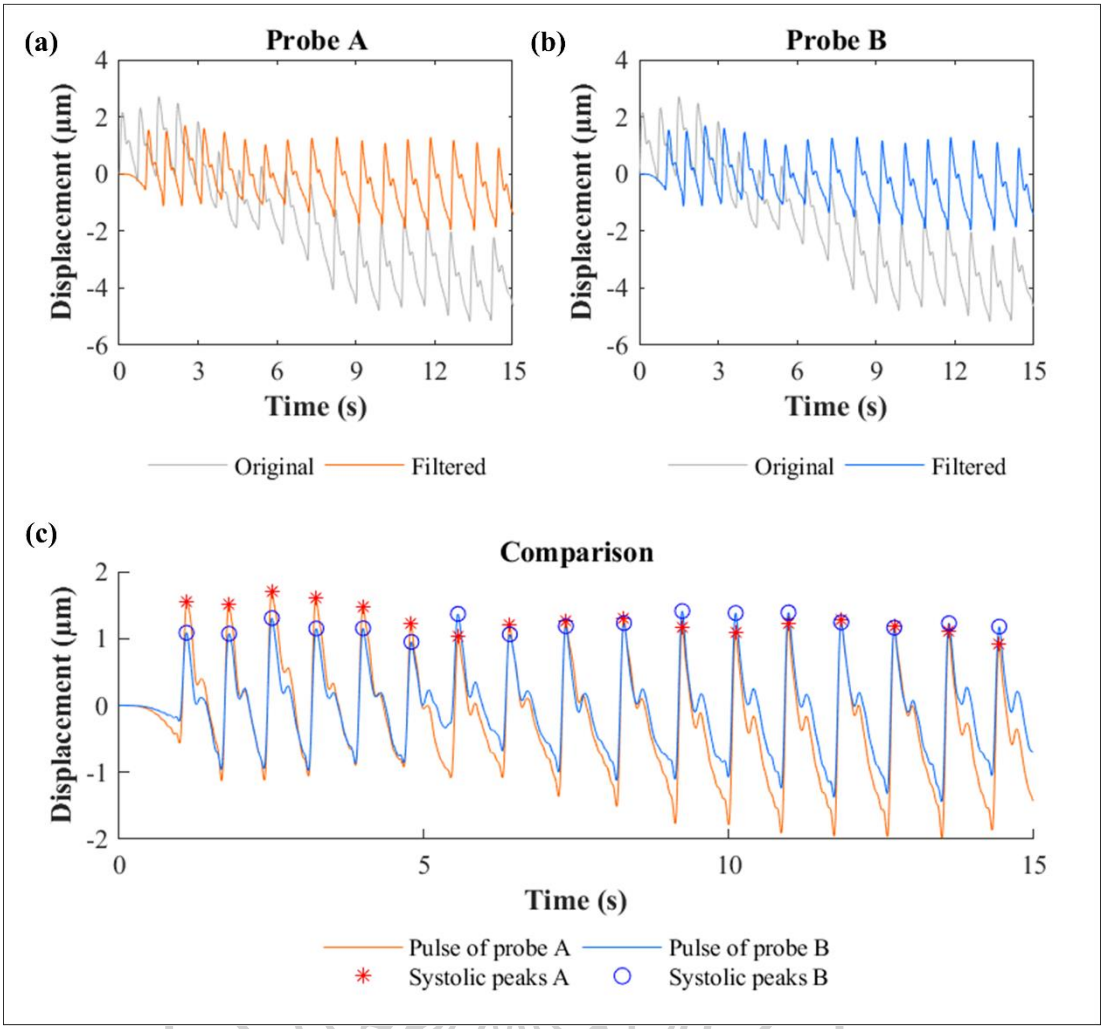

Fig. B21Pulse wave showcase of volunteer G no. 3 :
(a) Pulse wave of probe A, (b) pulse wave of probe B, and (c) pulse wave comparison

Table B33 Measured parameters of volunteer G measurement no. 3

Probe A				Probe B			
Displacement	=	2.7483	µm	Displacement	=	2.2383	µm
Measured PP	=	0.0194	mmHg	Measured PP	=	0.0158	mmHg
Calibrated PP	=	34.5372	mmHg	Calibrated PP	=	34.6711	mmHg
Combine							
HR of probe A	=	71.2296	bpm	Mean PP	=	34.6042	mmHg
HR of probe B	=	71.2183	bpm	PTT	=	2.7429	ms
Mean HR	=	71.2240	bpm	PWV	=	14.2185	m/s

Table B34 Blood pressure demodulation of volunteer G

Parameters	No. 1	No. 2	No. 3
PP measurement (mmHg)	32.5982	33.7976	34.6042
PWV measurement (m/s)	15.8106	5.0227	14.2185
DBP coefficient $\frac{\mathrm{PWV}^2 \rho \Delta r_{\mathrm{artery}}}{\mathrm{PP}}$	37.5370	3.7883	30.3579
m_{DBP}	0.0165	0.0165	0.0165
c_{DBP}	59.7732	59.7732	59.7732
DBP measurement (mmHg) $\mathrm{DBP} = m_{\mathrm{DBP}} \frac{\mathrm{PWV}^2 \rho \Delta r_{\mathrm{artery}}}{\mathrm{PP}} + c_{\mathrm{DBP}}$	60.3913	59.8355	60.2731
SBP measurement (mmHg) $\mathrm{SBP} = \mathrm{DBP} + \mathrm{PP}$	92.9896	93.6331	94.8773

Table B35 Error analysis of volunteer G

Parameters		SBP	DBP	PP	HR
No. 1	Measurement (mmHg)	92.99	60.39	32.60	82.36
	Reference (mmHg)	93.50	61.00	32.50	78.50
	Absolute error (AE: mmHg)	0.51	0.61	0.10	3.86
	AE percentage (%)	0.55	1.00	0.30	4.92
No. 2	Measurement (mmHg)	93.63	59.84	33.80	83.28
	Reference (mmHg)	94.00	60.00	34.00	79.00
	Absolute error (AE: mmHg)	0.37	0.16	0.20	4.28
	AE percentage (%)	0.39	0.27	0.60	5.42
No. 3	Measurement (mmHg)	94.88	60.27	34.60	71.22
	Reference (mmHg)	94.00	59.50	34.50	79.00
	Absolute error (AE: mmHg)	0.88	0.77	0.10	7.78
	AE percentage (%)	0.93	1.30	0.30	9.84

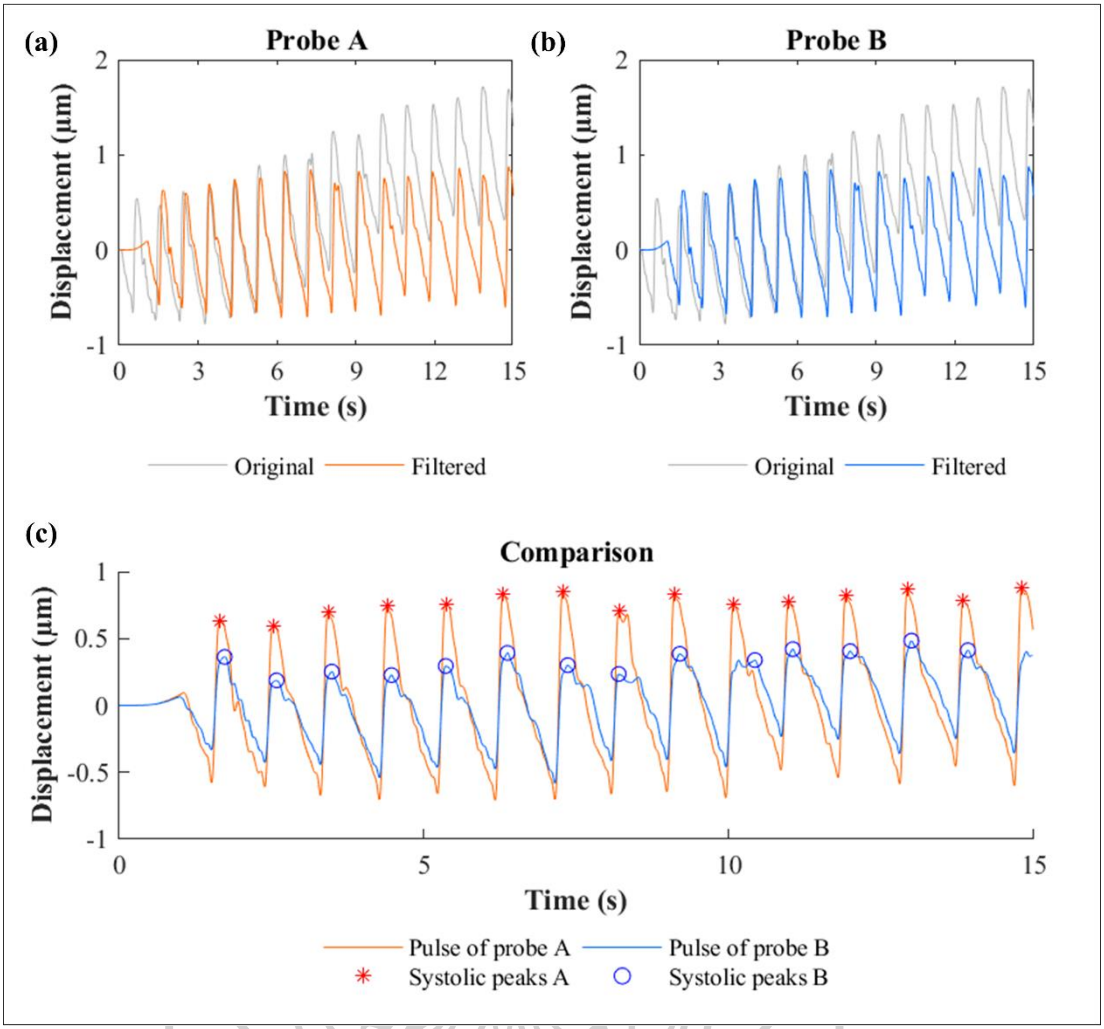

Fig. B22Pulse wave showcase of volunteer H no. 1 :
(a) Pulse wave of probe A, (b) pulse wave of probe B, and (c) pulse wave comparison

Table B36 Measured parameters of volunteer H measurement no. 1

Probe A				Probe B			
Displacement	=	1.3844	µm	Displacement	=	0.7339	µm
Measured PP	=	0.0083	mmHg	Measured PP	=	0.0044	mmHg
Calibrated PP	=	28.2500	mmHg	Calibrated PP	=	28.3041	mmHg
Combine							
HR of probe A	=	65.3524	bpm	Mean PP	=	28.2771	mmHg
HR of probe B	=	65.3645	bpm	PTT	=	60.1538	ms
Mean HR	=	65.3585	bpm	PWV	=	0.5652	m/s

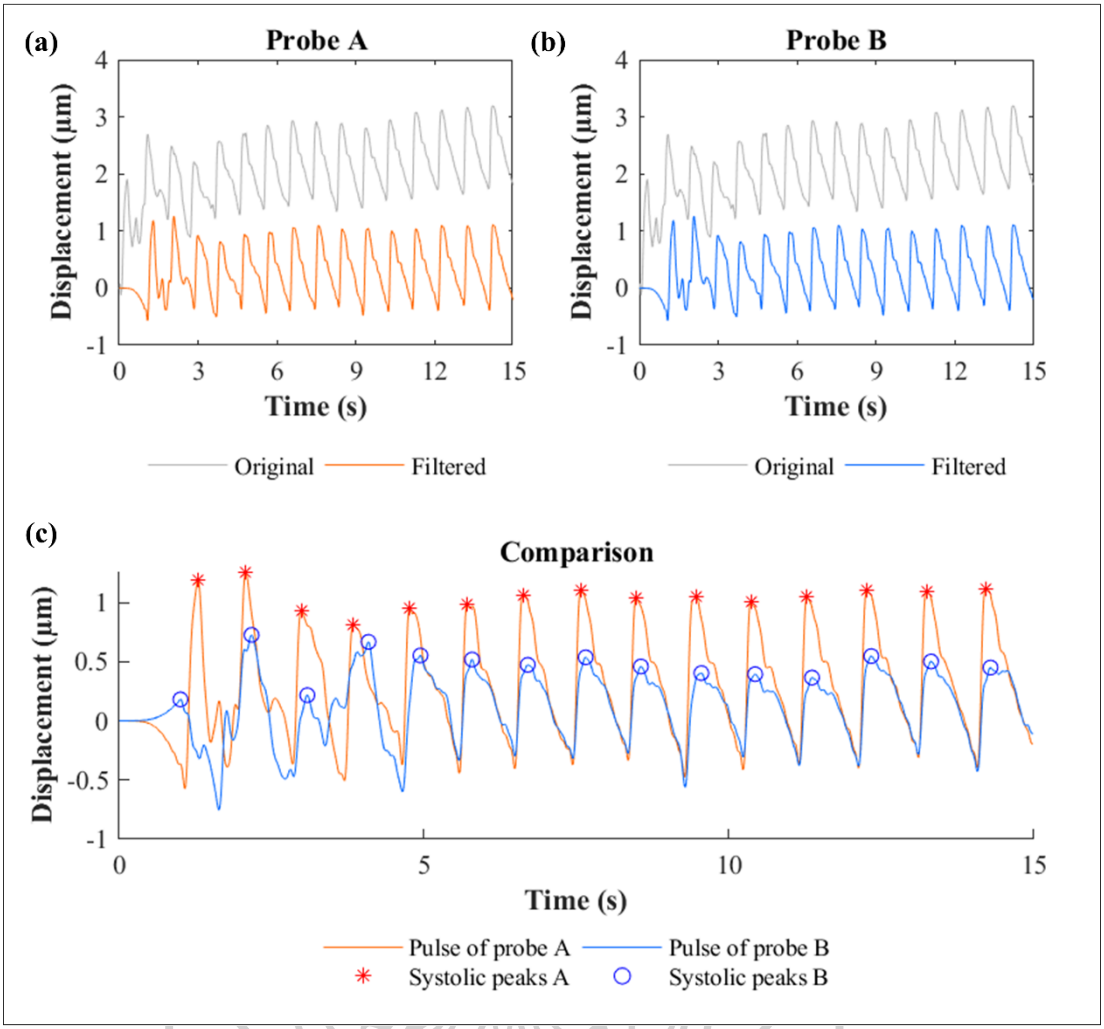

Fig. B23Pulse wave showcase of volunteer H no. 2 :
(a) Pulse wave of probe A, (b) pulse wave of probe B, and (c) pulse wave comparison

Table B37 Measured parameters of volunteer H measurement no. 2

Probe A				Probe B			
Displacement	=	1.4177	µm	Displacement	=	0.8673	µm
Measured PP	=	0.0085	mmHg	Measured PP	=	0.0052	mmHg
Calibrated PP	=	28.0000	mmHg	Calibrated PP	=	27.6443	mmHg
Combine							
HR of probe A	=	65.9044	bpm	Mean PP	=	27.8222	mmHg
HR of probe B	=	65.6181	bpm	PTT	=	78.1333	ms
Mean HR	=	65.7612	bpm	PWV	=	0.4352	m/s

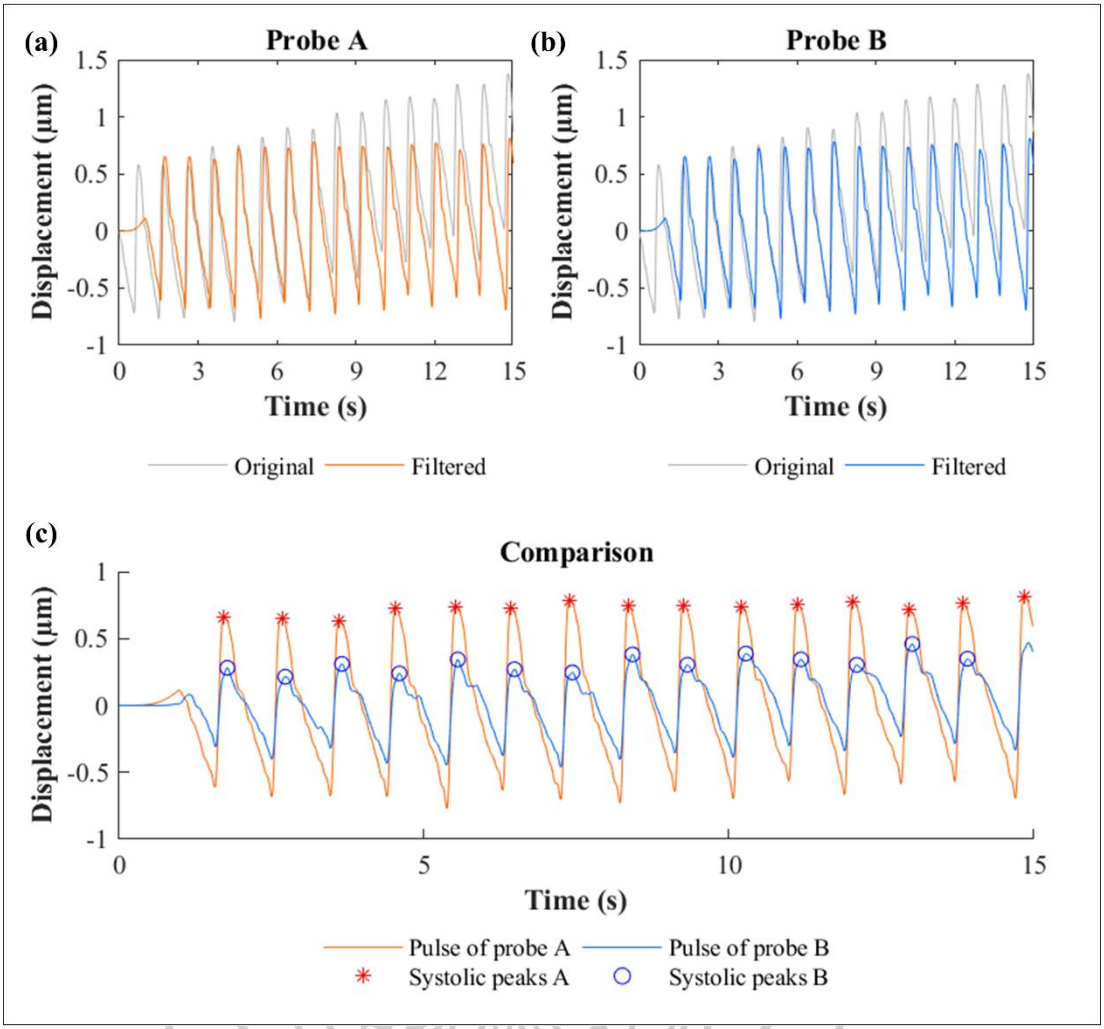

Fig. B24Pulse wave showcase of volunteer H no. 3 :
(a) Pulse wave of probe A, (b) pulse wave of probe B, and (c) pulse wave comparison

Table B38 Measured parameters of volunteer H measurement no. 3

Probe A				Probe B			
Displacement	=	1.3844	µm	Displacement	=	0.6838	µm
Measured PP	=	0.0083	mmHg	Measured PP	=	0.0041	mmHg
Calibrated PP	=	28.2500	mmHg	Calibrated PP	=	28.5515	mmHg
Combine							
HR of probe A	=	65.6499	bpm	Mean PP	=	28.4008	mmHg
HR of probe B	=	65.6298	bpm	PTT	=	57.1714	ms
Mean HR	=	65.6399	bpm	PWV	=	0.5947	m/s

Table B39 Blood pressure demodulation of volunteer H

Parameters	No. 1	No. 2	No. 3
PP measurement (mmHg)	28.2771	27.8222	28.4008
PWV measurement (m/s)	0.5652	0.4352	0.5947
DBP coefficient $\frac{\mathrm{PWV}^2 \rho \Delta r_{\mathrm{artery}}}{\mathrm{PP}}$	0.0565	0.0335	0.0625
m_{DBP}	-43.3611	-43.3611	-43.3611
c_{DBP}	61.5374	61.5374	61.5374
DBP measurement (mmHg) $\mathrm{DBP} = m_{\mathrm{DBP}} \frac{\mathrm{PWV}^2 \rho \Delta r_{\mathrm{artery}}}{\mathrm{PP}} + c_{\mathrm{DBP}}$	59.0882	60.0857	58.8261
SBP measurement (mmHg) $\mathrm{SBP} = \mathrm{DBP} + \mathrm{PP}$	87.3653	87.9079	87.2268

Table B40 Error analysis of volunteer H

Parameters		SBP	DBP	PP	HR
No. 1	Measurement (mmHg)	87.37	59.09	28.28	65.36
	Reference (mmHg)	86.50	59.50	27.00	66.00
	Absolute error (AE: mmHg)	0.87	0.41	1.28	0.64
	AE percentage (%)	1.00	0.69	4.73	0.97
No. 2	Measurement (mmHg)	87.91	60.09	27.82	65.76
	Reference (mmHg)	88.00	60.00	28.00	67.50
	Absolute error (AE: mmHg)	0.09	0.09	0.18	1.74
	AE percentage (%)	0.10	0.14	0.64	2.58
No. 3	Measurement (mmHg)	87.23	58.83	28.40	65.64
	Reference (mmHg)	88.00	58.50	29.50	65.50
	Absolute error (AE: mmHg)	0.77	0.33	1.10	0.14
	AE percentage (%)	0.88	0.56	3.73	0.21

Table B41 Pulse pressure and heart rate demodulation data

Test no.	Volunteer no.	Displacement probe A (μm)	Measured PP probe A (mmHg)	Calibrated PP probe A (mmHg)	Measured HR probe A (bpm)	Displacement probe B (μm)	Measured PP probe B (mmHg)	Calibrated PP probe B (mmHg)	Measured HR probe B (bpm)
1	1	5.7232	0.0404	49.3386	1.5016	0.0106	50.0988	77.0416	77.1248
2	1	3.5982	0.0254	48.9804	1.6716	0.0118	48.8081	80.2139	79.6284
3	1	4.7882	0.0338	49.1810	1.7000	0.0120	48.5930	78.2504	77.9626
4	2	2.5641	0.0181	36.4704	1.1758	0.0083	36.4283	85.3651	85.3319
5	2	2.5216	0.0178	36.5264	1.2325	0.0087	36.5549	89.8778	89.8311
6	2	2.9183	0.0206	36.0032	0.9916	0.0070	36.0169	84.1908	83.8301
7	3	3.1874	0.0225	35.2275	2.0258	0.0143	39.6667	64.7226	64.6389
8	3	3.3149	0.0234	37.1205	1.8416	0.0130	34.6667	65.5963	66.3088
9	3	2.9466	0.0208	31.6520	1.6575	0.0117	29.6667	68.6993	68.6993
10	4	3.2016	0.0226	39.6667	2.4083	0.0170	35.0830	56.1115	39.7720
11	4	3.5557	0.0251	34.6667	2.5358	0.0179	36.4245	54.6647	46.6066
12	4	3.2724	0.0231	38.6667	3.0174	0.0213	41.4925	61.7910	57.0505
13	5	0.8358	0.0059	46.5315	0.4958	0.0035	48.2568	76.8883	76.4526
14	5	0.9350	0.0066	48.5984	0.4533	0.0032	46.0676	85.3606	86.5426
15	5	1.0200	0.0072	50.3701	0.5525	0.0039	51.1757	75.6856	75.6744
16	6	3.0599	0.0216	38.9872	1.4308	0.0101	39.5290	74.2427	70.1328
17	6	4.6466	0.0328	38.7179	0.9208	0.0065	37.8958	74.0863	74.4171
18	6	4.1932	0.0296	38.7949	1.2891	0.0091	39.0753	83.3218	77.3395
19	7	4.0091	0.0283	40.2097	2.0825	0.0147	41.4247	58.7122	58.6147
20	7	3.9241	0.0277	40.5484	1.9550	0.0138	38.8973	63.9659	63.9741
21	7	4.3774	0.0309	38.7419	1.9691	0.0139	39.1781	61.2620	61.1621
22	8	1.0766	0.0076	28.2358	0.4675	0.0033	28.6071	73.1529	73.1351
23	8	1.0341	0.0073	27.7470	0.4392	0.0031	27.9286	76.0286	76.0218
24	8	1.2750	0.0090	30.5172	0.5242	0.0037	29.9643	75.4014	75.3969
25	9	4.4766	0.0316	37.8361	1.8558	0.0131	38.0181	80.8734	80.9389
26	9	4.8591	0.0343	34.3689	2.9891	0.0211	35.2058	84.1193	84.0422
27	9	4.6466	0.0328	36.2951	2.9608	0.0209	35.2761	88.2457	88.2976

Table B41 Pulse pressure and heart rate demodulation data (continued)

Test no.	Volunteer no.	Displacement probe A (μm)	Measured PP probe A (mmHg)	Calibrated PP probe A (mmHg)	Measured HR probe A (bpm)	Displacement probe B (μm)	Measured PP probe B (mmHg)	Calibrated PP probe B (mmHg)	Measured HR probe B (bpm)
28	10	4.3207	0.0305	31.4379	0.8075	0.0057	34.5000	72.5397	71.2533
29	10	3.8674	0.0273	34.6331	0.7225	0.0051	34.5000	76.1731	76.2079
30	10	3.4708	0.0245	37.4290	0.8075	0.0057	34.5000	83.0441	81.8246
31	11	5.5957	0.0395	37.7270	2.4933	0.0176	36.9286	58.8804	58.8590
32	11	7.0265	0.0496	37.0764	2.5074	0.0177	38.3469	58.9979	59.0176
33	11	6.5448	0.0462	38.4906	2.1249	0.0150	37.2449	58.7827	58.7420
34	12	3.4991	0.0247	46.5378	5.6524	0.0399	46.1644	54.7578	54.7628
35	12	2.9608	0.0209	45.6564	5.2699	0.0372	46.1723	54.5306	54.5025
36	12	3.3574	0.0237	46.3058	5.7090	0.0403	46.1632	50.4155	50.4325
37	13	3.0316	0.0214	39.4538	1.1900	0.0084	39.6210	87.1755	86.9229
38	13	4.0657	0.0287	40.4675	1.2183	0.0086	39.8548	93.6096	92.8103
39	13	4.1791	0.0295	40.5786	1.3600	0.0096	41.0242	86.5926	89.5656
40	14	1.6433	0.0116	35.5832	0.7225	0.0051	35.2568	74.6422	74.6771
41	14	2.3799	0.0168	35.0770	0.6942	0.0049	35.2058	80.1116	80.0190
42	14	1.9975	0.0141	35.3398	0.8783	0.0062	35.5374	74.1473	73.9280
43	15	4.6324	0.0327	32.8676	0.9775	0.0069	32.6786	65.7126	65.6359
44	15	4.8166	0.0340	31.8349	0.9916	0.0070	31.7143	69.1962	69.1802
45	15	4.3774	0.0309	34.2975	0.9491	0.0067	34.6071	75.5414	75.3895
46	16	4.4199	0.0312	42.2585	1.9125	0.0135	42.5464	77.6598	77.5595
47	16	5.8507	0.0413	38.7012	1.7991	0.0127	41.7388	73.2780	73.0994
48	16	4.3066	0.0304	42.5403	1.4450	0.0102	39.2148	74.2207	76.2583
49	17	2.6349	0.0186	48.5000	1.6150	0.0114	51.9076	53.2245	53.2434
50	17	2.3941	0.0169	52.5000	1.7425	0.0123	50.5416	62.1891	62.0347
51	17	2.6349	0.0186	48.5000	2.0683	0.0146	47.0508	57.9449	57.9747
52	18	2.9183	0.0206	32.3038	1.5016	0.0106	32.4649	70.1612	70.2510
53	18	2.2524	0.0159	32.3669	1.5158	0.0107	32.5307	69.3118	70.7948
54	18	2.6491	0.0187	32.3293	1.4025	0.0099	32.0044	70.2905	73.8552

Table B41 Pulse pressure and heart rate demodulation data (continued)

Test no.	Volunteer no.	Displacement probe A (μm)	Measured PP probe A (mmHg)	Calibrated PP probe A (mmHg)	Measured HR probe A (bpm)	Displacement probe B (μm)	Measured PP probe B (mmHg)	Calibrated PP probe B (mmHg)	Measured HR probe B (bpm)
55	19	3.1874	0.0225	25.8214	0.8783	0.0062	26.2027	62.1541	62.1228
56	19	3.7257	0.0263	27.0357	0.9208	0.0065	26.7703	63.5920	63.5747
57	19	3.9949	0.0282	27.6429	0.9775	0.0069	27.5270	62.7296	62.6641
58	20	3.8249	0.0270	31.2172	1.9266	0.0136	30.9615	108.7272	108.5666
59	20	4.8307	0.0341	30.7680	1.7141	0.0121	31.1538	101.4497	100.7299
60	20	4.2782	0.0302	31.0148	2.0116	0.0142	30.8846	102.4925	102.6969
61	21	4.9724	0.0351	40.1909	0.6942	0.0049	40.2403	65.3291	65.2988
62	21	4.9015	0.0346	40.0574	0.6233	0.0044	39.7752	68.4786	68.4452
63	21	5.2699	0.0372	40.7518	0.8075	0.0057	40.9845	75.2013	75.2079
64	22	2.5358	0.0179	36.6227	1.2891	0.0091	35.9624	64.1931	64.2398
65	22	2.8049	0.0198	37.8570	1.6008	0.0113	40.3091	68.3995	68.3761
66	22	3.3858	0.0239	40.5203	1.4875	0.0105	38.7285	68.6352	68.6331
67	23	2.7199	0.0192	30.9480	1.4591	0.0103	32.2185	69.7851	68.7930
68	23	2.5074	0.0177	31.8524	1.5300	0.0108	31.4676	69.6035	69.6723
69	23	3.1308	0.0221	29.1995	1.8275	0.0129	28.3139	79.4544	82.3271
70	24	3.0883	0.0218	29.0088	0.7225	0.0051	29.0101	95.5515	95.9079
71	24	3.7824	0.0267	26.4298	0.9491	0.0067	26.3288	85.9107	86.4886
72	24	3.8816	0.0274	26.0614	0.9633	0.0068	26.1612	99.5355	99.8004
73	25	4.1366	0.0292	44.4444	3.8816	0.0274	42.0714	59.5529	59.2489
74	25	2.0966	0.0148	39.6169	3.6832	0.0260	40.7857	59.1794	53.4156
75	25	3.7116	0.0262	43.4387	4.2782	0.0302	44.6429	68.9814	56.2641
76	26	3.8957	0.0275	43.1903	3.4283	0.0242	43.4388	79.2142	75.4603
77	26	4.2782	0.0302	43.5199	3.5557	0.0251	42.9317	72.5865	73.9098
78	26	5.7515	0.0406	44.7898	3.0033	0.0212	45.1295	74.5033	74.3679
79	27	2.8899	0.0204	54.8952	3.1166	0.0220	55.6696	73.7499	76.6518
80	27	2.9608	0.0209	54.2258	3.7824	0.0267	53.0961	70.4329	70.4784
81	27	3.3149	0.0234	50.8790	4.2641	0.0301	51.2344	63.6267	63.0782

Table B41 Pulse pressure and heart rate demodulation data (continued)

Test no.	Volunteer no.	Displacement probe A (μm)	Measured PP probe A (mmHg)	Calibrated PP probe A (mmHg)	Measured HR probe A (bpm)	Displacement probe B (μm)	Measured PP probe B (mmHg)	Calibrated PP probe B (mmHg)	Measured HR probe B (bpm)
82	28	3.1024	0.0219	43.5936	2.4508	0.0173	44.3077	64.7459	64.7249
83	28	3.8957	0.0275	44.1991	2.4366	0.0172	44.5192	67.6916	67.6916
84	28	4.5616	0.0322	44.7073	2.4933	0.0176	43.6731	72.3720	72.4069
85	29	4.7599	0.0336	42.2020	1.2325	0.0087	41.3141	81.8688	79.9829
86	29	4.0657	0.0287	40.1822	1.5300	0.0108	39.0256	80.7127	80.6548
87	29	3.5274	0.0249	38.6158	1.3175	0.0093	40.6603	91.1793	89.5582
88	30	5.1282	0.0362	32.1763	3.1874	0.0225	31.8532	62.0170	62.0111
89	30	4.4057	0.0311	31.0599	3.0883	0.0218	31.8792	58.0361	57.8391
90	30	5.1849	0.0366	32.2638	3.5132	0.0248	31.7676	63.9768	63.5378
91	31	5.2982	0.0374	52.0879	1.9833	0.0140	53.0385	74.2868	74.7906
92	31	5.9357	0.0419	52.8709	2.0400	0.0144	53.3462	75.3107	75.3107
93	31	7.2957	0.0515	54.5412	1.9975	0.0141	53.1154	77.1473	77.1473
94	32	3.0174	0.0213	54.1347	1.1475	0.0081	55.5000	91.0415	96.0184
95	32	2.8616	0.0202	53.1149	1.1900	0.0084	54.0000	102.2495	103.0574
96	32	3.5699	0.0252	57.7504	1.1475	0.0081	55.5000	89.2591	89.3788
97	33	4.1791	0.0295	43.2797	1.2750	0.0090	41.4942	78.4326	77.7724
98	33	4.5757	0.0323	43.7806	1.4733	0.0104	44.4651	75.2945	75.2745
99	33	3.9099	0.0276	42.9398	1.4450	0.0102	44.0407	77.4318	77.3869
100	34	4.8449	0.0342	33.8089	0.9208	0.0065	29.6019	93.7305	93.7026
101	34	4.3349	0.0306	28.3880	1.1333	0.0080	31.5883	100.7787	100.6957
102	34	4.7032	0.0332	32.3031	1.3175	0.0093	33.3098	94.0130	94.0214
103	35	2.9183	0.0206	42.6667	1.3741	0.0097	42.5723	74.1473	74.1388
104	35	2.5783	0.0182	42.4167	1.5016	0.0106	42.4448	68.9549	68.9465
105	35	3.2583	0.0230	42.9167	0.9633	0.0068	42.9829	75.0684	77.4487
106	36	4.3349	0.0306	30.1687	1.5441	0.0109	31.2675	69.5249	68.3423
107	36	3.3433	0.0236	28.7814	1.4308	0.0101	30.5142	68.2956	66.8946
108	36	4.2499	0.0300	30.0498	0.9350	0.0066	27.2183	60.1524	63.7123

Table B41 Pulse pressure and heart rate demodulation data (continued)

Test no.	Volunteer no.	Displacement probe A (μm)	Measured PP probe A (mmHg)	Calibrated PP probe A (mmHg)	Measured HR probe A (bpm)	Displacement probe B (μm)	Measured PP probe B (mmHg)	Calibrated PP probe B (mmHg)	Measured HR probe B (bpm)
109	37	3.8674	0.0273	38.0577	1.0341	0.0073	39.3718	85.1891	84.3370
110	37	3.8391	0.0271	37.4231	1.4166	0.0100	35.1954	79.3907	79.2998
111	37	3.7541	0.0265	35.5192	1.3033	0.0092	36.4328	75.3745	75.9854
112	38	3.5132	0.0248	52.3589	3.0316	0.0214	55.5364	70.5882	73.8068
113	38	3.3858	0.0239	53.0265	2.4366	0.0172	50.2935	63.9318	70.9471
114	38	4.0374	0.0285	49.6146	2.3091	0.0163	49.1700	73.1707	73.5114
115	39	3.8957	0.0275	65.2734	2.3091	0.0163	65.4881	76.0938	65.1890
116	39	2.4933	0.0176	60.2313	3.5416	0.0250	60.4771	60.8273	67.6387
117	39	2.7058	0.0191	60.9953	3.5274	0.0249	60.5347	55.6242	55.1538
118	40	2.4649	0.0174	51.8014	1.4591	0.0103	52.2500	91.7207	94.5656
119	40	1.9408	0.0137	49.0242	1.4591	0.0103	52.2500	90.3252	90.8174
120	40	1.9691	0.0139	49.1744	1.2750	0.0090	45.5000	83.9490	86.8056
121	41	2.6774	0.0189	24.4940	2.1816	0.0154	24.2254	75.6506	80.3686
122	41	3.6691	0.0259	25.8926	2.2383	0.0158	25.0943	79.2492	79.2763
123	41	3.1166	0.0220	25.1134	2.3091	0.0163	26.1803	80.8093	79.6272
124	42	4.5474	0.0321	51.0000	3.1024	0.0219	51.5478	65.5738	65.5594
125	42	4.7457	0.0335	50.0000	3.2299	0.0228	50.7280	67.2123	67.1943
126	42	4.7457	0.0335	50.0000	3.5416	0.0250	48.7241	66.6213	66.5897
127	43	3.3291	0.0235	53.4752	3.6407	0.0257	53.4857	86.9901	86.5884
128	43	4.5191	0.0319	53.5608	3.3149	0.0234	53.7327	76.9034	85.3606
129	43	3.1733	0.0224	53.4640	3.9099	0.0276	53.2817	85.6859	85.6885
130	44	2.8758	0.0203	32.2990	1.3175	0.0093	32.0454	74.9064	95.5718
131	44	4.0374	0.0285	36.7371	2.2666	0.0160	36.7894	77.0284	77.0152
132	44	3.4424	0.0243	34.4639	1.8416	0.0130	34.6652	79.7677	79.2522
133	45	5.9215	0.0418	26.1124	1.6575	0.0117	26.3658	74.9625	75.0657
134	45	5.7940	0.0409	26.3283	2.2666	0.0160	27.6854	74.3722	74.3484
135	45	4.4766	0.0316	28.5593	1.9266	0.0136	26.9489	74.5133	74.5550

Table B41 Pulse pressure and heart rate demodulation data (continued)

Test no.	Volunteer no.	Displacement probe A (μm)	Measured PP probe A (mmHg)	Calibrated PP probe A (mmHg)	Measured HR probe A (bpm)	Displacement probe B (μm)	Measured PP probe B (mmHg)	Calibrated PP probe B (mmHg)	Measured HR probe B (bpm)
136	46	3.3433	0.0236	30.9199	2.5924	0.0183	31.0268	104.2753	93.3707
137	46	2.5641	0.0181	30.2129	3.5557	0.0251	30.2907	100.0394	100.1062
138	46	2.7341	0.0193	30.3672	3.6974	0.0261	30.1825	87.9197	88.6820
139	47	4.1791	0.0295	36.3112	0.9066	0.0064	36.5451	75.5049	75.5525
140	47	4.1507	0.0293	36.2699	1.0625	0.0075	36.2329	76.9788	76.9718
141	47	3.9099	0.0276	35.9190	1.3175	0.0093	35.7220	77.4299	77.4370
142	48	1.5866	0.0112	35.4405	1.0341	0.0073	35.3026	86.0388	86.0363
143	48	1.5300	0.0108	35.2976	1.0625	0.0075	35.3289	80.9575	80.9139
144	48	1.5158	0.0107	35.2619	1.1050	0.0078	35.3684	86.7553	86.2252
145	49	2.2383	0.0158	39.2500	1.8133	0.0128	39.0822	89.3575	89.4188
146	49	2.2383	0.0158	39.2500	1.9125	0.0135	39.4075	96.6347	96.6198
147	49	3.2158	0.0227	42.0000	2.7058	0.0191	42.0103	96.8948	96.9440
148	50	3.9099	0.0276	33.9368	1.7425	0.0123	33.9274	67.0341	67.0341
149	50	3.7824	0.0267	33.6813	1.8983	0.0134	31.8871	64.9970	64.1245
150	50	2.6349	0.0186	31.3819	1.7991	0.0127	33.1855	66.9419	66.4599
151	51	2.8474	0.0201	30.0599	0.5525	0.0039	30.2500	87.0681	87.4689
152	51	1.5158	0.0107	33.2540	0.5525	0.0039	30.2500	85.0467	85.0518
153	51	1.5441	0.0109	33.1861	0.7650	0.0054	36.0000	81.5070	82.7891
154	52	5.2982	0.0374	28.2604	1.2466	0.0088	28.2795	83.6773	83.6680
155	52	4.1224	0.0291	31.6864	1.5725	0.0111	31.7347	84.6702	84.6778
156	52	3.8249	0.0270	32.5532	1.6433	0.0116	32.4858	80.4194	80.3811
157	53	2.0966	0.0148	29.8609	1.8416	0.0130	29.1310	65.2093	65.1830
158	53	2.5924	0.0183	33.3665	2.0116	0.0142	34.5546	67.6503	67.6525
159	53	3.1449	0.0222	37.2726	2.0825	0.0147	36.8144	68.7375	68.7285
160	54	1.6433	0.0116	44.0000	2.1391	0.0151	43.9792	115.6515	119.0161
161	54	1.6433	0.0116	44.0000	2.1533	0.0152	44.0004	116.5049	112.5704
162	54	1.8558	0.0131	45.0000	2.8333	0.0200	45.0204	124.2579	123.8816

Table B41 Pulse pressure and heart rate demodulation data (continued)

Test no.	Volunteer no.	Displacement probe A (μm)	Measured PP probe A (mmHg)	Calibrated PP probe A (mmHg)	Measured HR probe A (bpm)	Displacement probe B (μm)	Measured PP probe B (mmHg)	Calibrated PP probe B (mmHg)	Measured HR probe B (bpm)
163	55	2.4224	0.0171	42.1052	2.3941	0.0169	42.3794	71.8058	71.7128
164	55	2.7908	0.0197	40.0273	2.5499	0.0180	40.2861	78.2641	78.2737
165	55	2.8191	0.0199	39.8675	2.6208	0.0185	39.3346	75.0821	74.6687
166	56	1.3883	0.0098	24.1659	0.8783	0.0062	24.0663	76.4480	76.4457
167	56	1.2041	0.0085	24.9547	0.9208	0.0065	24.6939	77.7985	77.7747
168	56	1.1050	0.0078	25.3794	0.9916	0.0070	25.7398	77.9964	78.0076
169	57	2.9183	0.0206	58.8958	1.1191	0.0079	62.1397	84.2886	86.6051
170	57	3.3008	0.0233	53.9212	1.6575	0.0117	49.8818	87.6205	87.6278
171	57	3.8957	0.0275	46.1830	1.7850	0.0126	46.9786	89.7965	88.6350
172	58	0.8075	0.0057	27.6366	1.6858	0.0119	28.0374	72.6876	72.6656
173	58	1.0341	0.0073	28.1350	1.7708	0.0125	28.0020	72.5755	72.5711
174	58	1.0766	0.0076	28.2284	1.8700	0.0132	27.9606	75.2079	75.2612
175	59	1.6575	0.0117	42.3319	2.5074	0.0177	42.4111	86.3061	85.7014
176	59	2.0966	0.0148	39.5154	2.9466	0.0208	39.3394	81.5070	81.5119
177	59	2.3091	0.0163	38.1526	3.1024	0.0219	38.2495	90.8975	89.7044
178	60	4.8307	0.0341	44.7065	1.8133	0.0128	42.3224	77.1506	85.4457
179	60	3.7824	0.0267	40.9393	1.7991	0.0127	42.9863	86.0585	84.6979
180	60	1.6716	0.0118	33.3542	1.9975	0.0141	33.6913	87.0070	96.9619
181	61	3.7824	0.0267	42.6540	1.9408	0.0137	42.3360	90.4432	75.8725
182	61	5.1565	0.0364	42.9610	1.9833	0.0140	42.4848	65.0007	73.6016
183	61	2.5783	0.0182	42.3850	2.1816	0.0154	43.1791	89.6272	88.3496
184	62	5.0290	0.0355	36.5614	1.5158	0.0107	39.7622	73.1083	73.0861
185	62	4.2357	0.0299	36.9298	1.6716	0.0118	36.9246	73.7123	73.6852
186	62	5.1424	0.0363	36.5088	1.8700	0.0132	33.3132	72.4463	72.4485
187	63	2.7058	0.0191	40.9741	0.5667	0.0040	41.2537	80.6204	80.5647
188	63	4.0516	0.0286	42.8244	0.4392	0.0031	41.8582	92.5926	95.6023
189	63	2.5074	0.0177	40.7015	0.5383	0.0038	41.3881	74.3080	74.3379

Table B41 Pulse pressure and heart rate demodulation data (continued)

Test no.	Volunteer no.	Displacement probe A (μm)	Measured PP probe A (mmHg)	Calibrated PP probe A (mmHg)	Measured HR probe A (bpm)	Displacement probe B (μm)	Measured PP probe B (mmHg)	Calibrated PP probe B (mmHg)	Measured HR probe B (bpm)
190	64	1.1475	0.0081	46.4779	1.0341	0.0073	48.0000	78.9107	78.8327
191	64	0.9916	0.0070	48.9392	1.2041	0.0085	46.0000	75.5712	75.5779
192	64	1.2041	0.0085	45.5829	1.1191	0.0079	47.0000	79.2368	79.2615
193	65	2.3374	0.0165	50.0508	1.1616	0.0082	49.8973	81.7795	81.4244
194	65	2.5216	0.0178	47.8891	1.4875	0.0105	46.9220	81.8442	81.7494
195	65	2.6774	0.0189	46.0600	1.4591	0.0103	47.1807	84.9858	79.5439
196	66	3.3149	0.0234	42.1561	2.7199	0.0192	41.9093	73.2556	73.2377
197	66	3.7682	0.0266	43.1692	2.5358	0.0179	43.1641	74.5180	74.4856
198	66	2.8758	0.0203	41.1747	2.7908	0.0197	41.4266	77.8339	80.8031
199	67	4.0091	0.0283	37.3333	1.6858	0.0119	37.5714	66.6328	66.2335
200	67	4.3207	0.0305	37.3333	1.8133	0.0128	37.1429	66.5821	67.4894
201	67	4.1649	0.0294	37.3333	1.7708	0.0125	37.2857	69.6205	68.5678
202	68	1.2466	0.0088	29.1496	0.6517	0.0046	29.2143	86.2512	86.2225
203	68	1.5725	0.0111	29.3541	0.7366	0.0052	29.3571	91.0273	91.0405
204	68	1.7991	0.0127	29.4963	0.7791	0.0055	29.4286	88.6184	88.6708
205	69	1.2608	0.0089	34.6763	0.6517	0.0046	36.1484	71.8620	78.8091
206	69	1.1758	0.0083	34.9029	0.3825	0.0027	33.0165	66.6963	74.7384
207	69	1.5441	0.0109	33.9209	0.4958	0.0035	34.3352	77.2698	76.8640
208	70	4.4341	0.0313	34.2558	1.6716	0.0118	33.9474	75.2611	75.0962
209	70	4.6891	0.0331	36.2093	1.7566	0.0124	35.8816	78.3988	78.3506
210	70	4.7316	0.0334	36.5349	1.8133	0.0128	37.1711	79.8372	79.8397
211	71	2.5216	0.0178	56.3333	2.7341	0.0193	56.2370	70.0455	69.9518
212	71	2.5074	0.0177	55.8333	2.5641	0.0181	55.7418	71.5754	71.5780
213	71	2.5358	0.0179	56.8333	3.0033	0.0212	57.0211	61.7708	61.7814
214	72	1.4308	0.0101	50.5330	1.5583	0.0110	50.5000	60.8746	60.8519
215	72	1.5016	0.0106	51.4396	1.6433	0.0116	52.0000	57.9546	57.9822
216	72	1.5866	0.0112	52.5275	1.6433	0.0116	52.0000	58.8620	58.8659

Table B41 Pulse pressure and heart rate demodulation data (continued)

Test no.	Volunteer no.	Displacement probe A (μm)	Measured PP probe A (mmHg)	Calibrated PP probe A (mmHg)	Measured HR probe A (bpm)	Displacement probe B (μm)	Measured PP probe B (mmHg)	Calibrated PP probe B (mmHg)	Measured HR probe B (bpm)
217	73	3.2299	0.0228	40.5180	1.5441	0.0109	41.1067	56.8810	56.4511
218	73	3.5982	0.0254	40.3505	2.1108	0.0149	39.7216	64.1261	63.8026
219	73	4.0799	0.0288	40.1314	1.9266	0.0136	40.1717	63.9990	63.9600
220	74	3.9949	0.0282	59.3791	2.2808	0.0161	57.4876	66.2753	66.2900
221	74	4.1932	0.0296	60.3081	2.3658	0.0167	59.0565	66.6213	66.6015
222	74	3.9807	0.0281	59.3128	2.5499	0.0180	62.4558	70.6836	70.7592
223	75	4.0657	0.0287	35.9991	1.1900	0.0084	35.7500	55.9038	55.8981
224	75	4.4624	0.0315	34.5268	1.0766	0.0076	34.2500	60.1740	60.1703
225	75	4.4766	0.0316	34.4742	1.1333	0.0080	35.0000	55.6586	55.6965
226	76	1.5441	0.0109	28.5830	1.9550	0.0138	28.0920	76.9184	78.9889
227	76	2.2241	0.0157	29.7448	1.8558	0.0131	29.2254	75.5026	75.4836
228	76	2.1816	0.0154	29.6722	1.7283	0.0122	30.6826	78.9174	78.8713
229	77	2.4224	0.0171	44.9502	2.1674	0.0153	45.2143	69.6567	67.6336
230	77	2.3658	0.0167	45.0631	1.9125	0.0135	44.9286	68.3527	68.3553
231	77	2.1533	0.0152	45.4867	2.2949	0.0162	45.3571	70.8624	70.6732
232	78	2.4083	0.0170	32.5153	1.7425	0.0123	32.6812	82.3580	82.3628
233	78	2.6491	0.0187	33.9475	1.9833	0.0140	33.6477	83.2896	83.2742
234	78	2.7483	0.0194	34.5372	2.2383	0.0158	34.6711	71.2296	71.2183
235	79	1.3844	0.0083	28.2500	0.7339	0.0044	28.3041	65.3524	65.3645
236	79	1.4177	0.0085	28.0000	0.8673	0.0052	27.6443	65.9044	65.6181
237	79	1.3844	0.0083	28.2500	0.6838	0.0041	28.5515	65.6499	65.6298
238	80	1.0766	0.0076	40.5577	1.4025	0.0099	40.5833	65.2043	65.1825
239	80	1.1333	0.0080	40.1731	1.4308	0.0101	40.0833	69.4077	69.3344
240	80	1.1191	0.0079	40.2692	1.4166	0.0100	40.3333	71.4529	71.4334
241	81	2.3374	0.0165	54.3172	2.3374	0.0165	54.3360	90.9787	91.0020
242	81	1.9833	0.0140	53.6915	2.7058	0.0191	53.6932	84.9698	89.9041
243	81	1.8700	0.0132	53.4913	2.8333	0.0200	53.4707	87.6040	90.3955

Table B41 Pulse pressure and heart rate demodulation data (continued)

Test no.	Volunteer no.	Displacement probe A (μm)	Measured PP probe A (mmHg)	Calibrated PP probe A (mmHg)	Measured HR probe A (bpm)	Displacement probe B (μm)	Measured PP probe B (mmHg)	Calibrated PP probe B (mmHg)	Measured HR probe B (bpm)
244	82	3.4849	0.0246	33.7366	0.2267	0.0016	34.0000	108.2314	108.1876
245	82	3.1308	0.0221	34.4952	0.2550	0.0018	34.5000	102.6480	102.6511
246	82	3.0033	0.0212	34.7683	0.2550	0.0018	34.5000	107.5172	107.4787
247	83	2.3941	0.0169	32.5564	0.7933	0.0056	31.5051	88.1627	88.2016
248	83	2.0825	0.0147	32.3703	0.6800	0.0048	33.3418	96.2626	96.2626
249	83	2.4224	0.0171	32.5733	0.7225	0.0051	32.6531	88.0282	88.0204
250	84	3.2858	0.0197	36.3532	1.5011	0.0090	36.1105	78.8477	78.8457
251	84	3.2024	0.0192	35.8945	1.3010	0.0078	35.7267	73.4005	73.3811
252	84	3.0856	0.0185	35.2523	1.2676	0.0076	35.6628	72.9854	72.9915
253	85	4.0030	0.0240	66.9268	1.2676	0.0076	66.9643	70.1924	70.2012
254	85	4.8536	0.0291	64.8865	1.0174	0.0061	64.9286	72.4695	72.4767
255	85	4.5200	0.0271	65.6866	1.1008	0.0066	65.6071	72.4727	71.7188

Table B42 Summary of blood pressure demodulation

Test no.	Volunteer no.	Mean HR (bpm)	Mean PP (mmHg)	PTT (ms)	PWV (m/s)	DBP coefficient	m_{DBP}	c_{DBP}	Demodulated DBP (mmHg)	Demodulated SBP (mmHg)
1	1	77.0832	49.7187	19.1600	0.0522	0.0004	19682.2587	96.5742	104.6252	154.3439
2	1	79.9212	48.8943	28.2000	0.0355	0.0002	19682.2587	96.5742	100.2908	149.1850
3	1	78.1065	48.8870	25.6000	0.0391	0.0002	19682.2587	96.5742	101.0840	149.9711
4	2	85.3485	36.4493	35.3053	0.0283	0.0001	82667.9413	67.0557	77.0148	113.4641
5	2	89.8545	36.5406	34.8533	0.0287	0.0001	82667.9413	67.0557	77.2748	113.8154
6	2	84.0104	36.0100	34.1333	0.0293	0.0001	82667.9413	67.0557	77.7104	113.7205
7	3	64.6808	37.4471	9.0333	0.1107	0.0018	54.1291	63.1986	63.2982	100.7453
8	3	65.9526	35.8936	7.9429	0.1259	0.0024	54.1291	63.1986	63.3274	99.2210
9	3	68.6993	30.6593	6.8000	0.1471	0.0032	54.1291	63.1986	63.3744	94.0337
10	4	56.1115	37.3748	14.1333	0.0708	0.0008	619.6169	93.4365	93.9023	131.2771
11	4	54.6647	35.5456	13.0667	0.0765	0.0009	619.6169	93.4365	93.9814	129.5270
12	4	61.7910	40.0796	6.5333	0.1531	0.0035	619.6169	93.4365	95.6163	135.6959
13	5	76.6705	47.3941	40.8941	0.0245	0.0001	111744.0331	56.7840	66.8192	114.2133
14	5	85.9516	47.3330	51.7500	0.0193	0.0001	111744.0331	56.7840	63.0529	110.3859
15	5	75.6800	50.7729	46.2588	0.0216	0.0001	111744.0331	56.7840	64.6279	115.4008
16	6	72.1878	39.2581	34.0000	0.9706	0.1415	4.9974	73.9989	74.7058	113.9639
17	6	74.2517	38.3069	15.3333	2.1522	0.6955	4.9974	73.9989	77.4748	115.7816
18	6	80.3306	38.9351	50.5000	0.6535	0.0641	4.9974	73.9989	74.3194	113.2544
19	7	58.6635	40.8172	16.4333	0.0609	0.0006	-535.9812	65.2944	64.9963	105.8135
20	7	63.9700	39.7228	12.1600	0.0822	0.0010	-535.9812	65.2944	64.7501	104.4729
21	7	61.2121	38.9600	12.2000	0.0820	0.0010	-535.9812	65.2944	64.7536	103.7136
22	8	73.1440	28.4215	2.1333	22.0316	72.8878	0.0368	66.8324	69.5176	97.9391
23	8	76.0252	27.8378	3.9529	11.8900	21.2289	0.0368	66.8324	67.6145	95.4523
24	8	75.3991	30.2407	3.4353	13.6815	28.1080	0.0368	66.8324	67.8679	98.1087
25	9	80.9062	37.9271	30.2286	1.4225	0.3039	0.9902	71.9683	72.2691	110.1962
26	9	84.0808	34.7873	10.5818	4.0636	2.4796	0.9902	71.9683	74.4234	109.2108
27	9	88.2717	35.7856	18.1000	2.3757	0.8475	0.9902	71.9683	72.8074	108.5930

Table B42 Summary of blood pressure demodulation (continued)

Test no.	Volunteer no.	Mean HR (bpm)	Mean PP (mmHg)	PTT (ms)	PWV (m/s)	DBP coefficient	m_{DBP}	c_{DBP}	Demodulated DBP (mmHg)	Demodulated SBP (mmHg)
28	10	71.8965	32.9689	34.5000	0.0290	0.0001	-26663.3570	79.8874	76.5235	109.4925
29	10	76.1905	34.5666	29.3200	0.0341	0.0002	-26663.3570	79.8874	75.2299	109.7965
30	10	82.4344	35.9645	20.3789	0.0491	0.0004	-26663.3570	79.8874	70.2465	106.2110
31	11	58.8697	37.3278	34.0000	0.0294	0.0001	-34085.0655	69.1439	65.0001	102.3278
32	11	59.0078	37.7117	28.5333	0.0350	0.0002	-34085.0655	69.1439	63.0000	100.7117
33	11	58.7624	37.8677	29.9200	0.0334	0.0002	-34085.0655	69.1439	63.0000	100.8677
34	12	54.7603	46.3511	7.5000	6.0000	5.4059	0.1190	61.9162	62.5595	108.9106
35	12	54.5165	45.9143	7.7818	5.7827	5.0214	0.1190	61.9162	62.5138	108.4281
36	12	50.4240	46.2345	58.6667	0.7670	0.0883	0.1190	61.9162	61.9267	108.1613
37	13	87.0492	39.5374	8.8000	4.7727	3.4206	1.0700	66.2886	69.9487	109.4861
38	13	93.2099	40.1612	8.7200	4.8165	3.4836	1.0700	66.2886	70.0162	110.1774
39	13	88.0791	40.8014	19.4857	2.1554	0.6976	1.0700	66.2886	67.0351	107.8365
40	14	74.6597	35.4200	9.5059	4.4183	2.9314	0.4558	75.8302	77.1664	112.5864
41	14	80.0653	35.1414	10.5412	3.9844	2.3839	0.4558	75.8302	76.9168	112.0582
42	14	74.0377	35.4386	37.3600	1.1242	0.1898	0.4558	75.8302	75.9168	111.3554
43	15	65.6743	32.7731	4.0000	9.2500	12.8483	0.4354	70.7095	76.3041	109.0772
44	15	69.1882	31.7746	6.8000	5.4412	4.4458	0.4354	70.7095	72.6453	104.4199
45	15	75.4655	34.4523	16.2000	2.2840	0.7833	0.4354	70.7095	71.0506	105.5029
46	16	77.6097	42.4025	9.3333	4.6072	3.1873	-0.0628	70.0449	69.8448	112.2472
47	16	73.1887	40.2200	4.0000	10.7500	17.3532	-0.0628	70.0449	68.9554	109.1754
48	16	75.2395	40.8776	3.6000	11.9444	21.4237	-0.0628	70.0449	68.6998	109.5774
49	17	53.2340	50.2038	3.8000	11.3158	19.2279	-0.1438	58.7889	56.0233	106.2271
50	17	62.1119	51.5208	2.6000	16.5385	41.0727	-0.1438	58.7889	52.8814	104.4022
51	17	57.9598	47.7754	4.2667	10.0780	15.2516	-0.1438	58.7889	56.5953	104.3707
52	18	70.2061	32.3844	23.4133	1.9220	0.5547	-6.4559	86.4429	82.8618	115.2461
53	18	70.0533	32.4488	21.2800	2.1147	0.6715	-6.4559	86.4429	82.1078	114.5566
54	18	72.0728	32.1668	22.4000	2.0089	0.6060	-6.4559	86.4429	82.5305	114.6973

Table B42 Summary of blood pressure demodulation (continued)

Test no.	Volunteer no.	Mean HR (bpm)	Mean PP (mmHg)	PTT (ms)	PWV (m/s)	DBP coefficient	m_{DBP}	c_{DBP}	Demodulated DBP (mmHg)	Demodulated SBP (mmHg)
55	19	62.1385	26.0121	40.8000	0.9804	0.1443	21.3682	59.6326	62.7167	88.7288
56	19	63.5833	26.9030	52.1455	0.7671	0.0884	21.3682	59.6326	61.5207	88.4236
57	19	62.6969	27.5849	44.1818	0.9054	0.1231	21.3682	59.6326	62.2626	89.8476
58	20	108.6469	31.0894	32.8160	1.4627	0.3213	15.3528	78.4366	83.3690	114.4584
59	20	101.0898	30.9609	42.9043	1.1188	0.1880	15.3528	78.4366	81.3221	112.2830
60	20	102.5947	30.9497	37.0364	1.2960	0.2522	15.3528	78.4366	82.3089	113.2586
61	21	65.3140	40.2156	7.8333	5.6170	4.7378	0.0817	69.3859	69.7731	109.9887
62	21	68.4619	39.9163	7.2667	6.0550	5.5055	0.0817	69.3859	69.8359	109.7522
63	21	75.2046	40.8681	68.7000	0.6405	0.0616	0.0817	69.3859	69.3910	110.2591
64	22	64.2165	36.2926	16.9600	2.7123	1.1047	-0.1973	70.9948	70.7768	107.0694
65	22	68.3878	39.0831	14.1667	3.2471	1.5832	-0.1973	70.9948	70.6824	109.7655
66	22	68.6342	39.6244	8.1067	5.6743	4.8349	-0.1973	70.9948	70.0407	109.6651
67	23	69.2891	31.5833	23.8286	1.6367	0.4022	-3.0550	68.5472	67.3184	98.9016
68	23	69.6379	31.6600	12.8571	3.0333	1.3817	-3.0550	68.5472	64.3262	95.9862
69	23	80.8908	28.7567	16.1000	2.4224	0.8811	-3.0550	68.5472	65.8554	94.6121
70	24	95.7297	29.0094	11.4000	2.8947	1.2583	0.2349	72.2860	72.5816	101.5910
71	24	86.1997	26.3793	5.3333	6.1875	5.7491	0.2349	72.2860	73.6364	100.0157
72	24	99.6679	26.1113	8.8000	3.7500	2.1117	0.2349	72.2860	72.7820	98.8933
73	25	59.4009	43.2579	3.9692	9.8257	14.4973	-0.1212	78.1264	76.3690	119.6269
74	25	56.2975	40.2013	9.4000	4.1489	2.5849	-0.1212	78.1264	77.8131	118.0144
75	25	62.6227	44.0408	4.6000	8.4783	10.7939	-0.1212	78.1264	76.8179	120.8587
76	26	77.3373	43.3146	14.7200	3.2609	1.5967	6.7854	73.9925	84.8269	128.1414
77	26	73.2482	43.2258	21.2000	2.2642	0.7698	6.7854	73.9925	79.2158	122.4416
78	26	74.4356	44.9596	24.3333	1.9726	0.5843	6.7854	73.9925	77.9573	122.9169
79	27	75.2009	55.2824	47.5111	0.8840	0.1173	11.6485	63.8005	65.1674	120.4498
80	27	70.4556	53.6609	35.1200	1.1959	0.2148	11.6485	63.8005	66.3021	119.9630
81	27	63.3525	51.0567	18.8000	2.2340	0.7495	11.6485	63.8005	72.5305	123.5872

Table B42 Summary of blood pressure demodulation (continued)

Test no.	Volunteer no.	Mean HR (bpm)	Mean PP (mmHg)	PTT (ms)	PWV (m/s)	DBP coefficient	m_{DBP}	c_{DBP}	Demodulated DBP (mmHg)	Demodulated SBP (mmHg)
82	28	64.7354	43.9507	1.6000	25.0000	93.8519	0.0356	61.6173	64.9626	108.9133
83	28	67.6916	44.3592	3.9714	10.0720	15.2334	0.0356	61.6173	62.1602	106.5194
84	28	72.3895	44.1902	1.9467	20.5476	63.3994	0.0356	61.6173	63.8771	108.0673
85	29	80.9259	41.7581	8.9600	4.2411	2.7009	-0.2752	60.5678	59.8244	101.5824
86	29	80.6838	39.6039	6.9176	5.4932	4.5313	-0.2752	60.5678	59.3206	98.9245
87	29	90.3688	39.6380	16.7500	2.2687	0.7729	-0.2752	60.5678	60.3550	99.9931
88	30	62.0141	32.0147	14.4000	2.9167	1.2774	-11.1584	87.6803	73.4263	105.4410
89	30	57.9376	31.4696	14.9600	2.8075	1.1836	-11.1584	87.6803	74.4735	105.9431
90	30	63.7573	32.0157	14.0000	3.0000	1.3515	-11.1584	87.6803	72.6002	104.6159
91	31	74.5387	52.5632	26.4000	1.3636	0.2792	-0.9191	66.4439	66.1872	118.7504
92	31	75.3107	53.1085	35.1000	1.0256	0.1580	-0.9191	66.4439	66.2987	119.4072
93	31	77.1473	53.8283	20.4000	1.7647	0.4676	-0.9191	66.4439	66.0141	119.8424
94	32	93.5300	54.8174	11.4000	3.0702	1.4154	6.3739	72.0436	81.0655	135.8829
95	32	102.6534	53.5575	17.7333	1.9737	0.5850	6.3739	72.0436	75.7721	129.3295
96	32	89.3190	56.6252	18.0000	1.9444	0.5677	6.3739	72.0436	75.6624	132.2876
97	33	78.1025	42.3869	2.8267	16.9809	43.2998	0.1731	64.7116	72.2061	114.5930
98	33	75.2845	44.1228	3.2500	14.7692	32.7551	0.1731	64.7116	70.3810	114.5038
99	33	77.4093	43.4902	4.3250	11.0983	18.4958	0.1731	64.7116	67.9129	111.4032
100	34	93.7166	31.7054	25.1400	1.4718	0.3253	-5.0292	81.6451	80.0093	111.7147
101	34	100.7372	29.9882	17.2545	2.1444	0.6905	-5.0292	81.6451	78.1725	108.1606
102	34	94.0172	32.8065	19.1238	1.9348	0.5621	-5.0292	81.6451	78.8182	111.6247
103	35	74.1431	42.6195	4.7556	8.2009	10.0991	0.2017	63.5032	65.5399	108.1594
104	35	68.9507	42.4308	4.5231	8.6224	11.1640	0.2017	63.5032	65.7547	108.1854
105	35	76.2586	42.9498	15.0933	2.5839	1.0026	0.2017	63.5032	63.7054	106.6552
106	36	68.9336	30.7181	35.3333	1.0755	0.1737	-57.4563	72.4708	62.4916	93.2097
107	36	67.5951	29.6478	40.8000	0.9314	0.1303	-57.4563	72.4708	64.9866	94.6344
108	36	61.9324	28.6341	38.4000	0.9896	0.1471	-57.4563	72.4708	64.0218	92.6559

Table B42 Summary of blood pressure demodulation (continued)

Test no.	Volunteer no.	Mean HR (bpm)	Mean PP (mmHg)	PTT (ms)	PWV (m/s)	DBP coefficient	m_{DBP}	c_{DBP}	Demodulated DBP (mmHg)	Demodulated SBP (mmHg)
109	37	84.7630	38.7147	19.4105	1.7001	0.4340	3.6464	66.9360	68.5186	107.2334
110	37	79.3453	36.3092	49.7778	0.6629	0.0660	3.6464	66.9360	67.1767	103.4859
111	37	75.6799	35.9760	40.2154	0.8206	0.1011	3.6464	66.9360	67.3047	103.2807
112	38	72.1975	53.9477	12.6667	3.6316	1.9804	-0.3203	75.5527	74.9184	128.8661
113	38	67.4395	51.6600	15.8000	2.9114	1.2728	-0.3203	75.5527	75.1450	126.8050
114	38	73.3411	49.3923	29.6000	1.5541	0.3627	-0.3203	75.5527	75.4366	124.8289
115	39	70.6414	65.3808	77.5000	0.6710	0.0676	0.2628	62.7324	62.7502	128.1309
116	39	64.2330	60.3542	7.7333	6.7242	6.7895	0.2628	62.7324	64.5169	124.8711
117	39	55.3890	60.7650	453.4667	0.1147	0.0020	0.2628	62.7324	62.7329	123.4979
118	40	93.1431	52.0257	8.6667	4.0384	2.4490	-0.9362	78.8705	76.5776	128.6033
119	40	90.5713	50.6371	6.0000	5.8333	5.1097	-0.9362	78.8705	74.0866	124.7237
120	40	85.3773	47.3372	9.2000	3.8043	2.1733	-0.9362	78.8705	76.8358	124.1729
121	41	78.0096	24.3597	20.1600	2.0833	0.6517	-5.0588	69.8106	66.5136	90.8732
122	41	79.2628	25.4935	18.7200	2.2436	0.7559	-5.0588	69.8106	65.9868	91.4803
123	41	80.2183	25.6469	20.1176	2.0877	0.6545	-5.0588	69.8106	66.4996	92.1465
124	42	65.5666	51.2739	7.8286	4.3430	2.8324	-6.9015	94.5234	74.9757	126.2497
125	42	67.2033	50.3640	6.5867	5.1619	4.0012	-6.9015	94.5234	66.9095	117.2736
126	42	66.6055	49.3621	6.8000	5.0000	3.7541	-6.9015	94.5234	68.6147	117.9768
127	43	86.7893	53.4805	14.8000	2.9054	1.2676	-0.3759	72.8142	72.3377	125.8182
128	43	81.1320	53.6467	10.3000	4.1748	2.6171	-0.3759	72.8142	71.8304	125.4771
129	43	85.6872	53.3728	5.9158	7.2687	7.9337	-0.3759	72.8142	69.8319	123.2047
130	44	85.2391	32.1722	3.8000	0.2632	0.0104	962.6664	64.0115	74.0224	106.1946
131	44	77.0218	36.7632	12.6000	0.0794	0.0009	962.6664	64.0115	64.9220	101.6853
132	44	79.5100	34.5646	16.3000	0.0613	0.0006	962.6664	64.0115	64.5556	99.1202
133	45	75.0141	26.2391	13.6000	2.9412	1.2990	-1.1387	70.7444	69.2652	95.5043
134	45	74.3603	27.0069	10.0000	4.0000	2.4026	-1.1387	70.7444	68.0085	95.0153
135	45	74.5342	27.7541	13.4250	2.9795	1.3331	-1.1387	70.7444	69.2264	96.9804

Table B42 Summary of blood pressure demodulation (continued)

Test no.	Volunteer no.	Mean HR (bpm)	Mean PP (mmHg)	PTT (ms)	PWV (m/s)	DBP coefficient	m_{DBP}	c_{DBP}	Demodulated DBP (mmHg)	Demodulated SBP (mmHg)
136	46	98.8230	30.9734	17.6000	2.1591	0.7000	0.1510	72.1663	72.2720	103.2453
137	46	100.0728	30.2518	11.4182	3.3280	1.6632	0.1510	72.1663	72.4174	102.6692
138	46	88.3009	30.2748	15.0588	2.5234	0.9562	0.1510	72.1663	72.3107	102.5855
139	47	75.5287	36.4281	76.2750	0.4720	0.0335	-108.6121	76.9434	73.3102	109.7384
140	47	76.9753	36.2514	69.3412	0.5192	0.0405	-108.6121	76.9434	72.5473	108.7987
141	47	77.4335	35.8205	66.3529	0.5426	0.0442	-108.6121	76.9434	72.1424	107.9629
142	48	86.0376	35.3716	33.3263	1.1702	0.2056	-7.7337	69.7359	68.1455	103.5170
143	48	80.9357	35.3133	44.2000	0.8824	0.1169	-7.7337	69.7359	68.8318	104.1450
144	48	86.4903	35.3152	49.7684	0.7836	0.0922	-7.7337	69.7359	69.0228	104.3379
145	49	89.3882	39.1661	2.5556	13.6954	28.1652	-0.8800	112.1687	87.3823	126.5483
146	49	96.6273	39.3288	2.6095	13.4125	27.0137	-0.8800	112.1687	88.3956	127.7244
147	49	96.9194	42.0051	2.4286	14.4116	31.1880	-0.8800	112.1687	84.7221	126.7273
148	50	67.0341	33.9321	34.5846	1.1566	0.2009	34.0642	60.3121	67.1546	101.0867
149	50	64.5608	32.7842	41.2000	0.9709	0.1415	34.0642	60.3121	65.1336	97.9178
150	50	66.7009	32.2837	58.4000	0.6849	0.0704	34.0642	60.3121	62.7118	94.9954
151	51	87.2685	30.1549	33.4105	1.2571	0.2373	9.8807	71.8350	74.1797	104.3346
152	51	85.0493	31.7520	148.6667	0.2825	0.0120	9.8807	71.8350	71.9534	103.7054
153	51	82.1481	34.5930	41.3333	1.0161	0.1550	9.8807	71.8350	73.3669	107.9600
154	52	83.6727	28.2700	19.6000	2.2449	0.7568	-1.1991	72.7957	71.8883	100.1583
155	52	84.6740	31.7105	8.6737	5.0728	3.8642	-1.1991	72.7957	68.1623	99.8728
156	52	80.4003	32.5195	8.9556	4.9131	3.6248	-1.1991	72.7957	68.4494	100.9689
157	53	65.1962	29.4960	5.2000	7.6923	8.8854	-0.1730	75.8979	74.3611	103.8571
158	53	67.6514	33.9605	4.5429	8.8049	11.6417	-0.1730	75.8979	73.8844	107.8449
159	53	68.7330	37.0435	5.0286	7.9545	9.5014	-0.1730	75.8979	74.2545	111.2981
160	54	117.3338	43.9896	3.3333	12.0001	21.6239	-0.0554	68.8695	67.6717	111.6613
161	54	114.5377	44.0002	107.2000	0.3731	0.0209	-0.0554	68.8695	68.8683	112.8686
162	54	124.0698	45.0102	2.6400	15.1515	34.4727	-0.0554	68.8695	66.9600	111.9702

Table B42 Summary of blood pressure demodulation (continued)

Test no.	Volunteer no.	Mean HR (bpm)	Mean PP (mmHg)	PTT (ms)	PWV (m/s)	DBP coefficient	m_{DBP}	c_{DBP}	Demodulated DBP (mmHg)	Demodulated SBP (mmHg)
163	55	71.7593	42.2423	4.9250	8.9340	11.9855	-0.0178	77.0370	76.8242	119.0665
164	55	78.2689	40.1567	2.2353	19.6842	58.1831	-0.0178	77.0370	76.0039	116.1606
165	55	74.8754	39.6010	3.7600	11.7021	20.5633	-0.0178	77.0370	76.6719	116.2729
166	56	76.4469	24.1161	5.8000	6.7241	6.7895	0.4464	59.9981	63.0288	87.1449
167	56	77.7866	24.8243	19.4118	2.0091	0.6061	0.4464	59.9981	60.2687	85.0930
168	56	78.0020	25.5596	22.3333	1.7463	0.4579	0.4464	59.9981	60.2025	85.7621
169	57	85.4469	60.5177	10.4000	0.0962	0.0014	-26.5205	72.8202	72.7834	133.3011
170	57	87.6242	51.9015	2.8571	0.3500	0.0184	-26.5205	72.8202	72.3324	124.2339
171	57	89.2158	46.5808	3.0222	0.3309	0.0164	-26.5205	72.8202	72.3842	118.9650
172	58	72.6766	27.8370	4.8571	9.2648	12.8894	0.2077	53.7123	56.3888	84.2257
173	58	72.5733	28.0685	6.2133	7.2425	7.8767	0.2077	53.7123	55.3479	83.4163
174	58	75.2346	28.0945	4.9750	9.0452	12.2858	0.2077	53.7123	56.2634	84.3579
175	59	86.0038	42.3715	6.2933	6.5149	6.3734	-0.1493	89.0845	88.1332	130.5047
176	59	81.5095	39.4274	3.4000	12.0588	21.8360	-0.1493	89.0845	85.8251	125.2526
177	59	90.3010	38.2011	4.2947	9.5467	13.6856	-0.1493	89.0845	87.0417	125.2428
178	60	81.2981	43.5144	14.6000	2.4658	0.9130	6.7738	68.4978	74.6822	118.1966
179	60	85.3782	41.9628	20.4000	1.7647	0.4676	6.7738	68.4978	71.6654	113.6283
180	60	91.9845	33.5227	12.0000	3.0000	1.3515	6.7738	68.4978	77.6524	111.1751
181	61	83.1579	42.4950	13.2000	3.3333	1.6685	-0.0762	62.2550	62.1278	104.6228
182	61	69.3012	42.7229	3.0667	14.3477	30.9119	-0.0762	62.2550	59.8983	102.6212
183	61	88.9884	42.7821	8.8800	4.9550	3.6867	-0.0762	62.2550	61.9739	104.7560
184	62	73.0972	38.1618	71.9250	0.6396	0.0614	-3.4707	82.2927	82.0795	120.2413
185	62	73.6987	36.9272	58.1250	0.7914	0.0940	-3.4707	82.2927	81.9663	118.8935
186	62	72.4474	34.9110	16.9500	2.7139	1.1060	-3.4707	82.2927	78.4542	113.3652
187	63	80.5926	41.1139	7.8000	4.8718	3.5640	-0.0365	71.6603	71.5301	112.6441
188	63	94.0975	42.3413	1.9000	20.0000	60.0652	-0.0365	71.6603	69.4670	111.8083
189	63	74.3230	41.0448	7.0933	5.3572	4.3096	-0.0365	71.6603	71.5029	112.5477

Table B42 Summary of blood pressure demodulation (continued)

Test no.	Volunteer no.	Mean HR (bpm)	Mean PP (mmHg)	PTT (ms)	PWV (m/s)	DBP coefficient	m_{DBP}	c_{DBP}	Demodulated DBP (mmHg)	Demodulated SBP (mmHg)
190	64	78.8717	47.2390	5.2000	8.0769	9.7961	-0.5842	83.0475	77.3243	124.5632
191	64	75.5746	47.4696	6.9750	6.0215	5.4447	-0.5842	83.0475	79.8665	127.3362
192	64	79.2492	46.2914	9.4353	4.4514	2.9754	-0.5842	83.0475	81.3092	127.6006
193	65	81.6020	49.9741	10.5600	3.5985	1.9445	0.5550	62.8437	63.9229	113.8970
194	65	81.7968	47.4056	21.7143	1.7500	0.4599	0.5550	62.8437	63.0990	110.5045
195	65	82.2649	46.6204	10.3000	3.6893	2.0439	0.5550	62.8437	63.9781	110.5985
196	66	73.2467	42.0327	19.5556	2.0966	0.6601	-0.2593	74.8520	74.6809	116.7136
197	66	74.5018	43.1667	22.7600	1.8014	0.4873	-0.2593	74.8520	74.7257	117.8923
198	66	79.3185	41.3007	9.2889	4.4139	2.9255	-0.2593	74.8520	74.0935	115.3941
199	67	66.4332	37.4524	10.2286	5.1815	4.0316	0.5205	71.1984	73.2969	110.7493
200	67	67.0358	37.2381	9.4857	5.5874	4.6879	0.5205	71.1984	73.6385	110.8766
201	67	69.0942	37.3095	12.6769	4.1808	2.6248	0.5205	71.1984	72.5646	109.8741
202	68	86.2369	29.1819	2.3059	20.8162	65.0676	0.0000	88.0000	88.0000	117.1819
203	68	91.0339	29.3556	2.9200	16.4384	40.5770	0.0000	88.0000	88.0000	117.3556
204	68	88.6446	29.4624	1.9600	24.4898	90.0603	0.0000	88.0000	88.0000	117.4624
205	69	75.3356	35.4123	14.8000	2.3649	0.8398	1.9176	83.6226	85.2330	120.6453
206	69	70.7174	33.9597	18.8000	1.8617	0.5205	1.9176	83.6226	84.6206	118.5803
207	69	77.0669	34.1280	121.6000	0.2878	0.0124	1.9176	83.6226	83.6464	117.7745
208	70	75.1787	34.1016	11.8400	2.8716	1.2383	-0.4371	66.7539	66.2126	100.3142
209	70	78.3747	36.0454	8.6588	3.9266	2.3153	-0.4371	66.7539	65.7418	101.7873
210	70	79.8385	36.8530	10.3500	3.2850	1.6205	-0.4371	66.7539	66.0456	102.8985
211	71	69.9987	56.2852	10.4000	3.6538	2.0048	2.6009	72.1193	77.3335	133.6187
212	71	71.5767	55.7876	9.6308	3.9457	2.3378	2.6009	72.1193	78.1997	133.9873
213	71	61.7761	56.9272	15.5000	2.4516	0.9025	2.6009	72.1193	74.4668	131.3940
214	72	60.8633	50.5165	25.5333	1.6057	0.3872	-2.4304	77.5832	76.6422	127.1587
215	72	57.9684	51.7198	8.7077	4.7085	3.3291	-2.4304	77.5832	69.4922	121.2120
216	72	58.8640	52.2637	9.9333	4.1275	2.5583	-2.4304	77.5832	71.3656	123.6293

Table B42 Summary of blood pressure demodulation (continued)

Test no.	Volunteer no.	Mean HR (bpm)	Mean PP (mmHg)	PTT (ms)	PWV (m/s)	DBP coefficient	m_{DBP}	c_{DBP}	Demodulated DBP (mmHg)	Demodulated SBP (mmHg)
217	73	56.6661	40.8124	20.6667	1.9355	0.5625	-3.3333	77.3245	75.4495	116.2618
218	73	63.9643	40.0360	15.3455	2.6066	1.0203	-3.3333	77.3245	73.9236	113.9597
219	73	63.9795	40.1516	10.2000	3.9216	2.3093	-3.3333	77.3245	69.6269	109.7785
220	74	66.2827	58.4334	2.4615	18.6878	52.4420	0.1122	63.4063	69.2907	127.7241
221	74	66.6114	59.6823	2.3692	19.4158	56.6077	0.1122	63.4063	69.7581	129.4404
222	74	70.7214	60.8843	3.1714	14.5046	31.5920	0.1122	63.4063	66.9512	127.8355
223	75	55.9009	35.8745	21.4909	2.0008	0.6012	0.2579	50.9926	51.1476	87.0222
224	75	60.1722	34.3884	28.6154	1.5027	0.3391	0.2579	50.9926	51.0800	85.4684
225	75	55.6776	34.7371	16.0000	2.6875	1.0846	0.2579	50.9926	51.2723	86.0094
226	76	77.9537	28.3375	13.8353	3.3248	1.6600	0.0266	70.4511	70.4953	98.8328
227	76	75.4931	29.4851	4.7750	9.6335	13.9358	0.0266	70.4511	70.8221	100.3072
228	76	78.8944	30.1774	6.0444	7.6104	8.6971	0.0266	70.4511	70.6826	100.8600
229	77	68.6452	45.0822	2.2800	20.1754	61.1236	0.0647	58.6723	62.6298	107.7121
230	77	68.3540	44.9958	2.4667	18.6484	52.2211	0.0647	58.6723	62.0534	107.0493
231	77	70.7678	45.4219	5.6500	8.1416	9.9536	0.0647	58.6723	59.3167	104.7387
232	78	82.3604	32.5982	2.4667	15.8106	37.5370	0.0165	59.7732	60.3913	92.9896
233	78	83.2819	33.7976	7.7647	5.0227	3.7883	0.0165	59.7732	59.8355	93.6331
234	78	71.2240	34.6042	2.7429	14.2185	30.3579	0.0165	59.7732	60.2731	94.8773
235	79	65.3585	28.2771	60.1538	0.5652	0.0565	-43.3611	61.5374	59.0882	87.3653
236	79	65.7612	27.8222	78.1333	0.4352	0.0335	-43.3611	61.5374	60.0857	87.9079
237	79	65.6399	28.4008	57.1714	0.5947	0.0625	-43.3611	61.5374	58.8261	87.2268
238	80	65.1934	40.5705	46.5231	0.8813	0.1166	-591.1134	150.2035	81.2646	121.8351
239	80	69.3711	40.1282	46.6286	0.8793	0.1161	-591.1134	150.2035	81.5762	121.7044
240	80	71.4432	40.3013	45.8286	0.8946	0.1202	-591.1134	150.2035	79.1593	119.4606
241	81	90.9904	54.3266	6.8211	5.8642	5.1639	2.6387	66.7112	80.3370	134.6637
242	81	87.4370	53.6924	7.2000	5.5556	4.6347	2.6387	66.7112	78.9407	132.6330
243	81	88.9998	53.4810	6.8500	5.8394	5.1204	2.6387	66.7112	80.2223	133.7033

Table B42 Summary of blood pressure demodulation (continued)

Test no.	Volunteer no.	Mean HR (bpm)	Mean PP (mmHg)	PTT (ms)	PWV (m/s)	DBP coefficient	m_{DBP}	c_{DBP}	Demodulated DBP (mmHg)	Demodulated SBP (mmHg)
244	82	108.2095	33.8683	4.6833	7.9004	9.3727	2.0223	65.6700	84.6242	118.4925
245	82	102.6496	34.4976	4.5391	8.1514	9.9776	2.0223	65.6700	85.8476	120.3452
246	82	107.4980	34.6341	5.8000	6.3793	6.1110	2.0223	65.6700	78.0282	112.6623
247	83	88.1822	32.0307	7.3000	5.0685	3.8576	1.2139	62.6959	67.3785	99.4093
248	83	96.2626	32.8561	8.4000	4.4048	2.9135	1.2139	62.6959	66.2324	99.0885
249	83	88.0243	32.6132	8.2200	4.5012	3.0424	1.2139	62.6959	66.3890	99.0022
250	84	78.8467	36.2318	2.2750	17.1429	51.9571	-0.0951	64.8390	59.8969	96.1287
251	84	73.3908	35.8106	2.9000	13.4483	31.9751	-0.0951	64.8390	61.7975	97.6082
252	84	72.9885	35.4575	3.5467	10.9961	21.3776	-0.0951	64.8390	62.8056	98.2631
253	85	70.1968	66.9455	2.8267	15.5659	42.8375	0.1284	79.8161	85.3154	152.2610
254	85	72.4731	64.9076	4.7250	9.3122	15.3313	0.1284	79.8161	81.7843	146.6919
255	85	72.0958	65.6469	5.2667	8.3544	12.3398	0.1284	79.8161	81.4003	147.0472

Table B43 Blood pressure error analysis

Test no.	Volunteer no.	SBP (mmHg)				DBP (mmHg)				PP (mmHg)				HR (bpm)			
		χ_m	χ_t	AE	AE%	χ_m	χ_t	AE	AE%	χ_m	χ_t	AE	AE%	χ_m	χ_t	AE	AE%
1	1	154.34	154.00	0.34	0.22	104.63	104.00	0.63	0.60	49.72	50.00	0.28	0.56	77.08	78.50	1.42	1.80
2	1	149.19	147.00	2.19	1.49	100.29	97.50	2.79	2.86	48.89	49.50	0.61	1.22	79.92	75.50	4.42	5.86
3	1	149.97	152.50	2.53	1.66	101.08	104.50	3.42	3.27	48.89	48.00	0.89	1.85	78.11	81.00	2.89	3.57
4	2	113.46	114.00	0.54	0.47	77.01	77.50	0.49	0.63	36.45	36.50	0.05	0.14	85.35	86.50	1.15	1.33
5	2	113.82	113.00	0.82	0.72	77.27	76.50	0.77	1.01	36.54	36.50	0.04	0.11	89.85	84.00	5.85	6.97
6	2	113.72	114.00	0.28	0.25	77.71	78.00	0.29	0.37	36.01	36.00	0.01	0.03	84.01	84.00	0.01	0.01
7	3	100.75	103.50	2.75	2.66	63.30	63.50	0.20	0.32	37.45	40.00	2.55	6.38	64.68	68.50	3.82	5.58
8	3	99.22	97.00	2.22	2.29	63.33	63.00	0.33	0.52	35.89	34.00	1.89	5.57	65.95	74.50	8.55	11.47
9	3	94.03	93.50	0.53	0.57	63.37	63.50	0.13	0.20	30.66	30.00	0.66	2.20	68.70	72.00	3.30	4.58
10	4	131.28	128.50	2.78	2.16	93.90	91.50	2.40	2.63	37.37	37.00	0.37	1.01	56.11	64.50	8.39	13.01
11	4	129.53	130.50	0.97	0.75	93.98	96.50	2.52	2.61	35.55	34.00	1.55	4.55	54.66	64.00	9.34	14.59
12	4	135.70	137.50	1.80	1.31	95.62	95.50	0.12	0.12	40.08	42.00	1.92	4.57	61.79	62.50	0.71	1.13
13	5	114.21	115.00	0.79	0.68	66.82	67.50	0.68	1.01	47.39	47.50	0.11	0.22	76.67	83.00	6.33	7.63
14	5	110.39	110.50	0.11	0.10	63.05	64.00	0.95	1.48	47.33	46.50	0.83	1.79	85.95	82.00	3.95	4.82
15	5	115.40	114.50	0.90	0.79	64.63	63.00	1.63	2.58	50.77	51.50	0.73	1.41	75.68	84.00	8.32	9.90
16	6	113.96	113.00	0.96	0.85	74.71	74.50	0.21	0.28	39.26	38.50	0.76	1.97	72.19	65.00	7.19	11.06
17	6	115.78	115.00	0.78	0.68	77.47	77.50	0.03	0.03	38.31	37.50	0.81	2.15	74.25	68.00	6.25	9.19
18	6	113.25	115.00	1.75	1.52	74.32	74.50	0.18	0.24	38.94	40.50	1.57	3.86	80.33	66.50	13.83	20.80
19	7	105.81	106.50	0.69	0.64	65.00	65.00	0.00	0.01	40.82	41.50	0.68	1.65	58.66	62.50	3.84	6.14
20	7	104.47	104.50	0.03	0.03	64.75	65.00	0.25	0.38	39.72	39.50	0.22	0.56	63.97	63.00	0.97	1.54
21	7	103.71	103.00	0.71	0.69	64.75	64.50	0.25	0.39	38.96	38.50	0.46	1.19	61.21	62.50	1.29	2.06
22	8	97.94	95.00	2.94	3.09	69.52	69.50	0.02	0.03	28.42	25.50	2.92	11.46	73.14	70.50	2.64	3.75
23	8	95.45	97.50	2.05	2.10	67.61	67.50	0.11	0.17	27.84	30.00	2.16	7.21	76.03	70.50	5.53	7.84
24	8	98.11	99.00	0.89	0.90	67.87	68.00	0.13	0.19	30.24	31.00	0.76	2.45	75.40	72.00	3.40	4.72

Table B43 Blood pressure error analysis (continued)

Test no.	Volunteer no.	SBP (mmHg)				DBP (mmHg)				PP (mmHg)				HR (bpm)			
		χ_m	χ_t	AE	AE%	χ_m	χ_t	AE	AE%	χ_m	χ_t	AE	AE%	χ_m	χ_t	AE	AE%
1	1	154.34	154.00	0.34	0.22	104.63	104.00	0.63	0.60	49.72	50.00	0.28	0.56	77.08	78.50	1.42	1.80
2	1	149.19	147.00	2.19	1.49	100.29	97.50	2.79	2.86	48.89	49.50	0.61	1.22	79.92	75.50	4.42	5.86
3	1	149.97	152.50	2.53	1.66	101.08	104.50	3.42	3.27	48.89	48.00	0.89	1.85	78.11	81.00	2.89	3.57
4	2	113.46	114.00	0.54	0.47	77.01	77.50	0.49	0.63	36.45	36.50	0.05	0.14	85.35	86.50	1.15	1.33
5	2	113.82	113.00	0.82	0.72	77.27	76.50	0.77	1.01	36.54	36.50	0.04	0.11	89.85	84.00	5.85	6.97
6	2	113.72	114.00	0.28	0.25	77.71	78.00	0.29	0.37	36.01	36.00	0.01	0.03	84.01	84.00	0.01	0.01
7	3	100.75	103.50	2.75	2.66	63.30	63.50	0.20	0.32	37.45	40.00	2.55	6.38	64.68	68.50	3.82	5.58
8	3	99.22	97.00	2.22	2.29	63.33	63.00	0.33	0.52	35.89	34.00	1.89	5.57	65.95	74.50	8.55	11.47
9	3	94.03	93.50	0.53	0.57	63.37	63.50	0.13	0.20	30.66	30.00	0.66	2.20	68.70	72.00	3.30	4.58
10	4	131.28	128.50	2.78	2.16	93.90	91.50	2.40	2.63	37.37	37.00	0.37	1.01	56.11	64.50	8.39	13.01
11	4	129.53	130.50	0.97	0.75	93.98	96.50	2.52	2.61	35.55	34.00	1.55	4.55	54.66	64.00	9.34	14.59
12	4	135.70	137.50	1.80	1.31	95.62	95.50	0.12	0.12	40.08	42.00	1.92	4.57	61.79	62.50	0.71	1.13
13	5	114.21	115.00	0.79	0.68	66.82	67.50	0.68	1.01	47.39	47.50	0.11	0.22	76.67	83.00	6.33	7.63
14	5	110.39	110.50	0.11	0.10	63.05	64.00	0.95	1.48	47.33	46.50	0.83	1.79	85.95	82.00	3.95	4.82
15	5	115.40	114.50	0.90	0.79	64.63	63.00	1.63	2.58	50.77	51.50	0.73	1.41	75.68	84.00	8.32	9.90
16	6	113.96	113.00	0.96	0.85	74.71	74.50	0.21	0.28	39.26	38.50	0.76	1.97	72.19	65.00	7.19	11.06
17	6	115.78	115.00	0.78	0.68	77.47	77.50	0.03	0.03	38.31	37.50	0.81	2.15	74.25	68.00	6.25	9.19
18	6	113.25	115.00	1.75	1.52	74.32	74.50	0.18	0.24	38.94	40.50	1.57	3.86	80.33	66.50	13.83	20.80
19	7	105.81	106.50	0.69	0.64	65.00	65.00	0.00	0.01	40.82	41.50	0.68	1.65	58.66	62.50	3.84	6.14
20	7	104.47	104.50	0.03	0.03	64.75	65.00	0.25	0.38	39.72	39.50	0.22	0.56	63.97	63.00	0.97	1.54
21	7	103.71	103.00	0.71	0.69	64.75	64.50	0.25	0.39	38.96	38.50	0.46	1.19	61.21	62.50	1.29	2.06
22	8	97.94	95.00	2.94	3.09	69.52	69.50	0.02	0.03	28.42	25.50	2.92	11.46	73.14	70.50	2.64	3.75
23	8	95.45	97.50	2.05	2.10	67.61	67.50	0.11	0.17	27.84	30.00	2.16	7.21	76.03	70.50	5.53	7.84
24	8	98.11	99.00	0.89	0.90	67.87	68.00	0.13	0.19	30.24	31.00	0.76	2.45	75.40	72.00	3.40	4.72

Table B43 Blood pressure error analysis (continued)

Test no.	Volunteer no.	SBP (mmHg)				DBP (mmHg)				PP (mmHg)				HR (bpm)			
		χ_m	χ_t	AE	AE%	χ_m	χ_t	AE	AE%	χ_m	χ_t	AE	AE%	χ_m	χ_t	AE	AE%
25	9	110.20	112.00	1.80	1.61	72.27	74.00	1.73	2.34	37.93	38.00	0.07	0.19	80.91	82.00	1.09	1.33
26	9	109.21	109.50	0.29	0.26	74.42	75.00	0.58	0.77	34.79	34.50	0.29	0.83	84.08	83.50	0.58	0.70
27	9	108.59	106.50	2.09	1.97	72.81	70.50	2.31	3.27	35.79	36.00	0.21	0.60	88.27	83.50	4.77	5.71
28	10	109.49	109.00	0.49	0.45	76.52	77.50	0.98	1.26	32.97	31.50	1.47	4.66	71.90	82.00	10.10	12.32
29	10	109.80	108.50	1.30	1.19	75.23	74.00	1.23	1.66	34.57	34.50	0.07	0.19	76.19	79.00	2.81	3.56
30	10	106.21	108.00	1.79	1.66	70.25	70.50	0.25	0.36	35.96	37.50	1.54	4.09	82.43	75.50	6.93	9.18
31	11	102.33	101.00	1.33	1.31	65.00	65.00	0.00	0.00	37.33	36.00	1.33	3.69	58.87	57.50	1.37	2.38
32	11	100.71	101.00	0.29	0.29	63.00	63.50	0.50	0.79	37.71	37.50	0.21	0.56	59.01	56.00	3.01	5.37
33	11	100.87	100.50	0.37	0.37	63.00	62.50	0.50	0.80	37.87	38.00	0.13	0.35	58.76	56.50	2.26	4.00
34	12	108.91	111.00	2.09	1.88	62.56	63.50	0.94	1.48	46.35	47.50	1.15	2.42	54.76	49.50	5.26	10.63
35	12	108.43	107.50	0.93	0.86	62.51	61.50	1.01	1.65	45.91	46.00	0.09	0.19	54.52	50.00	4.52	9.03
36	12	108.16	107.00	1.16	1.09	61.93	62.00	0.07	0.12	46.23	45.00	1.23	2.74	50.42	52.00	1.58	3.03
37	13	109.49	111.00	1.51	1.36	69.95	71.50	1.55	2.17	39.54	39.50	0.04	0.09	87.05	88.00	0.95	1.08
38	13	110.18	108.50	1.68	1.55	70.02	68.50	1.52	2.21	40.16	40.00	0.16	0.40	93.21	87.00	6.21	7.14
39	13	107.84	108.00	0.16	0.15	67.04	67.00	0.04	0.05	40.80	41.00	0.20	0.48	88.08	89.00	0.92	1.03
40	14	112.59	113.00	0.41	0.37	77.17	77.50	0.33	0.43	35.42	35.50	0.08	0.23	74.66	77.50	2.84	3.66
41	14	112.06	111.50	0.56	0.50	76.92	76.50	0.42	0.54	35.14	35.00	0.14	0.40	80.07	77.00	3.07	3.98
42	14	111.36	111.50	0.14	0.13	75.92	76.00	0.08	0.11	35.44	35.50	0.06	0.17	74.04	77.50	3.46	4.47
43	15	109.08	106.50	2.58	2.42	76.30	76.50	0.20	0.26	32.77	30.00	2.77	9.24	65.67	67.50	1.83	2.70
44	15	104.42	105.50	1.08	1.02	72.65	72.00	0.65	0.90	31.77	33.50	1.73	5.15	69.19	72.00	2.81	3.91
45	15	105.50	107.00	1.50	1.40	71.05	71.50	0.45	0.63	34.45	35.50	1.05	2.95	75.47	76.00	0.53	0.70
46	16	112.25	114.50	2.25	1.97	69.84	69.50	0.34	0.50	42.40	45.00	2.60	5.77	77.61	72.00	5.61	7.79
47	16	109.18	109.00	0.18	0.16	68.96	70.50	1.54	2.19	40.22	38.50	1.72	4.47	73.19	71.00	2.19	3.08
48	16	109.58	107.50	2.08	1.93	68.70	67.50	1.20	1.78	40.88	40.00	0.88	2.19	75.24	75.00	0.24	0.32

Table B43 Blood pressure error analysis (continued)

Test no.	Volunteer no.	SBP (mmHg)				DBP (mmHg)				PP (mmHg)				HR (bpm)			
		χ_m	χ_t	AE	AE%	χ_m	χ_t	AE	AE%	χ_m	χ_t	AE	AE%	χ_m	χ_t	AE	AE%
49	17	106.23	109.00	2.77	2.54	56.02	58.50	2.48	4.23	50.20	50.50	0.30	0.59	53.23	52.00	1.23	2.37
50	17	104.40	105.00	0.60	0.57	52.88	52.50	0.38	0.73	51.52	52.50	0.98	1.87	62.11	52.50	9.61	18.31
51	17	104.37	101.00	3.37	3.34	56.60	54.50	2.10	3.84	47.78	46.50	1.28	2.74	57.96	62.00	4.04	6.52
52	18	115.25	116.50	1.25	1.08	82.86	84.00	1.14	1.36	32.38	32.50	0.12	0.36	70.21	70.50	0.29	0.42
53	18	114.56	115.50	0.94	0.82	82.11	83.00	0.89	1.07	32.45	32.50	0.05	0.16	70.05	68.50	1.55	2.27
54	18	114.70	112.50	2.20	1.95	82.53	80.50	2.03	2.52	32.17	32.00	0.17	0.52	72.07	67.50	4.57	6.77
55	19	88.73	89.00	0.27	0.30	62.72	63.50	0.78	1.23	26.01	25.50	0.51	2.01	62.14	63.50	1.36	2.14
56	19	88.42	90.00	1.58	1.75	61.52	62.00	0.48	0.77	26.90	28.00	1.10	3.92	63.58	64.00	0.42	0.65
57	19	89.85	88.00	1.85	2.10	62.26	61.00	1.26	2.07	27.59	27.00	0.59	2.17	62.70	64.00	1.30	2.04
58	20	114.46	115.50	1.04	0.90	83.37	84.00	0.63	0.75	31.09	31.50	0.41	1.30	108.65	107.00	1.65	1.54
59	20	112.28	113.00	0.72	0.63	81.32	82.00	0.68	0.83	30.96	31.00	0.04	0.13	101.09	104.00	2.91	2.80
60	20	113.26	111.50	1.76	1.58	82.31	81.00	1.31	1.62	30.95	30.50	0.45	1.47	102.59	105.00	2.41	2.29
61	21	109.99	110.50	0.51	0.46	69.77	69.00	0.77	1.12	40.22	41.50	1.28	3.09	65.31	68.50	3.19	4.65
62	21	109.75	109.50	0.25	0.23	69.84	70.50	0.66	0.94	39.92	39.00	0.92	2.35	68.46	69.50	1.04	1.49
63	21	110.26	110.00	0.26	0.24	69.39	69.50	0.11	0.16	40.87	40.50	0.37	0.91	75.20	69.00	6.20	8.99
64	22	107.07	106.00	1.07	1.01	70.78	70.50	0.28	0.39	36.29	35.50	0.79	2.23	64.22	67.50	3.28	4.86
65	22	109.77	110.50	0.73	0.66	70.68	71.00	0.32	0.45	39.08	39.50	0.42	1.06	68.39	66.00	2.39	3.62
66	22	109.67	110.00	0.33	0.30	70.04	70.00	0.04	0.06	39.62	40.00	0.38	0.94	68.63	69.00	0.37	0.53
67	23	98.90	100.50	1.60	1.59	67.32	67.50	0.18	0.27	31.58	33.00	1.42	4.29	69.29	67.00	2.29	3.42
68	23	95.99	95.00	0.99	1.04	64.33	64.50	0.17	0.27	31.66	30.50	1.16	3.80	69.64	67.00	2.64	3.94
69	23	94.61	94.00	0.61	0.65	65.86	65.50	0.36	0.54	28.76	28.50	0.26	0.90	80.89	70.50	10.39	14.74
70	24	101.59	101.00	0.59	0.59	72.58	72.00	0.58	0.81	29.01	29.00	0.01	0.03	95.73	83.50	12.23	14.65
71	24	100.02	100.00	0.02	0.02	73.64	73.50	0.14	0.19	26.38	26.50	0.12	0.46	86.20	87.50	1.30	1.49
72	24	98.89	99.50	0.61	0.61	72.78	73.50	0.72	0.98	26.11	26.00	0.11	0.43	99.67	92.00	7.67	8.33

Table B43 Blood pressure error analysis (continued)

Test no.	Volunteer no.	SBP (mmHg)				DBP (mmHg)				PP (mmHg)				HR (bpm)			
		χ_m	χ_t	AE	AE%	χ_m	χ_t	AE	AE%	χ_m	χ_t	AE	AE%	χ_m	χ_t	AE	AE%
73	25	119.63	123.00	3.37	2.74	76.37	79.00	2.63	3.33	43.26	44.00	0.74	1.69	59.40	64.00	4.60	7.19
74	25	118.01	118.50	0.49	0.41	77.81	79.00	1.19	1.50	40.20	39.50	0.70	1.78	56.30	63.00	6.70	10.64
75	25	120.86	117.00	3.86	3.30	76.82	73.00	3.82	5.23	44.04	44.00	0.04	0.09	62.62	60.50	2.12	3.51
76	26	128.14	128.50	0.36	0.28	84.83	84.50	0.33	0.39	43.31	44.00	0.69	1.56	77.34	74.00	3.34	4.51
77	26	122.44	123.50	1.06	0.86	79.22	81.00	1.78	2.20	43.23	42.50	0.73	1.71	73.25	74.00	0.75	1.02
78	26	122.92	121.50	1.42	1.17	77.96	76.50	1.46	1.90	44.96	45.00	0.04	0.09	74.44	73.50	0.94	1.27
79	27	120.45	120.50	0.05	0.04	65.17	65.00	0.17	0.26	55.28	55.50	0.22	0.39	75.20	73.50	1.70	2.31
80	27	119.96	120.00	0.04	0.03	66.30	66.50	0.20	0.30	53.66	53.50	0.16	0.30	70.46	71.50	1.04	1.46
81	27	123.59	123.50	0.09	0.07	72.53	72.50	0.03	0.04	51.06	51.00	0.06	0.11	63.35	72.00	8.65	12.01
82	28	108.91	108.50	0.41	0.38	64.96	65.50	0.54	0.82	43.95	43.00	0.95	2.21	64.74	65.00	0.26	0.41
83	28	106.52	108.00	1.48	1.37	62.16	62.50	0.34	0.54	44.36	45.50	1.14	2.51	67.69	66.50	1.19	1.79
84	28	108.07	107.00	1.07	1.00	63.88	63.00	0.88	1.39	44.19	44.00	0.19	0.43	72.39	68.00	4.39	6.46
85	29	101.58	101.00	0.58	0.58	59.82	58.50	1.32	2.26	41.76	42.50	0.74	1.75	80.93	80.50	0.43	0.53
86	29	98.92	99.50	0.58	0.58	59.32	60.00	0.68	1.13	39.60	39.50	0.10	0.26	80.68	81.50	0.82	1.00
87	29	99.99	100.00	0.01	0.01	60.36	61.00	0.65	1.06	39.64	39.00	0.64	1.64	90.37	82.00	8.37	10.21
88	30	105.44	107.50	2.06	1.92	73.43	74.50	1.07	1.44	32.01	33.00	0.99	2.99	62.01	57.50	4.51	7.85
89	30	105.94	105.00	0.94	0.90	74.47	74.00	0.47	0.64	31.47	31.00	0.47	1.51	57.94	60.50	2.56	4.24
90	30	104.62	103.50	1.12	1.08	72.60	72.00	0.60	0.83	32.02	31.50	0.52	1.64	63.76	61.50	2.26	3.67
91	31	118.75	119.50	0.75	0.63	66.19	67.50	1.31	1.94	52.56	52.00	0.56	1.08	74.54	74.50	0.04	0.05
92	31	119.41	118.50	0.91	0.77	66.30	65.50	0.80	1.22	53.11	53.00	0.11	0.20	75.31	77.00	1.69	2.19
93	31	119.84	120.00	0.16	0.13	66.01	65.50	0.51	0.78	53.83	54.50	0.67	1.23	77.15	80.00	2.85	3.57
94	32	135.88	134.00	1.88	1.41	81.07	81.00	0.07	0.08	54.82	53.00	1.82	3.43	93.53	94.00	0.47	0.50
95	32	129.33	133.00	3.67	2.76	75.77	79.00	3.23	4.09	53.56	54.00	0.44	0.82	102.65	96.50	6.15	6.38
96	32	132.29	130.50	1.79	1.37	75.66	72.50	3.16	4.36	56.63	58.00	1.37	2.37	89.32	94.50	5.18	5.48

Table B43 Blood pressure error analysis (continued)

Test no.	Volunteer no.	SBP (mmHg)				DBP (mmHg)				PP (mmHg)				HR (bpm)			
		χ_m	χ_t	AE	AE%	χ_m	χ_t	AE	AE%	χ_m	χ_t	AE	AE%	χ_m	χ_t	AE	AE%
97	33	114.59	114.50	0.09	0.08	72.21	73.00	0.79	1.09	42.39	41.50	0.89	2.14	78.10	76.50	1.60	2.09
98	33	114.50	113.50	1.00	0.88	70.38	69.00	1.38	2.00	44.12	44.50	0.38	0.85	75.28	76.50	1.22	1.59
99	33	111.40	112.50	1.10	0.97	67.91	68.50	0.59	0.86	43.49	44.00	0.51	1.16	77.41	77.50	0.09	0.12
100	34	111.71	112.50	0.79	0.70	80.01	81.00	0.99	1.22	31.71	31.50	0.21	0.65	93.72	99.50	5.78	5.81
101	34	108.16	107.50	0.66	0.61	78.17	80.00	1.83	2.28	29.99	27.50	2.49	9.05	100.74	100.00	0.74	0.74
102	34	111.62	111.50	0.12	0.11	78.82	76.00	2.82	3.71	32.81	35.50	2.69	7.59	94.02	94.50	0.48	0.51
103	35	108.16	110.00	1.84	1.67	65.54	67.50	1.96	2.90	42.62	42.50	0.12	0.28	74.14	74.00	0.14	0.19
104	35	108.19	106.50	1.69	1.58	65.75	64.00	1.75	2.74	42.43	42.50	0.07	0.16	68.95	73.50	4.55	6.19
105	35	106.66	106.50	0.16	0.15	63.71	63.50	0.21	0.32	42.95	43.00	0.05	0.12	76.26	74.50	1.76	2.36
106	36	93.21	95.00	1.79	1.88	62.49	62.50	0.01	0.01	30.72	32.50	1.78	5.48	68.93	65.00	3.93	6.05
107	36	94.63	94.00	0.63	0.67	64.99	65.00	0.01	0.02	29.65	29.00	0.65	2.23	67.60	65.50	2.10	3.20
108	36	92.66	91.50	1.16	1.26	64.02	64.00	0.02	0.03	28.63	27.50	1.13	4.12	61.93	70.00	8.07	11.53
109	37	107.23	108.00	0.77	0.71	68.52	68.50	0.02	0.03	38.71	39.50	0.79	1.99	84.76	81.50	3.26	4.00
110	37	103.49	102.50	0.99	0.96	67.18	67.00	0.18	0.26	36.31	35.50	0.81	2.28	79.35	77.50	1.85	2.38
111	37	103.28	103.50	0.22	0.21	67.30	67.50	0.20	0.29	35.98	36.00	0.02	0.07	75.68	80.00	4.32	5.40
112	38	128.87	130.50	1.63	1.25	74.92	75.00	0.08	0.11	53.95	55.50	1.55	2.80	72.20	72.00	0.20	0.27
113	38	126.81	125.50	1.31	1.04	75.15	75.00	0.14	0.19	51.66	50.50	1.16	2.30	67.44	70.50	3.06	4.34
114	38	124.83	124.50	0.33	0.26	75.44	75.50	0.06	0.08	49.39	49.00	0.39	0.80	73.34	72.00	1.34	1.86
115	39	128.13	130.00	1.87	1.44	62.75	64.50	1.75	2.71	65.38	65.50	0.12	0.18	70.64	65.00	5.64	8.68
116	39	124.87	126.00	1.13	0.90	64.52	64.50	0.02	0.03	60.35	61.50	1.15	1.86	64.23	63.50	0.73	1.15
117	39	123.50	120.50	3.00	2.49	62.73	61.00	1.73	2.84	60.77	59.50	1.27	2.13	55.39	62.50	7.11	11.38
118	40	128.60	129.50	0.90	0.69	76.58	77.50	0.92	1.19	52.03	52.00	0.03	0.05	93.14	91.00	2.14	2.36
119	40	124.72	126.50	1.78	1.40	74.09	74.00	0.09	0.12	50.64	52.50	1.86	3.55	90.57	88.50	2.07	2.34
120	40	124.17	121.50	2.67	2.20	76.84	76.00	0.84	1.10	47.34	45.50	1.84	4.04	85.38	88.00	2.62	2.98

Table B43 Blood pressure error analysis (continued)

Test no.	Volunteer no.	SBP (mmHg)				DBP (mmHg)				PP (mmHg)				HR (bpm)			
		χ_m	χ_t	AE	AE%	χ_m	χ_t	AE	AE%	χ_m	χ_t	AE	AE%	χ_m	χ_t	AE	AE%
121	41	90.87	91.00	0.13	0.14	66.51	67.00	0.49	0.73	24.36	24.00	0.36	1.50	78.01	79.50	1.49	1.87
122	41	91.48	91.50	0.02	0.02	65.99	66.00	0.01	0.02	25.49	25.50	0.01	0.03	79.26	78.00	1.26	1.62
123	41	92.15	92.00	0.15	0.16	66.50	66.00	0.50	0.76	25.65	26.00	0.35	1.36	80.22	80.00	0.22	0.27
124	42	126.25	126.00	0.25	0.20	74.98	75.00	0.02	0.03	51.27	51.00	0.27	0.54	65.57	66.00	0.43	0.66
125	42	117.27	118.50	1.23	1.03	66.91	67.00	0.09	0.14	50.36	51.50	1.14	2.21	67.20	63.50	3.70	5.83
126	42	117.98	117.00	0.98	0.83	68.61	68.50	0.11	0.17	49.36	48.50	0.86	1.78	66.61	67.50	0.89	1.33
127	43	125.82	127.00	1.18	0.93	72.34	73.00	0.66	0.91	53.48	54.00	0.52	0.96	86.79	84.50	2.29	2.71
128	43	125.48	124.50	0.98	0.78	71.83	71.00	0.83	1.17	53.65	53.50	0.15	0.27	81.13	87.00	5.87	6.74
129	43	123.20	123.00	0.20	0.17	69.83	70.00	0.17	0.24	53.37	53.00	0.37	0.70	85.69	87.50	1.81	2.07
130	44	106.19	105.00	1.19	1.14	74.02	74.00	0.02	0.03	32.17	31.00	1.17	3.78	85.24	77.00	8.24	10.70
131	44	101.69	101.00	0.69	0.68	64.92	65.50	0.58	0.88	36.76	35.50	1.26	3.56	77.02	75.00	2.02	2.70
132	44	99.12	101.00	1.88	1.86	64.56	64.00	0.56	0.87	34.56	37.00	2.44	6.58	79.51	75.00	4.51	6.01
133	45	95.50	94.50	1.00	1.06	69.27	69.00	0.27	0.38	26.24	25.50	0.74	2.90	75.01	75.50	0.49	0.64
134	45	95.02	95.00	0.02	0.02	68.01	68.00	0.01	0.01	27.01	27.00	0.01	0.03	74.36	76.50	2.14	2.80
135	45	96.98	98.00	1.02	1.04	69.23	69.50	0.27	0.39	27.75	28.50	0.75	2.62	74.53	74.00	0.53	0.72
136	46	103.25	103.50	0.25	0.25	72.27	72.50	0.23	0.31	30.97	31.00	0.03	0.09	98.82	98.50	0.32	0.33
137	46	102.67	103.00	0.33	0.32	72.42	72.50	0.08	0.11	30.25	30.50	0.25	0.81	100.07	101.00	0.93	0.92
138	46	102.59	102.00	0.59	0.57	72.31	72.00	0.31	0.43	30.27	30.00	0.27	0.92	88.30	102.00	13.70	13.43
139	47	109.74	110.50	0.76	0.69	73.31	73.50	0.19	0.26	36.43	37.00	0.57	1.55	75.53	78.00	2.47	3.17
140	47	108.80	107.50	1.30	1.21	72.55	72.00	0.55	0.76	36.25	35.50	0.75	2.12	76.98	77.00	0.02	0.03
141	47	107.96	108.50	0.54	0.50	72.14	72.50	0.36	0.49	35.82	36.00	0.18	0.50	77.43	80.00	2.57	3.21
142	48	103.52	103.50	0.02	0.02	68.15	68.00	0.15	0.21	35.37	35.50	0.13	0.36	86.04	78.00	8.04	10.30
143	48	104.15	104.50	0.36	0.34	68.83	69.50	0.67	0.96	35.31	35.00	0.31	0.89	80.94	83.00	2.06	2.49
144	48	104.34	104.00	0.34	0.32	69.02	68.50	0.52	0.76	35.32	35.50	0.18	0.52	86.49	85.50	0.99	1.16

Table B43 Blood pressure error analysis (continued)

Test no.	Volunteer no.	SBP (mmHg)				DBP (mmHg)				PP (mmHg)				HR (bpm)			
		χ_m	χ_t	AE	AE%	χ_m	χ_t	AE	AE%	χ_m	χ_t	AE	AE%	χ_m	χ_t	AE	AE%
145	49	126.55	129.00	2.45	1.90	87.38	90.00	2.62	2.91	39.17	39.00	0.17	0.43	89.39	91.00	1.61	1.77
146	49	127.72	126.00	1.72	1.37	88.40	86.50	1.90	2.19	39.33	39.50	0.17	0.43	96.63	91.00	5.63	6.18
147	49	126.73	126.00	0.73	0.58	84.72	84.00	0.72	0.86	42.01	42.00	0.01	0.01	96.92	91.00	5.92	6.50
148	50	101.09	102.50	1.41	1.38	67.15	67.50	0.35	0.51	33.93	35.00	1.07	3.05	67.03	67.00	0.03	0.05
149	50	97.92	97.00	0.92	0.95	65.13	64.50	0.63	0.98	32.78	32.50	0.28	0.87	64.56	66.00	1.44	2.18
150	50	95.00	94.50	0.50	0.52	62.71	63.00	0.29	0.46	32.28	31.50	0.78	2.49	66.70	67.00	0.30	0.45
151	51	104.33	106.00	1.67	1.57	74.18	76.00	1.82	2.40	30.15	30.00	0.15	0.52	87.27	79.50	7.77	9.77
152	51	103.71	103.50	0.21	0.20	71.95	73.00	1.05	1.43	31.75	30.50	1.25	4.10	85.05	81.50	3.55	4.35
153	51	107.96	106.50	1.46	1.37	73.37	70.50	2.87	4.07	34.59	36.00	1.41	3.91	82.15	85.50	3.35	3.92
154	52	100.16	100.50	0.34	0.34	71.89	72.00	0.11	0.16	28.27	28.50	0.23	0.81	83.67	79.00	4.67	5.91
155	52	99.87	100.00	0.13	0.13	68.16	69.50	1.34	1.92	31.71	30.50	1.21	3.97	84.67	78.50	6.17	7.86
156	52	100.97	100.50	0.47	0.47	68.45	67.00	1.45	2.16	32.52	33.50	0.98	2.93	80.40	76.50	3.90	5.10
157	53	103.86	105.50	1.64	1.56	74.36	76.50	2.14	2.80	29.50	29.00	0.50	1.71	65.20	65.00	0.20	0.30
158	53	107.84	109.50	1.66	1.51	73.88	74.50	0.62	0.83	33.96	35.00	1.04	2.97	67.65	68.00	0.35	0.51
159	53	111.30	108.00	3.30	3.05	74.25	71.50	2.75	3.85	37.04	36.50	0.54	1.49	68.73	71.00	2.27	3.19
160	54	111.66	113.00	1.34	1.18	67.67	70.00	2.33	3.33	43.99	43.00	0.99	2.30	117.33	121.00	3.67	3.03
161	54	112.87	113.00	0.13	0.12	68.87	68.00	0.87	1.28	44.00	45.00	1.00	2.22	114.54	120.00	5.46	4.55
162	54	111.97	110.50	1.47	1.33	66.96	65.50	1.46	2.23	45.01	45.00	0.01	0.02	124.07	118.00	6.07	5.14
163	55	119.07	121.00	1.93	1.60	76.82	79.00	2.18	2.75	42.24	42.00	0.24	0.58	71.76	77.00	5.24	6.81
164	55	116.16	118.00	1.84	1.56	76.00	76.50	0.50	0.65	40.16	41.50	1.34	3.24	78.27	81.00	2.73	3.37
165	55	116.27	112.50	3.77	3.35	76.67	74.00	2.67	3.61	39.60	38.50	1.10	2.86	74.88	78.50	3.62	4.62
166	56	87.14	87.50	0.36	0.41	63.03	63.00	0.03	0.05	24.12	24.50	0.38	1.57	76.45	78.00	1.55	1.99
167	56	85.09	85.50	0.41	0.48	60.27	61.50	1.23	2.00	24.82	24.00	0.82	3.43	77.79	79.50	1.71	2.16
168	56	85.76	85.00	0.76	0.90	60.20	59.00	1.20	2.04	25.56	26.00	0.44	1.69	78.00	84.00	6.00	7.14

Table B43 Blood pressure error analysis (continued)

Test no.	Volunteer no.	SBP (mmHg)				DBP (mmHg)				PP (mmHg)				HR (bpm)			
		χ_m	χ_t	AE	AE%	χ_m	χ_t	AE	AE%	χ_m	χ_t	AE	AE%	χ_m	χ_t	AE	AE%
169	57	133.30	135.50	2.20	1.62	72.78	73.00	0.22	0.30	60.52	62.50	1.98	3.17	85.45	79.50	5.95	7.48
170	57	124.23	122.00	2.23	1.83	72.33	74.00	1.67	2.25	51.90	48.00	3.90	8.13	87.62	78.50	9.12	11.62
171	57	118.97	119.00	0.03	0.03	72.38	70.50	1.88	2.67	46.58	48.50	1.92	3.96	89.22	78.00	11.22	14.38
172	58	84.23	85.00	0.77	0.91	56.39	57.50	1.11	1.93	27.84	27.50	0.34	1.23	72.68	69.50	3.18	4.57
173	58	83.42	84.50	1.08	1.28	55.35	55.50	0.15	0.27	28.07	29.00	0.93	3.21	72.57	73.00	0.43	0.58
174	58	84.36	82.50	1.86	2.25	56.26	55.00	1.26	2.30	28.09	27.50	0.59	2.16	75.23	76.50	1.27	1.65
175	59	130.50	132.50	2.00	1.51	88.13	90.00	1.87	2.07	42.37	42.50	0.13	0.30	86.00	88.00	2.00	2.27
176	59	125.25	126.50	1.25	0.99	85.83	87.50	1.67	1.91	39.43	39.00	0.43	1.10	81.51	86.50	4.99	5.77
177	59	125.24	122.00	3.24	2.66	87.04	83.50	3.54	4.24	38.20	38.50	0.30	0.78	90.30	87.50	2.80	3.20
178	60	118.20	118.00	0.20	0.17	74.68	73.00	1.68	2.30	43.51	45.00	1.49	3.30	81.30	86.00	4.70	5.47
179	60	113.63	113.00	0.63	0.56	71.67	72.50	0.83	1.15	41.96	40.50	1.46	3.61	85.38	86.50	1.12	1.30
180	60	111.18	112.00	0.82	0.74	77.65	78.50	0.85	1.08	33.52	33.50	0.02	0.07	91.98	89.00	2.98	3.35
181	61	104.62	105.00	0.38	0.36	62.13	63.50	1.37	2.16	42.50	41.50	0.99	2.40	83.16	74.00	9.16	12.38
182	61	102.62	103.50	0.88	0.85	59.90	60.00	0.10	0.17	42.72	43.50	0.78	1.79	69.30	74.50	5.20	6.98
183	61	104.76	103.50	1.26	1.21	61.97	60.50	1.47	2.44	42.78	43.00	0.22	0.51	88.99	75.00	13.99	18.65
184	62	120.24	123.50	3.26	2.64	82.08	83.50	1.42	1.70	38.16	40.00	1.84	4.60	73.10	70.00	3.10	4.42
185	62	118.89	117.00	1.89	1.62	81.97	80.50	1.47	1.82	36.93	36.50	0.43	1.17	73.70	71.50	2.20	3.08
186	62	113.37	112.00	1.37	1.22	78.45	78.50	0.05	0.06	34.91	33.50	1.41	4.21	72.45	72.50	0.05	0.07
187	63	112.64	117.50	4.86	4.13	71.53	74.00	2.47	3.34	41.11	43.50	2.39	5.49	80.59	75.50	5.09	6.75
188	63	111.81	112.00	0.19	0.17	69.47	69.50	0.03	0.05	42.34	42.50	0.16	0.37	94.10	72.50	21.60	29.79
189	63	112.55	107.50	5.05	4.70	71.50	69.00	2.50	3.63	41.04	38.50	2.54	6.61	74.32	74.50	0.18	0.24
190	64	124.56	128.00	3.44	2.69	77.32	78.00	0.68	0.87	47.24	50.00	2.76	5.52	78.87	73.50	5.37	7.31
191	64	127.34	126.00	1.34	1.06	79.87	78.00	1.87	2.39	47.47	48.00	0.53	1.10	75.57	72.00	3.57	4.96
192	64	127.60	125.50	2.10	1.67	81.31	82.50	1.19	1.44	46.29	43.00	3.29	7.65	79.25	76.00	3.25	4.28

Table B43 Blood pressure error analysis (continued)

Test no.	Volunteer no.	SBP (mmHg)				DBP (mmHg)				PP (mmHg)				HR (bpm)			
		χ_m	χ_t	AE	AE%	χ_m	χ_t	AE	AE%	χ_m	χ_t	AE	AE%	χ_m	χ_t	AE	AE%
193	65	113.90	115.50	1.60	1.39	63.92	65.50	1.58	2.41	49.97	50.00	0.03	0.05	81.60	82.00	0.40	0.49
194	65	110.50	111.00	0.50	0.45	63.10	63.00	0.10	0.16	47.41	48.00	0.59	1.24	81.80	83.00	1.20	1.45
195	65	110.60	108.50	2.10	1.93	63.98	62.50	1.48	2.36	46.62	46.00	0.62	1.35	82.26	83.50	1.24	1.48
196	66	116.71	118.50	1.79	1.51	74.68	76.00	1.32	1.74	42.03	42.50	0.47	1.10	73.25	70.00	3.25	4.64
197	66	117.89	116.50	1.39	1.20	74.73	73.50	1.23	1.67	43.17	43.00	0.17	0.39	74.50	74.50	0.00	0.00
198	66	115.39	115.00	0.39	0.34	74.09	74.00	0.09	0.13	41.30	41.00	0.30	0.73	79.32	78.00	1.32	1.69
199	67	110.75	111.50	0.75	0.67	73.30	73.50	0.20	0.28	37.45	38.00	0.55	1.44	66.43	69.00	2.57	3.72
200	67	110.88	111.50	0.62	0.56	73.64	73.50	0.14	0.19	37.24	38.00	0.76	2.00	67.04	69.50	2.46	3.55
201	67	109.87	108.50	1.37	1.27	72.56	72.50	0.06	0.09	37.31	36.00	1.31	3.64	69.09	67.00	2.09	3.13
202	68	117.18	117.50	0.32	0.27	88.00	88.00	0.00	0.00	29.18	29.50	0.32	1.08	86.24	86.00	0.24	0.28
203	68	117.36	116.50	0.86	0.73	88.00	88.00	0.00	0.00	29.36	28.50	0.86	3.00	91.03	86.50	4.53	5.24
204	68	117.46	118.00	0.54	0.46	88.00	88.00	0.00	0.00	29.46	30.00	0.54	1.79	88.64	86.00	2.64	3.08
205	69	120.65	121.50	0.85	0.70	85.23	85.00	0.23	0.27	35.41	36.50	1.09	2.98	75.34	74.00	1.34	1.80
206	69	118.58	118.50	0.08	0.07	84.62	85.00	0.38	0.45	33.96	33.50	0.46	1.37	70.72	75.00	4.28	5.71
207	69	117.77	117.00	0.77	0.66	83.65	83.50	0.15	0.18	34.13	33.50	0.63	1.87	77.07	76.00	1.07	1.40
208	70	100.31	103.00	2.69	2.61	66.21	68.50	2.29	3.34	34.10	34.50	0.40	1.15	75.18	76.50	1.32	1.73
209	70	101.79	101.50	0.29	0.28	65.74	67.00	1.26	1.88	36.05	34.50	1.55	4.48	78.37	78.00	0.37	0.48
210	70	102.90	100.50	2.40	2.39	66.05	62.50	3.55	5.67	36.85	38.00	1.15	3.02	79.84	77.00	2.84	3.69
211	71	133.62	136.50	2.88	2.11	77.33	81.50	4.17	5.11	56.29	55.00	1.29	2.34	70.00	68.50	1.50	2.19
212	71	133.99	131.50	2.49	1.89	78.20	75.00	3.20	4.27	55.79	56.50	0.71	1.26	71.58	65.00	6.58	10.12
213	71	131.39	131.00	0.39	0.30	74.47	73.50	0.97	1.32	56.93	57.50	0.57	1.00	61.78	63.50	1.72	2.71
214	72	127.16	127.50	0.34	0.27	76.64	77.00	0.36	0.46	50.52	50.50	0.02	0.03	60.86	60.00	0.86	1.44
215	72	121.21	122.00	0.79	0.65	69.49	70.50	1.01	1.43	51.72	51.50	0.22	0.43	57.97	56.50	1.47	2.60
216	72	123.63	122.50	1.13	0.92	71.37	70.00	1.37	1.95	52.26	52.50	0.24	0.45	58.86	59.00	0.14	0.23

Table B43 Blood pressure error analysis (continued)

Test no.	Volunteer no.	SBP (mmHg)				DBP (mmHg)				PP (mmHg)				HR (bpm)			
		χ_m	χ_t	AE	AE%	χ_m	χ_t	AE	AE%	χ_m	χ_t	AE	AE%	χ_m	χ_t	AE	AE%
217	73	116.26	117.50	1.24	1.05	75.45	76.50	1.05	1.37	40.81	41.00	0.19	0.46	56.67	60.00	3.33	5.56
218	73	113.96	112.00	1.96	1.75	73.92	72.50	1.42	1.96	40.04	39.50	0.54	1.36	63.96	61.50	2.46	4.01
219	73	109.78	110.50	0.72	0.65	69.63	70.00	0.37	0.53	40.15	40.50	0.35	0.86	63.98	65.00	1.02	1.57
220	74	127.72	128.50	0.78	0.60	69.29	72.00	2.71	3.76	58.43	56.50	1.93	3.42	66.28	64.50	1.78	2.76
221	74	129.44	128.00	1.44	1.13	69.76	67.50	2.26	3.35	59.68	60.50	0.82	1.35	66.61	67.50	0.89	1.32
222	74	127.84	128.50	0.66	0.52	66.95	66.50	0.45	0.68	60.88	62.00	1.12	1.80	70.72	70.50	0.22	0.31
223	75	87.02	86.50	0.52	0.60	51.15	50.50	0.65	1.28	35.87	36.00	0.13	0.35	55.90	57.50	1.60	2.78
224	75	85.47	86.00	0.53	0.62	51.08	51.50	0.42	0.82	34.39	34.50	0.11	0.32	60.17	58.50	1.67	2.86
225	75	86.01	86.00	0.01	0.01	51.27	51.50	0.23	0.44	34.74	34.50	0.24	0.69	55.68	60.00	4.32	7.20
226	76	98.83	99.50	0.67	0.67	70.50	71.00	0.50	0.71	28.34	28.50	0.16	0.57	77.95	80.00	2.05	2.56
227	76	100.31	100.00	0.31	0.31	70.82	71.50	0.68	0.95	29.49	28.50	0.99	3.46	75.49	80.00	4.51	5.63
228	76	100.86	100.50	0.36	0.36	70.68	69.50	1.18	1.70	30.18	31.00	0.82	2.65	78.89	80.00	1.11	1.38
229	77	107.71	108.50	0.79	0.73	62.63	63.50	0.87	1.37	45.08	45.00	0.08	0.18	68.65	66.00	2.65	4.01
230	77	107.05	106.00	1.05	0.99	62.05	61.00	1.05	1.73	45.00	45.00	0.00	0.01	68.35	65.50	2.85	4.36
231	77	104.74	105.00	0.26	0.25	59.32	59.50	0.18	0.31	45.42	45.50	0.08	0.17	70.77	65.00	5.77	8.87
232	78	92.99	93.50	0.51	0.55	60.39	61.00	0.61	1.00	32.60	32.50	0.10	0.30	82.36	78.50	3.86	4.92
233	78	93.63	94.00	0.37	0.39	59.84	60.00	0.16	0.27	33.80	34.00	0.20	0.60	83.28	79.00	4.28	5.42
234	78	94.88	94.00	0.88	0.93	60.27	59.50	0.77	1.30	34.60	34.50	0.10	0.30	71.22	79.00	7.78	9.84
235	79	87.37	86.50	0.87	1.00	59.09	59.50	0.41	0.69	28.28	27.00	1.28	4.73	65.36	66.00	0.64	0.97
236	79	87.91	88.00	0.09	0.10	60.09	60.00	0.09	0.14	27.82	28.00	0.18	0.64	65.76	67.50	1.74	2.58
237	79	87.23	88.00	0.77	0.88	58.83	58.50	0.33	0.56	28.40	29.50	1.10	3.73	65.64	65.50	0.14	0.21
238	80	121.84	123.00	1.16	0.95	81.26	82.50	1.24	1.50	40.57	40.50	0.07	0.17	65.19	70.50	5.31	7.53
239	80	121.70	120.50	1.20	1.00	81.58	80.50	1.08	1.34	40.13	40.00	0.13	0.32	69.37	70.50	1.13	1.60
240	80	119.46	119.50	0.04	0.03	79.16	79.00	0.16	0.20	40.30	40.50	0.20	0.49	71.44	75.50	4.06	5.37

Table B43　Blood pressure error analysis (continued)

Test no.	Volunteer no.	SBP (mmHg)				DBP (mmHg)				PP (mmHg)				HR (bpm)			
		χ_m	χ_t	AE	AE%	χ_m	χ_t	AE	AE%	χ_m	χ_t	AE	AE%	χ_m	χ_t	AE	AE%
241	81	134.66	135.00	0.34	0.25	80.34	81.00	0.66	0.82	54.33	54.00	0.33	0.61	90.99	93.50	2.51	2.68
242	81	132.63	134.00	1.37	1.02	78.94	79.00	0.06	0.08	53.69	55.00	1.31	2.38	87.44	93.50	6.06	6.48
243	81	133.70	132.00	1.70	1.29	80.22	79.50	0.72	0.91	53.48	52.50	0.98	1.87	89.00	91.00	2.00	2.20
244	82	118.49	122.00	3.51	2.87	84.62	88.00	3.38	3.84	33.87	34.00	0.13	0.39	108.21	106.50	1.71	1.61
245	82	120.35	116.50	3.85	3.30	85.85	83.00	2.85	3.43	34.50	33.50	1.00	2.98	102.65	105.00	2.35	2.24
246	82	112.66	113.00	0.34	0.30	78.03	77.50	0.53	0.68	34.63	35.50	0.87	2.44	107.50	103.50	4.00	3.86
247	83	99.41	98.50	0.91	0.92	67.38	67.50	0.12	0.18	32.03	31.00	1.03	3.33	88.18	88.00	0.18	0.21
248	83	99.09	99.50	0.41	0.41	66.23	67.00	0.77	1.15	32.86	32.50	0.36	1.10	96.26	90.50	5.76	6.37
249	83	99.00	99.50	0.50	0.50	66.39	65.50	0.89	1.36	32.61	34.00	1.39	4.08	88.02	89.50	1.48	1.65
250	84	96.13	96.00	0.13	0.13	59.90	60.00	0.10	0.17	36.23	36.00	0.23	0.64	78.85	70.50	8.35	11.84
251	84	97.61	98.00	0.39	0.40	61.80	61.50	0.30	0.48	35.81	36.50	0.69	1.89	73.39	69.50	3.89	5.60
252	84	98.26	98.00	0.26	0.27	62.81	63.00	0.19	0.31	35.46	35.00	0.46	1.31	72.99	75.50	2.51	3.33
253	85	152.26	152.00	0.26	0.17	85.32	85.00	0.32	0.37	66.95	67.00	0.05	0.08	70.20	67.50	2.70	4.00
254	85	146.69	150.00	3.31	2.21	81.78	85.00	3.22	3.78	64.91	65.00	0.09	0.14	72.47	66.50	5.97	8.98
255	85	147.05	144.00	3.05	2.12	81.40	78.50	2.90	3.69	65.65	65.50	0.15	0.22	72.10	68.50	3.60	5.25

APPENDIX C
ETHICS IN HUMAN RESEARCH DOCUMENTS

Owing to the experimentation in humans conducted in this dissertation, an approval of ethics in human research has been requested and granted for operation. In this section, the details and documents regarding the ethics in human research are achieved.

To initiate the research and development of a blood pressure measuring instrument, the approval of ethics in human research has been proposed to Silpakorn University Research, Innovation, and Creativity (SURIC) administrative office. Consequently, approval has been granted under the research project ID: REC 65.0131-017-0419 with certified document no. REC 65.0401-065. Furthermore, the experimentation can be carried out from 1st April 2022 to 31st March 2023, as referenced on Page 190.

However, the blood pressure measuring system had continuously been developed pass the initial human trial deadline of 31st March 2023. Meanwhile, the measuring system had implemented a novel demodulation technique of phase-shift demodulation which improved the resolution of the pulse wave monitoring. Thus, an extension to the previous deadline had been submitted to validate the system in continuous pulse wave monitoring applications. Consequently, the extended date is 18th August 2023 to 17th August 2024, a one-year period of human trial investigation. This is documented on Page 191.

To comply with the ethics in human research, the data shown in this dissertation do not represent an individual on an identifiable basis. Instead, the overall statistics are presented in the investigation. Since the following documents are written in Thai, the information written on this page shall serve as a summary of relevant details of the documents. For clarification, the human trial has only recruit Thai volunteers with supported documents approved by SURIC and fairly distributed to the volunteers before the examination for understanding of their rights, risks, and benefits in participation.

มหาวิทยาลัยศิลปากร

หนังสือฉบับนี้ให้ไว้เพื่อแสดงว่า

รหัสโครงการ: REC 65.0131-017-0419

ชื่อโครงการ (ภาษาไทย): การพัฒนาระบบตรวจจับชนิดใยแก้วนำแสงสำหรับการประยุกต์ใช้ในงานวิศวกรรมชีวการแพทย์: กรณีศึกษาการวัดความดันโลหิตแบบต่อเนื่อง

ชื่อโครงการ (ภาษาอังกฤษ): Development of a Fiber Optic Sensor for Biomedical Engineering Application: A Case Study of Continuous Blood Pressure Measurement

ผู้วิจัยหลัก: นายปิยวัฒน์ สามารถกิจ **สังกัด:** คณะวิศวกรรมศาสตร์และเทคโนโลยีอุตสาหกรรม

เอกสารที่รับรอง:

1. แบบเสนอเพื่อขอรับการพิจารณาจริยธรรมการวิจัยในมนุษย์ เวอร์ชั่น 02 ฉบับลงวันที่ 31 มีนาคม 2565
2. แบบเสนอโครงการวิจัยเพื่อการพิจารณาจริยธรรมการวิจัยในมนุษย์ (ฉบับภาษาไทย) เวอร์ชั่น 02 ฉบับลงวันที่ 31 มีนาคม 2565
3. เอกสารชี้แจงผู้เข้าร่วมการวิจัย เวอร์ชั่น 02 ฉบับลงวันที่ 31 มีนาคม 2565
4. หนังสือแสดงเจตนายินยอมการเข้าร่วมการวิจัย เวอร์ชั่น 01 ฉบับลงวันที่ 31 มกราคม 2565

ได้ผ่านการรับรองจากคณะกรรมการจริยธรรมการวิจัยในมนุษย์ มหาวิทยาลัยศิลปากร โดยยึดหลักเกณฑ์ตามคำประกาศ เฮลซิงกิ (Declaration of Helsinki) และมีความสอดคล้องกับหลักจริยธรรมสากล ตลอดจนกฎหมายข้อบังคับและข้อกำหนดภายในประเทศ โดยขอให้รายงานฉบับสมบูรณ์เมื่อโครงการเสร็จสิ้น

(ศาสตราจารย์ ดร.พรศิลป์ ศิริอมรศักดิ์)
ประธานคณะกรรมการจริยธรรมการวิจัยในมนุษย์
มหาวิทยาลัยศิลปากร

หมายเลขใบรับรอง COE 65.0401-065
วันที่รับรอง: 1 เมษายน พ.ศ. 2565
วันหมดอายุ: 31 มีนาคม พ.ศ. 2566

สำนักงานบริหารการวิจัย นวัตกรรมและการสร้างสรรค์
6 ถนนราชมรรคาใน ตำบลพระปฐมเจดีย์ อำเภอเมืองนครปฐม จังหวัดนครปฐม 73000
โทร 0-3425-5808 โทรสาร (Fax) : 0-3425-5808
email : su.ethicshuman@gmail.com

บันทึกข้อความ

ส่วนงาน สำนักงานบริหารการวิจัย นวัตกรรมและการสร้างสรรค์ มหาวิทยาลัยศิลปากร ภายใน 216004

ที่ อว 8603.16/4085 **วันที่** 14 สิงหาคม 2566

เรื่อง ผลการพิจารณาการต่ออายุเอกสารรับรองโครงการวิจัย

เรียน นายปิยวัฒน์ สามารถกิจ (นักศึกษาคณะวิศวกรรมศาสตร์และเทคโนโลยีอุตสาหกรรม)
ผ่านอาจารย์ที่ปรึกษา รองศาสตราจารย์ ดร.สาโรช พูลเทพ

ตามที่ท่านได้มีบันทึก ที่ อว 8615/18641 ลงวันที่ 10 สิงหาคม 2566 ขอต่ออายุโครงการวิจัยที่ผ่านการรับรองจากคณะกรรมการจริยธรรมการวิจัยในมนุษย์ พร้อมส่งรายงานความก้าวหน้าการดำเนินงานวิจัยครั้งที่ 1 ของโครงการวิจัย เรื่อง การพัฒนาระบบตรวจจับชนิดใยแก้วนำแสงสำหรับการประยุกต์ใช้ในงานวิศวกรรมชีวการแพทย์: กรณีศึกษาการวัดความดันโลหิตแบบต่อเนื่อง (เลขที่โครงการ REC 65.0131-017-0419) โดยโครงการดังกล่าวได้รับการรับรองจากคณะกรรมการจริยธรรมการวิจัยในมนุษย์ เมื่อวันที่ 1 เมษายน 2565 และหมดอายุวันที่ 31 มีนาคม 2566 ตามใบรับรองเลขที่ COE 65.0401-065 โดยผู้วิจัยดำเนินการไม่แล้วเสร็จ คิดเป็นร้อยละ 50 ของกระบวนการวิจัยที่วางแผนไว้ในโครงร่างการวิจัยให้เหตุผลว่าการพัฒนาระบบตรวจจับชนิดใยแก้วนำแสง ณ ห้องปฏิบัติการทางวิศวกรรมประเทศฝรั่งเศส ทำให้ระบบตรวจจับมีความเหมาะสมกับการตรวจวัดคลื่นชีพจรในมนุษย์ได้อย่างมีประสิทธิภาพมากยิ่งขึ้นส่งผลให้สามารถเก็บข้อมูลทางชีพจร (Cardiovascular information) จากผู้เข้าร่วมโครงการได้อย่างรวดเร็วและแม่นยำ อย่างไรก็ตามระบบที่ได้พัฒนาขึ้นไม่สามารถดำเนินการทดสอบกับกลุ่มตัวอย่างได้เต็มศักยภาพ เนื่องจากจำเป็นต้องทดสอบกับอาสาสมัครประชากรไทย (Thai population) ดังระบุไว้ในเอกสารโครงการ จึงจำเป็นต้องนำอุปกรณ์วิจัยกลับมาติดตั้งภายในห้องปฏิบัติการไทยและดำเนินการเก็บข้อมูลเพิ่มเติม นั้น

ในการนี้ ที่ประชุมคณะกรรมการจริยธรรมการวิจัยในมนุษย์ ครั้งที่ 4/2566 เมื่อวันที่ 18 สิงหาคม 2566 ได้พิจารณาตามเหตุผลข้างต้นแล้ว มีมติอนุมัติให้ต่ออายุ ระยะเวลา 1 ปี ตั้งแต่วันที่ 18 สิงหาคม 2566 และหมดอายุวันที่ 17 สิงหาคม 2567 ทั้งนี้ ผู้วิจัยจะไม่สามารถรับผู้เข้าร่วมการวิจัยรายใหม่ได้ในช่วงวันที่ 1 เมษายน 2566 ถึง 17 สิงหาคม 2566 ไปใช้ในโครงการวิจัยดังกล่าว

จึงเรียนมาเพื่อโปรดทราบ

(รองศาสตราจารย์ ดร.ประเสริฐ อัครมงคลพร)
ประธานกรรมการจริยธรรมการวิจัยในมนุษย์

VITA

NAME Piyawat Samartkit

INSTITUTIONS ATTENDED B.Tech (Engineering Business), Silpakorn University

PUBLICATION

P. Samartkit,S. Pullteap, and H.C. Seat, "Validation of Fiber Optic-Based Fabry-Perot Interferometer for Simultaneous Heart Rate and Pulse Pressure Measurements," IEEE Sensors Journal, vol. 21, no. 5, pp. 6195-6201, 2021.

S. Pullteap and P. Samartkit, "A High Sensitivity of Vital Signs Detector using Fiber Optic-based Fabry-Perot Interferometer," ECTI Transactions on Electrical Engineering, Electronics, and Communications, vol. 18, no. 2, pp. 98-106, 2020.

P. Samartkit and S. Pullteap, "Non-invasive continuous blood pressure sensors in biomedical engineering research: A review," Sensors and Actuators: A. Physical, vol. 367, p. 115084, 2024.